As opiniões expressas nesta publicação são da exclusiva responsabilidade do seu autor.

Universidade de Lisboa

Faculdade de Medicina de Lisboa

IMMUNE ENGAGEMENT THRESHOLDS FOR CD8$^+$ T CELL CONTROL OF γHERPESVIRUS-DRIVEN B CELL PROLIFERATION

by

Cristina Sofia Godinho da Silva

(Recipient of a scholarship – SFRH/BD/46416/2009 from Fundação para a Ciência e Tecnologia)

Degree of Doctor of Philosophy in Biomedical Sciences

Specialization in Biopathological Sciences

Thesis Supervised by Professor Doutor João Pedro Simas

PhD in Viral Pathogenesis, University of Cambridge, United Kingdom

A impressão desta dissertação foi aprovada pelo Conselho Científico da Faculdade de Medicina de Lisboa em reunião de 22 de Julho de 2014.

PREFACE

The current thesis presents data obtained during my PhD research project, developed at Instituto de Medicina Molecular in the period of January 2010 to December 2013, under the supervision of Professor Doutor João Pedro Simas (Faculdade de Medicina, Universidade de Lisboa).

This thesis is organized in 9 chapters, which are preceded by a summary written in Portuguese and an abstract. Before the description of the results, an introductory review of the subject is provided in chapter 1, followed by the aims of the work and the experimental strategy. In chapters 2, 3, 4, 5, 6 and 7 the original data obtained during this research project are presented. Final considerations, including the discussion of the results obtained in previous chapters, and future directions are presented in chapter 8. Finally, chapter 9 concerns the description of the materials and methodologies employed to carry out the presented work. The publications that resulted from the research carried out throughout the duration of this project are included in appendix 1 and 2.

Data presented in this dissertation were purely the result of work carried out by me and it is clearly acknowledge in the text whenever data or reagents produced by others were utilized. This work has not been submitted for any degree at this or any university.

Cristina Sofia Godinho da Silva

PUBLICATIONS

Godinho-Silva, C.*, Marques, S.*, Fontinha, D., Veiga-Fernandes, H., Stevenson, P. G. & Simas, J. P. (2014) **Defining Immune Engagement Thresholds for *In Vivo* Control of Virus-Driven Lymphoproliferation.** PLoS Pathog. 10(6): e1004220. *shared first authorship

Data presented in this publication were obtained by me, with the exception of panel B in figure 1, and panel B in figure 2. Data in figure 3A were obtained in collaboration. This publication resulted from my PhD research project.

Decalf, J.*, Godinho-Silva, C.*, Fontinha, D., Marques, S. & Simas, J. P. (2014) **Establishment of Murine Gammaherpesvirus Latency in B Cells Is Not a Stochastic Event.** PLoS Pathog. *Accepted, in press.* *shared first authorship

Data presented in panels B and C of figure 2, figure 5, figure S1, figure S2, figure S3B and figure S4 were obtained by me. Virus working stocks used in figure 4 were prepared and titrated by me and I helped with the initial set up of the experiment. Data presented in figure 9 were obtained by me, except for immunization at day 7 post-infection, and data regarding immunization at day 0 were obtained in collaboration. This publication resulted from research carried out throughout the duration of my PhD.

van de Pavert, S. A., Ferreira, M., Domingues, R. G., Ribeiro, H., Molenaar, R., Moreira-Santos, L., Almeida F. F., Ibiza, S., Barbosa, I., Goverse, G., Labão-Almeida, C., Godinho-Silva, C., Konijn, T., Schooneman, D., O'Toole, T., Mizee, M. R., Habani, Y., Haak, E., Santori, F. R., Littman, D. R., Schulte-Merker, S., Dzierzak, E., Simas, J. P., Mebius, R. E. & Veiga-Fernandes, H. (2014) **Maternal retinoids control type 3 innate lymphoid cells and set the offspring immunity.** Nature. 508 (7494): 123-7.

Data presented in panels i and j of figure 4, in panel e and f of extended data figure 7 and in extended data figure 8 were obtained in collaboration. This publication resulted from research carried out throughout the duration of my PhD.

ACKNOWLEDGMENTS

Em primeiro lugar, um agradecimento especial ao meu supervisor Pedro Simas por me ter dado a oportunidade de realizar o doutoramento no seu laboratório e de abraçar este desafiante e estimulante projecto de investigação. A sua orientação científica, conselhos e ensinamentos ao longo do meu doutoramento foram fundamentais. Obrigada pela compreensão e apoio, pela motivação e pela amizade demonstradas.

Quero também agradecer a todos os membros, do presente e passado, da unidade de Patogénese Viral, pela sua disponibilidade e apoio constantes e por toda a amizade, dentro e fora do laboratório. Em particular, um agradecimento muito especial à Sofia Marques a precursora deste projecto. A sua colaboração, inestimável ajuda, sugestões e inúmeras discussões científicas ao longo do meu doutoramento foram cruciais. Obrigada por me teres ensinado tanto do que hoje sei e, sobretudo, obrigada por todo o entusiasmo, confiança e motivação transmitidos, especialmente nos momentos mais difíceis. Obrigada à Lénia, que me introduziu ao "mundo" da biologia molecular, por partilhar comigo toda a sua experiência e conhecimento, e pelos nossos magníficos "momentos de 6ª à tarde". Obrigada à Marta Miranda, à Sofiazinha pela cumplicidade e apoio, à Diana pelas "madrugadas" a recolher LNs e finais de tarde com infindáveis iv's, à Inês, à Filipa, à Teresa, ao Bruno, ao Jérémie, à Marta Alenquer, à Ana e ao Alexandre, por terem feito do nosso grupo um grupo especial.

Gostaria também de agradecer ao Instituto de Medicina Molecular (IMM) por me ter recebido e por ter proporcionado todas as condições necessárias à realização do meu projecto de doutoramento. Este agradecimento é extensível aos investigadores e funcionários do instituto que, pela constante ajuda e disponibilidade, contribuíram para este trabalho. Em particular, agradeço aos funcionários do biotério por cuidarem dos meus ratinhos e aos membros da unidade de citometria de fluxo, nomeadamente à Ana Vieira pela ajuda com os *settings*, compensações e *sorts*. Agradeço também aos membros da unidade de Malária e posteriormente da unidade de Reumatologia, companheiros de espaço de cultura de células no IMM, pelo bom ambiente de trabalho e relacionamento proporcionados. Muito obrigada ao Angelo Chora por toda a sua disponibilidade, por partilhar os seus conhecimentos na área da célula T, pelas suas sugestões, conselhos e dicas experimentais e por me ter ensinado a fazer iv's.

Agradeço aos membros do meu comité de tese, Doutor Luís Graça, Doutora Maria Manuel Mota e Doutor Miguel Prudêncio, pela disponibilidade e críticas construtivas.

I would like to acknowledge Dr Philip Stevenson, to whom I am indebted for all his invaluable availability and contribution into my research article. His scientific expertise in the field, the exhaustive analysis and interpretation of all experiments and scientific discussions were crucial for improving the content as well as the reading of the manuscript.

Por fim, queria ainda agradecer aos meus amigos de sempre e para sempre e à minha família.

RESUMO

Os gama-herpesvírus (γHVs) são agentes com potencial oncogénico, que infectam mais de 95% da população adulta mundial, e persistem durante toda a vida do hospedeiro através do estabelecimento de infecções latentes em linfócitos B de memória. Para persistirem os γHVs exploram o normal ciclo de vida da célula B, induzindo a proliferação de células latentemente infectadas em centros germinativos e a sua posterior diferenciação em células B de memória de longa duração. Em indivíduos imunocompetentes, o equilíbrio dinâmico entre a capacidade linfoproliferativa do vírus e o controlo imunológico, em particular de linfócitos T citotóxicos (CTLs) $CD8^+$, permite que o vírus persista sem causar doença. Contudo, se o equilíbrio γHV-hospedeiro é perturbado, nomeadamente quando a função de $CD8^+$ CTLs é comprometida, as células B latentemente infectadas podem proliferar descontroladamente dando origem a doenças linfoproliferativas. Os dois γHVs humanos conhecidos até à data – vírus Epstein-Barr (EBV) e o vírus associado ao sarcoma de Kaposi (KSHV) – estão associados ao desenvolvimento de várias neoplasias como o linfoma de Burkitt, linfoma de Hodgkin, carcinoma da nasofaringe, sarcoma de Kaposi, entre outras. Consequentemente, o controlo dos γHVs constitui um objectivo clínico prioritário.

Os epítopos virais de latência apresentados no contexto de moléculas do complexo principal de histocompatibilidade (MHC) à superfície de células latentemente infectadas e de tumores constituem um alvo para $CD8^+$ CTLs. A apresentação destes epítopos latentes tem sido explorada com sucesso para prevenir e tratar doenças linfoproliferativas agudas causadas por EBV, através da transferência de CTLs, em pacientes submetidos a terapia imunossupressora após um transplante. Contudo, a optimização e a extensão deste tipo de imunoterapia a outras neoplasias induzidas por γHV, bem como o desenvolvimento de vacinas com fins profilácticos e terapêuticos tem-se revelado difícil, constituindo actualmente um importante desafio. A estrita especificidade de hospedeiro dos γHVs humanos tem limitado estudos *in vivo*. Consequentemente, um dos maiores desafios no estudo do controlo imunológico da infecção por γHVs consiste em relacionar a função efectora de $CD8^+$ CTLs determinada *in vitro* com um efeito imunoprotector efectivo *in vivo*.

Esta tese teve como principal objectivo identificar determinantes imunológicos críticos para o eficaz controlo *in vivo* da linfoproliferação induzida por γHV. Neste estudo utilizou-se a infecção de ratinhos de laboratório com o herpesvírus de murganho-4 (MuHV-4) como modelo experimental para identificar, *in vivo*, factores críticos para o eficaz reconhecimento e controlo imunológico da infecção latente por γHV. Em particular, analisou-se o impacto que a ligação de um epítopo de latência à molécula de MHC classe I e a avidez funcional da célula T para esse mesmo epítopo têm no controlo da infecção *in vivo*. O vírus MuHV-4 é um parasita natural de roedores selvagens, geneticamente relacionado com os γHVs humanos, EBV e KSHV, e que à semelhança destes, infecta latentemente células B, induzindo a sua proliferação em centros germinativos, e posterior diferenciação em células B de memória, como estratégia para persistir durante toda a vida do hospedeiro. A proteína de latência M2 codificada por MuHV-4 encontra-

se envolvida na modulação de vias de sinalização que promovem a activação da célula B e simultaneamente constitui um alvo para $CD8^+$ CTLs. M2 contem um epítopo restrito por $H2K^d$ ($M2_{84-92}/K^d$) cujo reconhecimento por $CD8^+$ CTLs de ratinhos BALB/c ($H2^d$), mas não de ratinhos C57BL/6 ($H2^b$), contribui para o controlo da proliferação das células B em centros germinativos, a longo termo após infecção. M2 codifica o único epítopo latente conhecido até à data para MuHV-4 e apresenta diversidade de aminoácidos na sua sequência primária, consistente com a possibilidade de selecção em resposta a pressão imunológica. Variações na sequência de aminoácidos de um epítopo latente que afectem a sua ligação à molécula de MHC classe I ou a avidez funcional da célula T $CD8^+$ para o epítopo poderão ter um impacto crucial no controlo da infecção latente e, consequentemente, na capacidade de persistência do vírus no hospedeiro. Para investigar esta hipótese, neste estudo construíram-se vírus recombinantes nos quais foi introduzido em fusão com o C-terminal da proteína M2 um epítopo $CD8^+$ bem caracterizado restrito por $H2K^b$ ($OVA_{257-264}/K^b$) ou variações do mesmo, que diferem num único aminoácido. Esta abordagem experimental permitiu que os epítopos introduzidos fossem apresentados num contexto fisiológico de latência, com a mesma cinética e no mesmo número de cópias do epítopo endógeno ($M2_{84-92}/K^d$).

Para avaliar a relevância da apresentação e do reconhecimento imunológico de cada epítopo no controlo da infecção latente procedeu-se à infecção intranasal de ratinhos do haplotipo $H2^b$ com os vírus recombinantes construídos. A escolha do haplotipo $H2^b$ permitiu analisar o impacto individual da introdução de cada epítopo no controlo da proliferação das células B latentemente infectadas por $CD8^+$ CTLs, sem que o epítopo endógeno de M2 ($M2_{84-92}/K^d$) fosse reconhecido. Cada epítopo foi caracterizado, *in vitro*, relativamente à sua capacidade de ligação à molécula de MHC classe I ($H2K^b$) e à sua avidez funcional para células T $CD8^+$, purificadas de ratinhos OT-I, e que expressam um TCR transgénico específico para o epítopo $OVA_{257-264}/K^b$.

O impacto que a ligação de um único epítopo latente derivado de M2 à molécula de MHC classe I tem na colonização do hospedeiro foi analisado, *in vivo*, após infecção de ratinhos C57BL/6 ($H2^b$), por comparação com a infecção com o vírus selvagem (WT). Cada vírus foi analisado para a capacidade de induzir a proliferação de células B latentemente infectadas em centros germinativos, durante a fase de expansão de latência, e para a persistência no hospedeiro a longo termo. Adicionalmente, analisou-se a resposta de células T $CD8^+$ induzida pelo reconhecimento de cada epítopo. Os resultados obtidos revelaram que o reconhecimento de um epítopo latente capaz de se ligar fortemente à molécula de MHC classe I comprometeu a capacidade do vírus estabelecer latência, traduzindo-se numa forte supressão da proliferação de células B latentemente infectadas em centros germinativos e numa diminuição dos níveis de persistência a longo termo no hospedeiro. Contudo, uma ligação subóptima à molécula de MHC classe I foi suficiente para permitir o estabelecimento de latência, a amplificação de células B infectadas em centros germinativos e o estabelecimento de níveis normais de persistência a longo termo. Logo, a forte ligação de um epítopo latente derivado de M2 à molécula de MHC classe I foi um determinante crítico para o eficaz controlo da linfoproliferação induzida pelo vírus. Pequenas variações na capacidade do epítopo se ligar a molécula de MHC classe I foram pouco

toleradas, resultando numa perda de controlo da infecção latente. Curiosamente, epítopos com ligação óptima à molécula de MHC classe I induziram respostas de $CD8^+$ CTLs relativamente pequenas comparativamente com um epítopo com ligação subóptima, o qual produziu a resposta com maior magnitude. Estes resultados indicam que respostas de $CD8^+$ CTLs de maior magnitude não são necessariamente mais eficazes e protectoras *in vivo*. Contudo, em ambas as situações as células T $CD8^+$ revelaram semelhante capacidade efectora, em termos de produção de interferão-gama (IFNγ) e de eliminação de células alvo *in vivo*.

A relevância da avidez funcional da célula T $CD8^+$ para o controlo *in vivo* da infecção latente foi analisada após infecção intranasal de ratinhos transgénicos OT-I ($H2^b$) com os diferentes vírus recombinantes e com o vírus WT em paralelo. O controlo da infecção latente foi tão mais eficaz quão maior a avidez funcional da célula T $CD8^+$ para o epítopo apresentado. Obteve-se, portanto, uma hierarquia de diferentes níveis de controlo de latência *in vivo,* a qual correlacionou com a avidez funcional *in vitro* das células OT-I para cada um dos epítopos apresentados. Adicionalmente, demonstrou-se inequivocamente que o controlo da infecção latente foi mediado por $CD8^+$ CTLs, visto que, após depleção de células T $CD8^+$ os níveis de latência estabelecidos por cada vírus recombinante reverteram para os níveis de latência do vírus WT. Logo, a avidez funcional da célula T $CD8^+$ para um epítopo latente revelou-se um factor importante para o controlo da infecção latente por MuHV-4.

O limitado repertório de células T $CD4^+$, inerente ao modelo OT-I, afecta a capacidade destes ratinhos desenvolverem centros germinativos, e consequentemente, a habilidade do vírus MuHV-4 expandir a população de células B latentemente infectadas em centros germinativos. Com o objectivo de avaliar a relevância da avidez funcional de $CD8^+$ CTLs para o controlo da infecção latente num ambiente mais favorável à linfoproliferação, cotransferiu-se para ratinhos $TCR\alpha^{-/-}$ ($H2^b$) células T $CD4^+$ policlonais purificadas de ratinhos C57BL/6 ($H2^b$) e células T $CD8^+$ monoclonais isoladas de ratinhos CD45.1 $Rag1^{-/-}$ OT-I ($H2^b$), um dia antes da infecção com os vírus recombinantes. O impacto da avidez funcional no desenvolvimento da resposta de $CD8^+$ CTLs e no controlo da linfoproliferação induzida por MuHV-4 foram determinados *in vivo*. A expansão *in vivo* das células OT-I, a sua activação e aquisição de função efectora demonstraram uma correlação com a avidez funcional determinada *in vitro* para cada um dos epítopos, tendo-se obtido uma hierarquia de resposta de $CD8^+$ CTLs. Por sua vez, esta traduziu-se numa hierarquia de diferentes níveis de controlo *in vivo* da linfoproliferação induzida por MuHV-4. Logo, obtiveram-se resultados concordantes com os obtidos previamente usando o modelo de ratinho OT-I. Adicionalmente, foi possível estabelecer uma relação entre a avidez funcional *in vitro* da célula T $CD8^+$ para cada epítopo e o controlo da linfoproliferação das células B latentemente infectadas em centros germinativos. Uma avidez funcional subóptima da célula T $CD8^+$ para um epítopo latente não comprometeu o controlo da linfoproliferação induzida por MuHV-4 em centros germinativos. Contudo, uma drástica diminuição na avidez funcional da célula T $CD8^+$ suprimiu o controlo da infecção, permitindo a expansão das células B latentemente infectadas. Logo, este aspecto do reconhecimento imunológico revelou-se mais flexível, quando comparado com o

efeito que semelhante perda de ligação à molécula de MHC classe I teve, no controlo da linfoproliferação induzida pelo vírus.

Em suma, este estudo demonstrou que a introdução de um único epítopo $CD8^+$ numa proteína de latência permitiu o eficaz controlo da linfoproliferação aguda induzida por MuHV-4 em centros germinativos e uma diminuição dos níveis de persistência no hospedeiro a longo termo, através de uma resposta de $CD8^+$ CTLs específica. Adicionalmente, os resultados obtidos nesta tese permitiram identificar a capacidade de ligação de um epítopo latente à molécula de MHC classe I e a avidez funcional da célula T $CD8^+$ para esse epítopo como determinantes imunológicos críticos do controlo *in vivo* da linfoproliferação induzida por γHV. A ligação óptima do epítopo à molécula de MHC classe I foi crucial para o eficaz controlo *in vivo* da linfoproliferação induzida pelo vírus, enquanto que variações na avidez funcional da célula T $CD8^+$ para o epítopo foram melhor toleradas, até se reflectirem numa perda de controlo da infecção *in vivo*. Logo, este estudo permitiu relacionar, para um epítopo latente, valores de interacção com a molécula de MHC classe I e com a célula T $CD8^+$ determinados *in vitro* com o respectivo efeito imunoprotector *in vivo*, destacando a importância e o potencial de se estabelecerem directrizes quantitativas para o controlo da infecção por γHV a partir de medidas bioquímicas.

Em conclusão, a identificação de determinantes imunológicos críticos para o eficaz controlo *in vivo* da linfoproliferação induzida por γHV é fundamental para o desenvolvimento de imunoterapias e estratégias de vacinação, tendo em vista a prevenção ou controlo da infecção persistente por γHV.

Palavras-chave: Gamma-herpesvírus; linfoproliferação induzida pelo vírus; linfócitos T citotóxicos $CD8^+$; epítopo de latência; ligação a MHC classe I; avidez funcional da célula T $CD8^+$.

ABSTRACT

Gamma-herpesviruses (γHVs) are oncogenic pathogens that drive the proliferation of latently infected cells in germinal centres to achieve long-term persistence in memory B cells in face of host competent immune responses. Persistence relies on a dynamic balance between virus-driven B cell proliferation and control by $CD8^+$ cytotoxic T lymphocytes (CTLs). If this virus-host equilibrium is disrupted, as is the case when $CD8^+$ CTL function is compromised, latently infected B cells can proliferate unchecked leading to the development of lymphoproliferative diseases. Viral latency epitopes presented in infected cells have been successfully exploited to prevent or treat γHV-associated lymphoproliferative disorders by adoptive CTL transfer in the transplantation setting. However, extending this approach to other γHV-associated tumours and to the development of prophylactic and therapeutic vaccines remains challenging. The narrow species tropism of human γHVs severely restricts *in vivo* analysis. Hence, an important unknown is how *in vitro* $CD8^+$ CTL killing correlates with effective *in vivo* immune protection.

The aim of this thesis was to identify immune engagement thresholds for effective *in vivo* $CD8^+$ CTL control of virus-driven B cell proliferation. Infection of laboratory mouse with murid herpesvirus-4 (MuHV-4) was used as an experimental model to investigate, for a single latently expressed epitope, how MHC class I binding and $CD8^+$ T cell functional avidity impact on infection control. The ability of MuHV-4 recombinants that differed only in latency epitope presentation to elicit epitope-specific $CD8^+$ CTL responses and to drive the proliferation of latently infected B cells was assessed. $CD8^+$ CTL control of latency amplification in GC B cells was critically dependent on strong epitope binding to MHC class I. By contrast, $CD8^+$ T cell recognition was effective over a broad range of functional avidities before control of virus-driven lymphoproliferation failed, thus showing relatively good tolerance for sub-optimal T cell receptor engagement. In summary, this study identified critical MHC class I and $CD8^+$ T cell engagement thresholds for *in vivo* $CD8^+$ CTL control of virus-driven B cell proliferation. Defining *in vivo* thresholds of immune engagement for the effective control of γHV persistent infection is fundamental for the development of successful immunotherapies and vaccines.

Keywords: Gamma-herpesvirus; virus-driven lymphoproliferation; $CD8^+$ cytotoxic T lymphocytes; latent epitope; MHC class I binding; $CD8^+$ T cell functional avidity.

ABBREVIATIONS

ACr	acidic central repeat
AIDS	acquired immunodeficiency syndrome
AP	alkaline phosphatase
APC	antigen-presenting cell
APL	altered peptide ligand
ATP	adenosine triphosphate
BAC	bacterial artificial chromosome
BCR	B cell receptor
BHK	baby hamster kidney
BL	Burkitt's lymphoma
bp	base pair
CFSE	carboxyfluorescein succinimidyl ester
CI	confidence interval
cpe	cytopathic effect
CSR	class switch recombination
CTL	cytotoxic T lymphocyte
DC	dendritic cell
DIG	digoxigenin
DMEM	Dulbecco's modified Eagle's medium
DNA	Deoxyribonucleic acid
EBER	EBV-encoded RNA
EBNA	EBV nuclear antigen
EBV	Epstein-Barr virus
EC_{50}	half-maximum effective concentration
EDTA	ethylenediaminetetraacetic acid
FACS	flow activated cell sorting
FCS	fetal calf serum
GAr	glycine-alanine repeat
GC	germinal centre
GMEM	Glasgow's modified Eagle's medium
GVHD	graft-versus-host disease
h	hour
HEL	hen egg lysozyme
HIV	human immunodeficiency virus
HL	Hodgkin's lymphoma
HLA	human leukocyte antigen
HMW	high molecular weight
Ig	immunoglobulin

i.n.	intranasal
i.p.	intraperitoneal
ICA	infectious centre assay
IFNγ	interferon-gamma
IL	interleukin
IM	infectious mononucleosis
IRF	interferon regulatory factor
ISH	*in situ* hybridization
ITAM	immunoreceptor tyrosine-based activation motif
i.v.	intravenous
kbp	kilo base pair
K_d	dissociation constant
KICS	KSHV-inflammatory cytokine syndrome
KS	Kaposi sarcoma
KSHV	Kaposi sarcoma-associated herpesvirus
LANA	latency-associated nuclear antigen
LB	Luria Bertani
LCL	lymphoblastoid cell line
LMP	latent membrane protein
MAb	monoclonal antibody
MARCH	membrane-associated RING-CH containing
MCD	multicentric Castleman disease
MFI	mean fluorescence intensity
MHC	major histocompatibility complex
min	minute
miRNA	microRNA
MHV-68	Murine herpesvirus 68
MOI	multiplicity of infection
MuHV-4	Murid herpesvirus 4
MZ	marginal zone
NCBI	National Centre for Biotechnology Information
NF-κB	nuclear factor-kappa B
NK	natural killer
NP	nucleoprotein
NPC	nasopharyngeal carcinoma
nt	nucleotide
OD	optical density
ORF	open reading frame
OVA	ovalbumin
p.i.	post-infection

PBS	phosphate-buffered saline
PCR	polymerase chain reaction
PEL	primary effusion lymphoma
PFU	plaque forming unit
pMHC	peptide-MHC
PTLD	post-transplant lymphoproliferative disease
RNA	RNA ribonucleic acid
RNase	ribonuclease
rpm	revolutions per minute
RT	room temperature
RTA	replication and transcriptional activator
s.e.m.	standard error of the mean
SH2	Src homology domain 2
SH3	Src homology domain 3
SHM	somatic hypermutation
SHPM	single-hit Poison Model
SSC	saline sodium citrate
SW_{HEL}	switch hen egg lysozyme
TAP	transporter associated with antigen processing
TCR	T cell receptor
TNF	tumour-necrosis factor
tRNA	transfer RNA
UV	ultraviolet
VSV	vesicular stomatitis virus
WT	wild type
YFP	yellow fluorescent protein
γHV	gamma-herpesvirus

TABLE OF CONTENTS

INDEX OF FIGURES

INDEX OF TABLES

CHAPTER 1

Introduction

Introduction

Gamma-herpesviruses, such as Epstein-Barr virus and Kaposi sarcoma associated herpesvirus, are human pathogens that establish lifelong latent infections in B lymphocytes. Latency is the hallmark of herpesviruses allowing them to persist in a non-infectious form, from which they periodically reactivate to disseminate to new hosts. It is characterized by limited gene expression, without virion production, and maintenance of the viral genome as a non-integrated circular episome, replicated by host cell DNA polymerase and equally distributed to daughter cells, when the latently infected cell divides during the course of cellular growth. In the immunocompetent host latent infection is kept under control by the immune system and the virus persists without causing disease, indicating that a fine co-evolutionary balance has favored the survival of both virus and humans. However, if the virus-host equilibrium is broken, usually when the $CD8^+$ T lymphocyte function is compromised, lymphoproliferative disorders can arise. In the absence of a competent immune response, latently infected cells can proliferate unchecked, leading to the development of lymphoproliferations that can range from controllable disease to highly aggressive life-threatening malignancy. This makes the control of gamma-herpesviruses an important clinical goal. Therefore, a major challenge consists in understanding the factors that regulate the fine balance between virus-driven proliferation of latently infected B cells and host immune control. This understanding is crucial in order to provide the opportunity to improve or develop new therapeutic strategies against these viruses. Furthermore, studying virus/T cell interaction will increase the knowledge on essential processes of viral pathogenesis and immune system function.

1.1. Epstein-Barr virus

Epstein-Barr virus, or EBV, was discovered 50 years ago in cultured tumour cells from patients with Burkitt's lymphoma (Epstein et al., 1964) and subsequently was found in several other lymphomas and carcinomas (Cesarman, 2014). If the success of a pathogen is defined by the number and extent of hosts it infects, EBV is the most successful human pathogen because it benignly infects more than 95% of the worldwide adult human population and persists for life (Kutok and Wang, 2006). Primary EBV infection *in vivo* generally occurs in the first decade of life and is usually asymptomatic. However, if the infection is acquired during adolescence or later, it can result in infectious mononucleosis (IM), a self-limiting lymphoproliferative disease (Henle et al., 1968; Kutok and Wang, 2006). Primary infection by EBV is rapidly controlled by both cellular and humoral immune mechanisms. Antibody limits the spread of infectious virus and cytotoxic T cells eliminate lytically and latently infected cells that express viral antigens (Hislop et al., 2007b). However, the immune system is unable to eliminate the virus, and as a consequence, EBV persists *in vivo* in a quiescent state in resting memory B lymphocytes that circulate in the peripheral blood for the life of healthy carriers (Babcock et al., 1998). Persistent infection is

characterized by stable low levels of latently infected memory B cells, approximately 1 in 10,000 to 100,000 memory B cells (Laichalk et al., 2002). A low level of active viral replication continues asymptomatically in EBV carriers, leading to virus secretion into the saliva and allowing EBV transmission from one human to another through the oral route. Nevertheless, the virus is continuously monitored by the host immune system, as cytotoxic T lymphocytes (CTLs) and serum antibodies accompany the lifelong persistent infection, which are also stable over time (Hislop et al., 2007b). Therefore, EBV persistence is understood as a dynamic equilibrium between the virus-driven B cell proliferation ability and the host immune control. By contrast, *in vitro* EBV is a potent transforming virus capable of infecting any resting B cell, driving it out of the resting state to become and activated proliferating lymphoblast (Aman et al., 1984; Pope et al., 1968; Thorley-Lawson and Mann, 1985).

Regardless of the benign and uneventful nature of EBV infection in the majority of humans, EBV has been associated with a number of diseases that generally fall into two categories: autoimmunity and cancer. EBV-associated malignancies, such as B cell lymphomas, develop more frequently in the individuals whose immune system is compromised, further indicating that the regulation of EBV infection in B cells is finely balanced.

1.1.1. Germinal centre model of EBV infection

Two biological models have been proposed to explain EBV persistence: the germinal centre (GC) model (Thorley-Lawson, 2001; Thorley-Lawson, 2005; Thorley-Lawson et al., 2008; Thorley-Lawson et al., 2013) and the direct infection model (Kurth et al., 2003; Kurth et al., 2000).

The GC model, proposed by Thorley-Lawson and co-workers, states that EBV persists by exploiting normal B cell biology (Figure 1.1). Hence, according to it newly latently infected B cells pass through a series of differentiation stages, each employing a discrete viral gene transcription programme. Following oral transmission, EBV establishes a lytic infection of permissive cells in the oropharynx, leading to high levels of virus shedding in saliva. It is thought that both squamous epithelial cells and locally infiltrating B cells support this lytic infection. Whether *de novo* infected B cells can enter the lytic cycle immediately or only after a phase of growth transformation is not known. Thereafter, the virus colonises the general B cell system via growth-transforming latent infection of B cells in local lymphoid tissue such as the tonsil. According to the GC model, EBV directly infects naïve B cells, causing their activation into proliferating latently infected blasts, through expression of the growth transcription programme also known as latency III (Table 1.1) (Babcock et al., 2000; Joseph et al., 2000). The growth transcription programme is characterized by the expression of the full *repertoire* of EBV latent proteins, consisting of six EBV nuclear antigens (EBNAs) 1, 2, 3A, 3B, 3C and LP, and three latent membrane proteins (LMPs) 1, 2A and 2B.

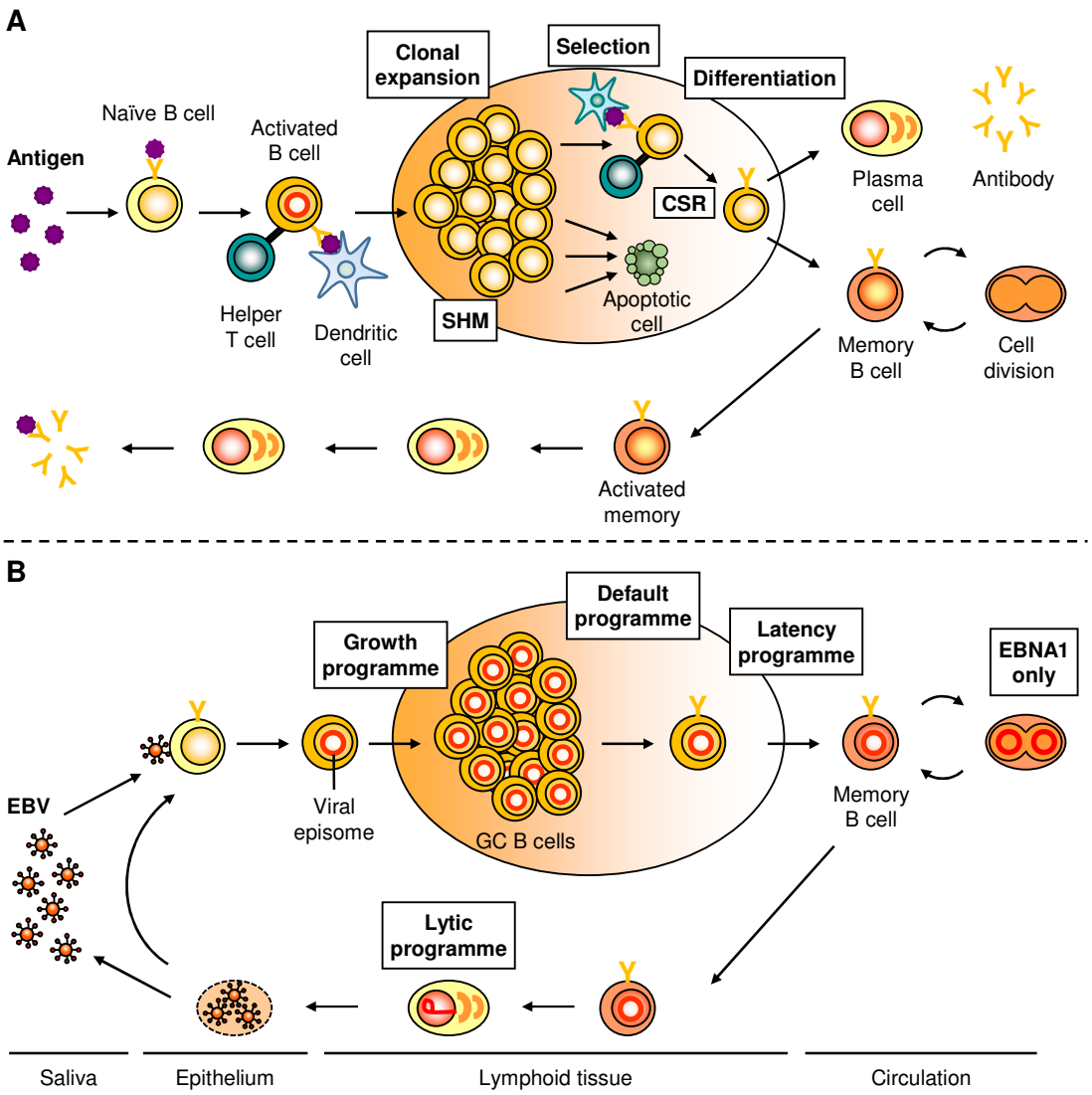

Figure 1.1. Normal B cell response and the parallel with the germinal centre (GC) model of EBV persistence. (A) Normal B cell response. The epithelium of the tonsil continuously samples antigens entering the mouth. Underneath the epithelium, naïve B cells that encounter cognate antigen become activated and migrate into a follicle where they receive further activation signals from dendritic cells and helper T cells, and establish a germinal centre (GC) reaction. In the GC, the blast undergoes repeated rounds of cell division, proliferating rapidly, in association with somatic hypermutation (SHM) and class switch recombination (CSR), followed by interaction with follicular dendritic and T cells to select those blasts that have the highest affinity for the antigen. The later receive further survival and differentiation signals, while the other cells die by apoptosis. The surviving ones differentiate into either a plasma cell or a memory B cell and leave the GC. Upon re-challenge with the antigen, memory B cells are quickly activated and differentiate into antibody producing plasma cells. (B) Germinal centre model of EBV persistence. EBV traverses the epithelium and infects a naïve B cell, activating it into a proliferating latently infected blast, as though the cell was responding to antigen, through expression of all nine known latent proteins – the growth transcription programme. These cells migrate to the follicle where the viral transcription programme changes to the more restricted default programme and a GC reaction is established. Subsequently the latently infected cells differentiate into memory B cells that leave the follicle. In the periphery, all viral protein expression is shut down – the latency programme – and the latently infected cells are maintained as normal memory B cells. These memory B cells can occasionally divide to maintain the pool of latently infected cells and so express the genome tethering protein EBNA1 – the EBNA1 only programme. At any time a small subset of latently infected memory B cells initiates lytic replication in association with terminal differentiation signals. Reactivation leads to the production of infectious virus and cell death. These virions can either replicate at a secondary tissue, where they are amplified and shed into saliva for transmission to new hosts,

or infect new naïve B cells, thus restarting the cycle of infection (adapted from Thorley-Lawson, 2005 and Thorley-Lawson et al., 2013).

In culture, EBV immortalises resting human B cells by expressing the growth programme, driving the establishment of continuously proliferating lymphoblastoid cell lines (LCLs) (Thorley-Lawson and Mann, 1985). *In vivo*, proliferating latently infected blasts then migrate into a follicle to participate in the GC reaction and switch the viral transcription programme to a more restricted pattern of latent protein expression, the default programme also referred to as latency II (Table 1.1) (Babcock et al., 2000; Roughan and Thorley-Lawson, 2009; Roughan et al., 2010). This viral transcription programme is characterized by the expression of only three latent proteins, EBNA1 (the viral genome tethering protein), LMP1 (a CD40 functional homologue) and LMP2A (a B cell receptor (BCR) homologue), that have the potential to mimic B cell survival and progression signals transmitted from helper T cells and through the BCR, respectively (Caldwell et al., 1998; Casola et al., 2004; Gires et al., 1997; He et al., 2003). Such signalling drives the differentiation of the latently infected B cells into memory B cells that leave the GC and enter the peripheral circulation (Thorley-Lawson, 2001). In latently infected memory B cells, EBV either only expresses the EBNA1 protein required for tethering the EBV DNA to the dividing host cell chromosomes, thereby maintaining and segregating the episomal DNA when B cells divide, EBNA1 only programme or latency I (Table 1.1); or no viral proteins at all, thereby shutting down all protein expression (Babcock et al., 2000). This later state, referred to as the latency programme or latency 0 (Table 1.1), is considered the "true" latency. Therefore, the memory compartment has been considered the site of long-term persistence because the virus is quiescent and, consequently, invisible to the host immune system.

Table 1.1. Patterns of EBV latent gene expression in different B cell subsets of healthy individuals and in malignancies. The corresponding expression profiles in malignant lymphomas have been designated latencies I, II and III (adapted from Thorley-Lawson, 2005).

Transcription programme	Genes expressed[a]	Infected normal B cell type	Function	Lymphoma type
Growth (Latency III)	EBNA1, 2, 3A, 3B, 3C, LP, LMP1, LMP2A and LMP2B	Naïve	B cell activation	Immunoblastic lymphoma, PTLD
Default (Latency II)	EBNA1, LMP1 and LMP2A	Germinal centre	Differentiation of activated B cell into memory	Hodgkin's disease Natural Killer-T cell lymphoma
EBNA1 (Latency I)	EBNA1	Dividing memory	Cellular division of latently infected memory B cells	Burkitt's lymphoma Primary effusion lymphoma
Latency (Latency 0)	None	Resting memory	Allow lifetime persistence	
Lytic	All lytic genes	Plasma cell	Viral replication in plasma cell	

[a]Does not include the noncoding EBER and BART RNAs.

PTDL – Post-transplant lymphoproliferative disease

In addition to these latent proteins, EBV expresses several noncoding RNAs. Among these are the EBV-encoded RNA (EBER) 1 and 2, which are small noncoding RNAs expressed ubiquitously and abundantly in EBV infected cells (Swaminathan, 2008). MicroRNAs (miRNAs) are also expressed during EBV latency. EBV encodes two clusters of miRNAs, one adjacent to the *BHRF1* gene and the other with the *BART* transcript. At least 22 precursor and 44 mature EBV miRNAs have been identified (Lopes et al., 2013; Swaminathan, 2008). Recently, distinct patterns of EBV miRNA expression associated with latency III and the restricted forms of latency, latency II, I and 0, have been found in latently infected cells *in vivo* (Qiu et al., 2011).

At any time a small subset of latently infected memory B cells can reactivate and initiate lytic replication, which is thought to occur in response to normal physiologic signals that drive terminal B cell differentiation into a plasma cell (Laichalk and Thorley-Lawson, 2005). EBV reactivation is subdivided into three distinct phases; immediate early when the transcription factors that initiate viral replication are expressed, early, when the proteins involved in viral DNA replication are produced, and late, when viral DNA and structural proteins are assembled into virions. The large amount of virus continually shed by healthy individuals suggests that the viruses released by plasma cells replicate at a secondary site (Thorley-Lawson et al., 2008). It is widely believed that epithelial cell infection amplifies the levels of infectious virus before shedding (Hadinoto et al., 2009). Released infectious virus can then either be shed into saliva for horizontal viral spread to new hosts or infect new naïve B cells, thus completing the infectious cycle. Each stage of this cycle has been demonstrated experimentally (Babcock et al., 1998; Babcock et al., 2000; Laichalk and Thorley-Lawson, 2005) and, with the exception of the memory compartment, is potentially regulated by the host immune system, which targets latently infected blasts and lytically infected plasma cells with cytotoxic T lymphocytes (CTLs) (Figure 1.2) and free virus with neutralizing antibodies (Hislop et al., 2007b).

Currently a major unanswered question concerns to the exact role of LMP1 and LMP2A on the GC process. Specifically, it remains unclear if the role of EBV is essentially passive as latently infected cells transit the GC or if the virus actually plays an active role. *In vitro* studies and evidence from transgenic mouse models have shown that LMP1 and LMP2A have the potential to drive GC B cell survival and differentiation in the absence of T cell help and antigen (Caldwell et al., 1998; Casola et al., 2004; Gires et al., 1997). However, latently infected memory B cells have molecular hallmarks of classical antigen-selected memory B cells, that is, their immunoglobulin (Ig) genes bear somatic mutations and are typically isotype switched (Souza et al., 2005; Souza et al., 2007; Tracy et al., 2012). Moreover, a recent study using a double LMP1 and LMP2A transgenic mouse model indicates that when co-expressed these two proteins have a modest impact on the GC process (Vrazo et al., 2012). Therefore, it has been suggested that LMP1 and LMP2A may simply provide the minimal signals required for the survival of EBV infected cells in the competitive environment of the GC, or may ensure that infected cells differentiate into memory rather than plasma cells (Thorley-Lawson et al., 2013). Further studies are needed to clarify this matter.

Rajewsky and co-workers have proposed that EBV infected cells do not participate in the GC reaction but, rather, that EBV directly infects memory B cells (Kurth et al., 2003; Kurth et al., 2000). Although proposed over 10 years ago, this direct infection model remains ill-defined, unverified at the biological level and unable to explain the origin of EBV-associated lymphomas.

The GC model remains the only experimentally validated model that explains both EBV biology and the origin and pathogenesis of EBV-associated lymphomas. However, a quantitative analysis of viral persistence and an understanding of the dynamic interactions between the different components of the GC model and how their regulation by the immune system produces the EBV pattern of persistence has been lacking. Recently, a mathematical description of the GC model has been developed that successfully recapitulates persistent EBV infection, correctly predicting the observed patterns of cytotoxic T cell regulation, namely which and by how much each infected population is regulated by the immune response, and the sizes of the infected GC and memory B cell populations (Delgado-Eckert and Shapiro, 2011; Hawkins et al., 2013). Importantly, this mathematical model predicts that it is the cycle of infection that explains persistence and provides the stability that allows EBV to persist at the extremely low levels observed, rather than quiescence in the memory B cell compartment. Thus, this moves the focus away from a single infected stage, the immunological invisible memory B cell compartment, to the entire cycle of infected stages (Figure 1.2). Experimental approaches that will distinguish between these two interpretations of the mechanism behind the GC model of persistence are now required.

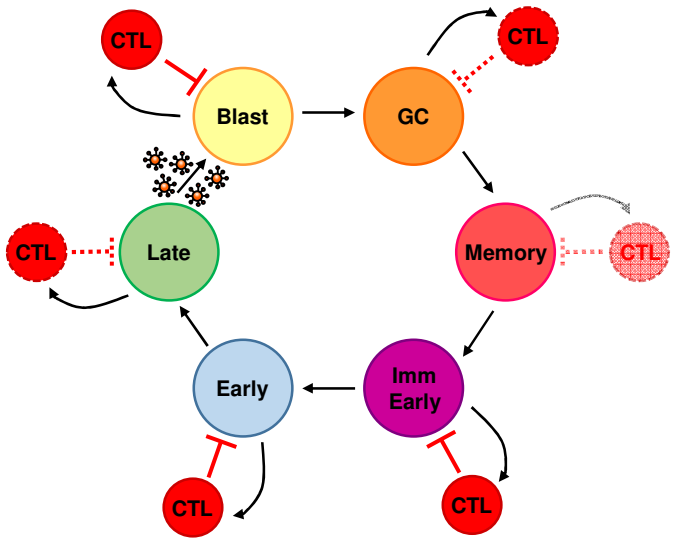

Figure 1.2. Cyclic EBV biological model. Naïve B cells infected by EBV, move into the follicle and enter the germinal centre (GC), where they continue to divide as EBV-infected GC B cells before differentiating into latently infected memory B cells that exit into the periphery. A small subset of memory B cells are induced to undergo lytic reactivation, processing through the lytic stages immediate early, early and late. Released infectious virus may be amplified through infection of the epithelium (not detailed in the model), but culminate in the infection of new naïve B cells which become blasts, thus completing the cycle. Theoretically each stage of the cycle has the capacity to elicit a $CD8^+$ cytotoxic T lymphocyte (CTL) response and to promote

the proliferation of its cognate CTL population (curved arrows) and is in turn controlled by those CTLs (red inhibitory arrows). Under biological conditions the blast, immediate early and early stages are always regulated by CTLs, while the GC and late stages may not always be recognized by CTLs, and there is never a CTL response against the memory stage (adapted from Thorley-Lawson, et al. 2013 and Hawkins et al., 2013).

1.1.2. EBV-associated malignancies

EBV-associated tumours can be categorized by those that occur in immunosupressed individuals versus those that occur in individuals without overt evidence of immunosuppression (Kutok and Wang, 2006). The first category comprises post-transplant lymphoproliferative diseases (PTLDs) in patients undergoing transplantation, who are iatrogenically immunosuppressed, and immunoblastic lymphomas in patients with acquired immunodeficiency syndrome (AIDS), who are immunocompromised by human immunodeficiency virus (HIV) infection. These B cell lymphoproliferative diseases reflect the failure of the immune system, particularly of the CTL response, to control EBV-driven B cell proliferation. The other category includes Burkitt's lymphoma (BL), Hodgkin's lymphoma (HL) and nasopharyngeal carcinoma (NPC), a small subset of natural killer (NK) and T cell lymphomas, gastric carcinomas, follicular dendritic tumours and other epithelial carcinomas. These are found in the immunocompetent host, typical occur many years after primary EBV infection, and EBV is considered has one factor in a complex multistep process of malignant transformation (Mesri et al., 2014). In these cases, EBV genes that affect cell proliferation and survival may contribute directly to tumorigenesis or increase the potential for genetic transformation events. The current understanding indicates that EBV contributes to lymphomagenesis by affecting genome stability and by subverting the cellular molecular signalling machinery and metabolism to avoid immune surveillance and enhance tumour growth and survival (Cesarman, 2014).

The GC model provided the first and, to date, only explanation for the origin of the EBV-associated lymphomas and the reason they express restricted patterns of latent proteins, despite having little to say about the origin of EBV-associated carcinomas (Thorley-Lawson and Gross, 2004). According to it any disruption of the immune system that interferes with the ability of EBV infected cells to become a resting memory B cell will increase the risk of tumour development. Therefore, different EBV-associated tumours are predicted to derive from different and discrete stages in the life cycle of latently infected B cells and represent a cell that is blocked from progressing into a resting state and thus continues to express the viral transcription programme of its progenitor. Using the GC latency model describing the predominant antigen expression and immunogenicity of infected cells, EBV-related tumours can be categorized into different latency types (Table 1.1).

The growth transcription programme or latency type III pattern of EBV expression characterizes the EBV-associated B cell lymphoproliferative diseases that occur in individuals severely immunocompromised by organ transplantation, HIV infection or congenital immunodeficiency.

The obvious explanation is that an impaired CTL response permits uninhibited growth of EBV latently infected blasts expressing the growth programme, which are unable to exit the cell cycle. In some cases, additional genetic defects may occur in EBV-infected cells. These can include genes encoding p53, c-myc, or BCL-6. Because EBV expression of the growth transcription programme elicits an immune response in immunocompetent individuals, latency III B cells are eliminated by CTLs, and thus lymphomas with EBV latency type III will only develop in immunodeficient individuals, while EBV lymphomas and cancers in immunocompetent hosts display latency II or I patterns.

HL is believed to derive from a latently infected GC B cell which have failed to successfully differentiate into a resting memory B cell and therefore constitutively expresses the default transcription programme or latency II (Thorley-Lawson and Gross, 2004). Latency type II is also observed in some types of T and NK cell lymphomas and in NPC. Why the default programme, usually found in GC B cells, is expressed in these tumours is completely unclear. BL was initially proposed to derive from a latently infected memory B cell and EBNA1 is the only latent protein expressed in this tumour. However, recent bioinformatics and genomics analysis indicate a GC origin also for BL (Victora et al., 2012). The interpretation for the origin of BL has been that it arises from a GC B cell that has left the follicle to become a resting memory B cell but is unable to do so because of a reciprocal *c-myc* translocation with one of three immunoglobulin chains, causing constitutively activation of the *c-myc* proto-oncogene; thus it maintains a GC cellular phenotype but attains the memory EBV phenotype (Thorley-Lawson and Gross, 2004).

Additionally, it is now known that EBV-associated tumours, such as BL, HL, NPC and gastric carcinoma, do also express a large number of miRNAs encoded in the BART region (Qiu et al., 2011). *In vitro*, these miRNAs have been shown to be dispensable for B cell transformation, but to confer an increased resistance to apoptosis (Marquitz et al., 2011; Seto et al., 2010). Furthermore, EBV encoded miRNAs have been shown to promote the survival of BL tumour cells *in vitro* (Vereide et al., 2014). Hence, currently BART miRNAs are believed to play a crucial role *in vivo* conferring survival/growth advantages for the tumours (Zhu et al., 2013).

1.1.3. Immune control of EBV infection

A potent innate and adaptive immune response occurs during primary EBV infection. This response, although it controls infection, does not eliminate it, and the virus remains for the lifetime of the infected individual. Thus, EBV persists in face of a host competent immune response in a lifelong dynamic balance with the host immune system.

Cell mediated immune responses are crucial at all stages of the virus-host interaction; acting both to bring the primary infection under control and to limit reactivation of the persistent infection from

its latent reservoir. The main effectors of these cellular responses are natural killer (NK) cells, $CD4^+$ and $CD8^+$ T cells (Figure 1.3) (Rickinson et al., 2014).

$CD8^+$ CTLs play a crucial role in protecting the host during EBV persistent infection. Their importance for the surveillance of EBV latently infected cells can be inferred from the fact that EBV-associated lymphomas frequently occur under conditions of compromised T cell function. Additionally, the importance of $CD8^+$ CTLs is further highlighted by the successful treatment of EBV-related lymphoproliferative disorders by adoptive transfer of EBV-specific CTLs (details in section 1.1.7) (Bollard et al., 2012).

Before focusing on the $CD8^+$ T cell control of EBV infection it is important to consider some aspects of $CD8^+$ cytotoxic T lymphocyte biology and response.

1.1.4. $CD8^+$ cytotoxic T lymphocytes

Virus-specific $CD8^+$ cytotoxic T lymphocytes (CTLs) recognize through their T cell receptor (TCR) viral epitopes, derived from the intracellular processing of viral proteins, that are displayed on the surface of infected cells by major histocompatibility complex (MHC) class I glycoproteins (called human leukocyte antigen (HLA) complex in humans) (Janeway et al., 2005). Antigen recognition drives $CD8^+$ T cell activation a process characterized by robust proliferation and differentiation into effector CTLs. These acquire the ability to produce effector cytokines such as interferon-gamma (IFNγ) and tumour-necrosis factor (TNF). $CD8^+$ CTLs can induce apoptosis of target cells displaying specific antigen, either by releasing cytotoxins (perforin and granzymes) or by Fas-Fas ligand interactions, and thus contribute to infection clearance. Subsequently most of the virus-specific CTLs die during the programmed contraction (cell death) phase while the surviving ones lead to the formation of a memory $CD8^+$ T cell pool (Janeway et al., 2005).

The specificity in the cellular immune response arises from an extensive TCR *repertoire*, as well as from MHC polymorphisms that control the size and diversity of the peptide *repertoire* presented (Janeway et al., 2005). The TCR diversity is critical to accommodate the myriad of potential peptide-MHC (pMHC) complexes comprising virus-derived peptides. Despite the potentially vast TCR *repertoire*, some immune responses, such as the CTL response to EBV, display strong biases in TCR selection. Although the understanding of the underlying mechanisms of TCR bias is far from complete, pMHC-I structure is considered to play a role. MHC molecules are encoded in a large cluster of genes that is inherited as a group or haplotype, which in the mouse are known as the H2 genes. Since laboratory mice are inbreed, each strain is homozygous and has a unique haplotype which is identified by a small letter (e.g. the MHC haplotype of BALB/c mice is $H2^d$, while the one of C57BL/6 is $H2^b$). Mice class I MHCs consist of three major loci, K, D and L.

$CD8^+$ T cell functional avidity is a critical attribute of the antiviral immunity. The *in vivo* effector capacity of $CD8^+$ T cells generally correlates well with functional avidity. The latter is a biological measure determined by *ex vivo* quantification of the ability of $CD8^+$ T cell clones exposed to different concentrations of cognate antigen to proliferate, produce cytokines and lyse target cells. The affinity of the TCR for the pMHC-complex, that is, the strength of the interaction between the TCR and pMHC; expression levels of the TCR and the CD4 or CD8 coreceptors; the distribution and composition of signaling molecules as well as expression levels of molecules that attenuate T cell function and TCR signaling; are crucial in determining the functional avidity of a $CD8^+$ T cell clone (Vigano et al., 2012).

During the course of an immune response and following pathogen re-exposure the functional avidity of a $CD8^+$ T cell population often increases (von Essen et al., 2012). However, it has also been reported that the functional avidity can decrease (Xiao et al., 2007) or remain similar (Zehn et al., 2009) during an infection. Despite that, in general it is well accepted that higher functional avidity $CD8^+$ T cell responses are of higher efficacy both at clearing acute virus infections and at eliminating cancer cells, with several studies sustaining this notion. Therefore, when developing new immunotherapy and vaccination approaches against infections and tumours the strategy is generally to enhance the functional avidity of T cell responses to viral and tumour antigens. This include the use of potent adjuvants during immunization, adoptive immunotherapy of high-avidity T cell clones, and immunization with optimized peptides, that although altered in sequence result in augmented T cell responses to the native epitope.

By contrast, the relevance of high versus low functional avidity $CD8^+$ T cells in the control of chronic viral infections and established tumours is not so clear, with an increasing number of studies challenging the benefit of high avidity $CD8^+$ T cells. In the context of HIV infection it has been reported that high functional avidity T cell responses can led to viral escape, T cell clonal exhaustion, and senescence (Almeida et al., 2007; Conrad et al., 2011; Iglesias et al., 2011; Leslie et al., 2006; O'Connor et al., 2002). Consequently, in the case of chronic and persistent infections, in which pathogen clearance cannot be accomplished, if the goal is to achieve a long-lasting effective infection control it has been proposed that when designing a vaccine the generation of low functional avidity T cell responses may be more suitable in order to attain a pool of durable effector competent $CD8^+$ T cells (Vigano et al., 2012).

Overall, the benefit of high versus low functional avidity $CD8^+$ CTLs for anti-viral and anti-tumour immunity remains a challenging question. Further studies are needed to improve the knowledge in this field, which will be invaluable for immunotherapy and vaccine design.

1.1.5. CD8+ T cell response to EBV infection

Analysis of infectious mononucleosis (IM), a clinical syndrome that can arise during primary EBV infection, has allowed the evolution of the EBV-specific CD8+ T cell response to be tracked over time, providing an understanding of the immune response to this pathogen.

Infectious mononucleosis is characterized by a dramatic large expansion of activated CD8+ T cells in blood, which are EBV-specific, with lytic antigen dominant over latent antigen specificities (Figure 1.3). This dominance becomes less marked as the acute infection subsides and the highly expanded lytic antigen response contracts. These changes are consistent with the order of events in primary EBV infection. Early lytic replication activates responses first from NK cells and then from lytic antigen-specific CD8+ T cells; thereafter, the virus colonises the B cell pool through a latent growth-transforming infection that elicits the latent antigen-specific CD8+ T cell response. There are coincident CD4+ T cell responses to EBV in IM but these are much smaller and, as yet, poorly characterized.

Originally the unusually large CD8+ T cell expansion in IM was thought to resemble nonspecific bystander activation (McNally and Welsh, 2002) or a polyclonal response to a virus-encoded or virus-induced superantigen (Sutkowski et al., 2001). However, the expanded populations were found to be markedly oligoclonal in TCR usage (Annels et al., 2000; Callan et al., 1996; Maini et al., 2000) and to contain EBV epitope-specific reactivities, detectable by *ex vivo* cytotoxicity assays (Steven et al., 1996), staining with HLA class I tetramers loaded with EBV-epitopes (Callan et al., 1998b) and *ex vivo* Elispot assays of IFNγ release (Catalina et al., 2001; Hislop et al., 2002; Hoshino et al., 1999; Pudney et al., 2005). Indeed, EBV represents the most dramatic case of conserved TCR usage within an epitope-specific CD8+ T cell response in humans. Still, responses to EBV epitopes can range from highly focused (Miles et al., 2005b), through varying degrees of oligoclonality (Annels et al., 2000; Couedel et al., 1999; Miles et al., 2005a), to a highly diverse *repertoire* (Silins et al., 1997).

Lytic epitope-specific CD8+ T cells are the major expanded populations in IM and individually can account for 1%-50% of the total CD8+ T cell population (Hislop et al., 2005; Hislop and Sabbah, 2008). Lytic cycle antigens display a reproducible hierarchy of immunodominace on many HLA I backgrounds. The numerically strongest responses focus on epitopes derived from the two immediate early expressed proteins, BZLF1 and BRLF1, or from a small subset of early proteins, and much weaker responses are elicited against the virion structural proteins that are expressed late in the cycle (Abbott et al., 2013; Hislop et al., 2007b; Pudney et al., 2005; Rickinson et al., 2014). Interestingly, this hierarchy of immunodominance seems to be shaped by viral immune evasion mechanisms. It directly matches the falling efficiency with which the successively expressed antigens are presented on the lytically infected cell surface (Pudney et al., 2005), as the HLA class I pathway becomes gradually impaired and the battery of CD8 evasion proteins of EBV takes increasing hold (Ressing et al., 2008; Rowe and Zuo, 2010). It has been suggested

that this correlation between immunogenicity and epitope display on infected cells implies either that the $CD8^+$ T cell response is initially primed by direct contact with lytically infected B cells, rather than crossprimed by antigen represented in dendritic cells, or; at least, its subsequent expansion is directly driven by such contacts (Rickinson et al., 2014).

Responses to latent cycle proteins are slower and smaller, with individual specificities accounting for 0.1%-3% of the $CD8^+$ T cell population (Hislop et al., 2002; Hislop and Sabbah, 2008). The latent cycle proteins are coexpressed in virus-transformed cells yet, as $CD8^+$ CTL targets, also display a striking hierarchy of immunodominance. The strongest responses across several HLA I types are markedly focused on immunodominant epitopes derived from the largest latent cycle proteins, the transcriptional regulators EBNAs 3A, 3B, and 3C (Hislop and Sabbah, 2008; Hislop et al., 2007b; Rickinson et al., 2014). Accompanying subdominant responses often map to epitopes from LMP2, much less often from EBNA2, EBNA1, EBNA-LP, or LMP1. However, this is not always the case. Particular HLA alleles can induce strong responses against epitopes from one of the usually subdominant antigens, for example, the virus genome maintenance protein EBNA1 (Blake et al., 2000). Indeed, EBNA1 can be a relevant $CD8^+$ CTL target despite impairment of its HLA I-restricted presentation by the glycine-alanine repeat (GAr) domain of the protein. This reflects the fact that the impairment is only partial and does not eliminate EBNA1 epitope display on the infected cell surface (Mackay et al., 2009). Similarly, EBNA2, EBNA-LP and LMP2 epitope-specific $CD8^+$ T cell responses were found to be immunodominant in the context of certain HLA class I alleles (Chapman et al., 2001; Lee et al., 1997). By contrast, although occasional responses to LMP1 epitopes have been detected these are usually very weak and detectable in only a small minority of certain allele-positive individuals. Therefore, most latent cycle proteins can clearly provide immunodominant epitopes given the right HLA context. Thus, it has been suggested that the marked immunodominance of the EBNA3 proteins does not need necessarily to reflect preferential handling by the HLA class I processing pathway. These three proteins collectively represent more than 60% of the unique sequences in all EBV latent proteins and may just happen to contain the strongest epitopes for the HLA alleles thus far tested, particularly alleles common in Caucasian populations (Hislop et al., 2007b).

Cell surface phenotype analysis of the EBV-specific cells in IM indicates that these cells show characteristics of armed effector cells, contain perforin and are potently cytotoxic (Callan et al., 2000; Catalina et al., 2002; Dunne et al., 2002; Hislop et al., 2002). However, these cells die rapidly by apoptosis *in vitro* unless given antigen stimulation. Accordingly, these cells express low levels of the anti-apoptotic Bcl-2 and Bcl-x proteins and high levels of the pro-apoptotic Bax protein (Callan et al., 2000; Dunne et al., 2002; Soares et al., 2004).

With the resolution of acute symptoms the expanded $CD8^+$ T cell pool rapidly decreases in size with the contraction of the EBV-specific responses (Catalina et al., 2001; Hadinoto et al., 2008). The highly expanded lytic epitope responses contract drastically, showing dramatic reductions both in absolute numbers and as a percentage of the diminishing $CD8^+$ T cell pool. The smaller

latent epitope-specific CD8+ T cell responses also show a reduction in absolute numbers, but they contract less heavily and consequently their percentage representation in the circulating CD8+ T cell pool often rises in the months following IM. Interestingly, in addition to the differential levels of contraction of the expanded lytic- and latent-specific CD8+ T cell responses, there are also qualitative changes in the content of the EBV-specific CD8+ T cell response over time. Some specificities are consistently lost post-IM, even in cases where these responses are numerically dominant to other surviving responses (Hislop et al., 2002). The reason for the loss of such specificities from the immune *repertoire* remains unclear. Other reactivities, typically against subdominant latent epitopes, may not appear in detectable numbers in the blood until 3-4 months after primary infection but are stably maintained thereafter (Hislop et al., 2002; Woodberry et al., 2005a). As a result of such qualitative changes, the distribution of EBV-specific CD8+ T cell reactivities established in CD8+ T cell memory can be quite different from that seen in acute infection.

Most studies on the T cell response to EBV during IM have focused on the CD8+ response as sampled from the peripheral circulation. However, the blood picture is not always representative of the situation in lymphoid tissues. That is, the percentage of EBV-specific CD8+ T cells in IM blood overestimates that seen in tonsils during acute infection. Comparative studies of the CD8+ T cell response to EBV in both blood and tonsillar tissue revealed that despite substantial numbers of EBV-specific CD8+ T cells in the tonsils they are relatively inefficiently recruited to this site. As a consequence, the peripheral circulation can contain approximately a 3-fold higher proportion of EBV-lytic epitope specific cells as compared to the tonsil, while latent specificities are generally more evenly distributed between the two compartments (Hislop et al., 2005). The relatively poor recruitment to the site of virus replication was shown to correlate with a lack of expression of lymphoid homing receptors, namely CCR7 and CD62L, by EBV-specific cells in the blood; and may explain why there is prolonged high-level secretion of virus in the aftermath of acute IM disease. Nevertheless, with the resolution of infection, EBV-specific CD8+ T cells re-express lymphoid homing markers, particularly latent specificities (Hislop et al., 2002), and begin to be more efficiently recruited to the tonsil, explaining the faster control of growth transforming infection at this site (Hislop et al., 2005). Therefore, in long-term carriers the situation is reversed and EBV-specific memory populations, specifically latent antigen-specific CD8+ T cells, are enriched in tonsils (Figure 1.3).

By contrast to the wealth of knowledge relating the understanding of the CD8+ T cell response to EBV during IM, relatively little is known about the response mounted in cases of asymptomatic primary infection. Healthy virus carriers, most likely contracting EBV years ago, have a similar response pattern to what is seen in patients with IM, though the magnitude of responses is smaller (Hislop and Sabbah, 2008). Lytic proteins elicit stronger CD8+ T cell responses when compared to latent proteins, with responses of up to 3% of CD8+ T cells being directed at one epitope (Catalina et al., 2001; Khan et al., 2004; Ouyang et al., 2003; Yang et al., 2000). The immediate early proteins, BZLF1 and BRFF1, and a subset of early proteins account for the majority of

detectable lytic CD8+ T cell responses (Benninger-Doring et al., 1999; Bihl et al., 2006; Saulquin et al., 2000; Tan et al., 1999). Latent-specific CD8+ T cells are directed towards epitopes processed from the EBNA3 family of proteins, with weaker responses to LMP2 and EBNA1, yet responses to LMP1, EBNA2 and EBNA-LP are rarely if ever seen (Saulquin et al., 2000). Responses to the EBNA3 family can range up to 1% of CD8+ T cells being specific for one epitope, but typically these are 0.5% or less (Benninger-Doring et al., 1999; Catalina et al., 2001; Hislop et al., 2001).

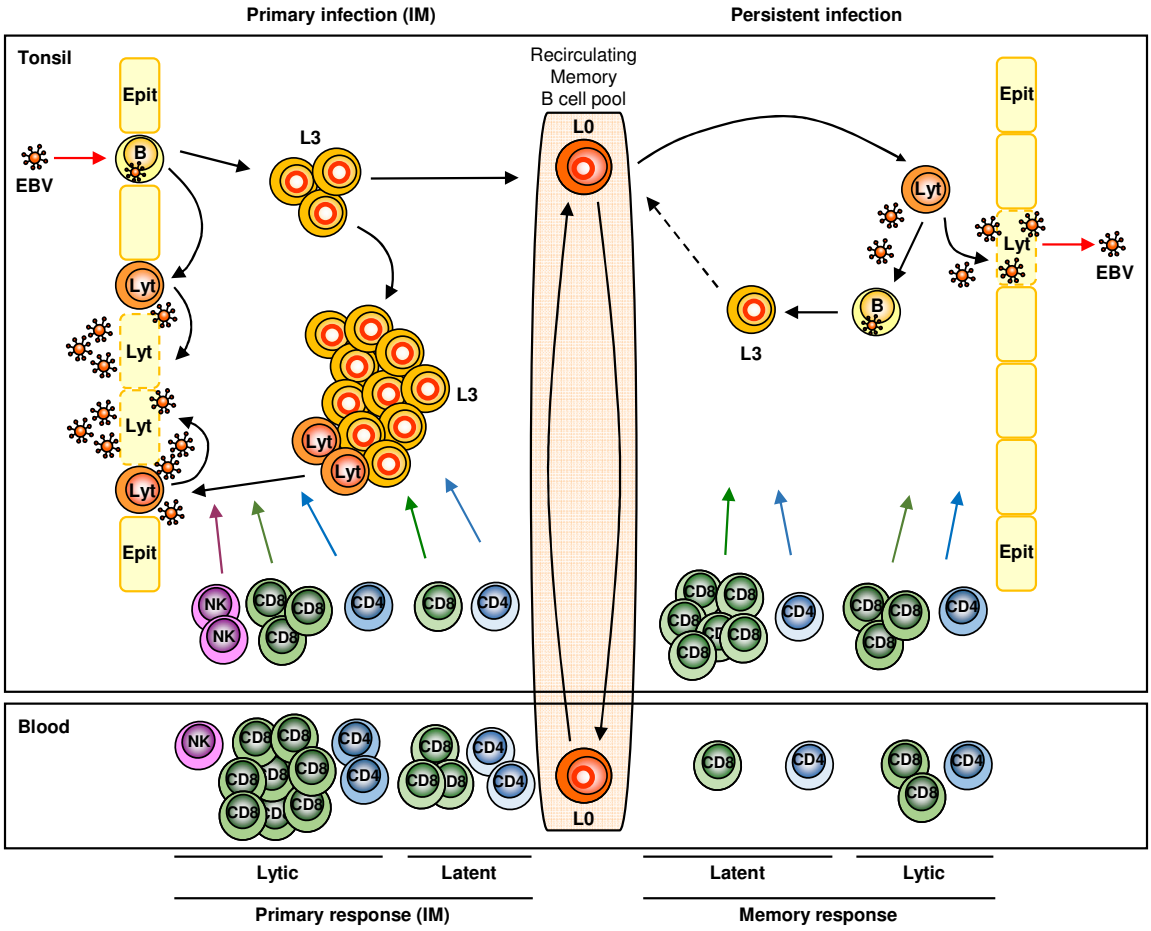

Figure 1.3. Cellular immune response to EBV infection. In the immunocompetent host, primary EBV infection, as seen in infectious mononucleosis (IM) patients, induces activation of natural killer (NK) cells, large expansions of virus-specific CD8+ T cells and smaller expansions of virus-specific CD4+ T cells in the blood. Lytic antigen-specific CD8+ T cells are the major expanded populations in IM; responses to latent cycle proteins are slower to develop and smaller in magnitude. By contrast, latent antigen-specific CD4+ T cells are at least as represented as lytic antigen reactivities. These initial T cell expansions are later culled and in the blood of long-term virus carriers the number of virus-specific memory T cells are generally low. The blood picture generally is not representative of the situation in lymphoid tissues. The percentage of EBV-specific T cells in blood overestimates that seen in tonsils during acute infection (IM), whereas the situation is reversed in long-term carriers where EBV-specific memory populations, particularly latent antigen-specific CD8+ T cells, are enriched in tonsils. Epit, epithelial cell; Lyt, litically infected cell; L3, latently infected B cell expressing the growth transcription programme or latency III; L0, memory B cell expressing the latency programme or latency 0 (adapted from Rickinson, et al., 2014).

Memory CD8+ T cell responses have been studied primarily in long-term asymptomatic EBV carriers, with no history of IM. These individuals shed low, often barely detectable, levels of infectious virus into the throat and have low numbers of latently infected cells in the blood (1-50 cells/million B cells). Individual epitope-specific responses account for 0.2%-2% (Benninger-Doring et al., 1999; Bihl et al., 2006; Saulquin et al., 2000) of the CD8+ T cell population in the case of lytic epitopes and 0.05%-1% for latent epitopes (Bihl et al., 2006). Most memory cells have a resting phenotype, they lack activation markers. However, at least some EBV-specific memory cells express perforin and are potently cytotoxic on peptide-loaded targets *ex vivo* (Catalina et al., 2002; Hislop et al., 2001). Although the proportion of EBV-specific CD8+ T cells appears to be quiet stable, over a longer time frame there is evidence for an age-related inflation of the EBV-specific response. Healthy individuals over age 60 can have individual EBV-specific responses constituting up to 14% of CD8+ T cells (Khan et al., 2004; Ouyang et al., 2003). Interestingly, this inflation of the EBV-specific CD8+ T cell response is not seen in older people carrying both EBV and cytomegalovirus (CMV); instead, dramatic expansions of CMV-specific CD8+ T cells are detected (Khan et al., 2004).

1.1.6. Viral evasion of CD8+ T cell immune response

Upon infecting a host, EBV is confronted by a coordinated and multi-faceted immune response. Therefore, it is not surprising that EBV has developed several strategies to evade the host immune surveillance. Active immune evasion mechanisms reduce the immunogenicity of EBV lytically and latently infected cells and are therefore of major importance for the virus to replicate and to establish a lifelong persistent infection in the immune competent host.

Prompted by findings that antigen presentation to CD8+ T cells falls dramatically during lytic cycle several studies have identified three EBV early lytic proteins with immune evasive effects that interfere with MHC class I antigen presentation: BNLF2a, BGLF5 and BILF1 (Ressing et al., 2008; Rowe and Zuo, 2010). BNLF2a is a small membrane-associated protein, composed of 60 amino acid residues, that localizes to the endoplasmic reticulum, physically associates with the transporter associated with antigen processing (TAP) complex and acts as a powerful inhibitor of it (Hislop et al., 2007a; Horst et al., 2009). BLNF2a is composed of two specialized domains, its hydrophobic C-terminal tail anchor ensures membrane integration and retention in the endoplasmic reticulum, whereas its cytosolic N-terminus blocks antigen translocation by TAP (Horst et al., 2011; Wycisk et al., 2011). BNLF2a inhibits both peptide and ATP binding to TAP, thus efficiently blocking peptide delivery to nascent MHC molecules. This way BNLF2a effectively impairs MHC class I-restricted antigen presentation of immediate early and early proteins in lytically infected B cells, allowing escape from CTL recognition (Croft et al., 2009). Additionally, a recent study indicates that BNLF2a can also reduce antigen presentation and recognition of newly infected B cells by EBV-specific CD8+ T cells (Jochum et al., 2012). Thus, BLNF2a seems to be

important to significantly diminish the immunogenicity of EBV-infected cells also during the initial, pre-latent phase of infection and this way may improve the establishment of EBV latency *in vivo*.

TAP transport is also hindered by BCRF1, the viral chemokine homologue of interleukin (IL)-10 (vIL-10), which reduces expression of the TAP1 subunit (Zeidler et al., 1997). Downregulation of TAP1 by vIL-10 hampers the transport of peptide antigens into the endoplasmic reticulum, their loading onto empty MHC class I molecules, and the subsequent translocation to the cell surface. As a consequence, vIL-10 causes a general reduction of surface MHC class I molecules on B lymphocytes that might also affect the recognition of EBV-infected cells by $CD8^+$ CTLs.

BGLF5 is a dual-function protein originally identified as a DNase enzyme (Baylis et al., 1989) essential for efficient infectious virus production. It is required for optimal viral DNA synthesis, genome encapsidation, and nuclear egress of the virus (Feederle et al., 2009). However, a second function of this protein was subsequently identified, a host protein-synthesis shutoff function which operates at the level of mRNA transcripts (Rowe et al., 2007). Thus, BGLF5 decreases expression of MHC class I molecules at the cell surface and reduces antigen presentation to $CD8^+$ CTLs by blocking the synthesis of new MHC class I molecules (Zuo et al., 2008). Resolution of BGLF5 crystal structure revealed an intrinsic RNase activity in the presence of Mn^{++} ions, which degraded unstructured mRNA (Buisson et al., 2009), indicating that the shutoff phenotype results from mRNA degradation (Horst et al., 2012).

BILF1 is a seven transmembrane spanning protein with structural and functional characteristics of a constitutively signalling vGPCR/chemokine receptor (Beisser et al., 2005; Paulsen et al., 2005). Through its cytoplasmic C-terminal tail BILF1 targets a broad range of MHC class I molecules decreasing cell surface levels of MHC I (Griffin et al., 2013; Zuo et al., 2009). This is achieved by BILF-1 mediated acceleration of endocytosis and subsequent lysosomal degradation of MHC class I molecules from the cell surface or by diversion of newly synthesized MHC class I molecules from the normal exocytic pathway that allows proteins to travel from the endoplasmic reticulum to the cell surface (Zuo et al., 2011).

Overall, the concerted actions of these EBV lytic proteins, which all target the MHC class I antigen-processing and presentation pathway, underscore the importance of the need for EBV to be able to evade $CD8^+$ T cell surveillance during the lytic replication cycle, at a time when a large number of potential viral targets are expressed. This strategy provides EBV a window for generation of viral progeny and is thought to be vital for EBV to colonize the host and upon reactivation for EBV to spread to new hosts.

Subsequently, the central strategy is to exist in a latent state, characterized by limited viral gene expression without virion production, enabling the virus to hide from the host immune response. Moreover, among the latent proteins EBNA1, which is expressed both in lytic and latently infected cells, is also able to interfere with antigen presentation although the mode of action is conceptually

distinct from BNLF2a, vIL-10, BGLF5 and BILF1, in that it only affects the processing of antigens from the EBNA1 protein itself. This unusual mechanism is the result of a large repetitive region in the *EBNA1* gene encoding a glycine-alanine repeat (GAr) domain comprising about one-third of the protein that impairs MHC class I-restricted presentation of *cis*-linked epitopes (Levitskaya et al., 1995). This is achieved by EBNA1 decelerating its own synthesis, either transcriptionally *via* interference of the nascent GAr polypeptide with ribosome assembly on the messenger RNA (Apcher et al., 2010; Apcher et al., 2009), or translationally *via* sub-optimal codon usage within the GAr sequence (Tellam et al., 2008) or through RNA secondary structural elements (Tellam et al., 2012). Independently of the mechanism, the GAr effect is only partial, reducing the presentation of native EBNA1 epitopes by 30%, similar to its reduction in rate of synthesis (Mackay et al., 2009). The latent membrane protein LMP1 paradoxically upregulates MHC class I processing, enhancing trans-presentation of $CD8^+$ T cell epitopes, yet itself is a poor $CD8^+$ T cell target, due to its ability to self-aggregate (Smith et al., 2009). The ability of LMP1 to drive both its own synthesis and degradation makes LMP1 levels fluctuate in individual EBV-transformed B lymphoblastoid cell lines (LCLs) (Lee and Sugden, 2008). Parallel fluctuations in antigen processing efficiency imply that, at any one time, only a fraction of cells in a LCL culture are visible to $CD8^+$ T cells (Brooks et al., 2009).

EBV has evolved several mechanisms to modulate the host $CD8^+$ T cell response that are essential for achieving a lifelong virus-host balance while minimizing the viral pathogenicity. Nevertheless, this multiple immune evasion mechanisms should be considered as strategies to dampen the efficiency of immune $CD8^+$ T cell responses, rather than to completely evade them. Knowledge of EBV immune evasion strategies is crucial to provide important guidance to improve T cell therapies and the immunogenicity of viral vaccines.

1.1.7. T cell therapy in the treatment of EBV-driven post-transplant lymphoproliferative disease

EBV-associated post-transplant lymphoproliferative disease (PTLD) is a life-threatening condition that develops after haematopoietic stem cell or solid organ transplantation, when the T cell immune response to EBV is ablated or severely compromised by immunosupression (Gottschalk et al., 2005). These lymphoproliferative diseases are lymphomas, resulting from uncontrolled proliferation of EBV infected B cells, that usually express all latent EBV viral proteins, and are therefore amenable to T cell-based immune therapies, such as donor lymphocyte infusions and the adoptive transfer of EBV-specific CTLs (Bollard et al., 2012).

PTLD developing after haematopoietic stem cell transplantation usually results from donor B cells and appears within the first 6-12 months post-transplantation, when profound deficiencies of EBV-specific CTLs are seen (Meij et al., 2003). Early attempts to threat PTLD using unselected donor

lymphocytes from the original EBV-immune stem cell donor were marred by collateral graft-versus-host disease (GVHD), due to the presence of alloreactive T cells in the lymphocyte infusions (Heslop et al., 1994; O'Reilly et al., 1997; Papadopoulos et al., 1994). Therefore, Heslop, Rooney, and colleagues adapted existing laboratory protocols of *in vitro* generation of EBV-specific CTL preparations for the clinic and by 1995 completed their first small trial demonstrating the effectiveness against PTLD (Rooney et al., 1995). The selective expansion of donor-derived T cell lines directed against EBV antigens uses EBV-transformed B cells (LCLs) as antigen presenting cells. LCLs are generated by infecting donor peripheral blood B cells with a laboratory strain of EBV and similar to PTLD, express type III latency. Thus, the generated EBV-specific CTLs usually contain both $CD8^+$ and $CD4^+$ T cells that recognize multiple latent and early lytic cycle viral antigens and, when infused into patients, can reconstitute an immune response to EBV and eliminate PTLD without inducing GVHD (Doubrovina et al., 2012; Heslop et al., 2010). Indeed, adoptive transfer of donor-derived LCL-stimulated EBV-specific CTLs has proved a safe and effective prophylactic approach and a remarkably successful therapy for classical PTLD after haematopoietic stem cell transplantation.

Failure to respond to EBV-specific CTL therapy has occurred when T cells of restricted specificity were infused, recipients lack HLA antigens through which EBV activity in the T cell line is restricted, or tumours express variants of the EBV antigens used to stimulate CTLs (Doubrovina et al., 2012; Gottschalk et al., 2001).

In general, generation of EBV-specific CTLs takes approximately 8-12 weeks. Half of the time is required for the generation of the antigen presenting cells (EBV-LCLs) and the other half for the generation and expansion of the EBV-specific CTLs in order to obtain the cell numbers that are required for clinical use and product testing (Smith et al., 1995). Consequently, the relatively long production time has limited the widespread use of EBV-specific CTLs to prevent or treat EBV-PTLD, as they cannot be generated in response to a patient developing PTLD. However, methodological improvements have now shortened the time required for the production of virus-specific CTLs. Three methods have already been used clinically. Firstly, multimer selection allows the selection of T cells directed against specific viral peptides in the context of a specific HLA class I molecule (Uhlin et al., 2010). Secondly, isolation of IFNγ secreting T cells is based on the selection of T cells that secret IFNγ in response to stimulation by viral antigens (Icheva et al., 2013; Moosmann et al., 2010). Lastly, faster *ex vivo* CTL culture methods use peptides or plasmid-derived viral antigens expressed in dendritic cells to stimulate T cells in the presence of cytokines (Gerdemann et al., 2009; Gerdemann et al., 2013; Gerdemann et al., 2012; Hao et al., 2014).

Establishing a bank of characterized HLA-typed EBV-specific T cell lines could make EBV CTLs rapidly available to a large number of patients. This third party approach was tested in the clinic in patients undergoing haemopoietic stem cell or solid organ transplantation who received closely HLA-matched EBV-specific CTLs generated from unrelated third-party blood donors (Barker et

al., 2010; Gallot et al., 2014; Haque et al., 2010; Haque et al., 2007; Leen et al., 2013). The best results were observed in patients receiving donor T cells which were best HLA matched with the recipient. In some instances multiple infusions were required to control PTLD (Doubrovina et al., 2012). Therefore, clinical protocols should allow for multiple infusions and for the substitution of donor CTL lines if patients fail to respond.

In recipients of solid organ transplant, PTLD most commonly arises from recipient B cells and the donor is often not accessible. Moreover, donor and recipient are rarely HLA-matched. Therefore, autologous EBV-specific CTLs have been used in this setting (Khanna et al., 1999; Savoldo et al., 2006). However, the need for ongoing immunosuppressive therapy has limited the persistence of infused EBV CTLs. Hence, CTLs have been genetically engineered to render them resistance to immunosuppressive drugs, namely to calcineurin inhibitors (cyclosporine or tacromilus) and rapamycin, in preclinical studies (Brewin et al., 2009; De Angelis et al., 2009; Huye et al., 2011; Ricciardelli et al., 2013). This strategy is also considered as an advantage for patients who after haemopoeitic stem cell transplant require immune suppression to avoid GVHD.

An important further development involving genetically manipulation of EBV-specific CTLs to render them therapeutically more effective *in vivo* aims at maximizing the chances of adoptively transferred cells to expand in their new host (Hoyos et al., 2010; Vera et al., 2009), to traffic to the tumour site and to resist the immunosuppressive environment that may exist there, overcoming tumour evasion mechanisms (Di Stasi et al., 2009; Foster et al., 2008).

LCL-stimulated effectors tend to be dominated by $CD8^+$ T cells against the EBNA 3A, 3B and 3C latent proteins. Therefore, using such effectors against other EBV-positive tumours is problematic since the tumours typically do not express these immunodominant targets (Hislop et al., 2007b). Nevertheless, this approach has revealed some success in the context of NPC (Louis et al., 2010), and in patients with EBNA3-negative HL-like or BL-like tumours (Haque et al., 2007; McAulay et al., 2009). Interestingly, the most successful EBV-CTL preparations were those with polyclonal TCR usage, implying requirement for a broadly target T cell response, and with significant $CD4^+$ T cell numbers. Although this may reflect the importance of $CD4^+$ T cell help in the adoptively transferred preparations, $CD4^+$ T cells may also be acting as effector cytotoxic cells by themselves. This is consistent with the finding that cytotoxic $CD4^+$ T cells, specific either for EBV lytic or latent proteins, are present in LCL-stimulated preparations and are capable of LCL recognition (Adhikary et al., 2007; Merlo et al., 2010; Taylor et al., 2006).

Efforts to optimise CTL therapies for EBV-positive tumours with limited antigen expression, such as NPC and HL, have focused attention on EBNA1 and the LMPs as target antigens (Bollard et al., 2014; Lutzky et al., 2014). Of these LMP2 is the richest source of $CD8^+$ epitopes and is expressed in EBV-positive HL and NPC. Various methods have been developed to produce CTL populations enriched in appropriate specificities. These include *ex vivo* selection with EBV-specific pentamers (Uhlin et al., 2010), *in vitro* stimulation with epitope peptides (Jones et al.,

2010; Moosmann et al., 2010), with the autologous LCL over-expressing the antigen of choice (Bollard et al., 2007), with an adenovirus encoding EBNA1/LMP1/LMP2 epitope strings (Duraiswamy et al., 2004) or a scrambled EBNA1, LMP1, LMP2 protein sequence (Lutzky et al., 2010). Moreover, there is an increasing argument that T cell based immunotherapy should be considered as a combination therapy with chemo/radiotherapy, particularly in advanced tumour disease to improve survival (Chia et al., 2014; Smith et al., 2012).

Overall, the success of adoptive T cell therapy for EBV-driven post-transplant lymphoproliferative disease is stimulating efforts to target other EBV-associated tumours by immunotherapeutic means, and has reawakened interest in the ultimate intervention strategy, a prophylactic EBV vaccine.

1.1.8. EBV vaccine development

The global burden of disease linked to EBV infection, namely IM, the various EBV-associated malignancies and possibly also autoimmune diseases, is driving renewed interest in the development of a prophylactic vaccine to reduce the EBV-associated disease load (Balfour, 2014; Cohen et al., 2011; Cohen et al., 2013). EBV vaccine development has been hampered by the lack of an animal model other than subhuman primates, selection of an appropriate dose and adjuvant, and debate about what an EBV vaccine could or should actually achieve.

The first EBV vaccine proposal was made by Epstein in 1976 (Epstein, 1976), who encouraged the use of EBV-determined membrane antigen as immunogen and assessment of vaccine efficacy in humans by protection of adolescents from IM. Epstein also highlighted the potential of a vaccine to prevent EBV-associated human cancers. Nevertheless, since then only three prophylactic EBV vaccines have been evaluated in controlled clinical trials. Two vaccines were constructed to induce neutralising antibody responses and one was designed to control the expansion of EBV infected cells by inducing $CD8^+$ T cell immunity to EBNAs.

One trial was conducted using vaccinia virus constructs expressing the EBV membrane glycoprotein gp350/220 (Gu et al., 1995). EBV causes infection predominantly by binding its major envelope glycoprotein gp350/220 to the CD21 receptor on the surface of B lymphocytes (Nemerow et al., 1987; Tanner et al., 1987) and antibodies against gp350/220 are able to neutralize EBV infectivity (Thorley-Lawson and Geilinger, 1980) and are the major component of neutralizing activity of human sera (Sashihara et al., 2009; Thorley-Lawson and Poodry, 1982). The vaccine was immunogenic and the authors concluded to have shown for the first time that protection and/or delay of EBV infection is possible in humans. However, no further work has been reported for this vaccine, possibly because of potential adverse events associated with the presence of live vaccinia (Maurer et al., 2003). Other trials have been conducted in healthy young

adults receiving recombinant gp350 protein with adjuvants (Moutschen et al., 2007; Sokal et al., 2007). In these cases the vaccine did not prevent primary infection but had a protective effect against IM. A small clinical trial of recombinant gp350 vaccine with an adjuvant was also conducted in paediatric renal transplant candidates (Rees et al., 2009). The vaccine was poorly immunogenic, probably due to low dose and weak adjuvant, and the trial could not assess protection from PTLD. However, the vaccine was safe and the trial demonstrated that immunization of children awaiting for transplantation is feasible. The potential of a gp350-based vaccine is further supported by studies conducted in rhesus macaques, in which a soluble gp350 vaccine afforded protection from infection after oral challenge and reduced blood levels of viral DNA for up to two years after infection with the challenge virus (Sashihara et al., 2011). Infection of rhesus macaques with rhesus lymphocryptovirus has been shown to reproduce many of the features of human EBV infection including long periods of viral shedding, viral latency, and the propensity to develop EBV associated malignancies if immunosupressed (Moghaddam et al., 1997). Finally, a different vaccination strategy is to control expansion of EBV-infected B cells by generating $CD8^+$ T cell responses to EBNAs (Khanna et al., 1992). Due to the potential role of EBNAs in B cell transformation, which precludes their use in whole protein-based vaccines, a single EBNA3A epitope vaccine restricted by HLA B8 was developed and tested in a trial (Elliott et al., 2008). This strategy was effective at generating an epitope-specific $CD8^+$ T cell response and did not predispose subjects to disease after primary EBV infection. Therefore, the trial was a “proof-of-principle”, which showed the safety and immunogenicity of EBV single-epitope vaccines aimed at inducing $CD8^+$ T cell immunity. While not practical for general use, because of HLA restriction, epitope vaccines might be useful for patients with PTLD, whose HLA type is known.

Therapeutic vaccines to treat EBV-associated cancers, although in their early stages, are currently also in development. The goal is to enhance immune recognition of tumour cells by targeting their expression of viral antigens. A vaccinia Ankara recombinant vector expressing the tumour-associated latent antigens EBNA1 and LMP2 was recently delivered to patients with NPC (Hui et al., 2013). Safety, immunogenicity and a dose-response effect were demonstrated, thus phase 2 studies are planned using the highest dosage regimen.

For prophylactic vaccines, ideal targets for efficacy trials in order of probable success have been proposed to be IM, PTLD and endemic BL (Balfour, 2007). A vaccine containing gp350 is a logical candidate, since neutralizing antibodies are presumably the best humoral defence against cell entry by EBV. The challenge now is to incorporate appropriate CTL target antigens into such vaccine constructs, thereby rendering the T cell response able to recognise and destroy *de novo* infected B cells upon which establishment of latency depends. However, the optimum vaccine formulation, including both the combination of EBV antigens and adjuvant, still needs to be determined (Cohen et al., 2013). Furthermore, a gp350-based vaccine may not be appropriate for all the suggested indications and more than one vaccine may need to be developed. For example, vaccines that induce T cell responses to EBV latent antigens expressed in tumour cells, especially EBNAs and LMPs, may be required to prevent or treat EBV-associated cancers.

One of the barriers to development of an effective vaccine has been the total reliance upon primates as animal models of EBV infection. The ability to reconstitute immunodeficient mouse strains with a functional human immune system (Leung et al., 2013) is now providing new models which not only allow EBV colonisation of the B cell system (Cocco et al., 2008) but also support the induction of EBV-specific $CD8^+$ and $CD4^+$ T cell responses (Shultz et al., 2010; Strowig et al., 2009). However, these humanized mouse models might not have all the features of a normal immune response; for example, EBV interacts with several cellular proteins to evade the immune response and it is unclear whether these proteins would have the same properties in a humanized mouse. In addition to the limitations in animal models to study protection against EBV infection and disease, other obstacles to development of an EBV vaccine include the lack of knowledge of immune correlates for protection against EBV infection and disease; the difficulty of performing clinical trials to prevent EBV associated malignancies in the absence of good surrogate markers for tumour development, and the long period of time between primary EBV infection and development of many EBV tumours.

Hence, one of the major EBV challenges to virologists and immunologists, to design a prophylactic vaccine that, even if cannot prevent primary infection, may limit virus load and protect against EBV-associated diseases, remains as potent as ever.

1.2. Kaposi sarcoma-associated herpesvirus

Kaposi sarcoma-associated herpesvirus, or KSHV, is the most recently identified human herpesvirus. The discovery of KSHV dates to 1994 and was made by Chang *et al.*, who found unique herpesvirus-like sequences present in most Kaposi sarcoma (KS) lesions from AIDS patients (Chang et al., 1994). KS tumours are comprised of KSHV-infected cells of endothelial origin. Subsequently, KSHV was found in other human malignancies, namely, two types of B cell tumours, primary effusion lymphoma (PEL) (Cesarman et al., 1995a) and multicentric Castleman disease (MCD) (Soulier et al., 1995), that frequently develop in AIDS patients, and in rare instances in diffuse large B cell lymphoma. Furthermore, novel epidemiologic evidence suggests that KSHV increases the risk of marginal zone lymphoma (Benavente et al., 2011). Primary KSHV infection is usually asymptomatic in immunocompetent individuals and like infection with EBV results in lifelong latency. Reports of KSHV-associated mononucleosis or rash are few and far between. Recently, however, a new clinical entity has been proposed as being associated with acute KSHV replication, KSHV-inflammatory cytokine syndrome (KICS) (Polizzotto et al., 2012; Tamburro et al., 2012; Uldrick et al., 2010).

Unlike EBV, KSHV is not ubiquitous in the human population. KSHV prevalence is low (<10%) in most areas of Europe, Asia and United States, moderate in some Mediterranean countries (4-35%) and high in sub-Saharan Africa (30-60%) (Uldrick and Whitby, 2011). The incidences of

KSHV-associated neoplastic diseases mirror the geographic KSHV seroprevalence, and certain groups of patients are at higher risk (Edelman, 2005). These include immunocompromised patients, such as HIV infected individuals and transplant recipients. The exact mechanism of transmission remains to be elucidated. However, saliva seems to be the major source of transmission because it contains virus more frequently and at a higher level than other body fluids (Johnston et al., 2009; Pauk et al., 2000). A much less frequent route of transmission is through organ transplants (Barozzi et al., 2003; Regamey et al., 1998) and via blood transfusion (Hladik et al., 2006), and sexual transmission remains controversial.

Similar to EBV, infection with KSHV has two distinct phases, lytic replication and latency, both of each contribute to pathogenesis. The latent programme allows the virus to persist in a relatively stable and immunological silent mode, whereas the lytic programme enables the virirons to be shed and transmitted to new hosts (Coscoy, 2007). In KSHV-associated malignancies, most tumour cells are latently infected, yet expression of viral lytic genes is detected in a small percentage of cells (Wen and Damania, 2010). This has led to the suggestion that lytic replication may enhance the growth of latently infected cells in a paracrine fashion, especially by expressing viral lytic proteins that are homologues of cellular cytokines and chemokines (Mesri et al., 2010; Nicholas, 2005). In addition, lytic replication can contribute to tumorigenesis indirectly by producing infectious virions to *de novo* infect naïve cells, thus replenishing the pool of latently infected cells, subsequently giving rise to transformed cells (Ganem, 2010). Individual KSHV genes and miRNAs have been shown to promote cell proliferation in multiple experimental systems and also to modulate autophagy and oncogene-induce senescence (Giffin and Damania, 2014; Lee et al., 2009a; Lei et al., 2010; Leidal et al., 2012). Recent evidence also indicates that during latency KSHV is able to modulate different metabolic pathways, both in B cells and endothelial cells, to its own profit (Bhatt et al., 2012; Delgado et al., 2010; Delgado et al., 2012).

1.2.1. KSHV latency

In contrast to EBV, attempts to generate human B cell lines immortalized *in vitro* by KSHV have failed and therefore the study of KSHV latency has largely focused on characterizing viral gene expression and function in B cell lines derived from PEL tumours and in epithelial cells.

During latency, as with EBV, KSHV expresses only a limited set of viral genes and miRNAs, thereby minimizing its exposure to the host immune system. KSHV latency locus includes the viral genes of the latency-associated nuclear antigen (*LANA*), the viral cyclin D homolog (*v-cyclin*), the viral Fas-associated death domain (FADD) interleukin-1B-converting enzyme (FLICE) inhibitory protein (*vFLIP*), *kaposin A*, *B* and *C*, and the viral miRNAs (Dittmer et al., 1998; Sin and Dittmer, 2013). *LANA*, *v-cyclin* and *v-FLIP* genes are encoded in a tricistronic transcript from a single promoter, also referred to as the KSHV oncogenic cluster, and are consistently expressed

in latency-associated diseases and B cell lines (Table 1.2) (Dittmer et al., 1998; Sarid et al., 1998). The latently expressed viral products ensure maintenance and faithful segregation of the viral genome during host cell division (LANA), continued survival of latently infected cells, and are also believed to be necessary for malignant transformation (Giffin and Damania, 2014). LANA can additionally interfere with several pathways that regulate cell proliferation and apoptosis, the cellular processes that are targeted by v-cyclin and v-FLIP as well (Ganem, 2010; Giffin and Damania, 2014; Mesri et al., 2010). Other viral genes expressed during latency include *viral IRF-3* (*vIRF-3*), *viral IL-6* (*vIL-6*), *K1* and *K15* (Table 1.2) (Wen and Damania, 2010). K1 is a transmembrane glycoprotein, encoded at the left end of the viral genome (Lagunoff and Ganem, 1997), that contains an immunoreceptor tyrosine-based activation motif (ITAM) (Lee et al., 1998a). K1 appears to function as a constitutively signaling BCR independent of ligand binding (Lee et al., 1998b) and thus may play a role similar to that of the EBV LMP2A. K1 expression has been detected in KS, PEL and MCD (Wen and Damania, 2010). K1 contains the two most variable regions across the entire viral genome, showing substantial diversity between viral isolates, and is used to sub-classify KSHV into A, B, C and D strains (Hayward, 1999; McGeoch, 2001; Zong et al., 1999).

KSHV also encodes a cluster of 12 miRNAs, all nestled within the latency-associated locus of the KSHV genome, which is highly active in gene expression in all forms of KSHV-associated malignancies (Gottwein et al., 2006; Samols et al., 2007). From the validated and the potential targets revealed so far, KSHV miRNAs appear to regulate the host immune response, cell survival and proliferation, apoptosis, as well as the control of lytic replication and maintenance of latency (Boss et al., 2009; Gottwein et al., 2011; Lei et al., 2010; Zhu et al., 2013).

Table 1.2. KSHV latent gene expression in different malignancies (adapted from Wen, K.W. & Damania, B., 2010 and Taylor, G.S. & Blackbourn D.J., 2011).

Malignancy	Viral latent gene expression
KS[a]	LANA, v-cyclin, v-FLIP, kaposin, vIL-6[b], K1[b]
PEL[a]	LANA, v-cyclin, v-FLIP, kaposin, vIRF-3, vIL-6[b], K1[b]
MCD[a]	LANA, v-cyclin, v-FLIP, vIRF-3[b], vIL-6[b], K1

[a]KSHV lytic gene expression can also be detected in these tumours.

[b]Represents a viral gene whose protein levels can be detected in only a small percentage of tumours.

In vivo, KSHV has been detected in endothelial cells, epithelial cells, B cells, and monocytes (Ambroziak et al., 1995; Blasig et al., 1997; Dupin et al., 1999; Pauk et al., 2000). However, the main target of KSHV latent infection is the B cell. KSHV infection and establishment of long-term latency seems to be restricted to a subset of only lambda (λ) expressing B cells (Chadburn et al., 2008; Hassman et al., 2011). KSHV infection drives primary B cells to proliferate (Hassman et al.,

2011) and individual KSHV latent genes, specifically *LANA*, *v-FLIP* and *vIL-6*, induce B cell proliferative phenotypes in transgenic mice (Ballon et al., 2011; Sin et al., 2010; Suthaus et al., 2012). Individual KSHV miRNAs also have transforming properties in B cell models *in vivo*, particularly the KSHV mir-155 ortholog (Boss et al., 2011). B cell specific expression of multiple viral latent genes, including *LANA*, *v-FLIP*, *v-cyclin*, all viral miRNAs, and *kaposin*, leads to sustained hyperplasia, lymphoma, and hyper-responsiveness to antigen stimulation in transgenic mice (Sin and Dittmer, 2013).

The mechanisms by which KSHV establishes and maintains latency are not as well studied as for EBV. The overall strategy, however, is believed to be the same – subversion of normal B cell developmental pathways to induce cell proliferation and achieve long-term persistence. A putative model of KSHV B cell pathogenesis has been proposed (Dittmer and Damania, 2013) that would start with the primary infection event, driving the infected cell into an activated state. In non-permissive cell subtypes, such as IgM+ kappa B cells, or T cells, the virus is rapidly lost or the cell dies. By contrast, in cells permissive for the establishment of latency, the virus persists, conferring a survival advantage to the infected cell. The molecular basis and the exact complement of viral genes that confer this advantage are not well defined. This model would be analogous to the establishment of EBV latency, which starts with expression of a set of genes that afterwards contracts to latency type I or even type 0.

1.2.2. KSHV-associated malignancies

Infection with KSHV increases the risk for development of several human malignancies, namely, Kaposi sarcoma (KS), primary effusion lymphoma (PEL) and multicentric Castleman disease (MCD). KS is grouped in four epidemiological forms: classic KS, which is a rare disease observed in elderly Mediterranean men; endemic KS, a frequent disease of children in sub-Saharan Africa; AIDS-associated KS, one of the most frequent malignancies developed in AIDS patients; and iatrogenic KS, which develops in immunossupressed individuals after organ transplant (Mesri et al., 2010). In all of these clinical categories of KS, the tumour represents aberrant angiogenesis or lymphangiogenesis through proliferation of KSHV infected elongated, spindle-shaped endothelial cells that line the vascular structures (Ganem, 2010; Mesri et al., 2010). KSHV infected endothelial cells express KSHV latent genes and all viral miRNAs (Dittmer, 2011; O'Hara et al., 2009). There is little evidence for long-term KSHV infected endothelial cells outside KS lesions, or before disease manifestation, and in infected endothelial lineage culture systems KSHV is rapidly lost unless latently infected cells undergo additional transforming events (Dittmer and Damania, 2013).

PEL is a diffuse large B cell lymphoma, which lacks expression of B cell-associated antigens, but instead expresses plasma cell markers, has immunoglobulin gene rearrangements and

hypermutation of the immunoglobulin genes, indicating a post-GC origin (Cesarman, 2011; Cesarman, 2014). It represents the extreme end of KSHV pathogenesis: a fully transformed cell, which maintains KSHV in high copy numbers, has acquired additional mutations, and which establishes tumours in immune deficient mice (Dittmer and Damania, 2013). PEL cells can be KSHV single positive or can be co-infected with EBV (Nador et al., 1996). These tumours have proven invaluable for laboratory-based studies of KSHV owing to the relatively consistent growth of PEL cell lines in culture. PEL-derived cell lines have provided both a source of KSHV genomic material for *in vitro* studies (Cesarman et al., 1995b) and an essential *in vitro* culture system for molecular studies in KSHV pathogenesis (Renne et al., 1996).

Unlike PEL, MCD cells do not show hypermutation of the immunoglobulin G locus, which could argue that these cells did not participate in the canonical GC reaction. MCD is an uncommon disseminated lymphadenopathy characterized by an abnormal proliferation of IgM λ-restricted plasmablasts within the mantle zone of B cell follicles (Cesarman, 2011; Cesarman, 2014). Interestingly, KSHV infection in MCD is quite lytic as compared to KS and PEL (Chadburn et al., 2008; Polizzotto et al., 2012).

1.2.3. CD8$^+$ T cell control of KSHV infection

Most KSHV infected healthy individuals are able to control persistent KSHV infection without developing disease. It is thought that adaptive T cell and neutralizing antibody responses are mounted against KSHV and are effective at controlling replication and concomitant pathogenesis of the persistent virus (Taylor and Blackbourn, 2011). Nevertheless, KSHV immune responses neither prevent *de novo* infection nor eliminate persistent infection.

Similar to what is seen with EBV, KSHV-associated disease originates when the host-pathogen equilibrium is disrupted. Specifically, when T cell immune control declines, for example, through AIDS or treatment with immunosuppressive drugs, both the prevalence of KSHV infection and the incidence of KS in KSHV carriers dramatically increase (Boshoff, 2002; Hislop and Sabbah, 2008; Robey et al., 2010). Moreover, a dramatic and spontaneous improvement in KS is frequently seen when immunity is restored, for example, through antiretroviral therapy or the cessation of iatrogenic drugs (Bower et al., 2009; Franceschi et al., 2008; Nagy et al., 2000). This indicates that successful T cell immunity targeted against KSHV plays a key role in containing KSHV infection, enabling the virus to establish controlled lifelong infection and to coexist with its host.

Much less is known about the cellular immune response to KSHV when compared to EBV. CD8$^+$ T cell responses to KSHV have been studied mostly in KS patients and asymptomatic carriers of KSHV. Few HLA-restricted KSHV-specific T cell epitopes have been identified, which are almost exclusively CD8$^+$ epitopes (Hislop and Sabbah, 2008; Robey et al., 2010), and these were found

to elicit weak CD8+ T cell responses when compared to EBV (Bihl et al., 2007). KSHV-specific CD8+ T cell responses have been detected against both lytic and latent proteins (Hislop and Sabbah, 2008; Robey et al., 2010). Some of these responses have been demonstrated to be functionally cytotoxic *in vitro*. In contrast to the lytic CD8+ T cell response to EBV, which is heavily skewed towards EBV immediate-early stage lytic genes, lytic CD8+ T cell responses against KSHV preferentially target both early and late lytic proteins (Robey et al., 2009). A study comparing the functionality of KSHV-specific CD8+ T cells directed against lytic or latent antigens, in HIV-positive asymptomatic carriers of KSHV, found that multifunctional KSHV-specific CD8+ T cells elicited to latent antigens are more frequently detected in CD8+ T cell populations than those targeted to lytic antigens (Bihl et al., 2007). Latent CD8+ CTL target epitopes have been identified in 4 latent proteins: LANA, Kaposin, K15 and the highly variable K1 (Brander et al., 2001; Guihot et al., 2006; Levitskaya et al., 1995; Robey et al., 2010; Stebbing et al., 2003). CD8+ T cell responses to KSHV epitopes have been found to be of higher frequency and of greater antigenic diversity in asymptomatic carriers compared to those with either AIDS-related, classic, or iatrogenic KS (Barozzi et al., 2008; Guihot et al., 2006; Lambert et al., 2006).

Overall, neither the breadth of the antigenic *repertoire* of the KSHV-specific CD8+ T cell immune response, nor its immunodominant targets, are fully understood. Even less is known about KSHV-specific CD4+ T cell responses. Neutralizing antibodies against KSHV are induced (Kimball et al., 2004), however their target has not been elucidated. Gamma delta (γδ) T cells (Barcy et al., 2008) and NK cells (Dewan et al., 2006) may also play a role in KSHV immune surveillance.

1.2.4. KSHV evasion of cytotoxic CD8+ T cell responses

Crucial to KSHV ability to establish a persistent viral reservoir is evasion of host immune recognition and attack that would otherwise eliminate the virus. As a sophisticated oncogenic virus, KSHV has evolved to possess a formidable *repertoire* of potent mechanisms to sabotage almost every aspect of the host immune system (Liang et al., 2008). Almost 50% of KSHV genome is dedicated to modulating host immune response. The immune evasion strategies of KSHV in the context of host innate and adaptive immunity include: interference with interferon (IFN) signaling, alteration of host chemokine signaling, inhibition of complement control, blockage of apoptotic and autophagic pathways, escape from NK cell lysis and cytotoxic T cell response (Feng et al., 2013; Hu and Usherwood, 2014; Liang et al., 2008). These evasion strategies ensure persistent infection and spread of KSHV, and contribute to the pathogenesis of KSHV-associated diseases. As before, special emphasis is given to KSHV evasion of CD8+ CTL response.

As with EBV, KSHV-specific mechanisms inhibiting CD8+ T cell responses tend to act on antigen processing and presentation. K3 and K5 gene products of KSHV act in concert to efficiently downregulate the expression of HLA molecules on the surface of infected cells, thus preventing

antiviral CD8+ CTL responses (Coscoy and Ganem, 2000; Ishido et al., 2000). K3 and K5 are highly homologous (~40% identity) and are expressed during the lytic replication cycle (Nicholas et al., 1997a). However, both genes may also be expressed during latency in response to Notch signaling (Chang et al., 2005). Both contain a RING-CH type zinc finger domain at the N-terminus, two transmembrane domains in the central region, but vary in the C-terminal tail (Nicholas et al., 1997a). Although predominantly located in the endoplasmic reticulum, K3 and K5 do not affect the assembly or transport of HLA molecules through the secretory pathway. Instead, they are the prototypical members of the membrane-associated RING-CH containing (MARCH) family of proteins and act as E3 ubiquitin ligases that mediate ubiquitination of the cytosolic tail of HLA molecules on the cell surface, which once ubiquitinated are rapidly internalized and degraded by the lysosome (Coscoy et al., 2001; Hewitt et al., 2002). K3 and K5 show different HLA allotype specificities. While K3 extensively downregulates the expression of HLA-A, -B, -C and –E; K5 effectively downregulates HLA-A and –B, HLA-C only weakly and is unable to target HLA-E (Coscoy and Ganem, 2000; Ishido et al., 2000). The E3 ligase activity of both K3 and K5 can be lysine-independent, in that they can alternatively ubiquitinate cysteine residues on HLA molecules (Cadwell and Coscoy, 2005; Cadwell and Coscoy, 2008). Moreover, K3 and K5 can downregulate not only HLA molecules from the cell surface, but also other components involved in T cell functions such as ICAM I and IFN-γR1 (Coscoy et al., 2001; Li et al., 2007).

Therefore, in addition to repressing antigen presentation, KSHV infection also causes downregulation of co-stimulatory molecules such as, CD80, CD86, CD1a, and CD83 on antigen-presenting cells (APCs) (Gregory et al., 2012). These co-stimulatory molecules are required for TCR-mediated activation of CTLs, so the downregulation of these proteins is another mechanism by which KSHV infection inhibits the adaptive T cell immune response.

The product of the DNase/alkaline exonuclease gene of KSHV, SOX, as EBV BGLF5, shuts down host cell protein synthesis, reducing surface HLA and concomitant antigen-specific CD8+ T cell recognition (Zuo et al., 2008). SOX induces host mRNA degradation by hyperadenylation of the transcripts and induces relocalization of cytoplasmic poly(A)-binding proteins, which are important for stability and translation of cytoplasmic mRNAs, into the nucleus. Thus, SOX may prevent nascent mRNA export and deplete preexisting cytoplasmic mRNAs (Kumar and Glaunsinger, 2010; Lee and Glaunsinger, 2009). vIRF-1 is another KSHV encoded protein known to inhibit HLA expression (Lagos et al., 2007). Overall K3, K5, SOX and vIRF-1 are lytic cycle proteins and their contribution to reducing antigen presentation *in vivo* in the context of KS and PEL are unknown. Nonetheless, downregulation of class I molecules and co-stimulators is also observed in latent KHSV infected cells (Tomescu et al., 2003) suggesting that CTL evasion is a constitutive demand for KSHV.

During latency, a minimal number of gene products is expressed, which reduces the number of antigens that can be presented to CD8+ T cells and invoke a response. LANA is a viral latent protein essential for the establishment and maintenance of KSHV latency in proliferating cells,

therefore contributing to the latent signature of KSHV infection. LANA tethers the viral episome to the host chromosomes during mitosis, ensuring partioning of the viral genome into progeny cells (Ballestas et al., 1999). Thus, consistent expression of LANA in latently infected cells creates a potential target for immune recognition. As seen with its functional EBV EBNA1 equivalent, LANA contains a repeat sequence, the acidic central repeat (ACr) domain, that similarly regulates LANA own translation and degradation to minimize antigen processing *in cis*, allowing escape from CTL recognition (Kwun et al., 2007; Zaldumbide et al., 2007). Nevertheless, $CD8^+$ T cell responses can be detected against LANA (Guihot et al., 2006; Woodberry et al., 2005b).

The sophisticated evasion of the host immune control by KSHV provides a foundation for persistent viral infection and pathogenesis. Nonetheless, due to the absence of *in vivo* models, as with EBV, it remains difficult to extrapolate *in vitro* observations to the *in vivo* viral infection.

1.2.5. KSHV vaccine prospect

Interests and efforts to develop a KSHV vaccine are limited. Since its discovery, research has focused essentially on the molecular virology and potential mechanisms of KSHV oncogenesis. Nevertheless, KSHV vaccines designed to prevent a naïve host from infection and to boost the immune control of KSHV in persistently infected people could have a major impact on individuals who are at a high risk of developing KSHV-associated diseases, namely, HIV infected individuals, those under immunosuppression, or living in endemic African areas (Wu et al., 2010). It has been proposed that a vaccine should increase immune control of lytic replication and decrease KSHV viral load in people already infected in order to reduce the risk of KS and shedding of virus for transmission (Wu et al., 2012). Furthermore, for a therapeutic vaccine incorporation of epitopes derived from latent proteins, such as LANA and Kaposin, is believed to increase its efficacy.

Twenty years after the discovery of KSHV, simple cytotoxic chemotherapy regimens remain the only clinically validated treatments, there exists no vaccine against this virus and except mTOR inhibitors, no targeted agents have been added to clinical practice (Bhatt et al., 2010; Krown et al., 2012; Roy et al., 2013; Sin et al., 2007).

1.3. Murid Herpesvirus-4

Both EBV and KSHV have a very narrow species tropism, and this has hampered *in vivo* studies. The discovery of Murid herpesvirus-4 (MuHV-4) (archetypal strain Murine herpesvirus 68 (MHV-68)) (Blaskovic et al., 1980), its relative simplicity and its capacity to establish a realistic infection in inbred mice have enabled rapid progress of the knowledge of gamma-herpesvirus (γHV) pathogenesis and provided the first opportunity to test directly the role of $CD8^+$ T cells in γHV pathogenesis. This system provides a tractable small animal model for studying key aspects of γHV infection in a natural host. It gives the opportunity to address *in vivo* the strategies used by γHVs to subvert the normal host cell function, characterize the immune effector mechanisms that control persistent infection and the mechanisms used by the virus to evade them and, finally, assess the effectiveness of different therapeutic strategies (Stevenson and Efstathiou, 2005).

MuHV-4 is a naturally occurring rodent pathogen, originally isolated from two species of free living small rodents: *Apodemus flavicollis* (yellow-necked mouse) and *Clethrionomys glareolus* (bank vole) in Slovakia, in 1980 (Blaskovic et al., 1980). Later studies indicated that this virus is endemic in wood mice (*Apodemus sylvaticus*) in the United Kingdom, suggesting that this may be the natural host species (Blasdell et al., 2003).

Genetically MuHV-4 is more closely related to KSHV than to EBV, its genome contains ~118 kbp of unique DNA flanked by terminal repeats with at least 80 genes, of which more than 60 open reading frames (ORFs) are homologous to those of KSHV (Efstathiou et al., 1990a; Virgin et al., 1997). Despite the fact that most ORFs are homologues of other γHVs or cellular genes, MuHV-4 genome also harbors a number of unique genes encoded at the left end of the genome, termed *M1-4*, most of which are dispensable for lytic replication and thus are presumably involved in persistent infection *in vivo* (Moorman et al., 2004; Song et al., 2005). Functional studies on some of these “unique” gene products have demonstrated conservation of key functions (e.g., MuHV-4 M2, EBV LMP2A and KSHV K1 and K15 all harbor SH2 and SH3 docking sites capable of interacting with Src or Syk family members, mimicking or interfering with BCR signaling) (Damania, 2004; Damania et al., 2000; Pires de Miranda et al., 2013). Like EBV, MuHV-4 causes an acute infectious mononucleosis syndrome, it is B cell tropic and shows a similar approach to host colonization, that is, both MuHV-4 and EBV drive B cell proliferation and exploit host GCs to persist in memory B cells (Blackman and Flano, 2002; Bowden et al., 1997; Doherty et al., 2001; Nash et al., 2001; Roughan and Thorley-Lawson, 2009; Simas and Efstathiou, 1998; Stevenson and Efstathiou, 2005). Moreover, persistent infection with MuHV-4 has been associated with increased frequencies of malignancies in mice with defective immune systems, mainly B cell lymphomas, but also other tumours of both lymphoid and non-lymphoid origin (Lee et al., 2009c; Sunil-Chandra et al., 1994; Tarakanova et al., 2005). Importantly, MuHV-4 also provides a natural *in vivo* infection model in which host immune evasion mechanisms are preserved (Stevenson et al., 2009). Adding to this the highly conserved nature of the innate and adaptive immune systems between mice and humans, studying MuHV-4 as a mouse model of γHV pathogenesis is believed

to allow the identification of conserved host and viral strategies for the simultaneous maintenance of lifelong persistence and prevention of disease.

An additional advantage of using MuHV-4 as a model is the possibility of infecting various genetically modified mice and manipulating the immune system, and the fact that MuHV-4 genome can be readily manipulated for mutational analysis.

Therefore, MuHV-4 presents as a unique experimental model for dissecting γHVs infection and immune control *in vivo*.

1.3.1. MuHV-4 model of infection

In the laboratory mouse, following intranasal inoculation MuHV-4 primary infection is characterized by acute lytic virus replication in lung alveolar epithelial cells (Figure 1.4) (Sunil-Chandra et al., 1992a). Lytic infection is resolved within 10 to 12 days by the host immune response, with $CD8^+$ T cells playing a prominent, but not exclusive, role. Subsequently, the virus establishes lifelong latency, predominantly in B cells (Marques et al., 2003; Sunil-Chandra et al., 1992b) of the secondary lymphoid organs, but also in dendritic cells (DCs), macrophages (Flano et al., 2000), and lung epithelial cells (Stewart et al., 1998). Latent infection in the spleen is characterized by an initial proliferation of the infected B cells and consequent amplification of the latent virus, reaching maximum levels around 14 days post-infection (p.i.), and decreasing thereafter to low but steady state levels of latently infected cells that persist throughout the entire life of the host without overt disease.

The peak of latent infection is accompanied by a transient splenomegaly and lymphadenopathy (Sunil-Chandra et al., 1992a), which are due to the proliferation of latently infected B cells, but also to a large increase in $CD4^+$ and $CD8^+$ T cell numbers, and are dependent on $CD4^+$ T cells (Ehtisham et al., 1993; Usherwood et al., 1996). This phase of infection is also accompanied by high levels of non-virus-specific antibodies and $CD8^+$ T cells in the peripheral blood thus resembling the IM caused by EBV (Blackman et al., 2000; Tripp et al., 1997). However, in contrast to the human IM in which the majority of T cells in the peripheral blood are oligoclonal outgrowths of lytic and latent-specific T cells and most are specific for a single or a few EBV lytic or latent epitopes, MuHV-4-induced IM results in selective expansion of $V\beta4^+CD8^+$ T cells (Hardy et al., 2000; Tripp et al., 1997). These cells are MHC-independent and are activated by the secreted M1 viral protein, in a manner reminiscent of a viral superantigen (Evans et al., 2008).

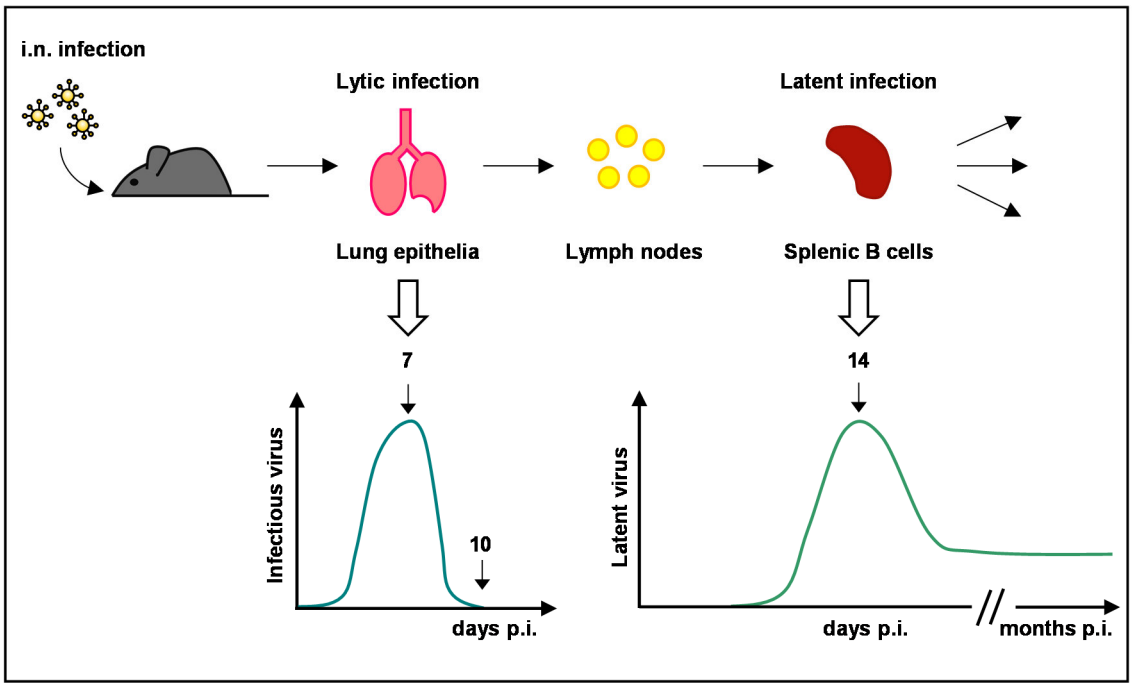

Figure 1.4. Model of MuHV-4 infection. After intranasal (i.n.) infection of inbred mice, MuHV-4 establishes a productive infection in the respiratory tract that peaks at around 4-7 days post-infection (p.i.) and is cleared to undetectable levels by 10-12 days p.i.. From the lung, the virus disseminates to the lymphoid tissue, with latent virus being first detected in the lymph nodes and subsequently in the spleen, mainly in B cells. During latent infection in the spleen there is an amplification of latent virus that reaches maximum levels at around 2 weeks p.i. and afterwards decreases to reach low steady-state levels of latently infected cells that persist for the lifetime of the host. From the spleen, the virus further disseminates to other sites probably via infected memory B cells (adapted from Stevenson, 2002).

In agreement to what has been proposed for EBV, the establishment of latent infection does not require a prior productive infection. In fact, latency is established in lung B cells as early as 3 days after respiratory inoculation, supporting the hypothesis that infection of B cells is a concurrent event with the ongoing lytic infection of the mucosal epithelium (Flano et al., 2005). Moreover, recombinant viruses that cannot undergo lytic replication still establish latency in mice (Flano et al., 2005; Moser et al., 2006). However, lytic replication is required for virus trafficking and establishment of latency in the spleen.

In vitro, MuHV-4 is able to productively infect epithelial and fibroblast cells from a variety of species raging from chickens to primates (Svobodova et al., 1982) and to latently infect murine B cell lines (Sunil-Chandra et al., 1993). MuHV-4$^+$ B cell lines have been established from tumours of infected mice, of which S11 is the best characterized (Usherwood et al., 1996). Infection of primary B cells with MuHV-4 results in their activation and increased proliferation, however the cells do not become transformed and usually die within two weeks (Dutia et al., 1999; Stevenson and Doherty, 1999). MuHV-4 has been shown to immortalize only fetal B cells *in vitro* (Liang et al., 2011). KSHV also colonizes B cells *in vivo*, but fails to transform them *in vitro*. Thus, EBV,

KSHV and MuHV-4 differ *in vitro* but remain strikingly similar regarding *in vivo* host B cell colonization.

1.3.2. MuHV-4 latency

MuHV-4 enters new hosts via the olfactory neuroepithelium (Milho et al., 2012) or genital tract (Francois et al., 2013), dendritic cells take it to lymph nodes (Gaspar et al., 2011), and from there it reaches the spleen. This epithelial/myeloid/lymphoid MuHV-4 infection pathway (Frederico et al., 2012) is consequently quite different to the epithelial cell/B cell exchange proposed for EBV (Borza and Hutt-Fletcher, 2002). Then, MuHV-4 enters the spleen by infecting marginal zone (MZ) macrophages, which provide a conduit to MZ B cells (Frederico et al., 2014). These relocate to the white pulp allowing virus transfer to follicular dendritic cells, which appear to transfer the virus without becoming infected (analogous to their presentation of immune complexes to GC B cells), and from there the virus reaches GC B cells to establish persistent infection (Frederico et al., 2014). Thus, MuHV-4 exploits normal splenic immune communication routes to spread by serial myeloid/lymphoid exchange (Frederico et al., 2014).

Several B cells subsets, and other cell types, namely macrophages and dendritic cells, are infected during the establishment of latency. However, B cells are the main reservoir of MuHV-4 latently infected cells. During the establishment of latency MuHV-4 is found in naïve, GC, memory B cells and plasma cells (Collins et al., 2009; Flano et al., 2002; Marques et al., 2003; Willer and Speck, 2003). At the peak of latent infection the majority of MuHV-4 latently infected cells correspond to B cells that are proliferating in a GC. This proliferation leads to the amplification of the pool of latently infected cells that reaches maximal levels at two to three weeks post-infection. Afterwards, most GCs regress and there is a consequent decline in the latent load to a low steady state that persists for the lifetime of the host. Therefore, latency in naïve and GC B cells wanes with time and at late times post-infection MuHV-4 latency is predominantly maintained in isotype switched memory B cells (Flano et al., 2002; Willer and Speck, 2003). GC B cell proliferation and differentiation into memory B cells is critical for maintenance of MuHV-4 long-term persistence (Kim et al., 2003; Moser et al., 2005). Although several B cell subsets can be initially infected by MuHV-4, only the ones that access a GC and differentiate into memory B cells are capable of maintaining long-term MuHV-4 latent infection. These observations imply similarities with the proposed model for EBV latency, indicating that MuHV-4 is also exploiting the normal B cell developmental pathways in order to achieve latency in the long-lived memory B cell compartment. Thus, the virus takes advantage of the GC reaction to expand the pool of latently infected cells and later to induce the differentiation of the infected cells into long-lived memory B cells.

MuHV-4-driven B cell activation, proliferation, expansion and differentiation of latently infected cells depends on $CD4^+$ T cells (Collins and Speck, 2014; Stevenson and Doherty, 1999;

Usherwood et al., 1996), CD40 ligand (Brooks et al., 1999), and CD40 (Kim et al., 2003), implying that MuHV-4 depends on normal T cell help to enter the GC reaction and differentiate into a memory B cell. In the absence of $CD4^+$ T cells, infected B cells show impaired proliferation in GCs, there is a reduced amplification of latency and no splenomegaly. In addition to $CD4^+$ T cell help, host colonization also requires T cell-independent survival signals provided by the B cell activating factor (BAFF) receptor (BAFF-R) (Frederico et al., 2014).

Several ORFs were shown to be transcribed during the establishment of latency, including *M1*, *M2*, *M3*, *M4*, *M8*, *M9*, *M11* (*v-bcl2*), *K3*, *ORF72* (*v-cyclin*), *mLANA* (*ORF73*) and *ORF74* (Marques et al., 2003). Furthermore, the pattern of transcription in B cells is selective and dependent upon the differentiation status of the B cell, which reflects the possibility of different latency programmes, as occurs with EBV.

Analogous to EBV and KSHV, MuHV-4 also encodes at least 15 miRNAs (miR-M1-1 to miR-M1-15) at the left end of its genome, which are expressed both in lytic and latently infected cells *in vitro* (Pfeffer et al., 2005; Zhu et al., 2010). An unusual feature of this miRNAs is that they are part of tRNA-like genes transcribed by RNA pol III and processed Drosha-independently by tRNaseZ (Bogerd et al., 2010; Diebel et al., 2010). Their targets and biological functions, particularly in the context of infection remain unknown. However, they are predicted to be expressed during latency *in vivo* and to modulate key aspects of the virus lifecycle. Uncharged viral tRNAs are also expressed in the spleens of latently infected mice and have been used as a marker to study the kinetics of viral latency (Bowden et al., 1997; Simas et al., 1999).

The mechanism by which MuHV-4 promotes the differentiation of newly infected naïve B cells into GC B cells, memory and plasma cells remains to be elucidated. Research conducted in our laboratory has focused on the latent phase of MuHV-4 infection, in particular in dissecting basic molecular mechanisms and characterizing the biological functions of both M2 and mLANA latent proteins, and their contribution to *in vivo* establishment of latency and host colonization. Our studies indicate that both proteins play important key functions during *in vivo* MuHV-4 expansion in GC B cells. The M2 protein has been shown to function as a modulator of B cell signaling, exhibiting functional homology with EBV LMP2A and KSHV K1 and K15, and to promote acute latency amplification *in vivo* (Pires de Miranda et al., 2008; Pires de Miranda et al., 2013; Rodrigues et al., 2006). mLANA, the virus episome maintenance protein, modulates cellular nuclear factor-kappa B (NF-κB) and c-myc through its E3 ubiquitin-ligase activity (Rodrigues et al., 2009; Rodrigues et al., 2013). Specifically, mLANA-mediated poly-ubiquitination of the p65/RelA subunit of NF-κB targets it for proteasomal degradation (Rodrigues et al., 2009), whereas heterotypic poly-ubiquitination of c-myc increases its stability resulting in increased progression through the cell cycle (Rodrigues et al., 2013). By simultaneously inhibiting NFκB signaling and increasing c-myc stability, mLANA is believed to be promoting the expansion of MuHV-4 in GC B cells and thereby contributing to MuHV-4 persistence in the host. Additionally, resolution of the crystal structure of mLANA C-terminal domain revealed a dimer, composed of a

ventral face mediating viral DNA binding and a dorsal face containing a novel structural motif with a patch of positively charged lysine residues, predicted to mediate interaction with host cell protein(s) (Correia et al., 2013). Mutations in the mLANA DNA binding motif abolished MuHV-4-driven GC B cell proliferation severely compromising virus persistence. Substitutions of lysine residues, located at the periphery of the positively charged dorsal motif, interfered with the efficient expansion of latently infected GC B cells (Correia et al., 2013).

Another study performed in our laboratory aimed at clarifying the role of BCR specificity in the establishment of MuHV-4 latency in B cells. This study demonstrated that MuHV-4 latency is not restricted to virus-specific B cells. Taking advantage of the switch hen egg lysozyme (SW_{HEL}) mice, which contain up to ~10% of hen egg lysozyme (HEL)-specific B cells, and the yellow fluorescent protein (YFP)-expressing MuHV-4, experiments were designed to investigate in parallel how MuHV-4 influences a normal B cell *repertoire* (HEL^-) and a clonal population of non-virus specific B cells (HEL^+) (Decalf, J. & Godinho-Silva C. *et al*., 2014, *accepted, in press*). *In vivo* tracking of HEL^- and HEL^+ B cells, revealed that latency was restricted to HEL^- B cells although both populations were equally sensitive to virus infection *in vitro*. MuHV-4 infection triggered two waves of B cell activation. The first wave was characterized by general B cell activation, with expansion of both HEL^- and HEL^+ B cells and upregulation of CD69 expression. The second wave was restricted to the population of HEL^- B cells which acquired GC and plasma cell phenotypes. HEL^+ B cells, despite being activated *in vivo*, did not support MuHV-4 latent infection and did not differentiate into GC B cells. Upon cognate antigenic stimulation, HEL^+ B cells differentiated into GC B cells, still MuHV-4 latent infection remained undetectable, indicating that the virus could not benefit from an acute B cell response to establish latency. Therefore, this study supports the idea that MuHV-4 establishment of latency in B cells is not a stochastic event in terms of BCR specificity relying on mechanisms that remain, however, to be identified.

Similarly, little is known about how MuHV-4 reactivates from latency and re-enters the lytic cycle. However, like with EBV and KSHV, plasma cell differentiation seems to be linked to MuHV-4 reactivation from latency, and it has been proposed that the M2 latency-associated protein is probably involved in this process (Liang et al., 2009).

1.3.3. M2 latency-associated protein

M2 was initially classified as a latency-candidate gene on the basis of its genomic position. *M2* is located at the left end of MuHV-4 genome, a region that contains four unique ORFs (M1-M4), eight viral tRNAs and at least fifteen miRNAs (Virgin et al., 1997). Comparative studies with closely related MuHV-4-like viruses revealed that M2 is the most divergent of the four proteins (Hughes et al., 2010). Among γHVs, this genomic region besides being very divergent is also known to encode latency-associated and transforming proteins (Virgin et al., 1999).

M2 is composed of two exons that, upon splicing, produce a unique 192 amino acid-long protein, bearing no discernible homology to any other viral or cellular proteins existent in the databases (Husain et al., 1999). This protein has no obvious conserved domains or intracellular signals and examination of its primary structure reveals only the presence of eight proline-rich regions and three tyrosine residues, two of which Y^{120} and Y^{129} are differentially and constitutively phosphorylated by Src family kinases (Figure 1.5) (Pires de Miranda et al., 2008; Rodrigues et al., 2006). Additionally, M2 contains an $H2K^d$-restricted epitope ($M2_{84-92}/K^d$) that is recognized by $CD8^+$ T cells from infected BALB/c ($H2^d$) mice (Husain et al., 1999). A CTL line that recognizes this epitope is able to kill the latently infected S11 cells, suggesting that the M2 protein is expressed during latent infection and is a target for the host $CD8^+$ CTL response (Husain et al., 1999).

MAPTPPQGKIPNPWPGGCSQNPVLWGDGTDGNYRPSEPWILGQVPCDQRFPHPSGNKNSSSTSGGR
PQRPPLPRTRFPKTIRRGFNKLRSTLKSPWKPRPSPVPSPEEVNPAGSPEENIY*ETANSEPVY*IQPIST
RSLMMLDSGSTDSPENLGPPTRPLPKLPNQHPMNPEIRLPIIPPSKCHKGFVEWGEE

Figure 1.5. Primary sequence of the M2 latency-associated protein. The proline residues organized in PxxP motifs (P represents a proline residue and x any amino acid) are shown in green, and the two tyrosine residues (Y^{120} and Y^{129}) with the potential to be phosphorylated by kynases are shown in pink and with an asterisk. The $H2K^d$-restricted $CD8^+$ CTL epitope is shown in blue and underlined, with the anchor residues, which are specific residues through which the peptide fragment binds to the MHC molecules, in yellow.

M2 transcripts were firstly detected in splenocytes of infected mice during the establishment of latency, but not in lytically infected fibroblasts (Husain et al., 1999; Virgin et al., 1999). Subsequently, work performed in our laboratory and another independent study demonstrated that the *M2* gene is consistently expressed during latency in the spleen in several B cell subsets, including the GC B cells, where it is one of the most expressed ORFs, and also in dendritic cells (Flano et al., 2002; Marques et al., 2003).

In vivo the M2 protein was shown to play a critical role in the establishment of latency as well as reactivation from latency (Herskowitz et al., 2005; Jacoby et al., 2002; Macrae et al., 2003). Following intranasal infection, disruption of M2 did not affect the acute phase of virus replication, but caused a severe decrease in the establishment of latency in the spleen and a profound reactivation defect. In a study from our group, a detailed phenotypical analysis of an M2-defective virus was performed, addressing the establishment and maintenance of latency in different spleen cell subsets and splenic regions (Simas et al., 2004). Disruption of M2 resulted in a reduction in the number of latently infected follicles at 14 days post-infection. However, the mean number of latently infected cells per infected follicle was equivalent between the M2-defective virus and wild type. In addition, the frequencies of infection in total B, GC and memory B cells were also significantly lower compared to the wild type. Late in infection, at 50 and 70 days post-infection,

disruption of M2 resulted in sustained and abnormally high levels of virus persistence in splenic total B and GC B cells but not in memory B cells. Both the percentage of infected follicles and the mean number of infected cells per follicle were increased late during infection with the M2-disrupted virus.

Taken together, these data are consistent with M2 playing a crucial role in two distinct steps of the GC reaction. During the establishment of latency, M2 is required for efficient colonization of splenic follicles but is dispensable for the expansion of latently infected GC B cells. Late in infection, M2 seems to be signaling the overall cessation of virus-driven expansion of infected GC B cells. The acute latency amplification deficit associated with disruption of M2 suggested that this protein might be modulating B cell signaling pathways in order to induce the initial activation of the infected B cell and to promote the establishment of long-term latency in the memory B cell pool. This strategy had previously been demonstrated for the human γHV latent proteins, LMP1 and LMP2A encoded by EBV and K1 and K15 encoded by KSHV, that interfere with different aspects of the host cellular signaling by mimicking the normal function of the B cell or CD40 receptors. Therefore, the *in vivo* work was complemented with biochemical studies in order to understand and characterize the molecular functions of M2 during latent infection.

The first biochemical study demonstrated that M2 is capable of inhibiting the IFN-mediated signal transduction, suggesting that by antagonizing IFN-mediated host immunity, M2 may be protecting latently infected cells from elimination (Liang et al., 2004). After, the same authors found that M2 could interact with several proteins involved in the DNA damage signaling, blocking DNA-damage-induced apoptosis (Liang et al., 2006). *In vitro* studies showed that M2 expression enhances B cell proliferation and survival, through secretion of high levels of IL-10 (Madureira et al., 2005; Rangaswamy and Speck, 2014; Siegel et al., 2008). *In vivo* high serum levels of IL-10 observed during MuHV-4 infection were dependent on a functional *M2* gene. Interestingly, recently LMP2A was also found to be capable of upregulating IL-10 production in mitogen-stimulated primary B cells and B cell lymphomas, and increased IL-10 promoted the survival of these cells (Incrocci et al., 2013). Furthermore, EBV encodes an IL-10 homolog, suggesting that manipulation of IL-10 expression may be a common strategy among γHV.

In vitro M2 was also shown to drive B cell differentiation towards a pre-plasma memory B cell phenotype in primary murine B cells and in a B lymphoma cell line (Liang et al., 2009; Siegel et al., 2008). *In vivo* infection of mice with a M2-null mutant results in an absence of virus infected plasma cells at the peak of latency expansion, whereas in mice infected with wild type MuHV-4 approximately 8-10% of virus infected splenocytes are plasma cells, with these cells accounting for the majority of reactivation observed upon explant of splenocytes (Liang et al., 2009). Thus, the role of M2 in MuHV-4 reactivation from latently infected B cells has been attributed to its ability to manipulate plasma cell differentiation. Moreover, a recent report demonstrates that *in vitro* M2 activates the NFAT pathway in a Src kinase-dependent manner leading to induction of the plasma cell-associated transcription factor, interferon regulatory factor-4 (IRF4), which can regulate the

IL-10 promoter in B cells, providing insights into how M2 potentially facilitates plasma cell differentiation and subsequent virus reactivation (Rangaswamy and Speck, 2014).

Biochemical research carried out in our laboratory has identified several intracellular targets of the M2 protein and demonstrated that M2 promotes the assembly of B cell signalling complexes downstream of the BCR (Pires de Miranda et al., 2008; Pires de Miranda et al., 2013; Rodrigues et al., 2006). The M2 C-terminal proline rich region was shown to be important for interaction of M2 with SH3 domains of Src family tyrosine kinases, for translocation of M2 to the plasma membrane, and for subsequent phosphorylation of two closely spaced tyrosine residues of M2 (Y^{120} and Y^{129}) present in a proposed unconventional ITAM (Pires de Miranda et al., 2013), with similar sequence identity to the ITAM of K1 (KSHV) (Lee et al., 1998a). Phosphorylation of M2 tyrosine residues creates additional docking sites that allow direct and selective interaction of M2 with SH2-containing molecules involved in B cell signalling, specifically, Fyn, Lyn, Vav1, Nck1, PLCγ2, PI3K and SHP2. Thus, M2 coordinates the formation of a signalosome similar to the one that is assembled by K1 (KSHV) and like K1 drives the phosphorylation of PLCγ2 (Lagunoff et al., 1999; Lee et al., 2005). M2 has also been shown to activate the Vav1/Rac1 pathway (Pires de Miranda et al., 2008; Rodrigues et al., 2006). Furthermore, efficient entry of latently infected B cells into GC reactions *in vivo* is dependent on M2, particularly on its C-terminal proline rich region and phosphotyrosines (Herskowitz et al., 2008; Jacoby et al., 2002; Macrae et al., 2003; Pires de Miranda et al., 2008; Simas et al., 2004). Hence, M2 modulation of B cell signaling is critical for the efficient colonization of splenic follicles *in vivo*. Interestingly, experiments being carried out in our group indicate that M2 is also promoting the formation of an immunological synapse between the B cell and $CD4^+$ T cell, which in normal B cell development is important to drive GC reactions (F. Lopes and D. Fontinha, unpublished). Therefore, it is possible that M2 is inducing a pre-synaptic state in the B cell that reduces the threshold or even replaces the need for cognate $CD4^+$ T cell help. Experiments are currently being performed by D. Fontinha to clarify this issue.

Globally, these studies indicate that M2 by modulating B cell signaling exhibits functional homologies with EBV LMP2A and KSHV K1, which mimic a constitutive activated BCR. Although EBV LMP2A and KSHV K1 manipulate B cell signaling events at the receptor level while MuHV-4 M2 modulates the signaling downstream of the BCR, the overall result is equivalent, implying that these latency-associated proteins exhibit convergent functions to allow the exploitation of the normal B cell developmental pathways in order to efficiently establish lifelong persistent infections in the host.

As previously mentioned, *in vivo* an unusual feature of the M2 knockout phenotype in BALB/c ($H2^d$) mice is that despite an acute latency deficit, long-term latent loads are increased (Simas et al., 2004). C57BL/6 ($H2^b$) mice, which are not known to recognize an M2 epitope, show the same acute latency deficit, but not the long-term increase (Jacoby et al., 2002). These observations suggested that long-term latency depends both on viral M2 expression and host H2 haplotype. Indeed, the increased long-term persistence observed in $H2^d$ mice infected with a M2 defective

virus results from an immunological effect rather than abrogation of the M2 molecular functions. A study conducted in our laboratory demonstrated that in BALB/c ($H2^d$) mice absence of the M2 epitope results in uncontrolled long-term MuHV-4-driven proliferation of latently infected cells in GCs (details in section 1.3.5) (Marques et al., 2008).

In summary, M2 modulates B cell signaling pathways in order to promote *in vivo* acute latency amplification in GC B cells and its $H2K^d$-restricted $CD8^+$ CTL epitope, in the appropriate host MHC haplotype, renders M2 indirectly responsible for setting the long-term viral load.

1.3.4. Adaptive immunity to MuHV-4

Adaptive immunity plays a major role in controlling MuHV-4 infection. Studies in MuHV-4, utilizing mice deficient for specific components of the adaptive host immune response, have provided important insights into their individual contribution for the control of both the lytic and latent phases of MuHV-4 infection (Table 1.3) (Barton et al., 2011; Stevenson et al., 2009).

The adaptive immune response to MuHV-4 acute infection is characterized by remarkable redundancy. That is, distinct components of the adaptive host immune response are individually dispensable for resolution of acute virus replication. Mice lacking $CD4^+$ T cells, $CD8^+$ T cells, B cells, or IFNγ effectively control acute virus replication, although the capacity of $IFN\gamma^{-/-}$ mice to control acute infection is strain specific (Cardin et al., 1996; Christensen et al., 1999; Lee et al., 2009b; Tsai et al., 2011). Therefore, $CD4^+$ T cells can be directly antiviral, independent of $CD8^+$ T cells or B cells. However, concurrent removal of both $CD4^+$ and $CD8^+$ T cell subsets is invariably fatal (Stevenson et al., 1999c). Nevertheless, in wild type mice the cells detected in the brochoalveolar lavages during lytic infection are mainly $CD8^+$ T lymphocytes, emphasizing the important role of $CD8^+$ CTLs in the control of primary acute infection. In fact, their depletion increases while their priming reduces the levels of infectious viruses in the lungs following intranasal infection (Ehtisham et al., 1993; Stevenson et al., 1999b; Stevenson et al., 1999c).

In contrast, control of persistent and reactivating MuHV-4 infection can be accomplished only by non-redundant, collaborative functions of $CD4^+$ and $CD8^+$ T cells, B cells and functional IFNγ signaling. Absence of any of these effector results in deregulated chronic infection.

$CD4^+$ T cell deficient mice are able to control the acute lytic lung infection but although they appear healthy for 2 to 3 months, MuHV-4 reactivates from latency at high levels, the mice develop severe chronic lung disease and eventually die, despite the presence of normal numbers and functional virus-specific $CD8^+$ T cells (Belz et al., 2003; Cardin et al., 1996; Ehtisham et al., 1993). IFNγ, at least partially derived from $CD4^+$ T cells, is critical for elimination of persistent lytic replication and for adequate control of reactivation. In the absence of either $CD4^+$ T cells or IFNγ, acute infection resolves but persistent replication continues at a low but pathologic level in multiple tissues,

leading to an array of pathologies that are uniformly fatal after several months (Christensen et al., 1999; Sparks-Thissen et al., 2005).

$CD4^+$ T cells may play a major effector role in controlling the establishment and maintenance of latency, still such a function has been hard to define. Yet, the finding that $CD4^+$ T cells lyse latently MuHV-4 infected B cells (Stuller and Flano, 2009) suggests that $CD4^+$ T cells may directly control latency rather than just provide helper T cell function. The effector function of $CD4^+$ T cells is possibly mediated by two independent mechanisms, IFNγ production and cytotoxicity, as persistently infected mice display two distinct effector populations, one producing IFNγ and the other possessing killing activity (Stuller et al., 2010). $CD4^+$ T cells seem to be continuously stimulated by infected B cells and dendritic cells (Freeman et al., 2011). However, it remains unclear which viral antigens are presented to $CD4^+$ T cells during latency and which targets $CD4^+$ T cells may recognize.

Another mechanism by which $CD4^+$ T cells may contribute to long-term MuHV-4 control is by enhancing $CD8^+$ T cell responses. Yet, the mechanism of $CD4^+$ T cell help operating during MuHV-4 chronic infection is not fully understood. $CD4^+$ T cell-mediated activation of dendritic cells, through CD40-CD40L interactions has been shown to be important for effective long-term control of MuHV-4 (Giannoni et al., 2008). $CD4^+$ T cell-mediated activation of dendritic cells could enable effective long-term activation of $CD8^+$ T cells encountering antigen-presenting dendritic cells in lymph nodes, however, this has not been demonstrated. Furthermore, recent reports indicate that in the absence of $CD4^+$ T cell help an IL-10-producing $CD8^+$ T cell population arises during persistent MuHV-4 infection that belongs to a subset of $CD8^+$ regulatory T cells (Hu et al., 2013; Molloy et al., 2011). IL-10 produced from these cells is partly responsible for erosion in immune surveillance, leading to spontaneous virus reactivation in lungs during the chronic stage (Molloy et al., 2011). IL-10-producing $CD8^+$ T cells showed partial overlap with the markers of regulatory $CD8^+$ T cells, and suppressed the proliferation of naïve $CD8^+$ T cells. Despite retaining cytotoxic activity and the ability to produce effector cytokines, these cells showed a proliferative defect that could be restored by addition of exogenous IL-2 or blockade of IL-10. (Hu et al., 2013).

In mice lacking $CD8^+$ T cells, the frequency of latently infected cells is increased, these cells are more likely to undergo reactivation and persistent low-level lytic replication occurs in the peritoneal compartment and to a lesser extent in the spleen (Tibbetts et al., 2002). In agreement, $CD8^+$ T cell depleted mice show a consistent rise in the level of latently infected cells in the spleen, suggesting an inability to control virus-driven proliferation of latently infected cells (Stevenson et al., 1999c). Moreover, in β2-microglobulin deficient BALB/c mice, which lack traditional $CD8^+$ T cells, MuHV-4 infection is associated with an increased incidence of lymphoproliferative diseases (Tarakanova et al., 2005). However, such disease does not occur in β2-microglobulin deficient C57BL/6 mice. A recent study has shown that fetal liver-derived B cells immortalized by MuHV-4 could be controlled by both $CD8^+$ and $CD4^+$ T cells *in vivo* (Liang et al., 2013).

Table 1.3. Key players in adaptive immune response to MuHV-4 (adapted from Barton, E. *et al.*, 2011).

Component of the adaptive immune response	Effect on MuHV-4 life cycle (*in vitro* or *in vivo*)	Potential mechanism
Conventional $CD8^+$ T cells	↓ acute replication ↓ latency ↓ persistent replication ↓ reactivation	Perforin-, granzyme- and Fas-dependent cytolysis; IFNγ-dependent control of reactivation.
Unconventional and $V\beta4^+$ $CD8^+$ T cells	↓ persistent replication ↓ reactivation	Unknown, $V\beta4^+$ $CD8^+$ T cells secret IFNγ; cytolytic activity unlikely.
$CD4^+$ T cells	↓ acute replication ↓ persistent replication ↓ reactivation	Long-term maintenance of effective $CD8^+$ CTL response via CD4-DC interactions; IFNγ-dependent control of reactivation; cytolysis.
IFNγ	↓ acute replication (in BALB/c mice) ↓ persistent replication ↓ reactivation	*In vitro* repression of viral RTA[a] promoter; *In vivo* mechanism unknown.
B cells	↓ persistent replication ↓ reactivation	B cell presentation of viral antigen to $CD8^+$ T cells and concomitant increase in IFNγ secretion.
Virus-specific antibody	↓ latency ↓ reactivation	Neutralization of virus produced upon reactivation

[a]MuHV-4 replication and transcriptional activator (RTA) is essential for virus lytic replication and reactivation from latency (lytic switch protein).

Overall, it remains uncertain if $CD4^+$ T cells function predominantly as direct cytolytic effectors, as a critical source of IFNγ, or through providing help to $CD8^+$ T cells and B cells, and how this help is mediated. Regarding $CD8^+$ T cells, it is not fully understood why $CD8^+$ T cells elicited in the absence of $CD4^+$ T cells initially control infection, yet subsequently fail to keep latent cells in check, despite maintaining high levels of cytokine expression and cytolytic function. However, it is undeniable that both $CD4^+$ and $CD8^+$ T cell subsets are needed to achieve optimal *in vivo* control of MuHV-4 persistent infection.

Neutralizing antibodies and total virus-specific antibodies slowly increase during MuHV-4 intranasal infection, reaching the peak one month later, and remaining high without declines (Stevenson and Doherty, 1998). Although it seems that virus-specific antibodies do not play an important role during the acute infection phase, the contribution of humoral responses to the control of persistent MuHV-4 infection has been demonstrated (Kim et al., 2002; Stevenson et al., 1999c; Tibbetts et al., 2003). These studies indicate to an important role for antibody in regulating latency, both by decreasing the number of latently infected cells and by inhibiting reactivation.

1.3.5. CD8+ T cell response to MuHV-4

MuHV-4 infection elicits a highly heterogeneous CD8+ T cell response that segregates into three kinetically and anatomically distinct waves of viral antigen presentation, during the lytic and latency amplification stages of infection, that are mirrored in the expansion and contraction of peptide-specific CD8+ T cells (Freeman et al., 2010; Gredmark-Russ et al., 2008; Liu et al., 1999a; Stevenson et al., 1999a). The first two waves are derived from viral lytic proteins, but they display distinct kinetics. The first wave of epitope-specific CD8+ T cells peaks at day 6 post-infection, while a second wave peaks around day 10 (Gredmark-Russ et al., 2008). Both are most abundant in the lungs and draining lymph nodes. These epitopes are thought to be presented solely during acute infection because CD8+ T cells specific for these epitopes contract more rapidly after resolution of acute lytic lung infection (Gredmark-Russ et al., 2008). A third, delayed class of lytic epitope-specific CD8+ T cells is detected coincident with the peak of latency expansion in the spleen, between days 15 and 20 post-infection, and is maintained at high levels for at least two months after resolution of acute infection (Freeman et al., 2010; Stevenson et al., 1999a). These epitope-specific CD8+ T cells show signs of continued antigen exposure *in vivo* during latency, they proliferate rapidly and exhibit functional avidity maturation over time, and their slow rate of decline is blunted following infection with a viral mutant that fails to establish latency (Freeman et al., 2010). CD8+ T cells analysed both during acute and latent infection retain functionality, as indicated by IFNγ and TNFα secretion and cytotoxic capacity upon antigen re-exposure, during persistent infection, with no evidence of functional exhaustion (Cush et al., 2007). CD8+ T cell transition from effector to effector-memory to central-memory phenotypic maturation is relatively prolonged, with effector contraction occurring over several months (Cush et al., 2007). It is believed that low-level antigen exposure, presumably driven by reactivation, plays a role in maintaining a highly functional CD8+ effector population for the life of the host, although this has not been formally demonstrated. Nevertheless, MuHV-4-specific memory CD8+ T cells do not require the presence of antigen for survival and are capable of homeostatic renewal if transferred into a lymphopenic host (Cush and Flano, 2009).

More than 30 MHC class I epitopes derived from MuHV-4 early and late genes have been identified in the C57BL/6 ($H2^b$) and BALB/c ($H2^d$) mice (Freeman et al., 2010; Gredmark-Russ et al., 2008). However, despite meaningful efforts to characterize the antigenic diversity, functionality and kinetics of MuHV-4-specific CD8+ T cell responses all class I-restricted epitopes identified thus far derive from lytic cycle proteins. The only MuHV-4 latent specific CD8+ CTL target known is the $H2K^d$-restricted epitope present in the M2 latency-associated protein ($M2_{84\text{-}92}/K^d$, GFNKLRSTL) recognized by CD8+ CTLs of BALB/c ($H2^d$) mice, but not of C57BL/6 ($H2^b$) mice (Husain et al., 1999). The M2-specific CD8+ T cell response is B cell dependent, transient and induced by the rapid increase in latently infected cells in the spleen around day 14 after infection (Usherwood et al., 2000). It expands and then contracts in parallel with latency amplification, reaching a peak 18 days after infection.

Attempts to improve $CD8^+$ CTL control of latency towards M2 had limited success. Adoptive transfer of $M2_{84-92}/K^d$-specific $CD8^+$ CTLs to BALB/c mice contributed to a reduction of the initial load of latently infected cells, however the long-term load was unaffected (Usherwood et al., 2000). Vaccination with the M2 antigen DNA also resulted in lower levels of latency *in vivo* at 14 days post-infection but did not prevent reaching normal long-term latent loads (Usherwood et al., 2001). A reduction in splenic long-term latent levels was only achieved by immunizing mice both intranasally and subcutaneously with adenoviral vectors encoding both M2 and M3 (Hoegh-Petersen et al., 2009). Thus, although a reduction in the latent loads was achieved neither strategy prevented the establishment of MuHV-4 latent infection. The relatively small contribution that M2-specific $CD8^+$ T cells apparently have in the control of latent infection is probably due to dominance of viral evasion over $CD8^+$ T cell function (details in section 1.3.6) (Stevenson and Efstathiou, 2005; Stevenson et al., 2009).

Thus, little is known about MuHV-4 latent antigenic-specific $CD8^+$ T cell responses and their importance for *in vivo* control of the virus-driven lymphoproliferation. A clear picture has come from a previous study conducted in our laboratory demonstrating that in BALB/c ($H2^d$) mice $CD8^+$ CTL recognition of the endogenous M2 epitope reduces MuHV-4 long-term latent loads (Marques et al., 2008). BALB/c mice display lower long-term latent loads than mouse strains not recognizing M2, such as C57BL/6 ($H2^b$), but not when infected with a recombinant virus in which the M2 epitope anchor residues have been mutated to prevent epitope binding to MHC class I and therefore presentation to $CD8^+$ T cells. Mutating the M2 epitope anchor residues increases long-term GC B cell colonization by MuHV-4 in $H2^d$ mice and restoring epitope presentation returns it to normal, consistent with the idea that disrupting $CD8^+$ T cell recognition of M2 allows more extensive proliferation of latently infected B cells (Marques et al., 2008). Thus, latent antigen-specific $CD8^+$ CTLs help to regulate long-term latent loads and for MuHV-4 this has been shown to depend on a single $CD8^+$ T cell epitope. Yet, the *in vivo* quantitative determinants of virus-driven lymphoproliferation control by $CD8^+$ CTL remain largely undefined.

Interestingly, in $H2^b$ mice, that do not recognize the endogenous M2 epitope, there is a massive expansion of non-classical $V\beta4^+$ $CD8^+$ T cells capable of producing IFNγ and TNFα (Braaten et al., 2006). The expansion of $V\beta4^+$ $CD8^+$ T cells begins 18 to 20 days post-infection (Evans et al., 2008) and has been shown to expand after the epitope-specific $CD8^+$ T cells already have declined (Stevenson et al., 1999a). This is considered as a back-up defence mechanism when classical $CD8^+$ T cell recognition of a key MuHV-4 target fails (Stevenson et al., 2009). However, the higher latent loads of $H2^b$ mice imply that the control exerted by $V\beta4^+$ $CD8^+$ T cells is not so efficient. In BALB/c ($H2^d$) mice infected with MuHV-4 (Evans et al., 2008) or in C57BL/6 ($H2^b$) mice infected with a viral recombinant deficient in viral $CD8^+$ T cell evasion (K3-deficient MuHV-4) (Stevenson et al., 2002), $V\beta4^+$ $CD8^+$ T cell expansion is minimal, probably because classical $CD8^+$ T cell recognition takes over. Nevertheless, non-classical $CD8^+$ T cell recognition seems to provide protection without overt disease when host genetics or viral evasion limit antigen presentation.

1.3.6. CD8+ T cell evasion during MuHV-4 infection

MuHV-4 represents a moving target for the host immune defences as it traffics from the lung to the lymphoid organs and from a lytic to a latent infection. Therefore, as with its human counterparts, immune evasion is a fundamental part of the MuHV-4 life cycle (Figure 1.6 and Table 1.4) (Feng et al., 2013; Hu and Usherwood, 2014; Stevenson et al., 2009). Studies with MuHV-4 have uncovered the importance of viral evasion for *in vivo* host colonization.

Two CD8+ T cell evasion genes have been identified in MuHV-4: *M3* and *mK3*. Both *M3* and *mK3* are expressed in the lytic cycle, but also in lymphoid tissue during latency establishment (Marques et al., 2003). *M3* and *mK3* mRNA has been detected in myeloid cells and in latently infected B cells, including in GC B cells (Marques et al., 2003). M3 and mK3 elicit two distinct CD8+ T cell evasion mechanisms that have been shown to be required to protect MuHV-4 infected cells from immune elimination by CD8+ T cells at the stage of acute latency amplification.

MuHV-4 M3 is a secreted broad-spectrum chemokine binding protein that binds selected CC and CXC chemokines with antiviral activity (Parry et al., 2000; van Berkel et al., 2000). After intranasal infection, an M3 deficiency had surprisingly little effect on lytic cycle replication, in the respiratory tract, or on the initial spread of virus to lymphoid tissues. However, there was a marked reduction in the amplification of latently infected B cells in the spleen (Bridgeman et al., 2001). *In vivo* this deficit was largely reverse by CD8+ T cell depletion, suggesting that the chemokine neutralization afforded by M3 may function to block effective CD8+ T cell recruitment into lymphoid tissue during MuHV-4 expansion of latency (Bridgeman et al., 2001; Rice et al., 2002). Human γHVs encode homologues of cellular cytokines and chemokines, including vIL-10 of EBV (Moore et al., 1990) and viral CC chemokine ligands (vCCLs, or MIPs) of KSHV (Moore et al., 1996; Nicholas et al., 1997b), that likely modulate the host immune response to favor viral infection.

mK3 is a homolog of KSHV-encoded K3 and K5, containing a RING domain and having E3 ubiquitin ligase activity. It is predominantly expressed in the endoplasmic reticulum membrane where it directly associates with and ubiquitinates the cytoplasmic tails of newly synthesized MHC class I glycoproteins, targeting them for proteosomal degradation, in contrast to KSHV K3 and K5, which induce rapid endocytose and lysosomal degradation of cell surface MHC class I molecules (Boname and Stevenson, 2001). mK3 can also degrade TAP and tapasin (Boname et al., 2004b; Boname et al., 2005), resembling EBV BLNF2a-mediated inhibition of TAP function. Thus, mK3 reduces cell surface expression of MHC class I molecules inhibiting recognition by antigen-specific CD8+ CTLs (Stevenson et al., 2000). *In vivo* depletion of MuHV-4 K3 has minimal effect on the viral clearance from the lung, but leads to attenuated viral latency amplification, a defect that can be reversed by CD8+ T cell depletion (Stevenson et al., 2002). Therefore, MHC class I inhibition seems to promote optimal seeding of latency without preventing the induction of

a robust and broad CD8⁺ T cell response during acute lytic infection (Freeman et al., 2010; Gredmark-Russ et al., 2008).

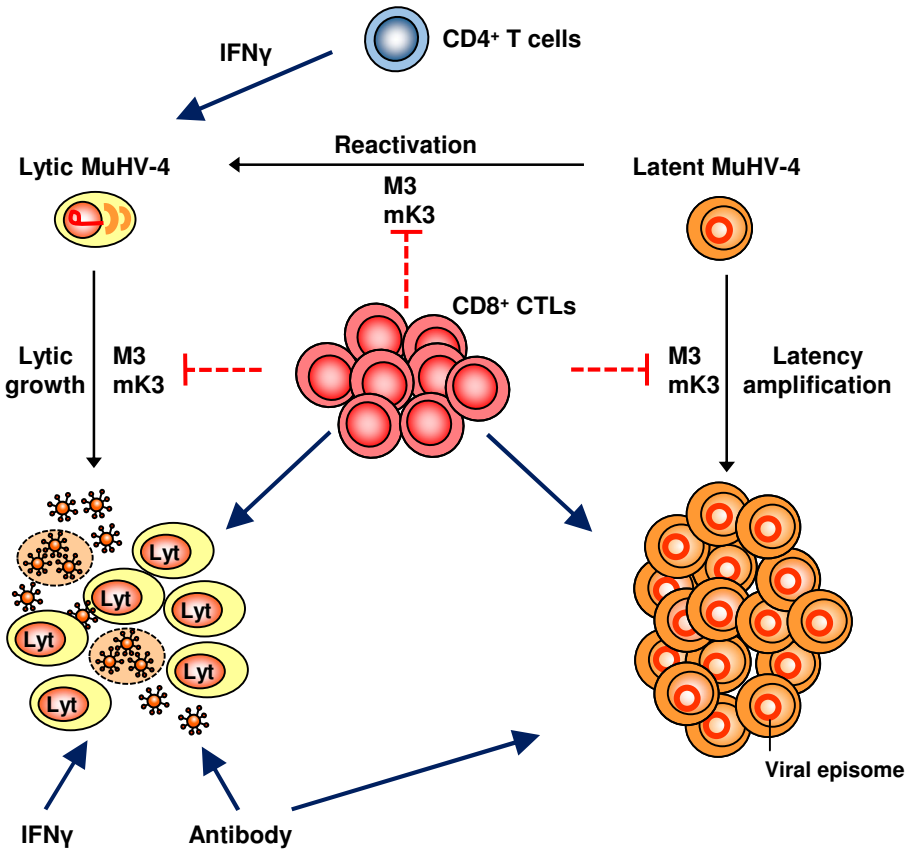

Figure 1.6. Immune evasion and immune control during MuHV-4 infection. CD8⁺ T cell evasion is a key aspect of MuHV-4 life cycle. MuHV-4 M3 and mK3 promote CD8⁺ T cell evasion during latency amplification and during lytic reactivation. CD4⁺ T cells play a role in limiting reactivation and low levels of lytic infection, likely through IFNγ signalling. Antibody also plays an important role in limiting the extent of viral reactivation as well as latency expansion (adapted from Stevenson et al., 2002).

Hence, MuHV-4 viral evasion of CD8⁺ T cell function increases the extent of acute virus-driven lymphoproliferation. Additionally, latency is a successful mechanism of evasion for all herpesvirus. Limiting antigen expression is the first and foremost long-term CD8⁺ T cell evasion mechanism. Even so, when latently infected cells divide, their viral episomes must be replicated and segregated by the viral episome maintenance protein. Thus, the MuHV-4 episome maintenance protein mLANA (Habison et al., 2012; Paden et al., 2012), although it lacks a glycine-alanine repeat (GAr) or an acidic central repeat (ACr) domain, similar to EBV EBNA1 and KSHV LANA, limits epitope presentation *in cis* through reduced protein synthesis and degradation (Bennett et al., 2005). Using MuHV-4 it was possible to define the *in vivo* contribution of *cis*-acting CD8⁺ CTL evasion to host colonization. If this *cis*-acting evasion is bypassed, CD8⁺ T cells ablate

latency, indicating that γHV have evolved mechanisms to keep episome maintenance immunologically silent and protected, since *cis*-acting evasion during episome maintenance was essential for normal host colonization (Bennett et al., 2005). Optimized expression of a $CD4^+$ T cell epitope during episome maintenance had no effect on host colonization *in vivo* (Smith et al., 2006).

In summary, studies in MuHV-4 have highlighted the importance of immune evasion for γHV to increase the number of latently infected cells and thus for effective host colonization.

Table 1.4. MuHV-4 $CD8^+$ T cell evasion mechanisms (adapted from Stevenson et al., 2009).

Gene	Site of action	Mechanism	Human γ-herpesvirus equivalents
K3	Lytic and latent	MHC class I and TAP degradation	EBV BNLF2a and KSHV K3 and K5
M3	Lytic and latent	Chemokine binding	Possibly EBV vIL-10 and KSHV vMIPs[a]
mLANA	Latency	Poor antigen presentation	EBV EBNA1 and KSHV LANA
M2	Latency	Selection of virus variants	EBV LMP2A and EBNA3B, KSHV K1

[a]These are functionally different from M3 but conform to the same strategy of a secreted lytic cycle protein that can afford immune evasion *in trans* in a mixed lytic/latent lesion.

1.3.7. MuHV-4 vaccination strategies

Owing to the oncogenic potential associated with EBV and KSHV persistent infection, vaccine development has focused on subunit vaccines. The discovery and establishment of MuHV-4 as an *in vivo* model of γHV infection has allowed researchers to explore and test proof of principle vaccination strategies (Wu et al., 2010; Wu et al., 2012). The goal is to pursue a vaccine strategy than can prevent or reduce long-term viral latency and hence lower tumour risk.

Peptide and subunit vaccination targeting lytic (glycoprotein150, glycoprotein B, ORF6, ORF61, M3) (Obar et al., 2004; Stevenson et al., 1999b; Stewart et al., 1999; Woodland et al., 2001b) and latency-associated viral proteins (M2) (Usherwood et al., 2001), heat-inactivated virions (Arico et al., 2004) and replication deficiency viruses (Kayhan et al., 2007) reduced the level of acute lung lytic replication and peak splenic latency of the challenge virus, however did not affect the establishment of long-term latency.

The only effective vaccination strategies that reduced long-term latency were based on live attenuated viruses, particularly viruses engineered to be deficient in the establishment of latency (Boname et al., 2004a; Fowler and Efstathiou, 2004; Freeman et al., 2012; Jia et al., 2010; Rickabaugh et al., 2004; Tibbetts et al., 2003). To achieve latency deficiency two principal strategies were exploited. One was to constitutively over-express the replication and

transcriptional activator (RTA), which is necessary and sufficient to disrupt latency and initiate the viral lytic cycle, thereby constantly driving the virus toward lytic replication (May et al., 2004; Rickabaugh et al., 2004). The other strategy was to eliminate the viral episome maintenance protein mLANA, thus preventing the virus from establishing splenic latency (Fowler et al., 2003; Moorman et al., 2003). Others have combined both strategies and generated a vaccine virus by replacing the locus containing mLANA and the potentially oncogenic proteins ORF72 (v-cyclin) and M11 (v-blc2) with the RTA expression cassete driven by a strong and constitutively active promotor (Freeman et al., 2012; Jia et al., 2010). These vaccines based on live attenuated viruses enable the presentation of a full *repertoire* of viral antigens in the context of active replication and thus effectively elicit humoral and cell-mediated immune responses. The next challenge is considered to be to attenuate viral lytic replication without losing immunogenicity. A rational approach is to eliminate viral immune evasion genes, especially those blocking MHC class I presentation, such as K3.

Based on these studies with MuHV-4 it has been proposed that live attenuated EBV and KSHV viruses unable to establish latency could be a viable option for vaccination (Wu et al., 2010). Furthermore, for post-exposure vaccination incorporation of epitopes derived from latent proteins is believed to be important to increase its efficacy. Overall, the development of safe and effective EBV and KSHV vaccines not only to induce protective immunity in naïve hosts, but also to enhance the immune control of virus carriers remains a major challenge.

1.4. Aims

The proliferation of latently infected cells and their control by $CD8^+$ T cells are central to γHVs pathogenesis. Latently expressed epitopes in B and tumour cells provide an immune target that has been successfully exploited to prevent and treat EBV-driven lymphoproliferative diseases in immunosuppressed transplant recipients by adoptive CTL transfer. However, efforts to optimize CTL-based immunotherapies to target other γHVs-associated tumours and to develop prophylactic and therapeutic vaccines have proved difficult. A major challenge consists in understanding the quantitative determinants of effective *in vivo* γHVs control by $CD8^+$ CTLs.

The narrow species tropism of human γHVs severely restricts *in vivo* analysis. Latent EBV transforms primary B cells *in vitro* and consequently immunological analysis has focused on *in vitro* recognition, mainly by $CD8^+$ T cells. However, most *in vivo* infected B cells have passed through GCs in lymphoid tissue and differentiated into long-lived resting memory B cells. Therefore, an important unknown is how far *in vivo* immune recognition matches the $CD8^+$ T cell mediated killing that is defined *in vitro*. That is, although many $CD8^+$ CTL targets have been identified, the functional impact of their engagement *in vivo* remains ill-defined.

MuHV-4 is a well-characterized animal model of γHV pathogenesis. Like EBV, it drives B cell proliferation in splenic GCs and persists in memory B cells. Hence, it provides a tractable experimental model that allows researchers to correlate biochemical interactions with *in vivo* immune function and infection control.

The aim of this thesis was to identify thresholds of immune engagement for effective *in vivo* $CD8^+$ CTL control of virus-driven B cell proliferation. Specifically, MuHV-4 was used to determine, for a single latently expressed epitope, how MHC class I binding and $CD8^+$ T cell functional avidity impact on *in vivo* infection control and host colonization.

1.5. Experimental strategy

During latency both transcriptional silencing and viral $CD8^+$ CTL evasion restrict the pool of possible epitopes. This creates a scenario in which amino acid variations in epitope sequences that affect peptide affinity for MHC class I and TCR functional avidity can have a major impact on *in vivo* immune control and consequently on host colonization. EBV LMP2A, KSHV K1 and MuHV-4 M2 are latently expressed functional homologues that modulate B cell signaling and represent potential $CD8^+$ CTL targets. Additionally, all show evidence of amino acid sequence diversity, consistent with immune selection. Therefore, the diversity of LMP2A, K1 and M2 prompt the *in vivo* analysis of the consequences of varying MHC class I binding and $CD8^+$ T cell functional avidity for a single epitope derived from M2.

MuHV-4 infection of mice makes addressing this question experimentally possible because long-term MuHV-4-driven proliferation of latently infected B cells in GCs was shown to be regulated by $CD8^+$ CTLs directed against a single $H2K^d$-restricted epitope present in the M2 protein - $M2_{84-92}/K^d$ – GFNKLRSTL (Figure 1.7 panel A). This epitope is recognized *in vivo* by $CD8^+$ CTLs of BALB/c ($H2^d$) mice but not of C57BL/6 ($H2^b$) mice and it constitutes the only latent-specific CTL epitope identified, thus far, for MuHV4. Thus, lack of an endogenous $H2^b$-restricted M2 epitope allowed the introduction of new $CD8^+$ CTL targets in a context where it is known to be important.

The experimental strategy involved infection of $H2^b$ mice with MuHV-4 recombinants engineered to express from the M2 C-terminus the well characterized $H2K^b$-restricted epitope comprising amino acid residues 257-264 of ovalbumin (OVA) or derived altered peptide ligands (APLs) (Figure 1.7 panel B). The choice of an $H2^b$ haplotype renders the endogenous $H2K^d$-restricted $M2_{84-92}$ epitope unrecognised by $CD8^+$ T cells of C57BL/6 mice, making possible to analyse the impact of OVA or APLs as single epitopes on the control of MuHV-4-induced lymphoproliferation. Furthermore, by attaching each epitope to the M2 C-terminus, this strategy allows expression of the introduced epitopes with the kinetics and copy number of a known endogenous latent epitope. Thus, this constitutes a physiologically relevant approach to epitope presentation since it conforms to normal latent gene expression.

First, OVA and APLs were characterized *in vitro* for MHC class I binding and $CD8^+$ T cell functional avidity was assessed using $CD8^+$ T cells purified from OT-I mice, which express a transgenic rearranged TCR designed to recognize $OVA_{257-264}$ in the context of $H2K^b$. Subsequently, the experimental approach involved infection of three independent but complementary $H2^b$ mouse models with the engineered MuHV-4 epitope recombinants (Figure 1.7).

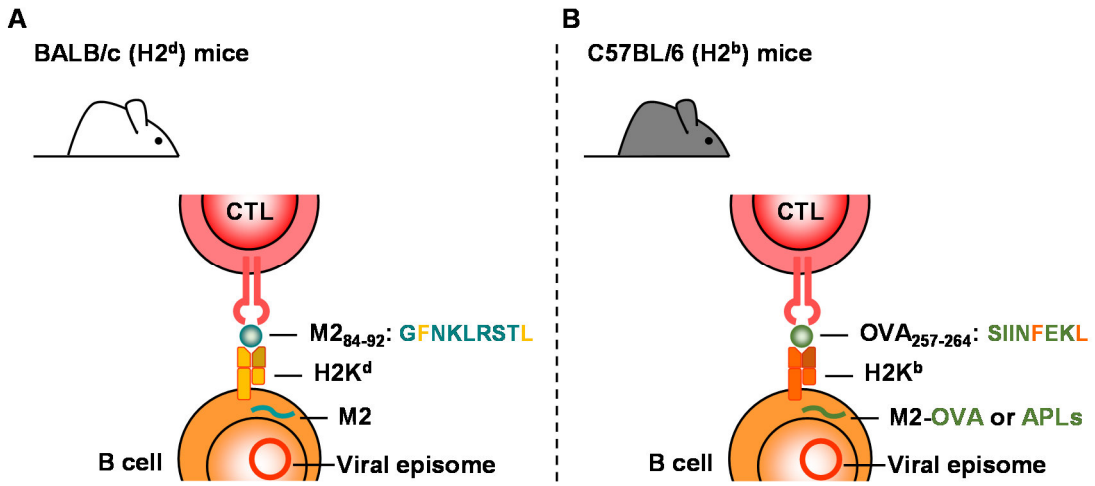

Figure 1.7. Generation of MuHV-4 recombinants expressing OVA or APLs thereof linked to M2. (A) $CD8^+$ cytotoxic T lymphocytes (CTLs) from BALB/c ($H2^d$) mice recognize latently infected B cells displaying on MHC class I ($H2K^d$) molecules the $H2K^d$-restricted epitope comprising amino acid residues 84-92 of the M2 latency-associated protein ($M2_{84-92}/K^d$ – GFNKLRSTL). $CD8^+$ CTL recognition of this single latent epitope controls long-term MuHV-4-driven B cell proliferation in GCs, in $H2^d$ mice. The epitope anchor residues, which are the amino acid residues that mediate binding to the MHC molecule, are shown in yellow. (B) MuHV-4 epitope recombinants were engineered to express from the M2 C-terminus the $H2K^b$-restricted epitope comprising amino acid residues 256-264 of chicken ovalbumin (OVA) or altered peptide ligands (APLs) thereof. Lack of an endogenous $H2^b$-restricted M2 epitope allowed to determine for a single latently expressed epitope how variations in MHC class I binding and $CD8^+$ T cell functional avidity impact on host colonization, in C57BL/6 ($H2^b$) mice. The epitope anchor residues are represented in orange.

The impact of MHC class I binding by a single latently expressed epitope derived from M2 on *in vivo* host colonization was addressed in C57BL/6 ($H2^b$) mice, which mount polyclonal $CD8^+$ T cell responses (Figure 1.8 panel A). Both the ability of MuHV-4 epitope recombinants to drive the proliferation of latently infected B cells in GCs and the $CD8^+$ T cell responses elicited were determined upon infection of mice.

Then, to investigate the relevance of $CD8^+$ T cell functional avidity for *in vivo* control of MuHV-4 latent infection, we focused on the well-established OT-I transgenic mouse model, which has a single TCR specificity for $OVA_{257-264}/K^b$ (Figure 1.8 panel B). OT-I ($H2^b$) mice were intranasally infected with MuHV-4 recombinants expressing epitopes with comparable $H2K^b$ binding but with different TCR functional avidities and the splenic latent loads established in the host were determined. The $CD8^+$ T cell functional avidity defined *in vitro* for each epitope was related to *in vivo* virus control.

Finally, to overcome the deficit in $CD4^+$ T cell help and GC formation inherent to OT-I transgenic mice, which impairs the ability of MuHV-4 to driven B cell proliferation in GCs, polyclonal $CD4^+$ T cells purified from C57BL/6 mice and OT-I cells isolated from CD45.1 $Rag1^{-/-}$ OT-I mice were adoptively transferred into $TCR\alpha^{-/-}$ ($H2^b$) recipients, one day prior to infection (Figure 1.8 panel C).

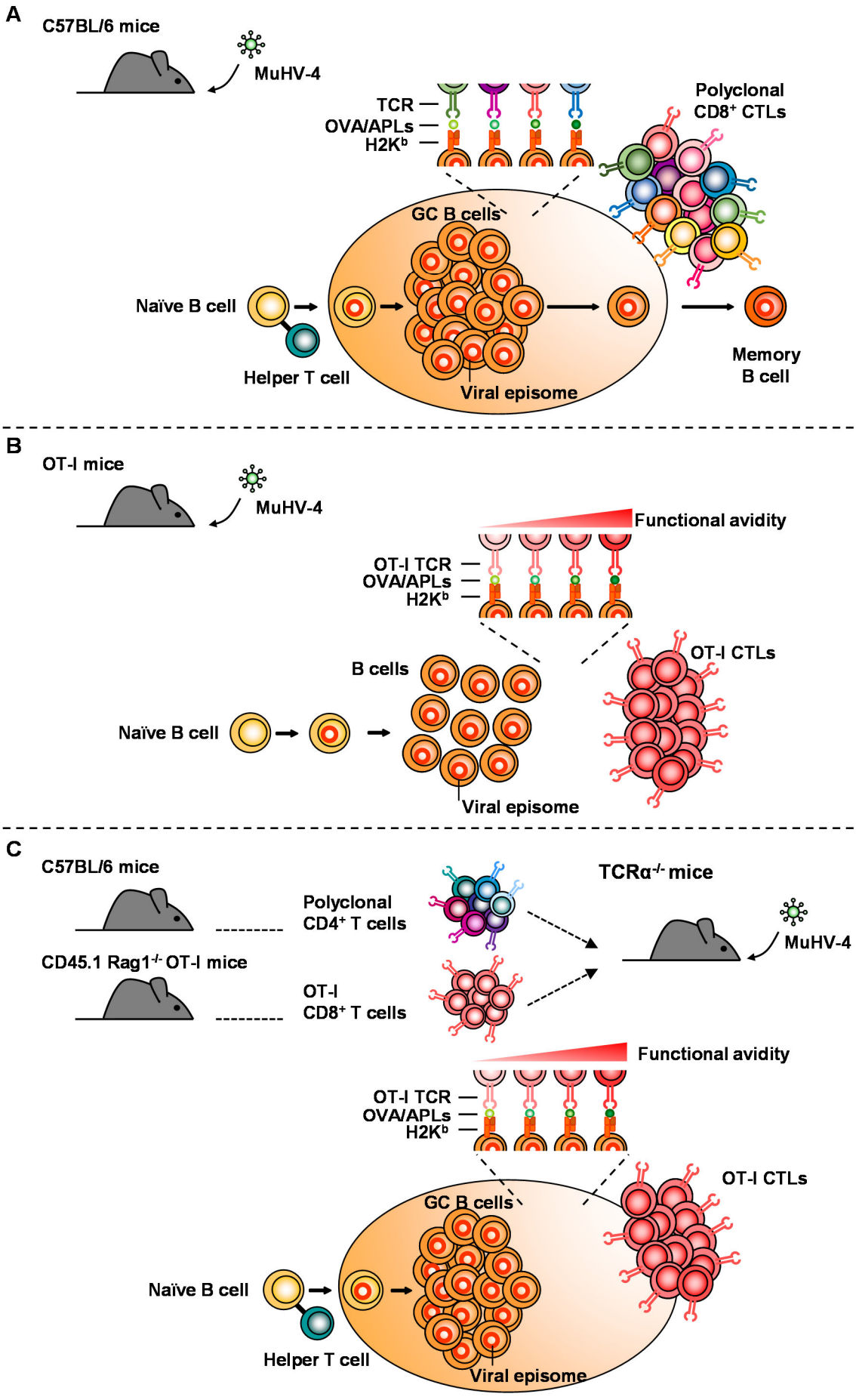
A
C57BL/6 mice
MuHV-4
TCR
OVA/APLs
H2K^b
Polyclonal
CD8$^+$ CTLs
GC B cells
Naïve B cell
Helper T cell
Viral episome
Memory
B cell
B
OT-I mice
MuHV-4
Functional avidity
OT-I TCR
OVA/APLs
H2K^b
OT-I CTLs
B cells
Naïve B cell
Viral episome
C
C57BL/6 mice
Polyclonal
CD4$^+$ T cells
CD45.1 Rag1$^{-/-}$ OT-I mice
OT-I
CD8$^+$ T cells
TCRα$^{-/-}$ mice
MuHV-4
Functional avidity
OT-I TCR
OVA/APLs
H2K^b
OT-I CTLs
GC B cells
Naïve B cell
Helper T cell
Viral episome

Figure 1.8. Experimental approach – MuHV-4 epitope recombinants were used to identify for a single latently expressed epitope functional immune engagement thresholds for *in vivo* CD8$^+$ CTL control of virus-driven B cell proliferation. (A) Impact of MHC class I binding on host colonization. C57BL/6 (H2^b) mice were intranasally infected with MuHV-4 recombinants expressing OVA or APLs linked to M2 (described in Figure 1.7, panel B). The ability of each MuHV-4 recombinant to drive the proliferation of latently infected cells in GCs and to elicit epitope-specific CD8$^+$ CTL responses were measured in the context of a polyclonal TCR *repertoire*. (B) Impact of CD8$^+$ T cell functional avidity on the control of MuHV-4 latent infection. OT-I transgenic (H2^b) mice, whose CD8$^+$ T cells express a transgenic TCR designed to recognize OVA$_{257-264}$ in the context of H2K^b, were intranasally infected with MuHV-4 epitope recombinants with similar MHC class I binding but that elicit OT-I T cell responses with different functional avidities. Latent infection levels established in the spleen were determined in this monoclonal CD8$^+$ T cell setting. The limited CD4$^+$ T cell *repertoire* of OT-I mice impairs GC formation. (C) Impact of CD8$^+$ T cell functional avidity on the control of MuHV-4-driven proliferation of latently infected cells in GCs. To overcome the deficit in CD4$^+$ T cell help and, thus, on GC formation inherent to OT-I mice, polyclonal CD4$^+$ T cells purified from C57BL/6 mice and OT-I cells isolated from CD45.1 Rag1$^{-/-}$ OT-I mice were adoptively transferred into TCRα$^{-/-}$ (H2^b) recipients, one day prior to infection with MuHV-4 epitope recombinants. Reconstituted mice had, therefore, polyclonal CD4$^+$ T cells and a monoclonal CD8$^+$ T cell compartment restricted to OT-I cells. These mice were used to determine how different TCR engagement thresholds by a latency epitope affect CD8$^+$ CTL of MuHV-4-driven B cell proliferation in GCs.

Thus, the reconstituted mice had polyclonal CD4$^+$ T cells and a monoclonal CD8$^+$ TCR transgenic compartment restricted to OT-I cells. This approach allowed to investigate the outcome of different TCR engagement thresholds on the in vivo CD8$^+$ CTL response and on the ability of MuHV-4 to driven the proliferation of latently infected B cells in GCs.

CHAPTER 2

Generation and characterization of MuHV-4 recombinants expressing OVA or APL derivates linked to M2

Generation and characterization of MuHV-4 recombinants expressing OVA or APL derivates linked to M2

Control of γHV latent infection is notorious complex. γHV colonize multiple cell types and infected cells can have distinct patterns of viral gene expression. Moreover, γHV have developed several strategies to subvert host immune surveillance in order to amplify the pool of latently infected cells and achieve long-term persistence. Evasion of immune recognition is further accomplished with transcriptional silencing during latency, which additionally restricts the pool of possible $CD8^+$ CTL targets. Thus, a major challenge consists in understanding the key determinants for efficient $CD8^+$ CTL control of virus-driven lymphoproliferation. EBV LMP2A, KSHV K1 and MuHV-4 M2, are latently expressed functional homologues that modulate B cell signaling and represent potential $CD8^+$ CTL targets. Additionally, all show evidence of amino acid sequence diversity, consistent with immune selection. Therefore, amino acid variations in epitope sequences that affect MHC class I binding or $CD8^+$ T cell functional avidity may have a major impact on *in vivo* infection control and, consequently, on host colonization.

To identify for a single latently expressed epitope how MHC class I binding and $CD8^+$ T cell functional avidity affect *in vivo* $CD8^+$ CTL control of γHV-driven lymphoproliferation, the well characterized $H2K^b$-restricted epitope comprising amino acid residues 257-264 of ovalbumin (OVA) or derived altered peptide ligands (APLs) were selected for expression from MuHV-4 M2 C-terminus. Q4, V4, G4, R4 and E1 APLs were selected since their biological properties have been extensively documented previously, namely their TCR affinity (Alam et al., 1999; Alam et al., 1996; Rosette et al., 2001), the fate they induce in thymocyte development (positive vs negative selection) (Daniels et al., 2006; Hogquist et al., 1994; Jameson et al., 1994) and their capacity to activate $CD8^+$ T cells in the periphery (Denton et al., 2011; Hommel and Hodgkin, 2007; Jameson et al., 1993; Zehn et al., 2009). As shown in Table 2.1 the group includes strong agonists, weak and very weak agonists and peptides that exhibit antagonist activity. This strategy allowed the generation of a very well-defined model epitope with the kinetics and copy number of a known endogenous epitope. The choice of an $H2^b$ haplotype renders the endogenous $H2K^d$-restricted $M2_{84-92}$ epitope unrecognised by $CD8^+$ T cells of C57BL/6 ($H2^b$) mice, making possible to analyse the impact of OVA or APLs as single epitopes on the control of MuHV-4-induced lymphoproliferation.

In this chapter OVA and APLs were first characterized for MHC class I binding and TCR functional avidity. Next, each epitope was introduced at the MuHV-4 M2 C-terminus and the engineered MuHV-4 epitope recombinants were analysed and characterized.

Table 2.1. Biological properties of OVA and APLs selected to generate MuHV-4 epitope recombinants.

Peptide	Sequence	TCR affinity K_d (μM)[a]	Thymocyte selection[b]	Mature $CD8^+$ T cell activation[c]
OVA	SIINFEKL	6.5	Negative	Strong agonist
Q4	SIIQFEKL	n.d.	Negative	Weak agonist
V4	SIIVFEKL	n.d.	Positive	Very weak agonist
G4	SIIGFEKL	10	Positive	Very weak agonist
E1	EIINFEKL	22.6	Positive	Partial agonist/ antagonist
R4	SIIRFEKL	57.1	Positive	Antagonist

n.d.; not determined.

[a]Alam et al., 1999; Alam et al., 1996; Rosette et al., 2001.

[b]Daniels et al., 2006; Hogquist et al., 1994; Jameson et al., 1994.

[c]Denton et al., 2011; Hommel and Hodgkin, 2007; Hogquist et al., 1994; Jameson et., 1993; Zhen et al., 2009.

2.1. Characterization of altered peptide ligands by MHC class I binding

OVA is known to bind to $H2K^b$ with high affinity (K_d 4.1nm) (Matsumura et al., 1992). To compare the ability of OVA and APLs to bind MHC class I a $H2K^b$ stabilization assay was performed on TAP-deficient RMA-S cells (Schumacher et al., 1990) using graded doses of each peptide (Figure 2.1, panel A). This experiment was performed by Dr Sofia Marques in our laboratory.

The mutant mouse lymphoma cell line RMA-S has a defect in class I assembly and expresses markedly reduced levels of empty class I molecules at the cell surface (Karre et al., 1986; Ljunggren and Karre, 1985; Powis et al., 1991). Cell surface assemble of class I molecules on RMA-S is stabilized both by incubation with peptide (Townsend et al., 1989) and by reduction of the temperature from 37ºC to 26ºC (Ljunggren et al., 1990). Therefore, RMA-S cells were first incubated overnight at 26°C to increase the level of empty surface H-$2K^b$ molecules. Then, RMA-S cells were loaded with graded concentrations of OVA and APL soluble peptides for 2h at 26°C and subsequently transferred to 37ºC to destroy empty $H2K^b$ molecules (Schumacher et al., 1990). The mean fluorescence intensity of $H2K^b$-specific staining on peptide-pulsed RMA-S cells was analysed by flow cytometry and the half-maximum effective concentration (EC_{50}) values required for surface $H2K^b$ stabilization were calculated for OVA and APL peptides from the constructed sigmoidal dose-response curves.

The concentration of OVA peptide required for inducing an half-maximum stabilization of $H2K^b$ was 40 nM, which is in close agreement with previous published data (Chen et al., 1994). The selected APLs Q4, V4, G4 and R4 were able to stabilize K^b cell surface expression to a similar degree as the native OVA peptide (EC_{50} within 2-fold) (Figure 2.1, panels A and B). This result is consistent with residue 4 being an important TCR contact residue and, consequently solvent-exposed according to the $H2K^b$-OVA complex crystal structure (Fremont et al., 1995; Jameson

and Bevan, 1992). For E1 peptide to achieve equivalent stabilization of $H2K^b$ a 6-fold higher peptide concentration was required (Figure 2.1, panel B). This result is in conformity with this residue being only partly exposed (Fremont et al., 1995) and with structural and biophysical analysis demonstrating decreased epitope stability for E1 (Denton et al., 2011). As expected, mutation of one anchor residue (leucine 8 to an alanine, A8 peptide) resulted in decreased surface $H2K^b$ stabilization. A8 required approximately 60-fold more peptide comparing to OVA (Figure 2.1, panel B). Finally, $H2K^b$ stabilization was completely lost when the two main anchor residues (phenylalanine 5 and leucine 8) were both mutated to alanines (A5A8 peptide) (Figure 2.1, panels A and B).

In agreement with published data (Denton et al., 2011; Zehn et al., 2009), all APLs were able to stabilize $H2K^b$ cell surface expression on RMA-S cells similarly to the OVA peptide, with the exception of E1 for which a 6-fold higher concentration of peptide was required to achieve equivalent stabilization.

2.2. Characterization of altered peptide ligands by TCR functional avidity

The functional avidity of OT-I cells for OVA and each APL was determined by *ex vivo* stimulation of $CD8^+$ T cells purified from OT-I mice with graded peptide doses. $CD8^+$ T cells from OT-I mice carry a transgenic TCR designed to recognize ovalbumin residues 257-264 (OVA) in the context of $H2K^b$ (Hogquist et al., 1994). Dose response curves of the capacity of each APL to stimulate IFNγ production in OT-I cells are shown (Figure 2.1, panel C). The concentration required for each peptide to achieve a half-maximum IFNγ response (EC_{50}) in OT-I cells is indicated (Figure 2.1, panel D). A detailed description of the experiment can be found in Material and Methods, section 9.2.11.1.

As expected, APLs differed in their potency for stimulating OT-I cells, showing a clear hierarchy in dose-response, with OVA>Q4>V4>G4>E1>R4. The original OT-I ligand, OVA, was the most potent in stimulating OT-I cells followed by Q4, for which a 14-fold higher concentration of peptide was required for equivalent IFNγ production. V4 and G4 required 3,760-fold and 198,000-fold higher concentrations of peptide, respectively. E1 exhibited the lowest functional avidity and R4 was not capable of stimulating IFNγ production by OT-I cells, which is in agreement with this APL as being described as an antagonist towards OT-I cells (Hogquist et al., 1994; Jameson et al., 1993).

Thus, the results obtained demonstrate that OT-I cells exhibit a hierarchy of functional avidities for the selected APLs, that match the reported TCR affinity and ability of each APL to support $CD8^+$ T cell activation (Table 2.1).

A

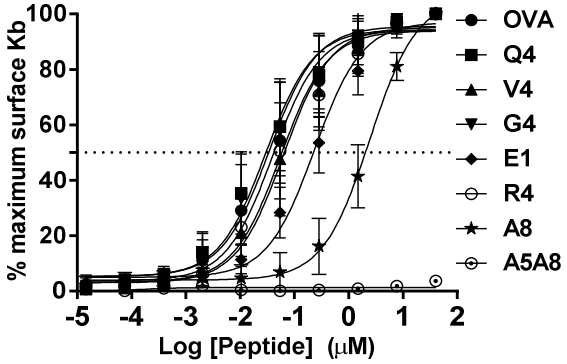

B

Peptide	EC_{50} (μM)	EC_{50} APL/OVA
OVA	0.040	1.0
Q4	0.030	0.8
V4	0.063	1.6
G4	0.034	0.9
R4	0.056	1.4
E1	0.235	5.9
A8	2.466	61.7
A5A8	------	------

C

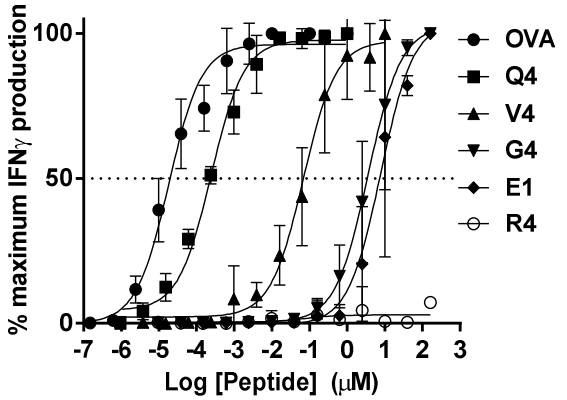

D

Peptide	EC_{50} (μM)	EC_{50} APL/OVA
OVA	1.82E-05	1.00E+00
Q4	2.43E-04	1.35E+01
V4	6.85E-02	3.76E+03
G4	3.61E+00	1.98E+05
E1	7.78E+00	4.27E+05
R4	------	------

Figure 2.1. Characterization of APLs by MHC class I binding and TCR functional avidity. (A) The capacity of OVA and individual APLs to stabilize surface $H2K^b$ on TAP-deficient RMA-S cells was determined using graded doses of each peptide. The mean fluorescence intensity of K^b-specific staining on peptide-pulsed RMA-S cells was obtained by flow cytometry. Shown is the percentage of maximum surface $H2K^b$ stabilization for each peptide. (B) The half-maximum effective concentration (EC_{50}) values required for surface $H2K^b$ stabilization were calculated for OVA and APLs from the sigmoidal dose-response curves using the GraphPad Prism software. EC_{50} APL/OVA values represent the ratio of the concentration of each APL divided by the concentration of native OVA peptide required for a half-maximum surface H-$2K^b$ stabilization. (A) and (B) were determined by Dr Sofia Marques in our laboratory. Data show results obtained in three independent experiments. (C) Functional avidity of OT-I cells for OVA and APL peptides was determined by constructing dose-response curves of the capacity of each peptide to stimulate IFNγ production in $CD8^+$ T cells purified from OT-I mice. (D) EC_{50} values required for inducing a half-maximum IFNγ response in OT-I cells and EC_{50} APL/OVA rations were determined as before. Data were reproducible over four independent experiments performed in duplicates each time.

2.3. Generation of MuHV-4 recombinants expressing OVA or derived APLs linked to M2

Each of the previously characterized epitopes was then introduced at the MuHV-4 M2 C-terminus (Figure 2.2, panel A). This strategy ensures expression of the introduced epitopes during latency without compromising M2 function, as shown before (Marques et al., 2008).

MuHV-4 recombinants were generated using a previously described methodology (Adler et al., 2000), which utilizes MuHV-4 cloned as a bacterial artificial chromosome (BAC). This technique allows the maintenance of the viral genome as a BAC in *Escherichia coli* and site-directed mutagenesis of the genome by homologous recombination (Adler et al., 2003). MuHV-4 recombinants expressing epitopes with comparable $H2K^b$ binding were also engineered with a yellow fluorescent protein (YFP) reporter construct to facilitate, based on YFP expression, tracking of infected cells, phenotypic analysis of infected cell populations and quantification of infection, by flow cytometry (Collins et al., 2009). The generation and initial characterization of these recombinant viruses are described in detail in Materials and Methods, section 9.2.5. Briefly, verification of the introduced epitopes was carried out by restriction enzyme digestion and sequencing across the *M2 ORF* in the BAC vector. The genomic structure and integrity of generated viruses was verified by examination of restriction enzyme digestion profiles of *E. coli*-derived BAC DNA.

Infectious viruses were reconstituted by transfection of BAC DNA into BHK-21 fibroblasts. Since MuHV-4 containing BAC sequences is attenuated *in vivo* compared to the wild type (WT) (Adler et al., 2001), these sequences were removed by propagating the viruses in fibroblasts expressing Cre recombinase. BAC sequences are flanked by *lox*P sites and Cre recombinase expression from the cellular genome allows efficient excision of the BAC sequences during cellular growth.

Viral genome integrity in the region subjected to homologous recombination was further analysed by PCRs across the *Hind*III-E region in plaque-purified viral DNA (Figure 2.2, panels B and C and Figure 2.3, panels A and B). The stability of the introduced epitopes was checked in viruses recovered from lytically infected BHK-21 cells or latently infected spleens, by sequencing the *M2* gene in viral high molecular height (HMW) DNA extracted from BHK-21 or from at least four different mice, respectively. This analysis confirmed the retention of the introduced epitopes following *in vitro* and *in vivo* infection.

A

MuHV-4 Recombinants	Epitope Sequence
vOVA	M2 - SIINFEKL
vQ4	M2 - SIIQFEKL
vV4	M2 - SIIVFEKL
vG4	M2 - SIIGFEKL
vR4	M2 - SIIRFEKL
vE1	M2 - EIINFEKL
vA8	M2 - SIINFEKA

B

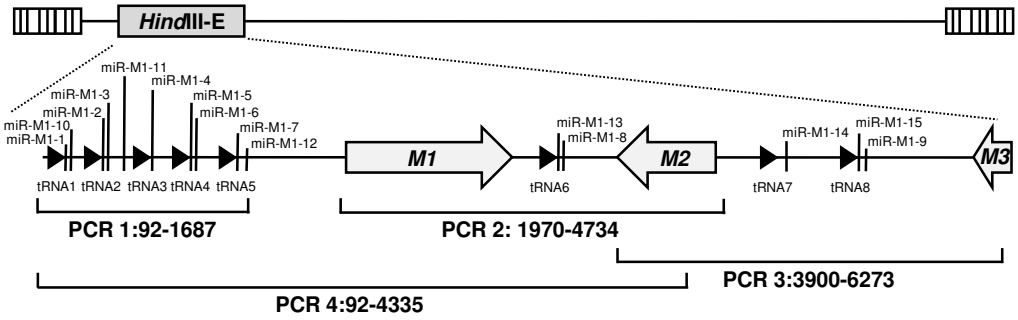

C

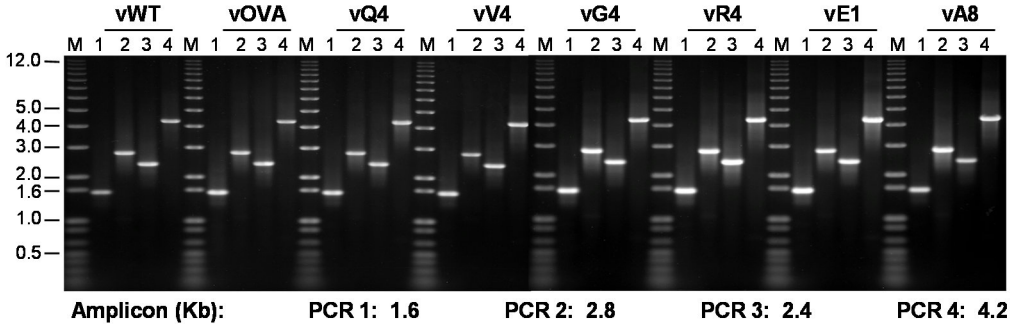

Figure 2.2. Construction and verification of the genomic integrity of MuHV-4 recombinants expressing OVA or APLs linked to M2. (A) MuHV-4 recombinant viruses were generated to express the well characterized H2K^b-restricted OVA$_{257-264}$ epitope or derived APLs from the *M2* C-terminus. Amino acid sequences of the introduced epitopes are shown. Blue residues denote single amino acid alterations introduced in native OVA epitope. (B) Schematic representation of the MuHV-4 genome and in particular of the *Hin*dIII-E region. ORFs are represented as shaded arrows and the eight viral tRNAs as small arrow heads. The fifteen miRNAs are shown. Amplicon genomic coordinates for PCRs performed across the *Hin*dIII-E region are indicated. (C) PCR analysis of recombinant viral DNA to confirm genome integrity in the *Hin*dIII-E region. High molecular weight DNA was purified from lytically infected BHK-21 cells. Expected size for each PCR is shown. PCR products were electrophoresed on a 0.8% agarose gel and stained with gel red. Markers consisting of a 1 Kb Plus DNA ladder (Invitrogen) are shown to the left of each virus.

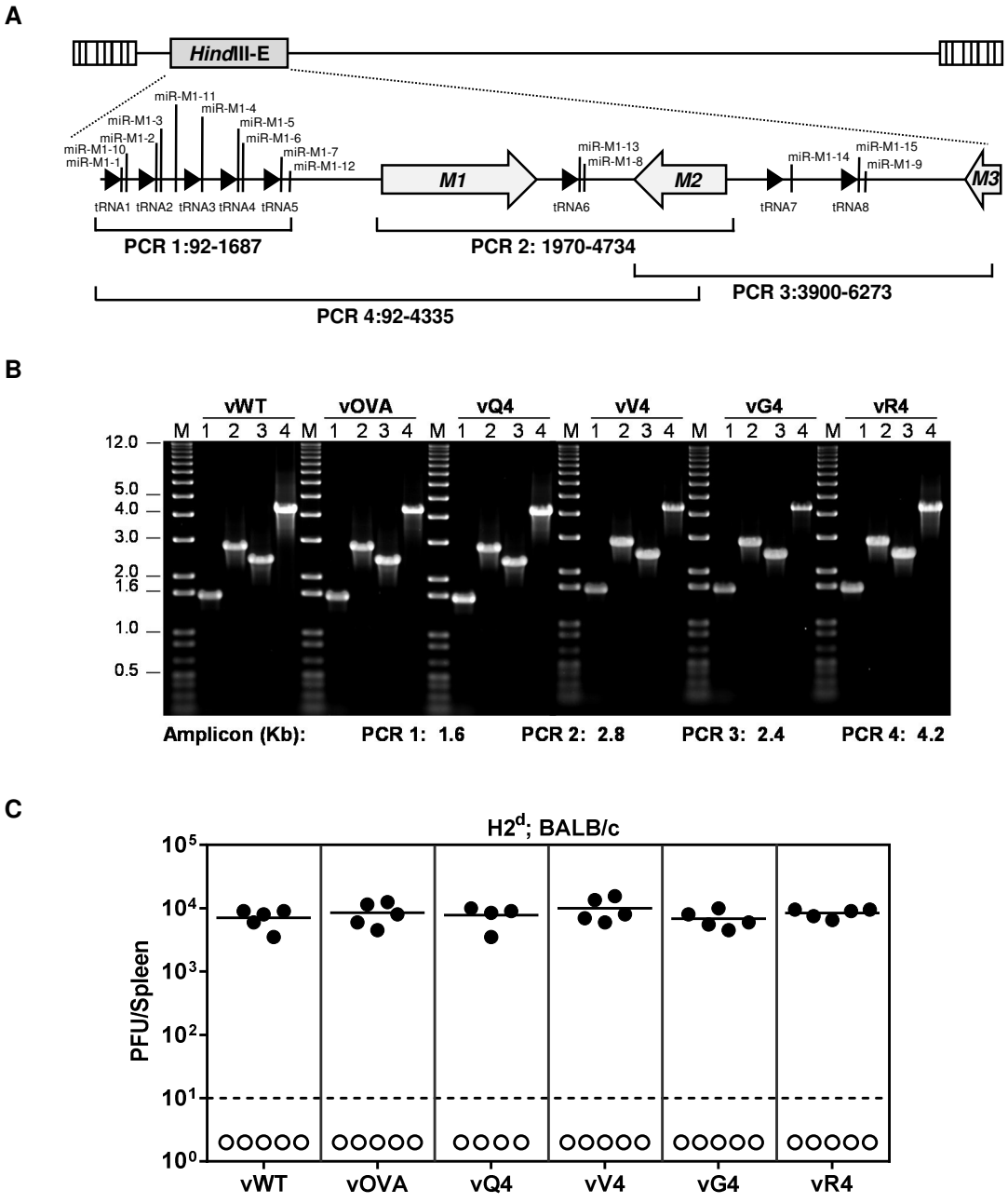

Figure 2.3. Generation and characterization of YFP-expressing MuHV-4 epitope recombinants. $H2K^b$-restricted $OVA_{257-264}$ epitope or APL derivates were introduced in fusion with the *M2* C-terminus of YFP-expressing MuHV-4. (A-B) PCR analysis of recombinant viral DNA to confirm genome integrity in the region subjected to homologous recombination during YFP BAC mutagenesis in *E.coli*. (A) Schematic representation of the MuHV-4 genome and in particular of the *Hin*dIII-E region. ORFs are represented as shaded arrows and the eight viral tRNAs and 15 miRNAs are shown. Amplicon genomic coordinates for PCRs performed across the *Hin*dIII-E region are indicated. (B) High molecular weight DNA extracted from MuHV-4 lytically infected BHK-21 fibroblasts (5 PFU/cell) was checked by PCR for genome integrity in the *Hin*dIII-E region. Expected size for each PCR is shown. PCR products were electrophoresed on a 0.8% agarose gel and stained with gel red. Markers consisting of a 1 Kb Plus DNA ladder (Invitrogen) are shown to the left of each virus. (C) $H2^d$ BALB/c mice were intranasally inoculated with 10^4 PFU of YFP-expressing MuHV-4 (vWT) or YFP-expressing MuHV-4 epitope recombinants. At 14 days p.i., spleens were removed, single cell splenocyte suspensions were prepared and latent infection in each sample was quantified by *ex vivo* reactivation assay (closed symbols). Pre-formed infectious viruses were analysed by plaque assay (open symbols). Each point represents the titre of an individual mouse. Horizontal bars show arithmetic means. The dashed horizontal line indicates the limit of detection of the assay. Latent loads of YFP-

expressing MuHV-4 epitope recombinants were not significantly different from those of vWT ($p>0.05$, by ordinary one-way ANOVA followed by Dunnett's multiple comparisons test). No pre-formed infectious viruses were detected for any of the viruses analysed.

2.4. MuHV-4 epitope recombinants display normal replication *in vitro* and *in vivo*

In vitro lytic replication kinetics for each of the engineered epitope recombinants was compared to that of the WT virus by constructing multi-step growth curves in permissive BHK-21 cells (Figure 2.4, panel A). Each recombinant virus showed equivalent *in vitro* growth kinetics.

The course of MuHV-4 infection upon intranasal inoculation is characterized by the establishment of a productive infection in alveolar epithelial cells that peaks at around 4-7 days and is then resolved to undetectable levels by 10 to 12 days post-infection (p.i.) (Sunil-Chandra et al., 1992a).

In vivo acute phase replication kinetics was determined for each MuHV-4 recombinant virus and compared to that of the WT virus in lung tissue of infected C57BL/6 mice (Figure 2.4, panel B). Following intranasal inoculation of C57BL/6 mice, lungs were removed at 4, 7 and 11 days p.i., subjected to freeze-thawing to disrupt cells, and the titre of infectious virus was determined in lung homogenates by plaque assay. All viruses showed identical *in vivo* replication kinetics in the lungs of infected mice, with peak titers at 4-7 days p.i. and clearance by day 11.

These results demonstrate that introducing an epitope at the M2 C-terminus does not affect the ability of MuHV-4 recombinants to replicate *in vitro* or *in vivo*, as previously reported (Marques et al., 2008). Additionally, obtained results are in agreement with previous studies demonstrating that M2 is dispensable for lytic replication *in vitro* and for normal acute phase replication kinetics in lung tissue following intranasal infection of mice (Jacoby et al., 2002; Macrae et al., 2003; Simas et al., 2004).

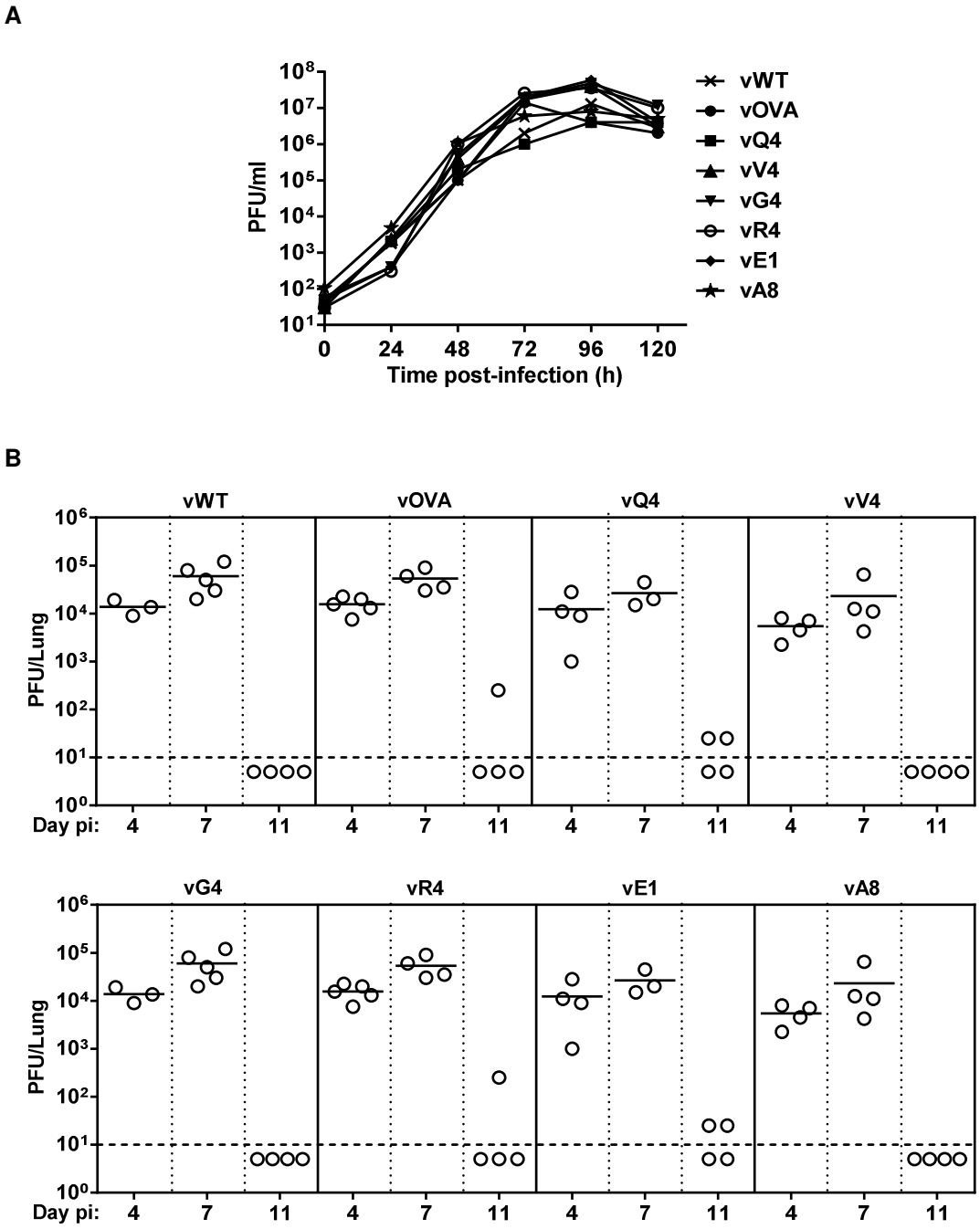

Figure 2.4. MuHV-4 epitope recombinants display normal *in vitro* and *in vivo* replication kinetics. (A) Multi-step growth curves were constructed for vWT and for the indicated recombinant viruses by infection of BHK-21 cells at low multiplicity (0.01 PFU/cell). At the indicated times post-infection (p.i.), samples were harvested, freeze-thawed and virus titres were determined by plaque assay on monolayers of BHK-21 cells. *In vitro* lytic replication kinetics of the recombinant viruses were not significant different from vWT ($p>0.05$, by ordinary one-way ANOVA followed by Dunnett's multiple comparisons test). (B) C57BL/6 ($H2^b$) mice were intranasally infected with 10^4 PFU of the indicated viruses and *in vivo* virus replication in lungs was quantified by plaque assay. Each point shows the titre of an individual mouse. Horizontal lines indicate arithmetic means. The dashed horizontal line represents the limit of detection of the assay. No MuHV-4 recombinant showed a deficit relative to vWT ($p>0.05$, using ordinary one-way ANOVA followed by Tukey's multiple comparisons test).

2.5. MuHV-4 epitope recombinants establish normal latency in $H2^d$ mice

Lytic replication in the lung is followed by dissemination to lymphoid tissue, namely lymph nodes and the spleen, where MuHV-4 establishes latent infection. Latent infection in the spleen is characterized by proliferation of infected B cells and consequent amplification of latent virus, peaking around 14 days p.i., and decreasing quickly thereafter to reach low but steady state levels of latency, that persist and remain stable throughout the entire life of the host (Cardin et al., 1996; Flano et al., 2003; Marques et al., 2003; Simas and Efstathiou, 1998; Sunil-Chandra et al., 1992a).

Introduction of an $H2K^b$-restricted epitope in M2 is not expected to impact on the ability of MuHV-4 to establish latency in $H2^d$ mice. Therefore, to analyse the ability of the engineered recombinants to establish latent infection, BALB/c ($H2^d$) mice were infected intranasally with the WT virus or MuHV-4 recombinants expressing OVA or APLs, and the latent load in the spleen was determined by quantification of *ex vivo* reactivation competent viruses by infectious centre assay.

Infectious centre assay is a well-established assay in which single cell suspensions are prepared from the harvested spleens and co-cultured with permissive fibroblast cells. The presence of latent virus in the splenocyte population is revealed by the observation of cytophatic effect (cpe) (plaques of cell lysis) on fibroblast monolayers. Unless preformed infectious virus are present at the time of harvest, the cpe can only result from viral reactivation from latency. Thus, to confirm that the results obtained for each virus reflect truly latent infection, spleen samples must also be analysed for the presence of pre-formed infectious viruses. To this end, replicate samples are subjected to freeze-thawing to disrupt the cells and, consequently, any possibility of reactivation from latency, without inactivating pre-formed infectious virus. Replicating viruses are then detected by incubation with permissive cells, which are subsequently analysed for the presence of cpe.

MuHV-4 epitope recombinants were evaluated at day 14 p.i. for their ability to establish and expand latent infection in the spleen. All recombinant viruses were capable of normal latency establishment in BALB/c ($H2^d$) mice, as demonstrated by equivalent splenic infectious centre assay titres (Figure 2.3, panel C and Figure 2.5). Furthermore, no pre-formed infectious viruses could be detected for any of the viruses analysed, indicating that splenic infection was only latent.

These results confirmed that introducing an $H2K^b$-restricted epitope in M2 did not impact on M2 latency associated functions and, thus, on the outcome of latent infection in BALB/c ($H2^d$) mice, given that all MuHV-4 recombinants established normal levels of splenic latency.

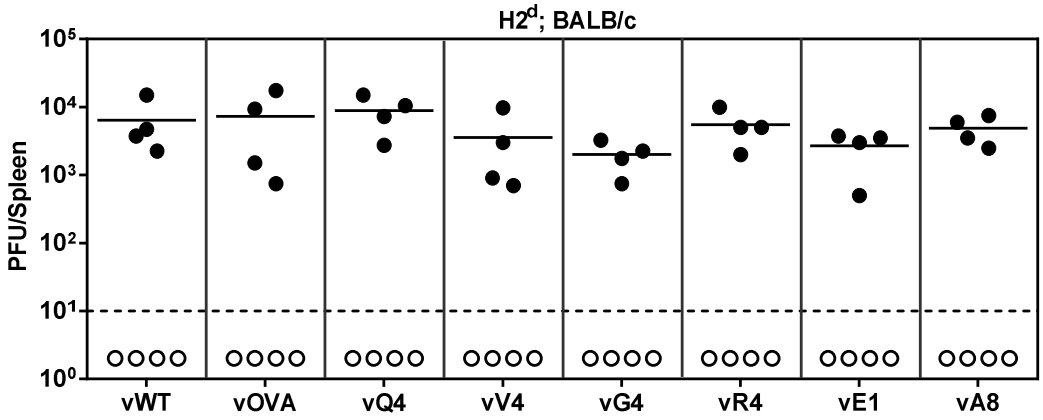

Figure 2.5. MuHV-4 epitope recombinants establish normal latency in BALB/c (H2^d) mice. BALB/c (H2^d) mice were intranasally inoculated with 10^4 PFU of the indicated viruses. At 14 days p.i., spleens were removed, single cell splenocyte suspensions were prepared and latent infection in each sample was quantified by *ex vivo* reactivation assay (closed symbols). Pre-formed infectious viruses were analysed by plaque assay (open symbols). Each point represents the titre of an individual mouse. Horizontal bars show arithmetic means. The dashed horizontal line indicates the limit of detection of the assay. Latent loads of MuHV-4 recombinants expressing OVA or APLs were not significantly different from vWT ($p>0.05$, by ordinary one-way ANOVA followed by Dunnett's multiple comparisons test). No pre-formed infectious viruses could be detected for any of the viruses analysed.

In summary, in this chapter MuHV-4 recombinants were engineered to express the well characterized H2K^b-restricted OVA epitope or derived APLs from the M2 C-terminus. APLs Q4, V4, G4 and R4 were able to stabilize H2K^b cell surface expression on RMA-S cells to a similar degree as native OVA, while E1 required 6-fold more peptide to achieve equivalent H2K^b stabilization. Additionally, all APLs differed in their potency for stimulating OT-I cells and showed a clear hierarchy in dose-response, with OVA>Q4>V4>G4>E1>R4. The engineered MuHV-4 epitope recombinants showed an otherwise intact *M2* locus, normal *in vitro* growth, equivalent *in vivo* lytic replication kinetics in the lungs of intranasally infected C57BL/6 (H2^b) mice and normal latency establishment in the spleens of BALB/c (H2^d) mice. Therefore, H2K^b-restricted epitopes were introduced at the M2 C-terminus, to ensure latent epitope expression, without causing any *in vitro* or *in vivo* replication defect in the engineered MuHV-4 recombinants.

CHAPTER 3

MHC class I binding by a latently expressed epitope impairs host colonization

MHC class I binding by a latently expressed epitope impairs host colonization

Experiments were set up to address how MHC class I binding by a latently expressed M2-linked epitope translates to *in vivo* recognition and *in vivo* control of MuHV-4-driven lymphoproliferation. Thus, C57BL/6 mice infected with the engineered MuHV-4 epitope recombinants were analysed during the establishment and maintenance of latency. Three independent, although complementary assays were performed. *Ex vivo* explant co-culture assays were performed in total splenocytes to evaluate the ability of the viruses to reactivate from latency. Limiting dilution combined with real time PCR to detect viral DNA-positive cells were applied to determine the frequency of infection of total splenocytes or of flow cytometrically purified splenic GC B cells. The latter constitute the major acute latency reservoir, are essential for amplification of the latently infected cell pool, and to gain access to the long-term latency reservoir of resting memory B cells. Finally, the presence of latently infected cells within splenic follicles was monitored by *in situ* hybridization in spleen sections using a probe specific for MuHV-4 tRNAs and miRNAs.

3.1. Expression of $H2K^b$ binding epitopes attenuates MuHV-4-driven lymphopholiferation

To assess the impact of $H2K^b$-restricted latent epitope expression on MuHV-4-driven lymphoproliferation, C57BL/6 ($H2^b$) mice were intranasally inoculated with WT virus and MuHV-4 epitope recombinants, and the latent load in the spleen was assessed by *ex vivo* reactivation assay. All viruses were evaluated, at day 7, 11, 14 and 21 p.i., for their ability to establish and expand a latent load in the spleen, and at day 50 p.i. for their ability to maintain long-term persistence. The results obtained are shown in Figure 3.1.

As expected, infection of mice with WT virus resulted in a peak of latency amplification at day 14 p.i. that subsided thereafter to reach by day 50 p.i. low long-term latency levels. In contrast, infection with MuHV-4 recombinants expressing OVA or APLs resulted in attenuation of any virus expressing an $H2K^b$ binding epitope. Splenic latency was established at day 11, but then was cleared rather than amplified by days 14-21 p.i.. This was characterized by an approximately 1000-fold reduction in the number of infectious centres at day 14 p.i. when compared with the WT virus. Interestingly vE1, which expresses an epitope with 6-fold lower EC_{50} for $H2K^b$ stabilization (Figure 2.1, panels A and B), showed an intermediate phenotype. vE1 established wild type splenic latency levels at day 11 p.i., followed by a gradual reduction in latent loads instead of latent expansion. This virus showed an approximately 100-fold reduction in the number of infectious centres at day 14 p.i. in comparison with the WT virus. In contrast vA8, in which epitope presentation was severely compromised by mutating one anchor residue, was able to establish

splenic latency levels undistinguishable from those of the epitope-null WT virus. This result indicates that the difference in latent loads of MuHV-4 epitope recombinant viruses were due to *in vivo* recognition of the H2K^b-restricted M2 derived epitopes.

Thus, H2K^b binding by a M2 derived latently expressed epitope severely compromised the ability of MuHV-4 to drive the amplification of the latently infected cell pool in spleens of C57BL/6 mice. Remarkably, a 6-fold reduction in H2K^b binding gave an intermediate latent phenotype.

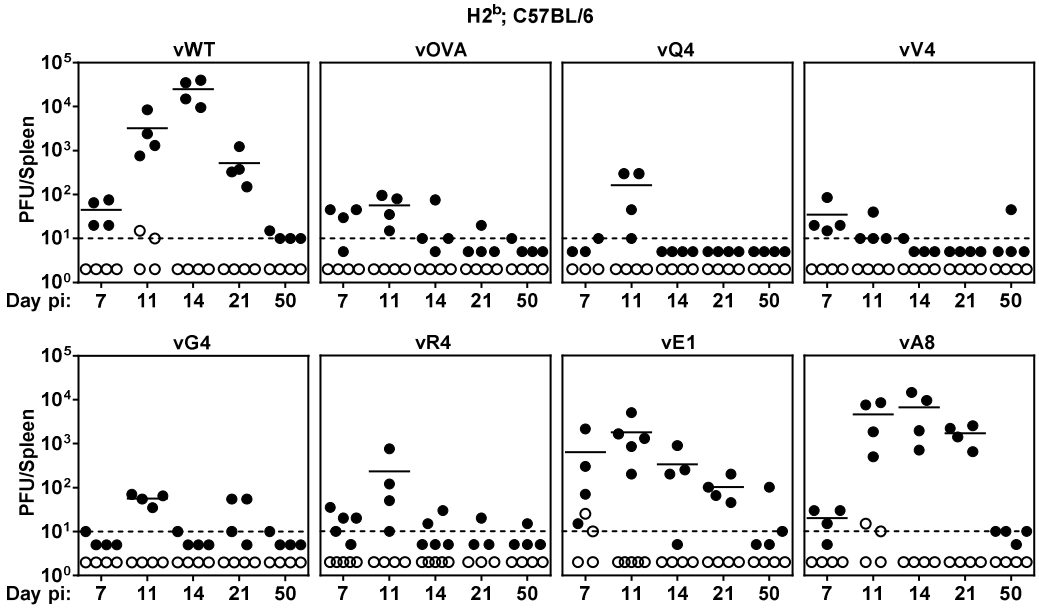

Figure 3.1. Expression of H2K^b binding epitopes attenuates MuHV-4-driven lymphoproliferation. C57BL/6 mice were intranasally infected with 10^4 PFU of vWT or MuHV-4 recombinants expressing the indicated epitopes. At the indicated days p.i. the latent load in spleens was determined by *ex vivo* reactivation assay (closed symbols) and pre-formed infectious viruses were quantified by plaque assay (open symbols). Each point represents the titre of an individual mouse. Horizontal bars indicate arithmetic means. The dashed horizontal line represents the limit of detection of the assay. At day 14 p.i., vOVA, vQ4, vV4, vG4, vR4 and vE1 latent loads were significantly below those of vWT ($p<0.05$, by two-tailed unpaired t-test). vA8 latency loads were not significantly different from vWT ($p=0.07$).

3.2. H2K^b binding by latency-associated epitopes compromises both acute MuHV-4-induced lymphoproliferation and long-term persistence

Not every latently infected cell necessarily reactivates its virus *ex vivo* and this becomes more evident at long-term. Therefore, the *ex vivo* reactivation assay was complemented with quantification of the frequency of viral DNA-positive total splenocytes, as a second measure of infected cell frequency. This was performed by Dr Sofia Marques in our laboratory by limiting dilution followed by real time PCR as originally described in (Marques et al., 2003).

C57BL/6 mice intranasally infected with the different viruses were analysed during establishment and maintenance of latency, at 14 and 50 days p.i., respectively. Total splenocytes were subjected to 2-fold serial dilutions, with 8 replicates per dilution, and lysed. Cell lysates were then analysed by real time PCR for the presence of viral genomes, using the fluorescent TaqMan methodology with primers and probe specific for the *M9 ORF*. Details of this methodology can be found in Materials and Methods, section 9.2.9.

The results obtained are in agreement with results from *ex vivo* reactivation assay (Figure 3.1). At the peak of latency amplification, day 14 p.i., the frequency of vOVA, vQ4, vV4, vG4 and vR4 DNA-positive cells was markedly reduced (>100-fold reduction) in comparison with vWT or vA8, which showed equivalent frequencies of infection (Figure 3.2 and Table 3.1). vE1 showed the previously reported intermediate phenotype. Moreover, the incapability of vOVA, vQ4, vV4, vG4 and vR4 to amplify latency also resulted in a severe deficit of virus persistence at day 50 p.i., when compared to vWT or vA8 (Figure 3.2 and Table 3.1). Despite the strongly decreased acute latent load, vE1 displayed a normal long-term frequency of latently infected cells (Figure 3.2 and Table 3.1). Indeed, the frequency of vE1 DNA-positive cells at 50 days p.i. was close to the frequency of vWT and vA8.

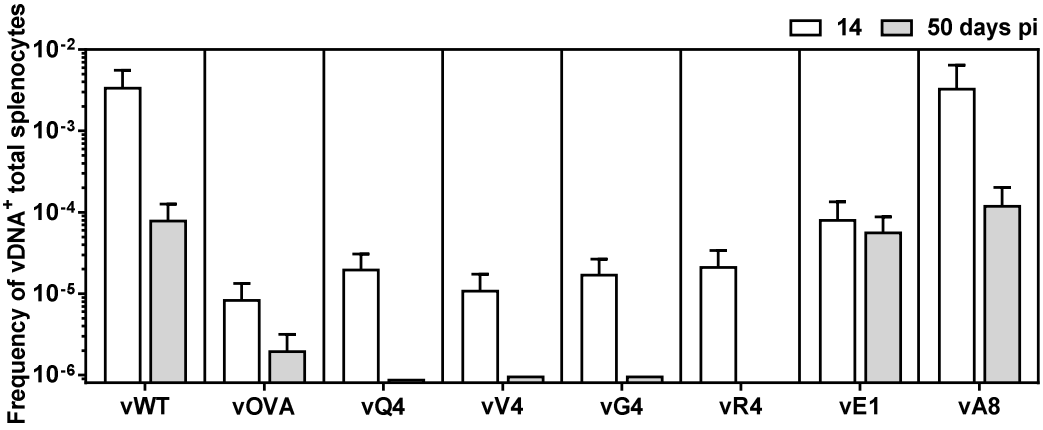

Figure 3.2. H2K^b binding by latency-associated epitopes compromises acute MuHV-4-driven lymphoproliferation and long-term persistence. C57BL/6 mice were intranasally inoculated with 10^4 PFU of the indicated viruses. At 14 and 50 days p.i. spleens were dissected and the frequency of cells positive for viral genome was determined in total splenocytes by limiting dilution followed by real time PCR. Data were obtained from pools of 4 or 5 spleens per group. Bars represent the frequency of viral DNA positive cells with 95% confidence intervals. This experiment was performed by Dr Sofia Marques in our laboratory.

Table 3.1. Frequency of MuHV-4 latent infection in total splenocytes[a] of C57BL/6 mice.

Virus	Day p.i.	Reciprocal frequency[b] of viral DNA$^+$ cells (95% CI)	
vWT	14	296	(179-856)
	50	12,770	(7,900-33,288)
vOVA	14	121,005	(75,230-309,065)
	50	517,114	(316,845-1,405,472)
vQ4	14	51,426	(32,333-125,586)
	50	id	≥1,149,446[c]
vV4	14	92,857	(57,599-239,405)
	50	id	≥1,053,659[c]
vG4	14	59,253	(37,537-140,588)
	50	id	≥1,053,659[c]
vR4	14	47,755	(29,622-123,123)
	50	id	≥1,264,391[c]
vE1	14	12,576	(7,445-40,375)
	50	17,810	(11,400-40,677)
vA8	14	307	(212-962)
	50	8462	(4970-28,436)

[a] Data were obtained from pools of 4 to 5 spleens.
[b] Frequencies were calculated by limiting-dilution analysis with 95% confidence intervals (CI).
[c] Estimated based upon less than 3 different dilution sets.
id; indeterminable.
This experiment was performed by Dr Sofia Marques in our laboratory.

These results demonstrate that strong H2K^b binding by a latently expressed epitope not only impaired acute MuHV-4-driven lymphoproliferation but also caused a severe deficit in long-term persistence. Interestingly, H2K^b binding by the weaker E1 epitope affected acute latency amplification without compromising long-term latent loads. Thus, a weaker MHC class I binding epitope allowed some immune control during acute virus-driven lymphoproliferation, but not in the long-term.

3.3. Strong MHC class I binding abolishes MuHV-4-driven lymphoproliferation in GC B cells

MuHV-4 colonizes multiple cell types during the establishment of acute latent infection in the spleen. However, the main target of MuHV-4 latent infection are undoubtedly B lymphocytes (Flano et al., 2000; Marques et al., 2003). Analysis of different splenic B cell subpopulations demonstrated that GC B cells constitute the main viral reservoir during the establishment of latency and that these cells also connect most directly to the long-term latency reservoir of resting memory B cells (Flano et al., 2002; Kim et al., 2003; Marques et al., 2003). To understand better the relationship between acute and long-term latent loads, the frequency of virus genome-positive GC B cells was determined by limiting dilution combined with real time PCR.

C57BL/6 mice were intranasally infected and at the peak of latency amplification, day 14 p.i., spleens were harvested and splenocyte suspensions were prepared and stained with three cell surface markers: anti-CD19, anti-CD95 and anti-GL7 T and B cell activation marker. GC B cells were flow cytometrically sorted, by enriching for $CD19^{+}CD95^{hi}GL7^{hi}$ cells. Purity of the isolated GC B cell population as well as the percentage of representation in total spleen were assessed. The purity of the sorted GC B cell population was consistently higher than 96% and corresponded to approximately 4-6% of total spleen (Table 3.2). Purified GC B cells were serially 2-fold diluted and 8 replicates of each dilution were analysed by real time PCR for the presence of viral genomes using a set of primers and probe specific for MuHV-4 *M9* gene.

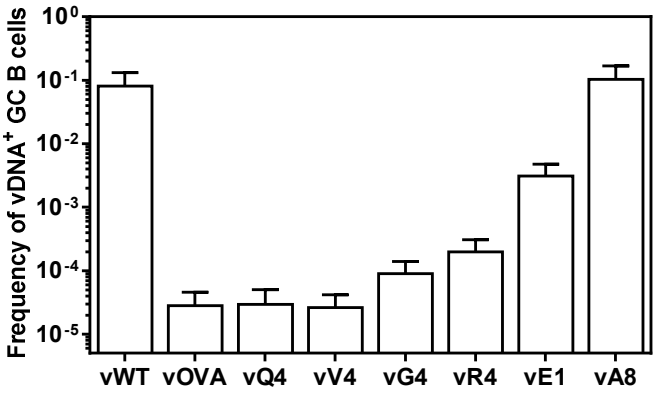

Figure 3.3. Strong MHC class I binding suppresses MuHV-4-driven lymphoproliferation in GC B cells. C57BL/6 mice were intranasally infected with 10^4 PFU of the indicated viruses. At 14 days p.i. GC B cells ($CD19^{+}CD95^{hi}GL7^{hi}$) were flow cytometrically purified and frequencies of MuHV-4 DNA-positive cells were determined by limiting dilution followed by real time PCR. Purity of sorted population was always ≥96%. Data were obtained from pools of 5 spleens per group. Bars represent the frequency of viral DNA-positive cells with 95% confidence intervals.

Table 3.2. Frequency of MuHV-4 latent infection in GC B cells[a] of C57BL/6 mice at day 14 p.i..

Virus	Reciprocal frequency[b] of viral DNA+ cells (95% CI)		% Cells[c]	% Purity[d]
vWT	12	(8-34)	4.63	96.1
vOVA	35,463	(21,819-94,657)	4.06	96.3
vQ4	33,847	(19,882-113,738)	3.63	97.6
vV4	44,687	(23,952-92,597)	4.03	97.4
vG4	11,092	(7,184-24,318)	5.76	96.0
vR4	5,016	(3,268-10,785)	5.66	97.5
vE1	323	(211-687)	4.13	96.5
vA8	10	(6-25)	4.18	96.6

[a] Data were obtained from pools of 5 spleens.
[b] Frequencies were calculated by limiting-dilution analysis with 95% confidence intervals (CI).
[c] The percentage of GC B cells from total spleen was estimated by FACS analysis.
[d] The purity of sorted cells was determined by FACS analysis.

During acute latency amplification, at day 14 p.i., the severe latency deficit previously reported for vOVA, vQ4, vV4, vG4 and vR4 reflected a marked impairment in the ability of MuHV-4 to drive the expansion of latent infection in GC B cells (Figure 3.3 and Table 3.2). This was characterized by an approximately 1000-fold lower frequency of virus DNA-positive GC B cells comparatively to vWT. The frequency of viral DNA-positive GC B cells of vA8 was equivalent to vWT, and vE1 presented and intermediate frequency of infection (Figure 3.3 and Table 3.2). The frequency of GC B cells infected with vE1 was only approximately 25-fold lower when compared to vWT. Thus, vE1 showed a strong acute reduction in viral DNA-positive total splenocytes frequencies with relative sparing of GC B cells.

Hence, strong MHC class I binding by a latently expressed epitope abolished MuHV-4-driven lymphoproliferation in GC B cells. A 6-fold decrease in E1 epitope binding to MHC class I allowed MuHV-4 to amplify the pool of latently infected GC B cells to some extent, explaining the high long-term frequencies of infection.

3.4. Decreased MHC class I binding allows MuHV-4 colonization of splenic follicles

The data of frequencies of infection in GC B cells, during acute virus-driven lymphoproliferation, was further supported by addressing the ability of each virus to colonise splenic follicles and induce the expansion of latency in GCs by *in situ* hybridization, using a probe specific for MuHV-4 tRNAs and miRNAs (Bowden et al., 1997; Pfeffer et al., 2005). These transcripts are abundantly

expressed in the GC and constitute an important marker for latency, allowing the analysis of the colonization and expansion of latent infection in GCs (Bowden et al., 1997; Simas et al., 1999).

Mice were infected with vWT or MuHV-4 epitope recombinants and 14 days latter spleens were dissected, fixed and paraffin-embedded. Spleen sections were made and processed for *in situ* hybridization with viral tRNA/miRNAs specific riboprobes (details in Materials and Methods, section 9.2.10). At least four spleens and six sections per spleen were analysed per virus. Pictures of representative spleen sections were taken from each group of animals.

Mice infected with either vWT or vA8 showed the expected pattern of infection characterized by the detection of large clusters of infected cells within GCs, at day 14 p.i., that reflected cellular proliferation and, thereby, expansion of the latently infected cell pool (Figure 3.4, panels a and h respectively) (Simas et al., 1999). In contrast, vOVA, vQ4, vV4, vG4 and vR4 showed a severe impairment in GC colonization and, consequently, abolishment of the proliferation of latently infected cells within splenic follicles (Figure 3.4, panels b to f). These results are in agreement with the previous data, demonstrating that infection with these recombinant viruses is cleared rather than amplified by days 14-21 p.i.. Again, mice infected with vE1 displayed an intermediate phenotype, characterized by a reduction both in the number of vmiRNA/vtRNA positive follicles and in the number of infected cells within positive follicles in comparison to vWT (Figure 3.4, panel g).

Taken together, these results demonstrate that expression of a strong $H2K^b$ binding epitope during latent infection severely impaired host GC colonization. However, small drops in MHC class I binding were poorly tolerated, allowing some expansion of latently infected cells in GCs.

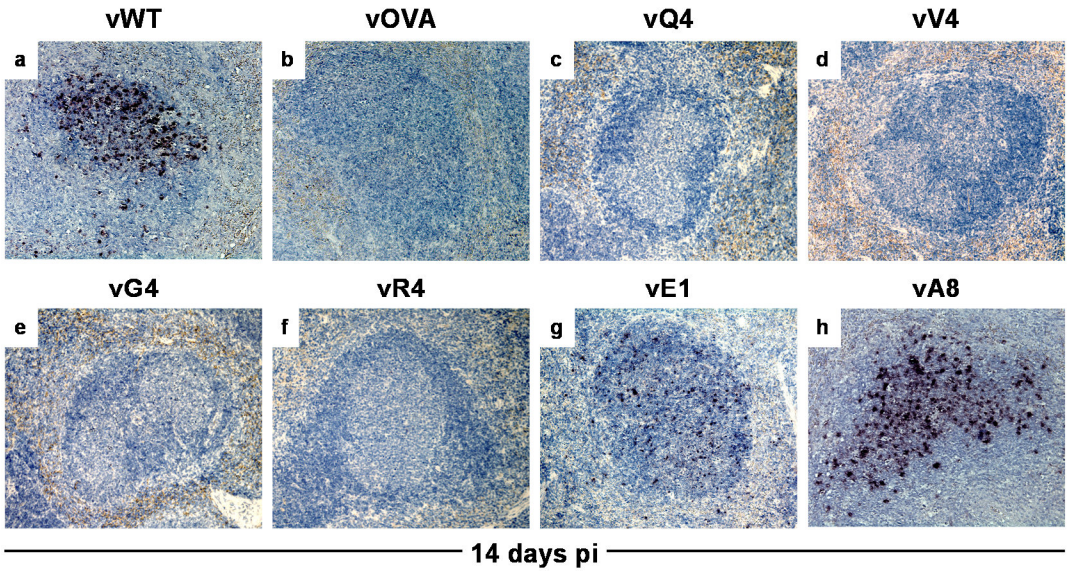

Figure 3.4. Decreased MHC class I binding allows MuHV-4 colonization of splenic follicles. C57BL/6 mice were intranasally infected with 10^4 PFU of the indicated viruses. At 14 days p.i., spleens were dissected and processed for *in situ* hybridization with a viral miRNA/tRNA-specific riboprobe. Representative spleen sections from each group of animals are shown. Dark staining indicates cells positive for viral encoded miRNA/tRNAs. All sections are magnified at x200 and counter stained with haematoxylin.

Overall the results from the three independent but complementary assays used in this chapter, *ex vivo* reactivation assay, limiting dilution combined with real time PCR and *in situ* hybridization, corroborate that *in vivo* recognition of a single M2-linked epitope allowed control of MuHV-4-driven lymphoproliferation. However, control was critically dependent on strong MHC class I binding by the latently expressed epitope. That is, strong MHC class I binding abolished MuHV-4-driven B cell proliferation in GCs and, consequently, severely compromised long-term persistence. Nevertheless, a 6-fold reduction in MHC class I binding was sufficient to allow escape of latently infected GC B cells and reaching normal long-term latent loads.

CHAPTER 4

$CD8^+$ CTL responses to epitopes expressed in latent infection

CD8+ CTL responses to epitopes expressed in latent infection

The severe impairment in host colonization observed upon infection of C57BL/6 ($H2^b$) mice with MuHV-4 recombinants expressing $H2K^b$-restricted epitopes during latent infection implied that latency-specific $CD8^+$ CTL responses were generated towards the introduced M2-linked epitopes. Therefore, experiments were set up to detect and evaluate the effector function of epitope-specific $CD8^+$ CTL responses.

4.1. Epitope-specific CD8+ T cell responses are generated *in vivo* in C57BL/6 mice infected with MuHV-4 epitope recombinants

C57BL/6 mice were intranasally inoculated with MuHV-4 epitope recombinants and at 11, 14 and 21 days p.i., spleens were harvested, splenocyte suspensions prepared and epitope-specific $CD8^+$ CTL responses were measured *in vivo* by tetramer staining.

Class I MHC tetramer reagents are uniquely able to stain $CD8^+$ T cells in an antigen-specific fashion (Altman et al., 1996). Using a strategy that temporarily inserts a photocleavable peptide into class I MHC molecules, the peptide fragments during exposure to long-wave UV irradiation, thus evacuating the peptide binding groove (Toebes et al., 2006). If the emptied MHC molecule is subsequently supplied with an epitope of interest, a novel peptide-MHC complex of defined specificity is generated in a single step from a common precursor (Toebes et al., 2006). Thus, $H2K^b$ epitope-specific tetramers were produced by exchange of conditional ligand for OVA, APLs, A8 or a peptide derived from vesicular stomatitis virus (VSV) nucleoprotein (NP) (VSV NP_{52-59}), which was used as a control. The generated $H2K^b$ epitope-specific tetramers were subsequently used in combination with anti-CD8α to stain freshly isolated splenocytes from infected mice (details in Materials and Methods, section 9.2.11.2).

$CD8^+$ T cell responses specific to vOVA, vQ4, vV4, vG4 and vR4 were detectable, although small in magnitude (Figure 4.1, panel A). As expected, responses to vA8 were barely detectable, despite vA8 high latent loads, consistently with A8 epitope having one anchor residue mutated. *In vivo* this epitope was probably not produce in sufficient amounts to compensate for its poor $H2K^b$ binding (Figure 2.1, panels A and B) and, consequently, was unable to generate an epitope-specific $CD8^+$ T cell response. Surprisingly vE1, which has an intermediate latent phenotype (Figure 3.1) and expresses an epitope with 6-fold lower EC_{50} for $H2K^b$ stabilization (Figure 2.1, panel B), elicited the $CD8^+$ T cell response with the highest magnitude. This result could not be ascribed to lytic infection, since *in vivo* lytic replication in lungs of infected mice was indistinguishably high for all viruses (Figure 2.4, panel B).

4.2. Epitope-specifc CD8+ T cells display effector function

The effector function of epitope-specific CD8+ T cells was assessed by analyzing their ability to produce IFNγ. Freshly isolated splenocytes from C57BL/6 mice infected with MuHV-4 epitope recombinants were analysed by intracellular staining for IFNγ after *ex vivo* stimulation with the corresponding epitope peptide at 11, 14 and 21 days p.i.. Intracellular staining for IFNγ after *ex vivo* stimulation with VSV NP_{52-59} peptide was also performed for each virus at each time point as control.

The results obtained corroborate the previous data of $H2K^b$ epitope-specific tetramer staining. CD8+ T cells specific for vOVA, vQ4, vV4, vG4 and vR4 were capable of producing IFNγ after *ex vivo* stimulation with the corresponding epitope peptide, despite the fact that those viruses elicited small CD8+ T cell responses (Figure 4.1, panel B). No IFNγ production could be detected in mice infected with vA8, consistently with the lack of vA8-specific CD8+ T cells, demonstrated by $H2K^b$ epitope-specific tetramer staining. Again, the largest CD8+ T cell response was elicited by vE1.

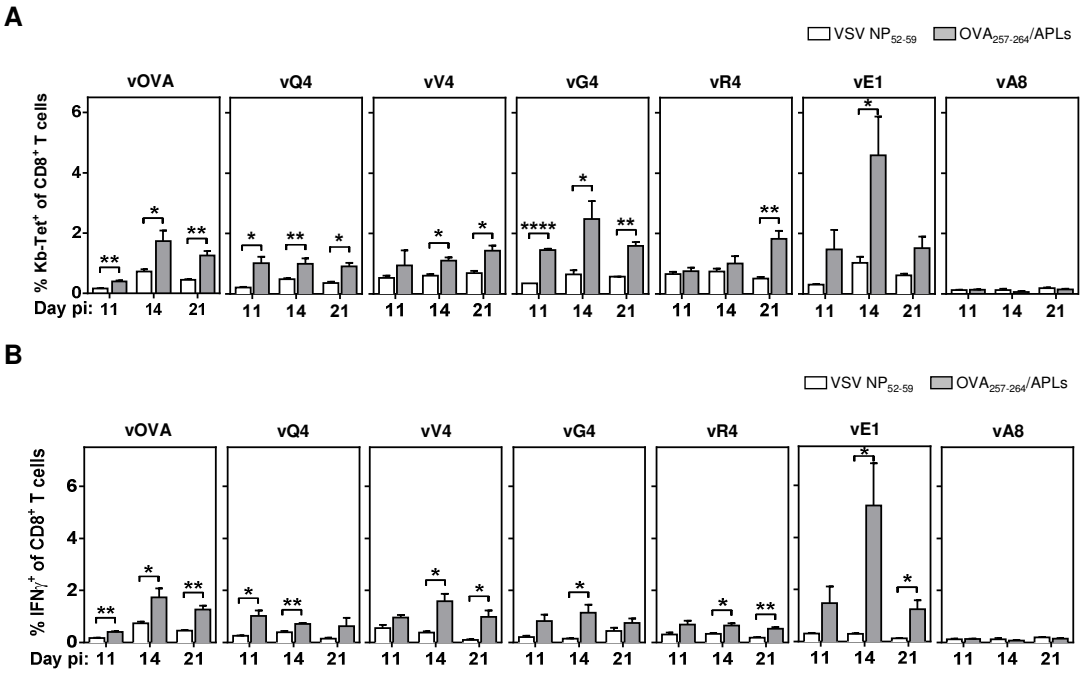

Figure 4.1. *In vivo* CD8+ T cell responses to epitopes expressed in latent infection. C57BL/6 mice were intranasally inoculated with 10^4 PFU of MuHV-4 recombinants expressing OVA, APLs or the A8 anchor residue mutant. At the indicated times post-infection (p.i.) spleens were removed and epitope-specific CD8+ T cell responses were measured. (A) Splenocytes from infected mice were cell surface co-stained with anti-CD8α and with an $H2K^b$ tetramer loaded with the VSV NP_{52-59} peptide (with bars) as a control or the correspondent epitope peptide (grey bars). The data show the percentage of tetramer positive cells among CD8+ T cells at each time point (arithmetic means ± s.e.m. from 3 independent measurements). (B) The effector function of splenic CD8+ T cells was determined by intracellular interferon-gamma (IFNγ) staining of splenocytes after *ex vivo* stimulation with the VSV NP_{52-59} peptide (with bars) or the correspondent epitope peptide (grey bars). Data show the percentage of CD8+ T cells responding to each peptide at the indicated time points (arithmetic means ± s.e.m. from 3 independent measurements). *p<0.05, **p<0.01, ****p<0.0001; using a two-tailed unpaired t-test.

4.3. E1-specific CD8+ T cells exhibit *in vivo* cytolytic activity despite less efficient control of virus-driven lymphoproliferation

The functionality and effector capacity of vE1-specific CD8+ CTLs was further confirmed and compared to that of vOVA- and vA8-specific CD8+ CTLs by an *in vivo* cytotoxicity assay.

C57BL/6 mice were intranasally infected with vOVA, vE1 or vA8. Total splenocytes from naïve congenic CD45.1 C57BL/6 mice were used as target and control cells. Target cells were pulsed with OVA, E1 or A8 peptides and labeled with a high concentration of carboxyfluorescein succinimidyl ester (CFSE). Control cells were left unpulsed and were labeled with a low concentration of CFSE. At day 10 p.i. 50:50 mixes of target and control cells were then transferred intravenously into the previously infected mice (Figure 4.2, panel A). Prepared mixes were also transferred into vWT infected C57BL/6 controls to ensure equal transfer. In the next day, spleens were dissected from recipient mice, the proportion of $CFSE^{high}$ and $CFSE^{low}$ cells among transferred CD45.1+ splenocytes was analysed by flow cytometry and the percentage of target cell killing determined (detailed description of the assay in Material and Methods, section 9.2.11.4).

vE1-specific CD8+ CTLs killed E1-pulsed target cells *in vivo* (Figure 4.2, panel B) and showed target cell elimination comparable to vOVA (Figure 4.2, panel C). As expected, mice infected with vWT showed no target cell elimination when transferred with the same mixes. Mice infected with vA8 were not capable of *in vivo* target cell elimination (Figure 4.2 panels B and C) in agreement with absence of A8 epitope-specific CD8+ T cell responses in those mice (Figure 4.1).

Hence, expression of the weaker $H2K^b$ binding E1 epitope allowed the generation of large functional E1-specific CD8+ CTL responses, however those CTLs were less efficient at controlling virus-driven lymphoproliferation.

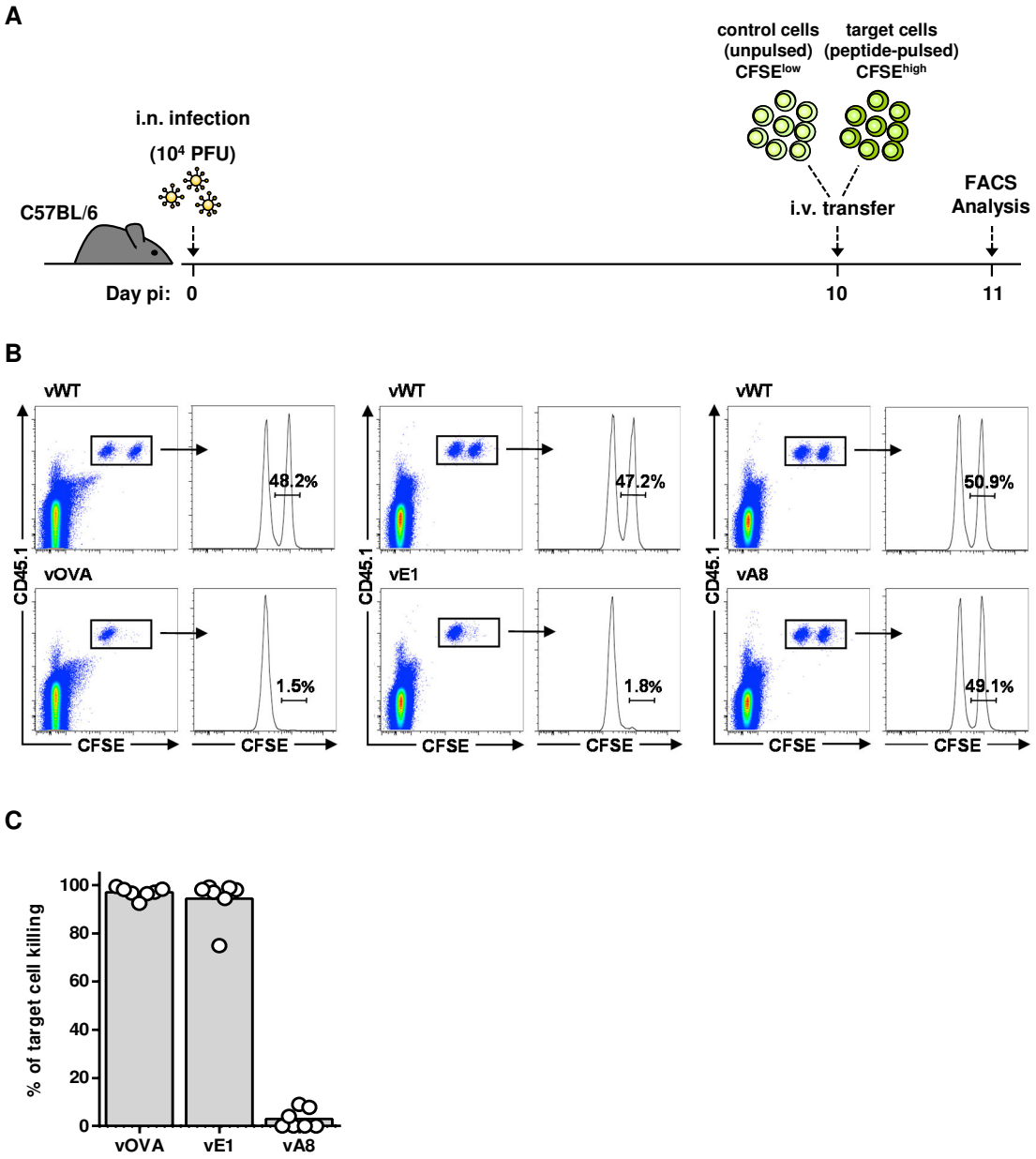

Figure 4.2. vE1-specific CD8⁺ T cells exhibit *in vivo* cytolytic activity comparable to vOVA. C57BL/6 mice were intranasally inoculated with 10^4 PFU of the indicated viruses and CTL activity of splenic CD8⁺ T cells was measured *in vivo*. At day 10 p.i. $2x10^6$ OVA-, E1- or A8-pulsed CD45.1⁺ splenocytes labeled with high concentration of CFSE and $2x10^6$ unpulsed CD45.1⁺ splenocytes labeled with low concentration of CFSE were transferred intravenously into vOVA, vE1 or vA8 infected mice. The same mix of cells was transferred into vWT infected mice as internal control. In the next day, the proportion of $CFSE^{high}$ and $CFSE^{low}$ cells among CD45.1⁺ cells recovered from the spleen was analysed by FACS. (A) Schematic diagram of the experimental setting. (B) Representative FACS plots show the proportions of high and low CFSE-positive cells in indicated groups of mice. (C) Bar diagram shows the percentage of target cell killing calculated as described in Materials and Methods section 9.2.11.4. For each group three to four mice were analysed and experiments were repeated three times.

Taken together, data presented in this chapter demonstrate that the strong impairment of acute virus-driven lymphoproliferation, upon infection of C57BL/6 mice with MuHV-4 expressing $H2K^b$ binding epitopes, was mediated by functional epitope-specific $CD8^+$ CTL responses. Strong $H2K^b$ binding elicited $CD8^+$ CTL responses that, despite small in magnitude, were very efficient at controlling acute MuHV-4-induced lymphoproliferation. Interestingly, expression of the weaker $H2K^b$ binding E1 epitope elicited the largest $CD8^+$ CTL response. Regardless of the higher magnitude of vE1-specific $CD8^+$ CTL response and its capacity of *in vivo* target cell killing, those $CD8^+$ CTLs were less efficient at curtailing MuHV-4 latency amplification.

CHAPTER 5

$CD8^+$ CTL functional avidity for a latency associated epitope is a key determinant of infection control

CD8+ CTL functional avidity for a latency associated epitope is a key determinant of infection control

CD8+ CTL control of MuHV-4-driven lymphoproliferation in C57BL/6 mice, through the recognition of latently expressed M2-linked OVA, Q4, V4, G4 and R4 epitopes, indicated that in these mice there is a TCR *repertoire* specific for each of these epitope variants. Indeed, all of the APLs induced epitope-specific CD8+ T cell responses implying that CD8+ T cell clones could be recruited from the naïve *repertoire* that recognized and responded either to OVA or to an APL. Hence, in the context of a polyclonal TCR *repertoire* the key requirement was the availability of an epitope capable of strong MHC class I binding. Nevertheless, the immune response to EBV can involve selective and massive expansion of a few dominant clones of CD8+ T cells, that is, large oligoclonal or even monoclonal CD8+ CTL expansions (Callan et al., 1996; Hislop et al., 2007b). In most cases, CD8+ T cell responses to latent cycle antigens are markedly focused on a relatively small number of immunodominant viral epitopes (Hislop et al., 2007b). Therefore, to investigate the quantitative requirements of CD8+ T cell functional avidity for *in vivo* control of MuHV-4 latent infection, we focused on a mouse model with a single TCR specificity, the well characterized OT-I transgenic mice (Clarke et al., 2000; Hogquist et al., 1994). CD8+ T cells from OT-I mice express a transgenic TCR designed to recognize $OVA_{257-264}$ in the context of $H2K^b$ (Clarke et al., 2000; Hogquist et al., 1994).

5.1. *In vivo* infection control correlates with CD8+ CTL functional avidity by latency epitope recognition

OT-I mice were intranasally infected with MuHV-4 expressing OVA or APLs with equivalent $H2K^b$ binding (Q4, V4, G4 and R4) and host colonization was examined by quantification of reactivation-competent virus by infectious centre assay of spleens 9 and 11 days later. For comparative purposes OT-I mice were analysed alongside with the epitope-null vWT, to assess the level of infection in the absence of epitope recognition. vE1 and vA8 were not utilized since they bind $H2K^b$ less efficiently precluding analysis of CD8+ T cell functional avidity because target concentrations are different.

Expression of the original OT-I ligand, OVA, resulted in the lowest infection levels both at 9 and 11 days p.i. (Figure 5.1, panel A). Expression of APLs resulted in a subsequent hierarchy of latent infection control (OVA>Q4>V4>G4>R4) that matched their hierarchy of functional avidities and not their slightly differences in $H2K^b$ binding (Figure 5.1, panel A). Expression of the antagonist R4 epitope allowed no infection control since infectious centre titres were equivalent to those of the vWT. Expression of epitopes with decreased functional avidity was also associated with a concomitant increase in the titres of pre-formed infectious virus in some mice. Thus, both at 9 and

11 days p.i. there was a clear correlation between CD8+ T cell functional avidity and *in vivo* virus control. This was further demonstrated by plotting the functional avidity of OT-I cells for OVA and APLs against the latent load established in the spleen of OT-I mice infected with MuHV-4 recombinants expressing the correspondent epitope (Figure 5.1, panel B).

These results indicate that variations in CD8+ T cell functional avidity for a latently expressed epitope had a profound impact on host control of MuHV-4 latent infection. Moreover, MuHV-4 splenic latent loads established in OT-I mice correlated with the functional avidity of CD8+ T cells for the latently recognized epitope.

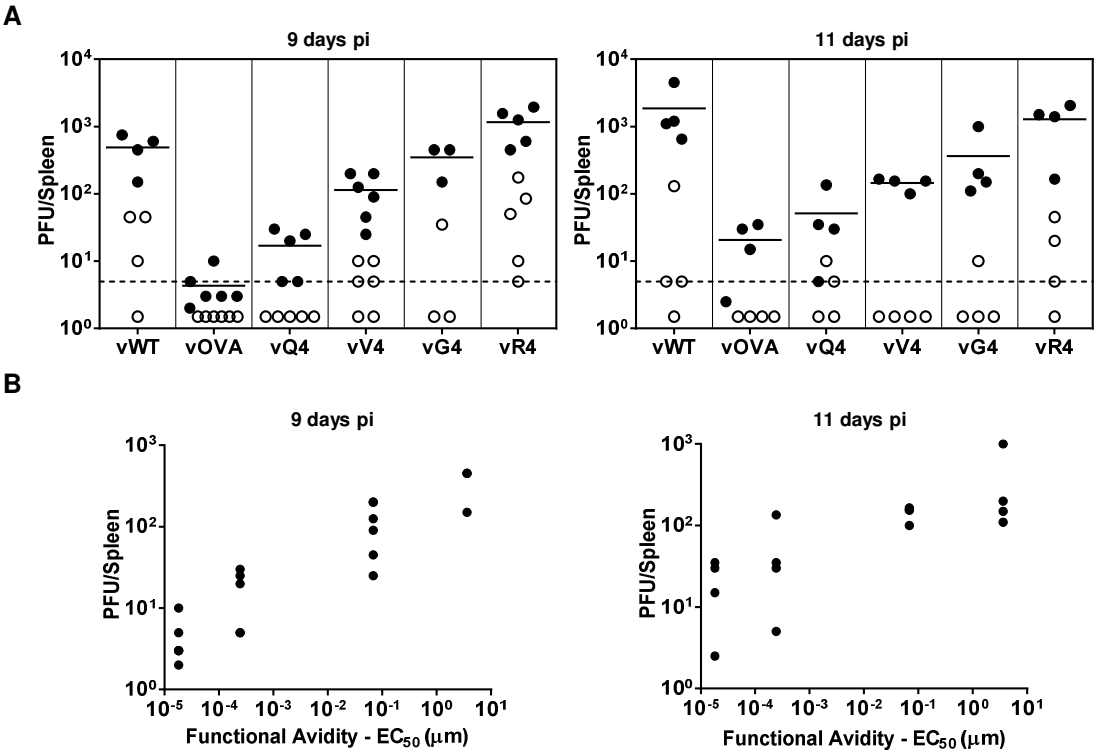

Figure 5.1. *In vivo* infection control correlates with CD8+ CTL functional avidity by latency epitope recognition. OVA_{257}-specific TCR transgenic (OT-I) mice were intranasally infected with 10^3 PFU of the indicated viruses. (A) At 9 and 11 days p.i., spleens were dissected and splenocytes were titrated for latent virus by infectious centre assay (closed symbols). Pre-formed infectious viruses were quantified by plaque assay (open symbols). Each circle represents the titre of an individual mouse. Horizontal bars indicate arithmetic means. The dashed horizontal line represents the limit of detection of the assay. At 9 days p.i. vOVA, vQ4 and vV4 showed significantly less latent infection compared to vWT (vOVA p=0.0014, vQ4 p=0.0042, vV4 p=0.0087; by Student's two-tailed unpaired t-test). vG4 and vR4 latent infection was not significantly different from vWT (vG4 p=0.4631, vR4 p=0.0885). (B) Graphs show the correlation between CD8+ T cell functional avidity and splenic latent loads at 9 and 11 days p.i.. The functional avidity of OT-I cells for OVA or APLs (Q4, V4 and G4) (data from Figure 2.1, panel D) was plotted against the latent load established in spleens of OT-I mice (data from panel A) infected with the correspondent MuHV-4 epitope recombinant. Day 9: r_s=0.9148, p=0.0435; day 11: r_s=0.8977 p=0.0525; according to Pearson's correlation. Data in panel A were obtained in collaboration with Dr Sofia Marques in our laboratory.

5.2. Attenuation of MuHV-4 infection by latent epitope recognition is mediated by CD8+ CTLs

To further confirm that immune control of MuHV-4 latent infection was mediated by CD8+ CTLs, CD8+ T cells were depleted from infected OT-I mice. Following intranasal infection with each virus, CD8+ T cells were depleted by 5 intraperitoneal injections of CD8-specific monoclonal antibody (Figure 5.2, panel A). A group of vWT infected OT-I mice was left non-depleted as experimental control. At day 11 p.i. mice were sacrificed, spleens were dissected, single cell splenocyte suspensions were prepared and stained for CD8α followed by flow cytometry analysis to determine the efficacy of depletions, or analysed by *ex vivo* reactivation assay to determine splenic latent titres.

CD8+ T cell depletions were very effective (Figure 5.2, panel B) and had little effect on infectious centres titres of vWT infected mice when compared to those of vWT infected non-depleted mice (Figure 5.2, panel C). This result is consistent with the lack of known $H2^b$-restricted MuHV-4 latency epitopes and with previous published data showing that numbers of acute latently infected spleen cells are not significantly higher in CD8-depleted mice (Ehtisham et al., 1993; Stevenson et al., 1999c).

CD8+ T cell depletions reverted splenic latent infection of all MuHV-4 epitope recombinant viruses to vWT infection levels (Figure 5.2, panel C), demonstrating that the activity of CD8+ CTLs was responsible for the different latent loads established in OT-I mice (Figure 5.1, panel A).

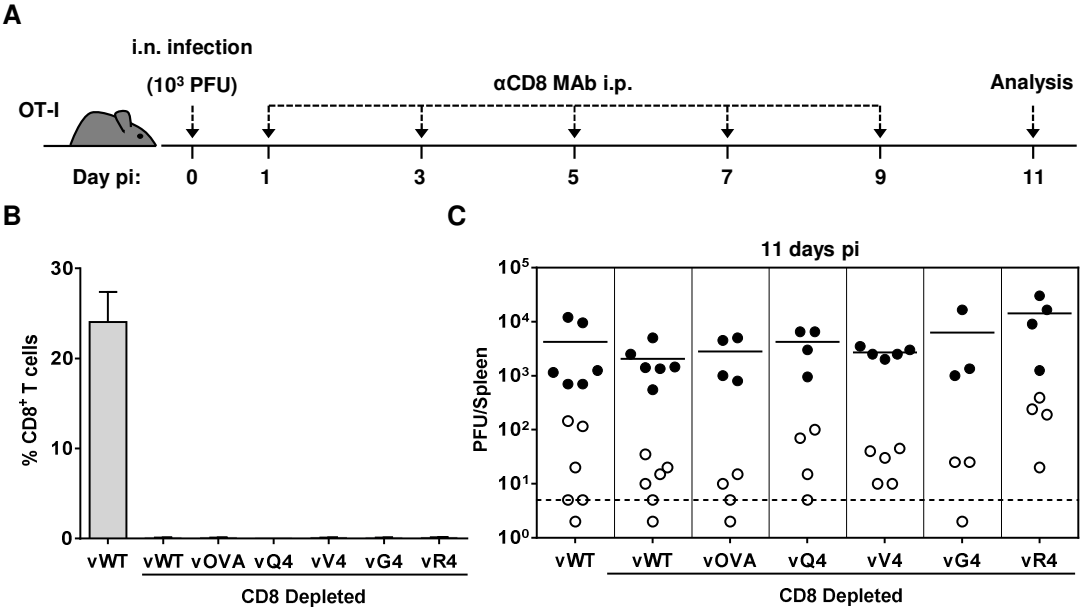

Figure 5.2. Attenuation of MuHV-4 infection by latent epitope recognition is mediated by CD8⁺ CTLs. OT-I mice were intranasally infected with the indicated viruses (10^3 PFU) and CD8⁺ T cells were depleted by intraperitoneal (i.p.) injection of anti-CD8 monoclonal antibody (MAb). At 11 days p.i. spleens were removed for analysis. A group of vWT infected OT-I mice was left non-depleted as control. (A) Schematic diagram of the experimental setting. (B) Splenocytes were stained for CD8α and analysed by flow cytometry. The data show the percentage of CD8⁺ T cells of total splenocytes (arithmetic means ± s.e.m) in depleted mice and control (non-depleted) mice. (C) Splenocytes were titrated for latent infection by explant co-culture (closed symbols). Lytic virus were analysed by plaque assay (open symbols). Each symbol represents the titre of an individual mouse. Horizontal bars indicate arithmetic means. The dashed horizontal line represents the limit of detection of the assay. Data were reproducible over two independent experimental groups. Latent loads of the epitope recombinants were not significantly different from vWT latent loads in non-depleted or CD8-depleted mice ($p>0.05$; ordinary one-way ANOVA followed by Dunnett's multiple comparisons test).

Overall, the results obtained in this chapter demonstrate that introducing latent CD8⁺ CTL targets where no latency epitope recognition existed before caused a CD8⁺ CTL-dependent attenuation of MuHV-4 latent loads, in proportion to the functional avidity of the expressed epitope for the dominant TCR. Thus, CD8⁺ CTL functional avidity is also a key determinant of immune control of MuHV-4 latent infection.

CHAPTER 6

$CD8^+$ CTL functional avidity in the context of normalized T cell *repertoire*

CD8$^+$ CTL functional avidity in the context of normalized T cell *repertoire*

In the previous chapter OT-I mice provided a useful starting point to address the impact of CD8$^+$ CTL functional avidity on *in vivo* control of MuHV-4 latent infection. However, OT-I mice display a limited CD4$^+$ T cell *repertoire*. The total number of T cells OT-I transgenic mice possess is similar to that of non-transgenic littermates, but those transgenic cells are strongly skewed towards the CD8$^+$ T cell subset (Clarke et al., 2000). Moreover, several reports indicate that MuHV-4-driven activation, proliferation and differentiation of latently infected B cells are dependent on CD4$^+$ T cell help (Collins and Speck, 2014; Ehtisham et al., 1993; Kim et al., 2003; Sangster et al., 2000; Stevenson and Doherty, 1999). Consequently, in this chapter a strategy developed to understand the impact of CD8$^+$ CTL functional avidity in a setting more advantageous to B cell proliferation is described.

6.1. OT-I mice exhibit low frequencies of GC B cells that sustain MuHV-4 latent infection

CD4$^+$ T cell help is critical for the generation and maintenance of GCs (Nutt and Tarlinton, 2011; Vinuesa et al., 2005). Therefore, OT-I mice were characterized and compared with C57BL/6 mice for their capacity to induce GC formation and to sustain MuHV-4-driven lymphoproliferation. To this end, OT-I and C57BL/6 mice were intranasally infected with YFP-expressing MuHV-4 recombinant virus (vYFP) and at the peak of latency amplification, day 14 p.i., splenocytes were stained for GC B cells (CD19$^+$CD95^{hi}GL7^{hi}) and analysed by flow cytometry. MuHV-4 infected cells were identified based on YFP expression.

OT-I mice showed an impairment in GC formation in comparison to C57BL/6 mice (Figure 6.1, panel A). This was accompanied by a reduction in the frequency of MuHV-4 infected GC B cells in OT-I mice when compared to C57BL/6 mice (Figure 6.1, panel B). This result was further confirmed by analysing the phenotype of the infected cells. Approximately 50% of MuHV-4 infected B cells (CD19$^+$ YFP$^+$) in OT-I mice had a GC B cell phenotype (CD19$^+$CD95^{hi}GL7^{hi}) in contrast to the characteristic 80% exhibited by C57BL/6 mice (Figure 6.1, panel C).

Thus, the limited CD4$^+$ T cell *repertoire* of OT-I mice impaired GC formation and so the ability of MuHV-4 to drive B cell proliferation.

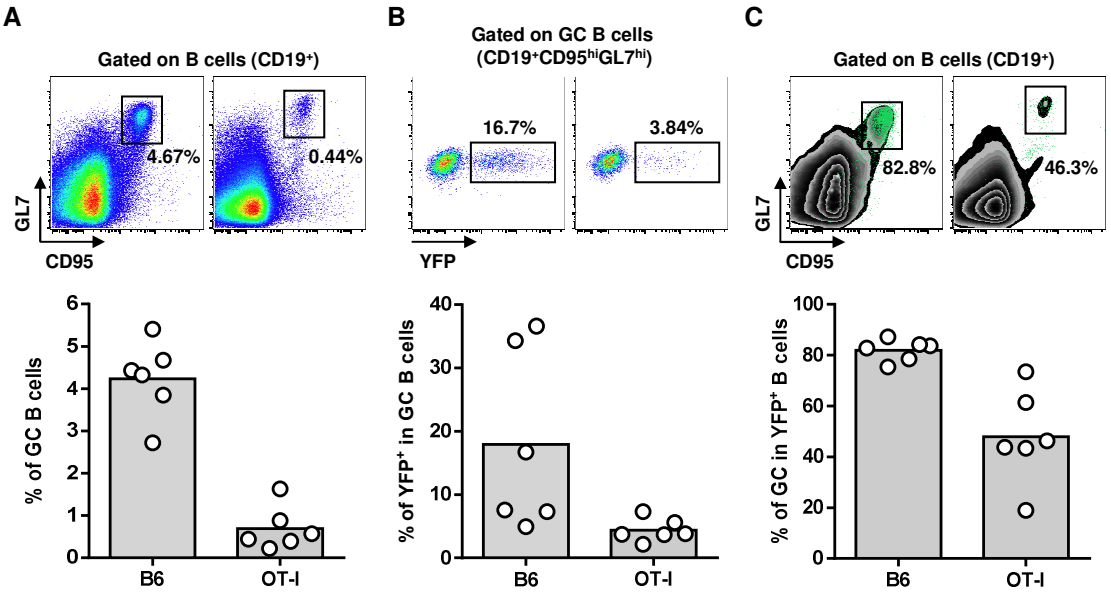

Figure 6.1. OT-I mice exhibit low frequencies of GC B cells that sustain MuHV-4 latent infection. C57BL/6 or OT-I mice were intranasally infected with 10^3 PFU of YFP-expressing MuHV-4 and at 14 days p.i., spleens were dissected, single splenocyte suspensions were prepared and analysed by flow cytometry. (A) Frequencies of GC ($CD19^+CD95^{hi}GL7^{hi}$) B cells. (B) Frequency of YFP-positive cells in GC B cells evaluated by gating on the $CD19^+CD95^{hi}GL7^{hi}$ population. (C) Phenotype of infected cells analysed by overlapping GC B cells and YFP-positive B cells FACS plots. Representative FACS plots from individual animals are shown (top panels) and compiled percentages are presented in the graphics below. Each point represents an individual mouse; 6 mice were analyzed for each experimental condition; grey bars indicate the average percentage.

6.2. $TCR\alpha^{-/-}$ mice reconstituted with $CD4^+$ T cells exhibit robust proliferation of MuHV-4 infected GC B cells

To address the importance of $CD8^+$ CTL functional avidity in an environment more favourable to MuHV-4-driven B cell proliferation, $CD4^+$ T cells purified from pooled lymph nodes of naïve C57BL/6 mice were intravenously transferred into $TCR\alpha^{-/-}$ recipients one day prior to infection with YFP-expressing MuHV-4 (Figure 6.2, panel A). $TCR\alpha^{-/-}$ mice are deficient for the αβ TCR and so very few $CD4^+$ T cells are found in the periphery (Mombaerts et al., 1992; Philpott et al., 1992), which severely compromises GC formation in these mice (Figure 6.2, panel B). At day 16 and 18 p.i. reconstituted $TCR\alpha^{-/-}$ mice were characterized for their ability to sustain GC reactions and MuHV-4-induced lymphoproliferation.

Adoptive transfer of polyclonal $CD4^+$ T cells to subsequently infected $TCR\alpha^{-/-}$ mice led to a robust proliferation of GC B cells (Figure 6.2, panels B and C) in which MuHV-4 was able to establish latent infection (Figure 6.2, panel D). Moreover, approximately 80% of the infected B cells ($CD19^+YFP^+$) had a GC phenotype ($CD19^+CD95^{hi}GL7^{hi}$) (Figure 6.2, panel E) similarly to infection in C57BL/6 mice (Figure 6.1, panel C).

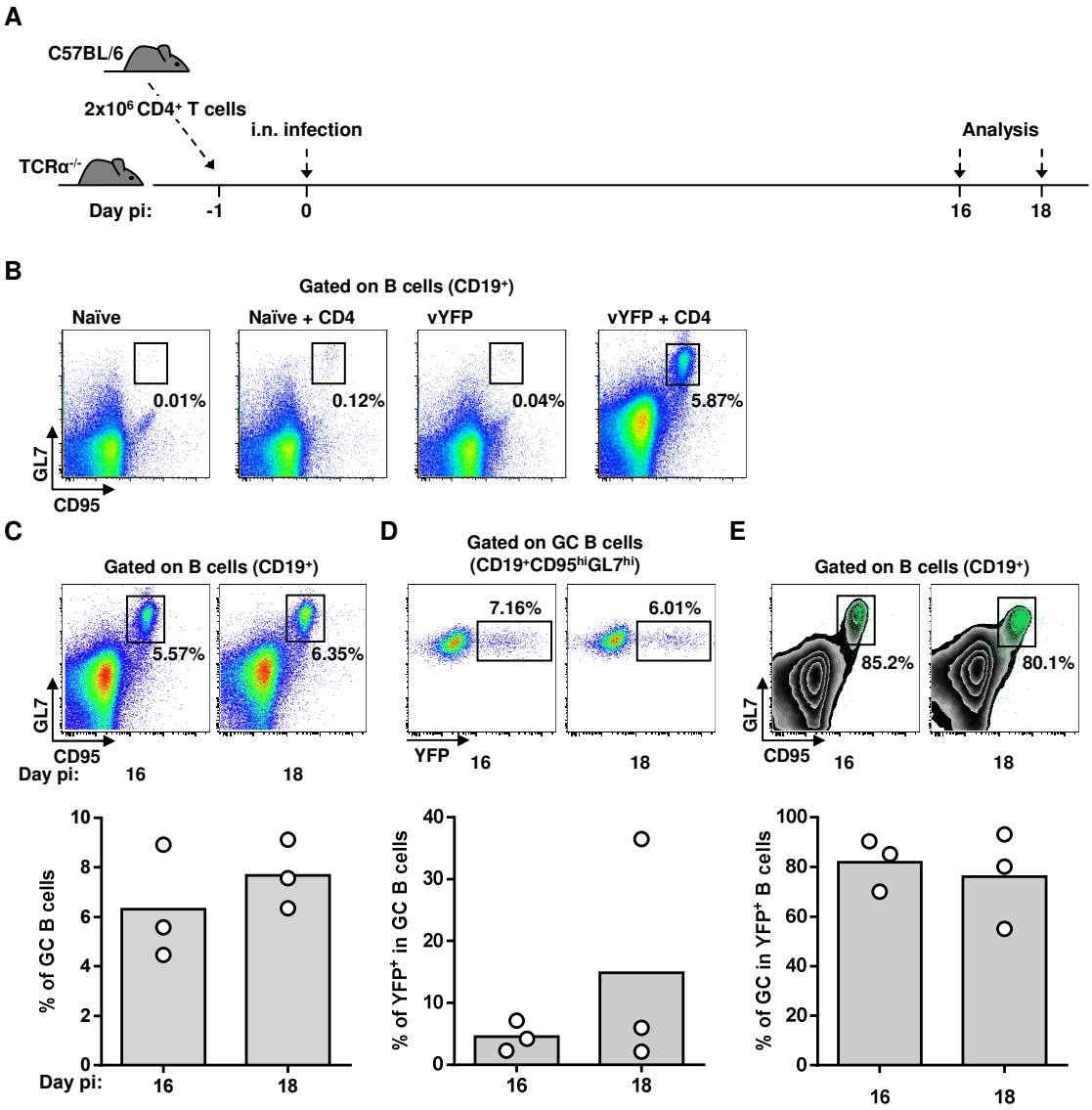

Figure 6.2. TCRα$^{-/-}$ mice reconstituted with CD4$^+$ T cells display robust proliferation of MuHV-4 infected GC B cells. 2x10^6 CD4$^+$ T cells purified from pooled lymph nodes of naïve C57BL/6 mice were intravenously transferred into age and sex matched TCRα$^{-/-}$ mice one day prior to infection with 10^3 PFU of YFP-expressing MuHV-4 (vYFP). At 16 and 18 days p.i. mice were sacrificed, spleens were dissected and single splenocyte suspensions were stained for GC B cells and analysed by flow cytometry. (A) Schematic diagram of the experimental setting. (B) Representative FACS plots show the frequency of GC B cells (CD19$^+$CD95^{hi}GL7^{hi}) in spleens of the following experimental controls: naïve TCRα$^{-/-}$ mice, naïve TCRα$^{-/-}$ mice reconstituted with CD4$^+$ T cells, TCRα$^{-/-}$ mice infected with vYFP and TCRα$^{-/-}$ mice reconstituted with CD4$^+$ T cells one day prior to infection with vYFP. (C-E) Spleens of reconstituted TCRα$^{-/-}$ mice infected with vYFP were analysed by flow cytometry for (C) frequencies of GC B cells, (D) frequencies of infection in GC B cells and (E) phenotype of the infected cells, at 16 and 18 days p.i.. Representative FACS plots from individual animals are shown (top panels) and compiled percentages are presented in the graphics below. Each point represents an individual mouse; grey bars indicate the average percentage.

Thus, providing polyclonal CD4$^+$ T cells to TCRα$^{-/-}$ mice restored the normal pattern of MuHV-4 latent infection in GC B cells.

6.3. OVA recognition by reconstituted TCRα$^{-/-}$ mice elicits a strong OT-I response that suppresses splenic colonization

To compare the effect of optimal CD8$^+$ T cell recognition with absence of CD8$^+$ T cell control in this setting, CD4$^+$ T cells purified from pooled lymph nodes of naïve C57BL/6 mice and OT-I T cells obtained from pooled lymph nodes of naïve CD45.1 Rag1$^{-/-}$ OT-I mice were intravenously transferred into TCRα$^{-/-}$ recipients one day prior to infection with recombinant MuHV-4 YFP expressing the high avidity OVA epitope (vOVA) or the R4 antagonist (vR4) (Figure 6.3, panel A). TCRα$^{-/-}$ mice are deficient for the αβ TCR so most CD8$^+$ T cells express the γδ TCR (Mombaerts et al., 1992; Philpott et al., 1992). Therefore, reconstituted TCRα$^{-/-}$ mice had polyclonal CD4$^+$ T cells and a TCRαβ CD8$^+$ T cell compartment of modest size and restricted to OT-I T cells, so to a single CD8$^+$ TCR specificity.

In vivo kinetics of OT-I T cell expansion were determined at different times p.i. by staining of splenic OTI (CD45.1$^+$CD8α$^+$) T cells followed by flow cytometry analysis (Figure 6.3, panel B). Infection with vOVA elicited a strong OT-I response that reached maximal levels at day 16 p.i.. As expected, infection with vR4 did not cause any increase in OT-I cell numbers during the course of viral infection, in agreement with expression of an antagonist ligand for the OT-I TCR. Notably, the late kinetics of OT-I expansion induced by vOVA infection were consistent with the expression kinetics of a latent antigen.

CTL function of OT-I cells was analysed by intracellular staining for IFNγ and granzyme B after *ex vivo* stimulation of infected splenocytes with the OVA or R4 peptide at days 12, 14, 16 and 19 p.i.. vOVA-induced OT-I cell expansion correlated with the acquisition of effector function demonstrated by production of IFNγ (Figure 6.2, panel C) and the expression of granzyme B (Figure 6.2, panel D). The inability of vR4 to induce OT-I expansion was consistent with the absence of IFNγ production and granzyme B expression (Figure 6.2, panels C and D).

The impact of such CD8$^+$ CTL response differences in the ability of MuHV-4 to colonize the spleen and induce the expansion of latency was addressed by quantification of reactivation-competent virus by infectious centre assay from day 10 to day 19 p.i.. The strong OT-I response elicited by vOVA infection supressed splenic colonization, while absence of CD8$^+$ CTL control allowed vR4 colonization of the spleen and amplification of latency (Figure 6.3, panel E).

Hence, *in vivo* recognition of a high avidity M2-linked epitope allowed optimal latent specific CD8$^+$ CTL control of MuHV-4-driven lymphoproliferation.

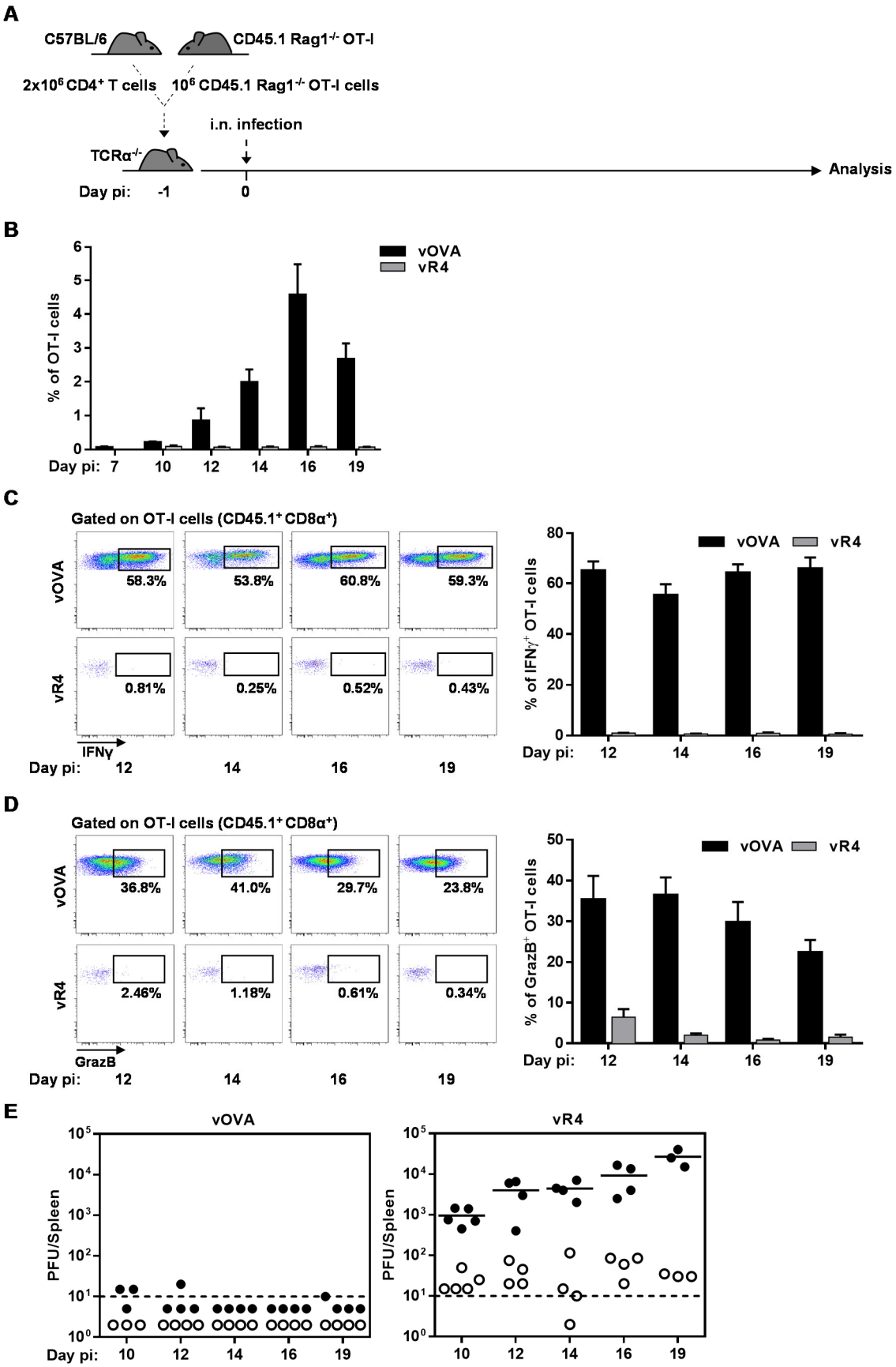

Figure 6.3. *In vivo* recognition of high avidity M2-linked OVA epitope elicits optimal latent specific CD8⁺ CTL control of MuHV-4 infection in reconstituted TCRα$^{-/-}$ mice. 2x10^6 CD4$^+$ T cells purified from

C57BL/6 lymph nodes and 10^6 CD45.1 Rag1$^{-/-}$ OT-I cells isolated from pooled lymph nodes of naïve CD45.1 Rag1$^{-/-}$ OT-I mice were intravenously transferred into age and sex matched TCRα$^{-/-}$ recipients one day prior to infection (10^3 PFU) with recombinant MuHV-4 YFP expressing OVA (vOVA) or R4 (vR4) epitopes. (A) Schematic representation depicting the experimental setting. (B) Kinetics of *in vivo* OT-I cells expansion upon infection with vOVA (black bars) or vR4 (grey bars). At the indicated time p.i. the frequency of OT-I cells in the spleen was determined by FACS staining of CD45.1$^+$CD8α$^+$ cells (arithmetic means ± s.e.m). (C-D) Effector function of splenic OT-I cells was determined by analyzing their ability to produce IFNγ and express granzyme B. Splenocytes of infected mice were *ex vivo* stimulated with the OVA (black bars) or R4 (grey bars) peptides and then stained for (C) intracellular IFNγ or (D) granzyme B. Data show the percentage of OT-I cells (CD45.1$^+$CD8α$^+$) responding to peptide at each time point. Representative FACS plots from individual animals are shown (left panels) and compiled percentages are presented in the graphics at the right (arithmetic means ± s.e.m.). (E) Latent infection in spleens of infected mice was quantified by *ex vivo* reactivation assay (closed circles) and pre-formed infectious viruses were analysed by plaque assay (open circles). Each circle represents the titre of an individual mouse. Horizontal bars represent the mean titre per group of animals. The dashed horizontal line represents the limit of detection of the assay. For each time point groups of 3 to 5 mice were analysed.

Globally, the results presented in this chapter demonstrate that reconstituted TCRα$^{-/-}$ mice provide a novel and valuable setting to investigate how TCR engagement by a latently expressed epitope impacts on MuHV-4-driven B cell proliferation.

CHAPTER 7

In vivo thresholds of $CD8^+$ CTL engagement regulate MuHV-4-driven lymphoproliferation

In vivo thresholds of CD8$^+$ CTL engagement regulate MuHV-4-driven lymphoproliferation

CD8$^+$ CTL functional avidity was previously shown to be an important determinant of MuHV-4 latent infection control in OT-I mice (Chapter 5). To further understand the quantitative requirements of TCR functional avidity for *in vivo* control of MuHV-4-driven B cell proliferation in GCs reconstituted TCRα$^{-/-}$ mice were used. As demonstrated in the previous chapter, these mice provide an environment more conducive to MuHV-4-driven lymphoproliferation. Upon intranasal infection of mice with MuHV-4 YFP recombinants expressing OVA or APLs, experiments were designed first to investigate the outcome of different TCR engagement thresholds on the *in vivo* CD8$^+$ CTL response. Then, the ability of MuHV-4 to driven the proliferation of latently infected cells, both in total splenocytes and in GC B cells, was assessed. Thus, *in vivo* CD8$^+$ CTL engagement thresholds were related to the outcome of MuHV-4-driven lymphoproliferation.

7.1. Sub-optimal TCR engagement compromises *in vivo* CD8$^+$ CTL expansion rather than effector function

The *in vivo* impact of OT-I TCR engagement by latently expressed OVA or APL epitopes on CD8$^+$ T cell expansion, activation and acquisition of effector function was determined in the spleens of reconstituted TCRα$^{-/-}$ mice at day 16 p.i..

In vivo CD8$^+$ T cell expansion was quantified by flow cytometry analysis of stained OT-I (CD45.1$^+$CD8α$^+$TCRβ$^+$) cells in freshly isolated splenocytes (Figure 7.1, panel A). OT-I T cell expansion was greatest for vOVA, followed by vQ4 and further reduced for vV4. Infection with vG4 and vR4 failed to induce *in vivo* OT-I cell expansion, similarly to infection with the epitope-null vWT. Thus, OT-I cell expansion correlated well with the epitope functional avidity measured before (Figure 2.1, panels C and D). Namely, the 14-fold reduction in functional avidity of Q4 only modestly affected OT-I cell expansion, while the 3,760-fold reduction of V4 caused a more pronounced reduction, still without supressing it completely. However, the 198,000-fold reduction in functional avidity of G4 caused the CD8$^+$ T cell response to decline to background levels.

In vivo virus-driven OT-I cell expansion was paralleled by the acquisition of an activation phenotype, characterized by increased cell surface expression of CD44 and down regulation of CD62L expression (CD44^{hi}CD62L^{lo} phenotype) (Figure 7.1, panel B). Indeed, the different expansion profiles of OT-I cells matched the extent of their activation status. Recognition of epitopes with higher functional avidity was consistent with the detection of higher percentages of CD44^{hi}CD62L^{lo} OT-I cells. By contrast, infection with vG4 and vR4 was associated with maintenance of CD62L cell surface expression on OT-I cells, similarly to infection with vWT.

Next, the effector function of OT-I cells was analysed by *ex vivo* stimulation of infected splenocytes with the corresponding epitope peptide followed by intracellular staining for IFNγ and granzyme B (Figure 7.1, panels C and D respectively). $CD8^+$ T cell responses to vQ4 and vV4 showed comparable functionally to vOVA. That is, in each situation OT-I cells were capable of producing IFNγ and expressing granzyme B following *ex vivo* peptide stimulation. Responses to vG4 and vR4 were hard to evaluate due to reduced OT-I cell numbers. Hence, reducing TCR functional avidity affected the overall magnitude of the $CD8^+$ CTL response rather than CTL functionality.

These results are in agreement with previous *in vivo* studies on how TCR avidity impacts on pathogen-specific $CD8^+$ T cell responses. As observed by Zhen and colleagues upon infection of mice with recombinant *Listeria monocytogenes* expression of OVA, Q4 and V4 activates OT-I T cells *in vivo*, but the magnitude of CTL expansion is dictated by the strength of TCR ligation (Zehn et al., 2009). Failure of G4 to induce *in vivo* OT-I cell expansion is consistent with subsequent studies using recombinant Influenza A virus expressing the G4 APL that also demonstrated the inability of K^bG4 to activate naïve OT-I cells and induce CTL effector function following *in vivo* priming, suggesting that this ligand likely falls the minimal threshold required for TCR-mediated effective CTL activation under *in vivo* conditions (Denton et al., 2011).

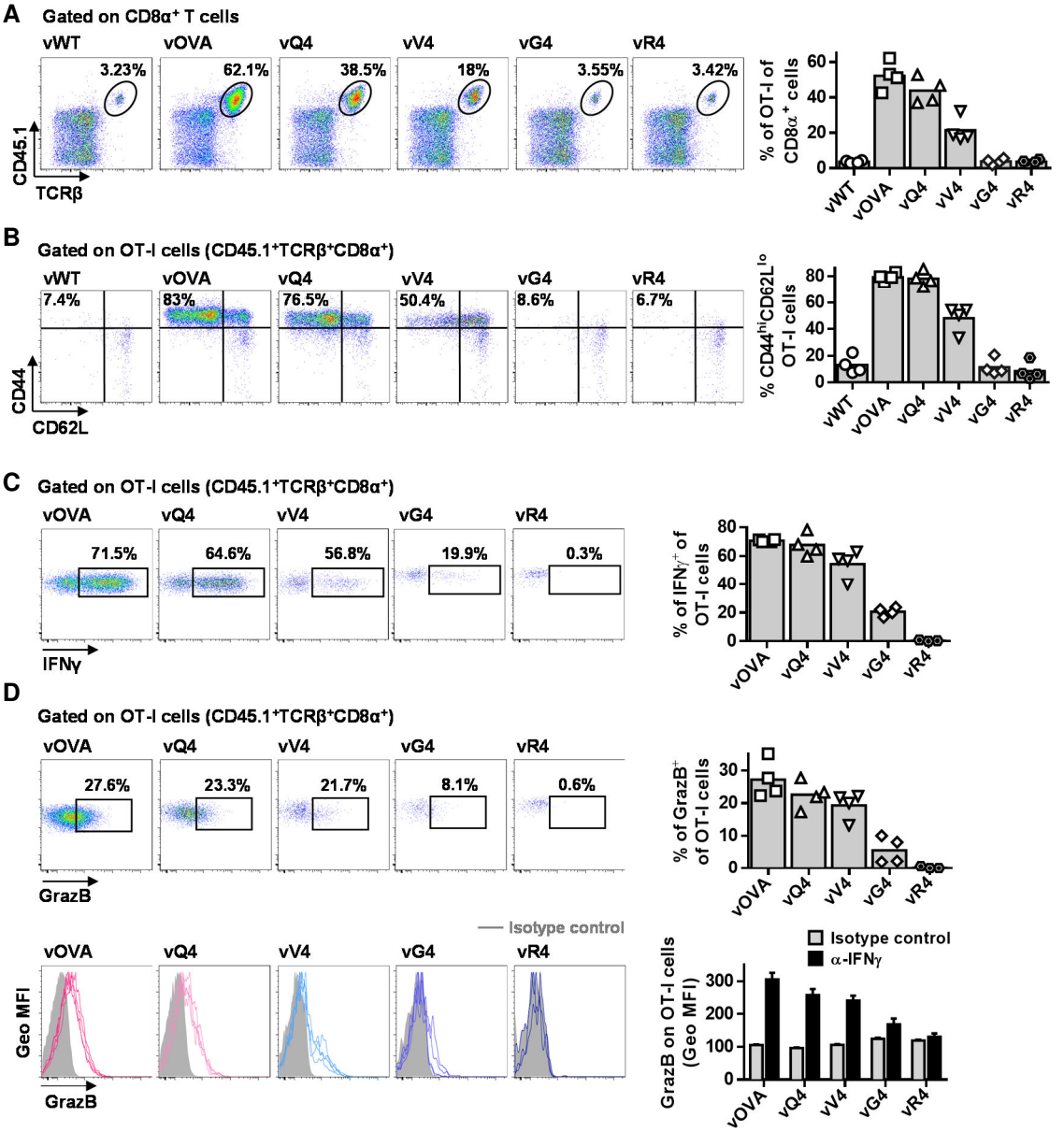

Figure 7.1. Sub-optimal TCR engagement affects the magnitude of *in vivo* CD8⁺ CTL expansion rather than effector function. Reconstituted TCRα$^{-/-}$ mice (details in Figure 6.3, panel A) were intranasally inoculated with 10^3 PFU of MuHV-4 YFP (vWT) or MuHV-4 YFP recombinants expressing the indicated M2-linked epitopes. At day 16 p.i. spleens were removed and the frequency, phenotype and effector function of transferred OT-I cells was analyzed by flow cytometry. (A) Magnitude of the *in vivo* OT-I T cell response to the indicated viruses. Representative FACS plots from individual animals show the frequency of OT-I (CD45.1⁺ TCRβ⁺ CD8α⁺) cells within total CD8⁺ T cells. vOVA, vQ4 and vV4 induced significant expansion of OT-I cells in comparison with vWT ($p<0.0001$, $p<0.0001$, $p=0.002$, respectively; by ordinary one way ANOVA followed by Tukey's multiple comparisons test). vWT, vG4 and vR4 did not significantly increase OT-I cell numbers ($p>0.9$). (B) The activation phenotype of OT-I cells was determined by analyzing the frequency of CD44^{hi}CD62L^{lo} cells gated on the CD45.1⁺ TCRβ⁺ CD8α⁺ population. vOVA, vQ4 and vV4 induced significantly more OT-I cell activation than vWT ($p<0.0001$); vG4 and vR4 were not significantly different from vWT ($p>0.9$). (C-D) The effector function of OT-I cells was determined by analyzing their capacity for (C) interferon-gamma (IFNγ) and (D) granzyme B (GrazB) production, by intracellular cytokine staining following *ex vivo* stimulation with OVA or the corresponding APL peptide. The data show the percentage of OT-I cells (CD45.1⁺ TCRβ⁺ CD8α⁺) producing (C) IFNγ and (D) GrazB in response to each peptide. Histograms show geometric mean fluorescence intensities (MFI) of granzyme B staining relative to an antibody isotype control (shaded area).Representative FACS plots from individual animals (left panels)

and compiled percentages (right panels) are shown. Each point represents an individual mouse; 4 mice were analyzed per group; bars represent the average percentage.

7.2. TCR engagement thresholds determine the outcome of MuHV-4-driven lymphoproliferation

To investigate how the different TCR engagement thresholds, triggered by recognition of latently expressed OVA or APLs, affect MuHV-4-driven lymphoproliferation, reconstituted TCRα$^{-/-}$ mice were analysed following intranasal infection with MuHV-4 epitope recombinants by *ex vivo* reactivation assay. Analysis was performed during the establishment and expansion of latency (16 and 21 days p.i.), always in comparison with vWT.

OVA expression severely impaired the establishment of latency (Figure 7.2). Both at 16 and 21 days p.i. latent viruses were below the limit of detection of the infectious centre assay. Q4 expression caused an equivalent marked suppression of splenic colonization, only marginally less than vOVA. V4 expression gave an intermediate phenotype, allowing the establishment and amplification of latency, with latent titres significantly below those of the vWT and above those of vOVA. vG4 and vR4 established and amplified splenic latency, reaching latent titres equivalent to the epitope-null vWT. Infection with vWT, vG4 and vR4 was also associated with a concomitant increase in the titres of pre-formed infectious virus. *In vivo* control of MuHV-4-driven lymphoproliferation showed, therefore, a titratable correlation with CD8^{+} CTL functional avidity (Figure 7.3).

Hence, infection of reconstituted TCRα$^{-/-}$ mice with MuHV-4 epitope recombinants reproduced the previous CD8^{+} CTL-dependent attenuation of latency observed in OT-I mice, in proportion to the functional avidity of the latently expressed epitope.

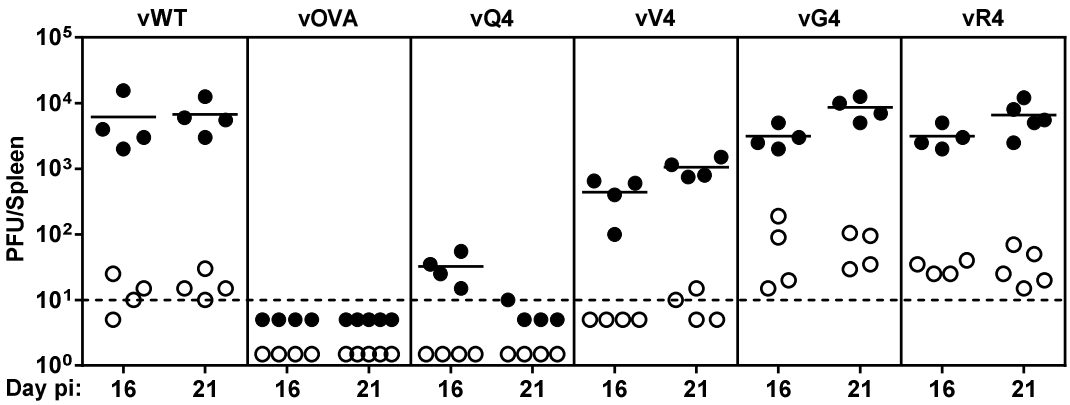

Figure 7.2. *In vivo* thresholds of TCR engagement affect the outcome of MuHV-4-driven lymphoproliferation. Reconstituted TCRα$^{-/-}$ mice were intranasally infected with 10^3 PFU of the indicated viruses. At 16 and 21 days p.i. spleens were dissected and titrated for latent virus by *ex vivo* reactivation assay (closed circles). Pre-formed infectious viruses were quantified by plaque assay in frozen/thawed splenocyte suspensions (open cicles). Each circle shows the titre of one mouse and the horizontal bar represents the mean titre per group of animals. The dashed line indicates the limit of detection of the assay. At 16 and 21 days p.i. vOVA, vQ4 and vV4 showed significantly lower latent loads than vWT (d16: vOVA p=0.02, vQ4 p=0.02, vV4 p=0.03; d21: vOVA p=0.004, vQ4 p=0.006, vV4 p=0.02; by ordinary one-way ANOVA followed by Dunnett's multiple comparisons test). Latent loads of vG4 and vR4 were not significantly different from vWT (d16: vG4 p=0.4, vR4 p=0.4; d21: vG4 p=0.8, vR4 p=1.0).

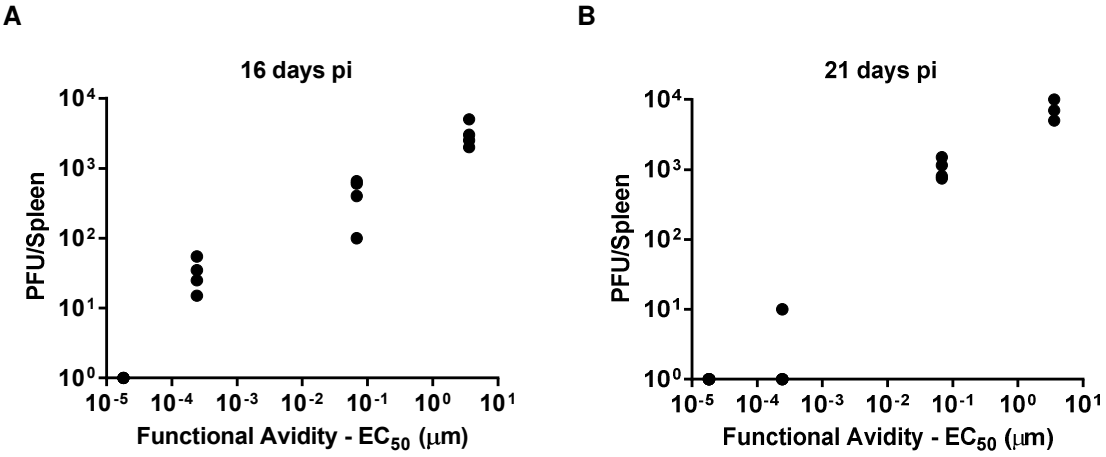

Figure 7.3. *In vivo* control of MuHV-4-driven lymphoproliferation correlates with CD8+ CTL functional avidity. To study the association between CD8+ T cell functional avidity and MuHV-4-driven lymphoproliferation, the functional avidity of OT-I cells for OVA or APLs (Q4, V4 and G4) (data from Figure 2.1, panel D) was plotted against the latent load established in spleens of reconstituted TCRα$^{-/-}$ mice infected with the correspondent MuHV-4 epitope recombinant at (A) 16 and (B) 21 days p.i. (data from Figure 7.2). Day 16: r_s=0.9868, p=0.0066; day 21: r_s=0.9899, p=0.0051; according to Pearson's correlation coefficient.

7.3. Sub-optimal CD8$^+$ CTL functional avidity allows MuHV-4-driven lymphoproliferation

As a second measure of virus-driven lymphoproliferation, the frequency of viral genome positive cells in total splenocytes was quantified, at 16 and 21 days p.i., by using the previously described real time PCR at limiting dilution method.

The inability of vOVA to amplify latency was corroborated by an approximately 1000-fold difference in the frequency of vOVA DNA-positive cells in comparison with vWT at day 21 p.i. (Figure 7.4 and Table 7.1). Q4 expression led to a slightly less efficient control of latent infection. This was illustrated by an approximately 5-fold higher frequency of vQ4 DNA-positive cells in comparison with that of vOVA. vV4 showed an intermediate phenotype, characterized by establishment and amplification of viral latency, nevertheless the frequency of virus DNA positive splenocytes was approximately 5-fold lower when compared to vWT. Infection with vG4 and vR4 reproduced the wild type pattern of latent infection observed in these mice. That is, the frequency of virus DNA-positive splenocytes was similar to vWT at both time points measured. Thus, the frequencies of viral genome-positive cells in total splenocytes supported the results of the *ex vivo* reactivation assay, showing a similar hierarchy of MuHV-4-driven lymphoproliferation control (vWT=vG4=vR4>vV4>vQ4>vOVA).

Notably, while recognition of latently expressed OVA and Q4 epitopes, which have higher functional avidity for the dominant TCR, was associated with a decrease in the frequency of latently infected cells in the spleen from day 16 to day 21 p.i., reducing TCR functional avidity further allowed the establishment and amplification of the latently infected cell pool. Hence, these results indicate that there is an *in vivo* immune threshold of TCR engagement that determines the outcome of MuHV-4-induced lymphoproliferation.

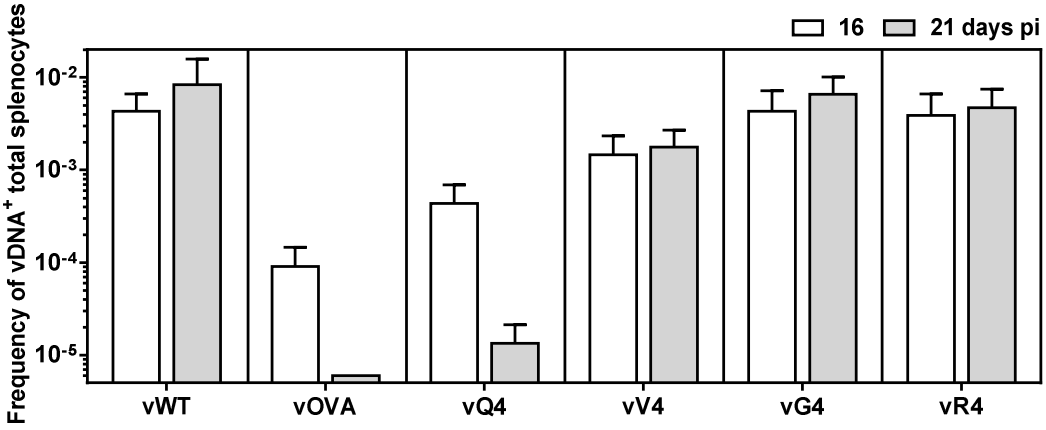

Figure 7.4. Sub-optimal TCR engagement allows MuHV-4-driven lymphoproliferation. Reconstituted TCRα$^{-/-}$ mice were intranasally infected with 10^3 PFU of the indicated viruses. At 16 and 21 days p.i. the frequency of cells positive for MuHV-4 genome was determined in total splenocytes by limiting dilution followed by real time PCR. Data were obtained from pools of 4 to 5 spleens per group. Bars represent the frequency of viral DNA-positive cells with 95% confidence intervals.

Table 7.1. Frequency of MuHV-4 latent infection in total splenocytes[a] of reconstituted TCRα$^{-/-}$ mice.

Virus	Day p.i.	Reciprocal frequency[b] of viral DNA+ cells (95% CI)	
vWT	16	232	(150-509)
	21	119	(63-991)
vOVA	16	11,010	(6,845-28,119)
	21	id	>161,924[c]
vQ4	16	2,296	(1,442-5,630)
	21	74,799	(47,030-182,682)
vV4	16	687	(427-1,755)
	21	567	(371-1,201)
vG4	16	231	(139-688)
	21	152	(99-331)
vR4	16	257	(150-870)
	21	211	(134-491)

[a] Data were obtained from pools of 4 to 5 spleens.
[b] Frequencies were calculated by limiting-dilution analysis with 95% confidence intervals (CI).
[c] Estimated based upon less than 3 different dilution sets.
id; indeterminable.

7.4. Sub-optimal CD8+ CTL functional avidity allows MuHV-4-driven GC B cell proliferation

To further investigate the impact of CD8+ CTL functional avidity in MuHV-4 ability to drive the proliferation of latently infected GC B cells, the frequency of virus genome-positive cells was determined in the flow cytometrically purified CD19+CD95^{hi}GL7^{hi} population, as before.

As expected, the frequency of viral DNA-positive cells for vOVA and vQ4 revealed a severe impairment in the ability of MuHV-4 to establish and expand latency in GC B cells (Figure 7.5 and Table 7.2). This was characterized by a reduction rather than amplification of the latently infected GC B cell pool from day 16 to day 21 p.i.. Infection with vV4, vG4 and vR4 was characterised by expansion of latently infected GC B cells with frequencies of viral DNA-positive cells equivalent to those of vWT.

The obtained results were supported by the analysis of YFP expression in GC B cells (Figure 7.6). These data further corroborate that the latently infected cells expanding in the spleen correspond to GC B cells.

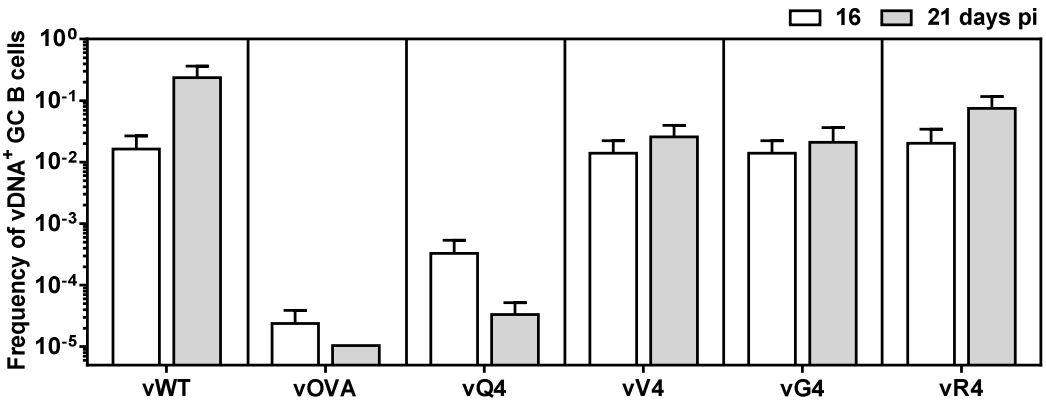

Figure 7.5. Sub-optimal CD8⁺ CTL control allows amplification of the pool of latently infected GC B cells. Reconstituted TCRα$^{-/-}$ mice were intranasally infected with the indicated viruses and frequencies of viral DNA-positive cells in flow cytometrically purified GC B cells (CD19^{+}CD95^{hi}GL7^{hi}) were determined by limiting dilution and real time PCR at 16 and 21 days p.i.. Purity of sorted population was always ≥97%. Data were obtained from pools of 4 to 5 spleens per group. Bars represent the frequency of viral DNA-positive cells with 95% confidence intervals.

Table 7.2. Frequency of MuHV-4 latent infection in GC B cells[a] of reconstituted TCRα$^{-/-}$ mice.

Virus	Day p.i.	Reciprocal frequency[b] of viral DNA^{+} cells (95% CI)		% Cells[c]	% Purity[d]
vWT	16	61	(38-158)	3.13	97.3
	21	4	(3-9)	6.36	97.4
vOVA	16	41,748	(25,873-108,104)	1.95	97.0
	21	id	>96,432[e]	4.88	98.4
vQ4	16	3,042	(1,874-8,064)	3.50	97.0
	21	29,920	(19,237-67,294)	4.87	97.0
vV4	16	72	(45-176)	3.00	98.2
	21	39	(25-84)	8.83	99.0
vG4	16	72	(45-176)	3.08	97.0
	21	32	(18-108)	6.68	98.0
vR4	16	50	(29-167)	2.46	97.4
	21	16	(9-53)	7.99	97.0

[a] Data were obtained from pools of 4 to 5 spleens.
[b] Frequencies were calculated by limiting-dilution analysis with 95% confidence intervals (CI).
[c] The percentage of GC B cells from total spleen was estimated by FACS analysis.
[d] The purity of sorted cells was determined by FACS analysis.
[e] Estimated based upon less than 3 different dilution sets.
id; indeterminable.

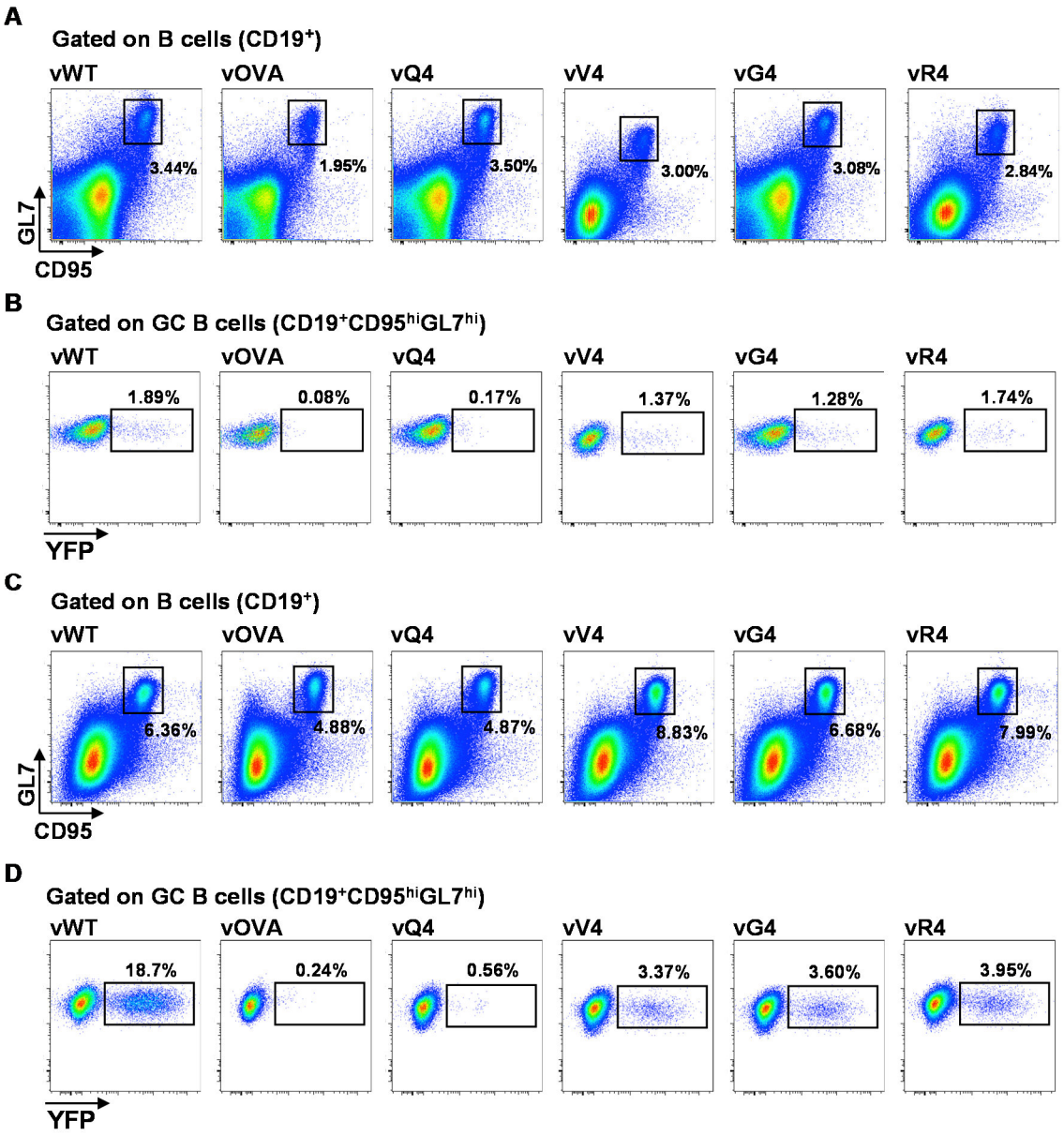

Figure 7.6. YFP expression in GC B cells of reconstituted TCRα$^{-/-}$ mice infected with MuHV-4 recombinants expressing OVA or APLs. TCRα$^{-/-}$ mice were adoptively transferred with polyclonal CD4^{+} T cells and CD45.1 Rag1$^{-/-}$ OT-I cells one day prior to infection (10^3 PFU) with MuHV-4 YFP (vWT) or MuHV-4 YFP recombinants expressing the indicated epitopes. At 16 (A and B) and 21 (C and D) days p.i. single cell suspensions were prepared, stained for GC B cells and analysed by flow cytometry. (A and C) Frequencies of GC (CD19^{+}CD95^{hi}GL7^{hi}) B cells. (B and D) Frequency of YFP-positive cells in GC B cells. FACS plots show data obtained from pools of 4 or 5 spleens per group of animals.

Taken together, data presented in this chapter indicate that *in vivo* immune thresholds of TCR engagement affect the outcome of MuHV-4-induced lymphoproliferation. The $CD8^+$ CTL response displayed a surprisingly large tolerance for sub-optimal TCR engagement. Reducing $CD8^+$ CTL functional avidity compromised viral control through reduced T cell expansion instead of differentially affecting CTL effector function. Recognition of the latently expressed OVA epitope elicited marked $CD8^+$ CTL expansion and severely impaired MuHV-4-driven lymphoproliferation. A 14-fold reduction in functional avidity (vQ4) gave remarkably similar results; a 4,000-fold reduction (vV4) gave an intermediate phenotype; and a 200,000-fold reduction (vG4) abolished $CD8^+$ CTL control of virus-induced lymphoproliferation. Thus, OT-I TCR engagement by M2-derived OVA or Q4 was considerably above the threshold required for *in vivo* viral control and low functional avidity allowed MuHV-4-driven lymphoproliferation.

CHAPTER 8

General Discussion

General Discussion

γHVs are worldwide distributed pathogens that despite their oncogenic potential have evolved to persist for the lifetime in the human population. γHVs drive the proliferation of latently infected GC B cells to achieve long-term persistence in memory B cells in face of host competent immune responses (Hislop et al., 2007b; Thorley-Lawson, 2001). Therefore, in the immunocompetent host a dynamic interaction between virus-driven B cell proliferation and the host immune response, in particular by $CD8^+$ CTLs, produces the observed pattern of lifelong persistence without overt disease. However, when the virus-host equilibrium is disrupted γHV can cause severe sometimes life-threatening diseases. This is particularly evident in individuals in which $CD8^+$ T cell surveillance is ablated or severely compromised, either by iatrogenic immunosuppression during transplantation or by chronic HIV-1 infection. In the absence of $CD8^+$ CTL control latently infected B cells can proliferate unchecked leading to the development of lymphoproliferative diseases (Thorley-Lawson and Gross, 2004). Hence, notwithstanding its benign appearance, EBV is aetiologically linked to three B cell malignancies, BL, HL and PTLD, to a subset of T and NK cell lymphomas and to an epithelial tumour, NPC (Cesarman, 2014; Kutok and Wang, 2006). KSHV is similarly associated to B cell lymphoproliferative diseases, such as PEL and MCD, and to a tumour of endothelial origin, KS (Cesarman, 2014; Dittmer and Damania, 2013). The frequency of lymphoid malignancies associated with γHV infection and its greater incidence in individuals with immunodeficiency, places the proliferation of latently infected cells and their control by $CD8^+$ CTLs at the center of γHV pathogenesis.

Viral latency epitopes that are presented at the surface of latently infected B cells, B cell lymphomas or carcinomas provide an immune target and are a focus of current immunotherapies and vaccination strategies (Bollard et al., 2012; Elliott et al., 2008; Hui et al., 2013; Long et al., 2011). However, despite the success of adoptive T cell therapy to prevent and treat EBV-driven PTLD, targeting other EBV-associated tumours and developing prophylactic and therapeutic vaccines remains a major challenge. Because of the narrow species tropism of human γHVs the quantitative determinants of *in vivo* γHV control by $CD8^+$ CTL remain unclear. An important unknown is how far the $CD8^+$ T cell mediated killing that is defined *in vitro* relates to effective *in vivo* immune protection. Despite extensive studies on the $CD8^+$ T cell response to γHV and the identification of many γHV $CD8^+$ CTL targets, the outcome of their engagement *in vivo* remains poorly defined.

In this thesis, infection of laboratory mouse with MuHV-4 was used as an experimental model to identify immune engagement thresholds for effective *in vivo* $CD8^+$ CTL control of virus-driven B cell proliferation. MuHV-4 provides a natural *in vivo* infection model for dissecting γHV infection and immune control, in which viral immune evasion mechanisms are preserved. Importantly, it shares with EBV the same strategy of host colonization, that is, it exploits the proliferation of latently infected cells in GCs to establish lifelong persistence in memory B cells. Thus, MuHV-4

presents as a well-established mouse model of γHV pathogenesis that provides an invaluable opportunity to correlate biochemical interactions with *in vivo* immune control.

The M2 latency-associated protein encoded by MuHV-4, like EBV LMP2A and KSHV K1, is expressed in latently infected B cells and modulates B cell signalling, displaying functional homologies with the aforementioned viral proteins (Burkhardt et al., 1992; Caldwell et al., 1998; Damania, 2004; Lagunoff et al., 1999; Lee et al., 2005; Lee et al., 1998a). Experiments carried out in our laboratory have demonstrated that M2 promotes the assembly of B cell signalling complexes downstream of the B cell receptor (Pires de Miranda et al., 2008; Pires de Miranda et al., 2013; Rodrigues et al., 2006) and that M2 it is required for efficient entry of latently infected B cells into GC reactions *in vivo* (Simas et al., 2004). It is noteworthy that besides promoting B cell activation, proliferation and survival, providing an advantage in the competitive environment of the GC, these latent proteins are also themselves a source of $CD8^+$ CTL targets. As with EBV LMP2A (Lee et al., 1997; Murray et al., 1992; Rickinson and Moss, 1997; Steven et al., 1996) and KSHV K1 (Osman et al., 1999), M2 contains an $H2K^d$-restricted epitope that is recognized by $CD8^+$ T cells from infected $H2^d$ mice (Husain et al., 1999; Usherwood et al., 2000). So far, this is the only latent epitope identified for MuHV-4. Importantly, recognition of this single latent epitope by $CD8^+$ CTLs of BALB/c ($H2^d$) mice was shown to regulate the proliferation of latently infected B cells in GCs, during long-term MuHV-4 infection (Marques et al., 2008). Therefore, presentation of these latently expressed epitopes at the surface of infected cells and tumours, and their potential for recognition by the host $CD8^+$ CTL response have been exploited. LMP2A is a candidate vaccine target for NPC (Chen et al., 2008; Hui et al., 2013) and also a potential target for prospective CTL-based immunotherapies (Lutzky et al., 2010; Smith et al., 2012). Similar efforts have focused on the potential of M2-based vaccination strategies (Hoegh-Petersen et al., 2009; Usherwood et al., 2001) and of adoptive transfer of M2-specific CTLs (Usherwood et al., 2000) to improve $CD8^+$ T cell control of MuHV-4 latency, however with limited success. Thus, how LMP2A/K1/M2 immune recognition functions *in vivo* is important to understand. Additionally, all these three proteins show evidence of amino acid sequence diversity, consistent with the possibility of selection as a result of immune pressure from host $CD8^+$ CTL responses (Marques et al., 2008; Stebbing et al., 2003; Wang et al., 2010). The diversity of LMP2A, K1 and M2 prompted the hypothesis that amino acid variations in epitope sequences that affect epitope binding to MHC class I or $CD8^+$ T cell functional avidity are likely to have a major impact on immune control of virus-driven B cell proliferation and, thus, on host colonization.

This thesis set out to investigate *in vivo* how MHC class I binding and $CD8^+$ T cell functional avidity, for a single latently expressed epitope derived from M2, impact on the control of virus-driven B cell proliferation. The adopted strategy consisted in generating MuHV-4 recombinants expressing from the M2 C-terminus the well characterized $H2K^b$-restricted OVA epitope or derived APLs, and characterizing both the $CD8^+$ T cell responses elicited and the ability of MuHV-4 to drive B cell proliferation upon infection of mice. MuHV-4 infection of mice presents as a unique model to experimentally address this question since long-term virus-driven B cell proliferation in

GCs has been shown to be regulated by latent-specific $CD8^+$ CTLs directed towards a single epitope derived from M2, in BALB/c ($H2^d$) mice (Marques et al., 2008). Hence, it offers the opportunity to relate directly quantitative changes in epitope recognition to the control of virus-driven B cell proliferation. Furthermore, attaching each epitope to the M2 C-terminus, provides a physiological relevant approach to epitope presentation, as it conforms to latent gene expression, in striking contrast to the use of exogenous promoters, which are active independently of endogenous viral gene expression. Thus, each introduced $CD8^+$ CTL target was expressed with the kinetics and copy number of the endogenous M2 epitope.

All the selected epitopes showed equivalent capacity to stabilize $H2K^b$ cell surface expression on TAP deficient RMA-S cells with the exception of E1, for which a 6-fold higher peptide concentration was required to achieve equivalent $H2K^b$ stabilization, in agreement with published data (Denton et al., 2011). By contrast, OT-I T cells exhibited a broad range of functional avidities for the selected epitopes with OVA>Q4>V4>G4>E1>R4. Since all $CD8^+$ CTL epitopes introduced were $H2^b$-restricted a major prediction was that MuHV-4 epitope recombinants would not be attenuated in BALB/c ($H2^d$) mice. This was found to be the case.

$CD8^+$ T cell control vs evasion: a matter of thresholds

Upon infection of C57BL/6 ($H2^b$) mice, introduction of a single latently expressed epitope, where none existed before, caused a severe $CD8^+$ CTL-dependent suppression of acute MuHV-4-driven B cell proliferation in GCs. This result is consistent with the previously reported impact of *in vivo* recognition of the endogenous M2 epitope in BALB/c ($H2^d$) mice (Marques et al., 2008). However, while the latter only affected long-term latent loads, OVA or APLs expression in C57BL/6 ($H2^b$) mice affected the infection outcome during acute MuHV-4-driven B cell proliferation, when trans-acting immune evasion operates (Stevenson et al., 2009). These results demonstrate that latent-specific $CD8^+$ CTL responses can physiologically be attained and show that during acute virus-driven lymphoproliferation, even though viral evasion is fully operational, it can be overcome by $CD8^+$ CTL function. Thus, even with viral evasion some epitope restriction is necessary for MuHV-4 to amplify the pool of latently infected B cells. The obtained results suggest that viral evasion simply raises the threshold for *in vivo* latent epitope recognition by $CD8^+$ CTLs and demonstrate that breaking through is possible with strong epitope presentation. This implies that selection for poor latent epitope presentation is even stronger than previously found (Marques et al., 2008). The effectiveness of viral immune evasion seems to be partially host-dependent. That is, the greater effect of epitope presentation observed in C57BL/6 ($H2^b$) mice possibly reflected differences in host susceptibility to immune evasion, as mK3 degrades $H2K^b$ relatively poorly (Boname and Stevenson, 2001) and degrades TAP better in $H2^d$ than $H2^b$ cells (Boname et al., 2004b). Thus, the extent of virus-driven B cell proliferation seems to reflect an immunological battle between viral $CD8^+$ T cell evasion and host $CD8^+$ CTL control, which is partially host dependent and determined by thresholds of immune engagement (Figure 8.1).

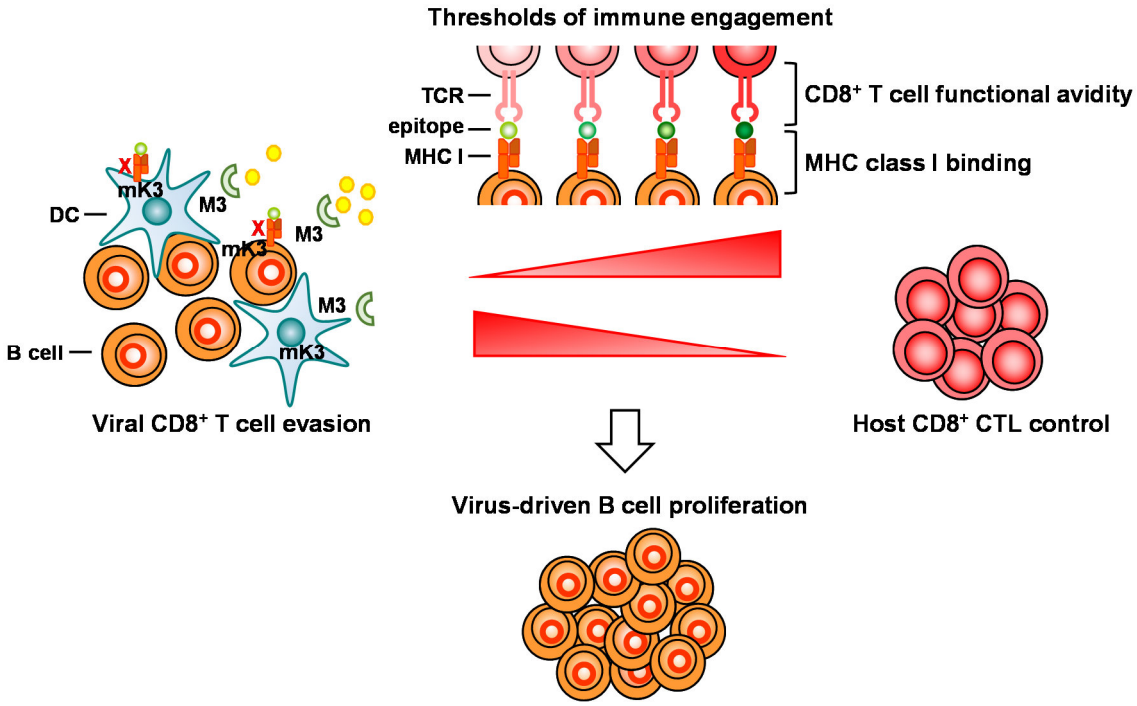

Figure 8.1. Critical MHC class I binding and CD8⁺ T cell engagement thresholds determine the effectiveness of CD8⁺ CTL control of virus-driven B cell proliferation. A dynamic interplay between viral CD8⁺ T cell evasion and CD8⁺ cytotoxic T lymphocyte (CTL) function occurs in the infected host. Viral CD8⁺ T cell evasion afforded by mK3 and M3 expression in dendritic cells (DC) and possibly also in B cells promotes acute latency amplification. M3 is a secreted chemokine binding protein, which may block effective CD8⁺ T lymphocyte recruitment. mK3 promotes the degradation of MHC class I heavy chains and TAP inhibiting antigen presentation to CD8⁺ T cells. Viral evasion probably raises the threshold for *in vivo* latent epitope recognition by CD8⁺ CTLs. Hence, effective CD8⁺ CTL control of latency expansion critically relies on overcoming this threshold with strong epitope presentation. Both MHC class I and CD8⁺ T cell engagement by a latent epitope dramatically affect the balance between virus-driven lymphoproliferation and CD8⁺ CTL control.

In vivo thresholds of MHC class I engagement

In vivo CD8⁺ CTL control of virus-driven B cell proliferation was critically dependent on strong epitope binding to MHC class I. Upon infection of C57BL/6 ($H2^b$) mice with MuHV-4 recombinants expressing epitopes that bound strongly to $H2K^b$, virus-driven B cell proliferation in GCs was cleared rather than amplified and long-term persistence was severely compromised (Figure 8.2). Slightly differences in $H2K^b$ binding, less than 1.6-fold, had no obvious impact on *in vivo* CD8⁺ CTL efficacy. However, a 6-fold reduction in $H2K^b$ binding was poorly tolerated, allowing escape of latently infected GC B cells and the establishment of normal long-term persistence levels. A 60-fold reduction completely abolished CD8⁺ CTL protection. Thus, *in vivo* M2-linked epitope presentation showed very little latitude for sub-optimal MHC class I binding before CD8⁺ CTL control failed. Similar results were obtained in our laboratory upon infection of C57BL/6 ($H2^b$) mice with MuHV-4 recombinants expressing from the M2 C-terminus the $H2K^b$-restricted lytic epitope, derived from MuHV-4 ORF8 glycoprotein B ($ORF8_{604-612}/K^b$), or APLs thereof (Supplementary

Figure 1, C. Godinho-Silva unpublished results). This indicates that the drastic suppression of acute MuHV-4-driven B cell proliferation did not result from introducing in M2 an unusually strong heterologous epitope, since the endogenous ORF8 epitope has been shown to stabilize cell surface $H2K^b$ to a similar degree as OVA (EC_{50} within 2- to 3- fold) (Sehrawat et al., 2012).

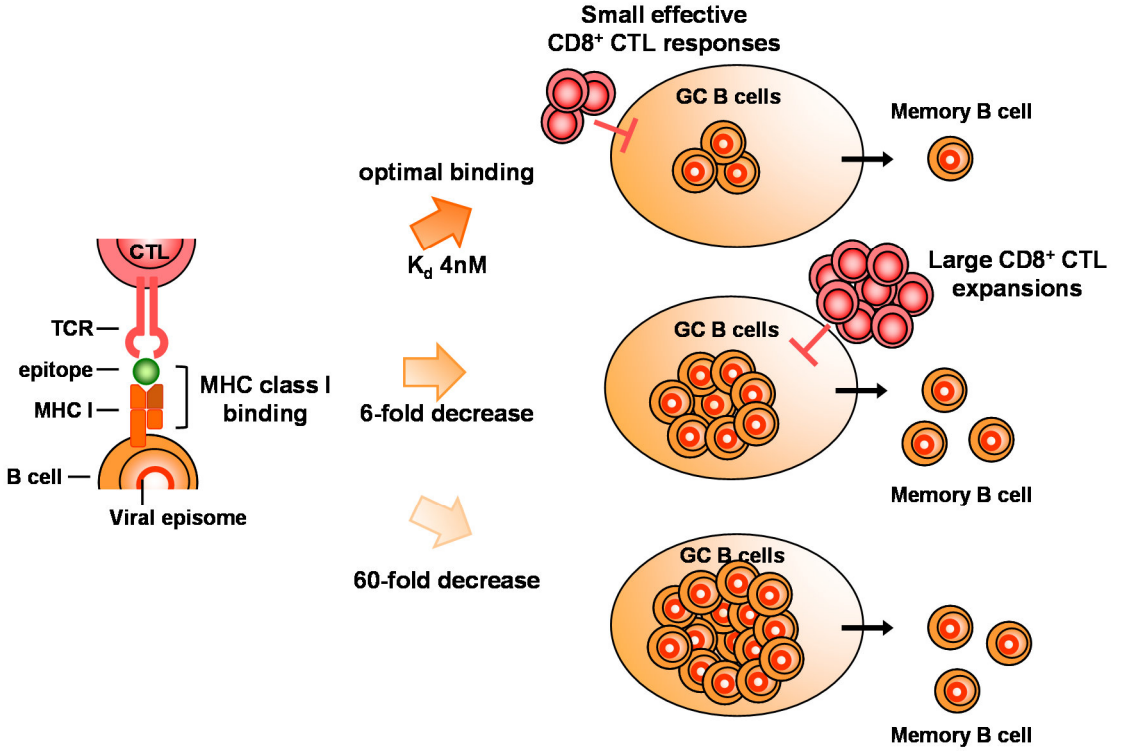

Figure 8.2. *In vivo* MHC class I engagement thresholds critically affect $CD8^+$ CTL control of virus driven B cell proliferation. MHC class I binding by the M2-linked OVA epitope, which as a K_d of 4nM for $H2K^b$ (Matsumura et al., 1992), elicited small but very effective latent-specific $CD8^+$ cytotoxic T lymphocyte (CTL) responses, which suppressed MuHV-4 driven B cell proliferation in GCs and severely compromised long-term persistence. A 6-fold reduction in MHC class I binding allowed large latent-specific $CD8^+$ T cell responses to develop, however they were less efficient at curtailing virus-driven lymphoproliferation in GCs and resulted in normal long-term latent loads. A 60-fold decrease in MHC class I binding abolished $CD8^+$ CTL protection.

Evidence of selection for poor epitope presentation – relevance of MHC class I engagement

The drastic impact of strong MHC class I binding by a latent epitope on MuHV-4-driven B cell proliferation is in agreement with epidemiological evidence of immune pressure from MHC-restricted CTL responses for epitope loss, in the latently expressed EBV EBNA3B protein, by selective mutation of anchor residues (Burrows et al., 1996; de Campos-Lima et al., 1993; de Campos-Lima et al., 1994; Levitsky et al., 1997; Midgley et al., 2003a; Midgley et al., 2003b). The sequence of two unusually strong HLA-A11 restricted immunodominant epitopes within EBNA3B were described to be often mutated in EBV strains prevalent in highly HLA-A11 positive

populations. The changes in the epitope regions altered the amino acid sequence at key anchor residues for HLA-A11 binding and rendered the epitopes non-immunogenic *in vivo*. For KSHV, epidemiological evidence also indicates that several functional MHC class I restricted epitopes, identified in the most variable region of the latent K1 protein, have been positively selected for amino acid diversity (Stebbing et al., 2003). In line with this, comparative studies with closely related MuHV-4 viruses revealed that M2 is the most divergent of the four proteins encoded by the left end of the viral genome (Hughes et al., 2010), showing a higher frequency of non-synonymous mutations (1.01) when compared to M1, M3, M4 and ORF4 (0.20-0.27) (Marques et al., 2008). Thus, the divergence of the *M2* gene in a region of low overall variation may reflect strong immune selection. Evidence of strong positive selection for amino acid diversity in EBV LMP2A and EBNA3B, KSHV K1 and MuHV-4 M2, which provide important $CD8^+$ CTL targets, presumably reflects that less well-recognized viruses establish higher latent loads and therefore transmit better to new hosts (Stevenson et al., 2009). Overall, it seems that the long co-evolution of γHV with their hosts, under immune pressure from $CD8^+$ CTL responses, has resulted in selection for poor epitope presentation. Therefore, it would be interesting to characterize the endogenous M2 latent epitope ($M2_{84\text{-}92}/K^d$) for MHC class I binding and to compare it with the epitopes used in this study. In BALB/c ($H2^d$) mice the $M2_{84\text{-}92}/K^d$-specific $CD8^+$ CTL response allows MuHV-4 expansion of latency in GC B cells and only thereafter control of the virus-induced lymphoproliferation. Thus, MHC class I engagement by the endogenous M2 epitope will probably be close to the threshold of vE1. Furthermore, since the effectiveness of viral immune evasion seems to be partially host-dependent, it would be interesting to infect $H2^{b/d}$ F1 hybrids (BALB/c x C57BL/6) with the MuHV-4 epitope recombinants differing in epitope presentation, and to relate the MHC class I binding characteristics of the endogenous M2 epitope and of OVA and APL epitopes with the ability of each virus to expand the pool of latently infected B cells in $H2^{b/d}$ F1 hybrids.

$CD8^+$ CTL targets

The precise cellular targets for $CD8^+$ CTL recognition of M2-linked epitopes remain unknown. MuHV-4 colonizes the spleen via serial lymphoid/myeloid virus exchange (Frederico et al., 2014) and M2 expression has been detected in several B cell subpopulations, but also in dendritic cells (Marques et al., 2003). Therefore, $CD8^+$ CTLs could suppress virus-driven B cell proliferation indirectly before the onset of lymphoproliferation, by targeting infected myeloid cells, which transfer infection to B cells. However, myeloid cells are probably protected by viral evasion (Smith et al., 2007; Stevenson et al., 2009). Therefore, another possibility is infected B cells, which are a major site of M2 expression (Husain et al., 1999; Marques et al., 2003) and could be directly recognized by $CD8^+$ T cells before latency amplification. Finally, the other possibility is proliferating GC B cells, consistent with the observation that disrupting $CD8^+$ T cell recognition of M2 allows more extensive proliferation of latently infected B cells in GCs of BALB/c mice (Marques et al., 2008).

Susceptibility to CD8$^+$ CTL attack

Susceptibility to CD8$^+$ CTL attack during acute virus-driven B cell proliferation varied with the cell type. vE1 showed a severe acute reduction in the frequency of latently infected total splenocytes, but relative sparing of latently infected GC B cells. This suggests that the latently infected GC B cell population may be more protected from CD8$^+$ CTLs. It is possible that viral evasion operating at the level of GC B cells makes this population of latently infected cells harder to target. Several evidences support this hypothesis. Transcription of both m*K3* and *M3* has been detected in splenic latently infected GC B cells during the acute phase of MuHV-4-driven lymphoproliferation, at day 14 p.i. (Marques et al., 2003). mK3 promotes the degradation of MHC class I heavy chains (Boname and Stevenson, 2001; Lybarger et al., 2003) and the TAP peptide transporter (Boname et al., 2004b). M3 is a secreted protein (van Berkel et al., 1999) that binds chemokines blocking chemokine signalling (Jensen et al., 2003; Parry et al., 2000; van Berkel et al., 2000). Although m*K3* and *M3* are transcribed both in the lytic cycle and during latency (Marques et al., 2003), loss of mK3 and M3 function has no discernable impact on primary lytic lung infection following intranasal inoculation, but causes a CD8-dependent defect in latency-associated lymphoproliferation in GCs *in vivo* (Bridgeman et al., 2001; Stevenson et al., 2002). Therefore, mK3 and M3 could protect B cells and in particular GC B cells directly against CD8$^+$ CTL attack. On the other hand, extensive interplay between lytic and latent infection could provide indirect protection to GC B cells. It has been proposed that mK3 might act by downregulating MHC class I-restricted antigen presentation in lytically infected myeloid cells (Smith et al., 2007), which carry virus to lymphoid tissue (Frederico et al., 2012) and, once there, express early lytic evasion genes such as M3, which binds chemokines and inhibits CD8$^+$ T cell function (Bridgeman et al., 2001; Rice et al., 2002). This way, lytic infection of myeloid cells, expressing mK3 and M3, could both increase virus seeding to B cells and help to protect indirectly latently infected GC B cells (Stevenson et al., 2009).

Infection of C57BL/6 (H2^b) mice with a MuHV-4 recombinant expressing the M2-linked E1 epitope but defective for K3, could help clarifying if GC B cells are indeed more protected from CD8$^+$ CTL attack through viral evasion. If the proposed hypothesis is correct the frequencies of infection for this viral recombinant in GC B cells should be as low as in total splenocytes.

The relative sparing of vE1$^+$ GC B cells allowed the establishment of normal long-term latent loads. This further emphasises the reliance of MuHV-4 on the amplification of the pool of latently infected B cells in GCs in order to establish a long-term latent reservoir, and highlights the importance of targeting acute latency amplification in order to prevent, or at least minimize, long-term persistence.

Where does CD8$^+$ CTL stimulation come from?

Interestingly, the rather modest epitope-specific CD8$^+$ CTL responses elicited by MuHV-4 epitope recombinants expressing M2-linked OVA, Q4, V4, G4 and R4 epitopes (approximately 1-2% of total CD8$^+$ T cells) contrasted with the large E1-specific CD8$^+$ CTL response (approximately 5% of total CD8$^+$ T cells). Despite small in magnitude, CD8$^+$ CTL responses elicited by epitopes capable of strong MHC class I binding completely supressed MuHV-4-driven GC B cell proliferation and severely compromised long-term persistence. This finding is consistent with latent epitope presentation downstream of mLANA eliciting similarly low but very effective CD8$^+$ CTL responses (approximately 1-2% of total CD8$^+$ T cells), which cause a strong CD8$^+$ CTL-dependent latency attenuation (Bennett et al., 2005). Surprisingly, despite decreased MHC class I binding, vE1 stimulated large, functional specific CD8$^+$ CTL responses, but those CTLs were not able to efficiently curtail virus-driven GC B cell proliferation. This suggests that, at least for vE1, most CD8$^+$ CTL stimulation comes from a population distinct from the one engaged in B cell proliferation. During acute MuHV-4 latent expansion many latently infected GC B cells do not make it through to long-term latency, and so a lot may reactivate. Therefore, it is possible that a GC-derived B cell population could be stimulating the larger vE1-specific CD8$^+$ T cell response, but not GC B cells themselves which, as previously suggested, may be more protected through viral evasion, and so harder to target and also incapable of providing CD8$^+$ T cell stimulation. However, it remains unclear which cell type(s) are stimulating the small but very efficient epitope-specific CD8$^+$ CTL responses. During acute MuHV-4-driven lymphoproliferation, latency is established preferentially in B cells, specifically in the main proliferative population of GC B cells, but also in dendritic cells and macrophages (Flano et al., 2000; Flano et al., 2003; Marques et al., 2003). M2 expression has been detected in several B cells subpopulations, besides GC B cells, and in dendritic cells but not in macrophages (Marques et al., 2003). All these cell types express MHC class I molecules at the cell surface and are capable of antigen presentation and mediating CD8$^+$ T cell activation. Additionally, expression of the endogenous M2 latency-associated epitope ($M2_{84\text{-}92}/K^d$) has been detected predominantly in B cells and to a lesser extent in dendritic cells, but again not in macrophages (Woodland et al., 2001a); and B cells have been shown to be needed for efficient priming of the $M2_{84\text{-}92}/K^d$-specific CD8$^+$ T cell response (Usherwood et al., 2000). Therefore, it is possible that the CD8$^+$ CTL responses towards the M2-linked epitopes can be stimulated by the self-renewing population of latently infected B cells, when infection is supressed, but also by other infected cell types, when CD8$^+$ T cells fail to abolish latency amplification. This suggests that the important population for effective *in vivo* control and the main CD8$^+$ T cell stimulating population do not necessarily match.

Discrepancy between CD8$^+$ T cell numbers and effective *in vivo* protection

The small but very efficient latent-specific CD8$^+$ CTL responses found in this study contrast with MuHV-4 large lytic antigen-specific CD8$^+$ T cell responses (Freeman et al., 2010; Gredmark-Russ et al., 2008; Stevenson et al., 1999a). The latter clearly do not control latency amplification as

priming them fails to prevent it (Liu et al., 1999b; Stevenson et al., 1999b). Likewise, both in healthy carriers and in IM large EBV lytic antigen-specific $CD8^+$ T cells are the major expanded populations when compared to latent epitope-specific $CD8^+$ T cells (Hislop and Sabbah, 2008). An equivalent discrepancy between large T cell numbers and effective immune protection is also seen in beta-herpesvirus, in which large $CD8^+$ T cell responses to cytomegalovirus infection are not associated with better control (Karrer et al., 2003; Khan et al., 2002). Therefore, it seems that large $CD8^+$ T cell expansion reflects a failure to control latency. The results obtained in mice infected with vE1 followed the same trend. Those mice showed larger latent $CD8^+$ T cell stimulation yet poor control of virus-driven B cell proliferation, suggesting that bigger responses come from $CD8^+$ T cells acting too late.

In vivo thresholds of $CD8^+$ T cell engagement

EBV provides a dramatic example of conserved TCR usage within an epitope-specific T cell response in humans (Annels et al., 2000; Argaet et al., 1994; Callan et al., 1998a; Miles et al., 2005b). Therefore, domination by a single TCR prompted the analysis of the impact of varying $CD8^+$ T cell functional avidity, for a single latently expressed epitope, on *in vivo* control of MuHV-4-driven lymphoproliferation. Two TCR transgenic mouse models were used, OT-I mice and reconstituted $TCR\alpha^{-/-}$ mice, both with a single $CD8^+$ TCR specificity for $OVA_{257-264}$ in the context of $H2K^b$. Once antigen presentation has broken through, $CD8^+$ CTL functional avidity was an important determinant of *in vivo* control of MuHV-4 latent infection. Specifically, for constant MHC class I binding, MuHV-4 recombinants expressing OVA or APLs showed a titratable correlation between $CD8^+$ CTL functional avidity and *in vivo* control of virus-driven lymphoproliferation. However, this effect was again more evident in total splenocytes, emphasizing the immune privilege of GC B cells from acute $CD8^+$ CTL attack. Low $CD8^+$ CTL functional avidity, elicited by vV4, gave intermediate infectious centre titres and intermediate frequencies of latently infected cells in total splenocytes, with relative sparing of latently infected GC B cells. The $CD8^+$ CTL response displayed a surprisingly large tolerance for sub-optimal TCR engagement, with low $CD8^+$ T cell functional avidity compromising control of virus-driven lymphoproliferation through reduced CTL expansion, rather than differentially affecting CTL effector function. In contrast to MHC class I binding, $CD8^+$ CTL control of virus-driven B cell proliferation remained effective across a wide range of T cell functional avidities. Specifically, high $CD8^+$ CTL functional avidity dramatically suppressed MuHV-4 expansion of latency in GC B cells (Figure 8.3). Reducing $CD8^+$ T cell functional avidity 14-fold had little impact on the control of virus-driven B cell proliferation, with latently infected cells being cleared rather than amplified. However, while a 4,000-fold reduction allowed some $CD8^+$ CTL control of latently infected total splenocytes, MuHV-4 ability to expand latency in GC B cells was unaffected. Finally, a 200,000-fold reduction completely abrogated $CD8^+$ CTL control of virus-driven B cell proliferation. Therefore, this aspect of recognition was more flexible in the two $CD8^+$ T cell monoclonal mouse models used, and a polyclonal $CD8^+$ CTL population could attack any variant epitope so long as its MHC class I binding was strong.

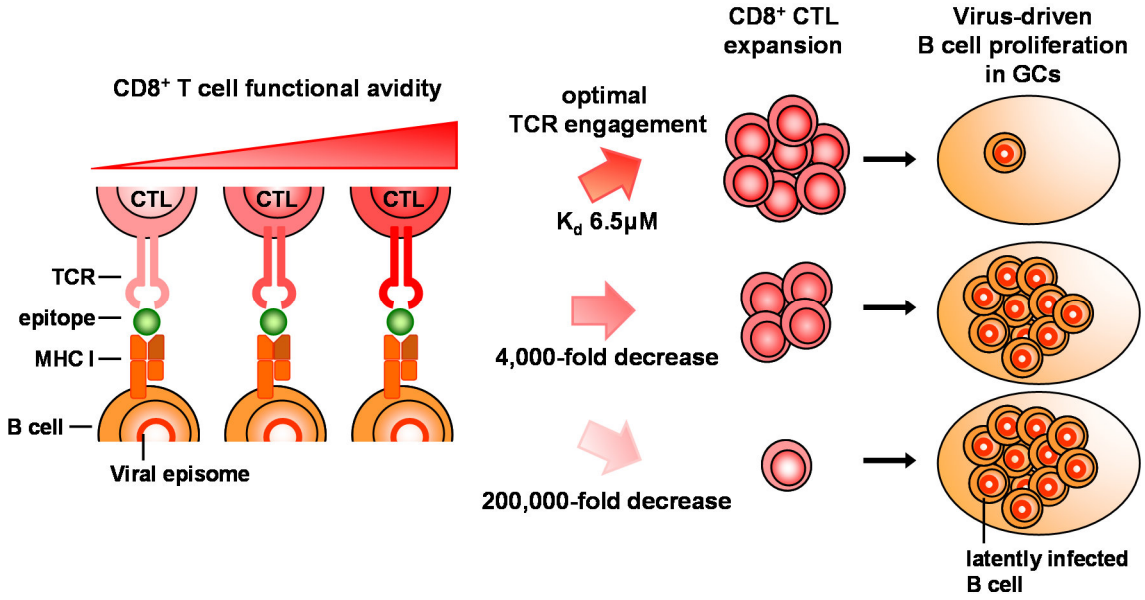

Figure 8.3. *In vivo* thresholds of CD8⁺ T cell engagement by a latently expressed epitope regulate virus-driven B cell proliferation. TCR engagement by the M2-linked OVA epitope, for which the OT-I TCR has a K_d of 6.5 µM (Alam et al., 1996), abolished virus-driven B cell proliferation in GCs. Reducing CD8⁺ T cell functional avidity affected CTL control through reduced CD8⁺ T cell expansion. Still, CD8⁺ CTL control remained effective over a broad range of CD8⁺ T cell functional avidities, showing relatively good tolerance for sub-optimal TCR engagement. CD8⁺ CTL protection started to fail with an epitope with 4,000-fold lower CD8⁺ T cell functional avidity and a 200,000-fold reduction completely abrogated CD8⁺ CTL control of virus-driven B cell proliferation.

Major achievements

In summary, work presented in this thesis demonstrated that a single latently expressed CD8⁺ CTL target allowed acute control of virus-driven B cell proliferation, even with active viral immune evasion at play. Both MHC class I binding and CD8⁺ T cell functional avidity were critical determinants of the *in vivo* control of virus-driven B cell proliferation. Specifically, CD8⁺ CTL control of virus-driven B cell proliferation in GCs was critically dependent on strong epitope binding to MHC class I. By contrast, infection control was effective over a broader range of CD8⁺ T cell functional avidities, showing relatively good tolerance for sub-optimal TCR engagement. Infection of mice with vOVA illustrated the impact of strong epitope presentation, infection with vWT or vA8 that of poor epitope presentation, and OVA APLs covered the range in between, and thus allowed the identification of critical MHC class I and CD8⁺ T cell engagement thresholds for the *in vivo* CD8⁺ CTL control of virus-driven B cell proliferation. The capacity of MuHV-4 to correlate biochemical interactions with *in vivo* immune function underscores the importance of predicting *in vivo* CTL efficacy from biochemical measures and of establishing quantitative guidelines for γHV infection control, with implications for vaccination and anti-cancer immunotherapy.

Final considerations

MuHV-4-driven B cell proliferation seems to be finely balanced, within limits set ultimately by the host immune system. With restricted latent gene expression and with viral immune evasion raising the threshold for *in vivo* epitope recognition, $CD8^+$ CTL efficacy critically relies on overcoming this threshold and on the attack of the appropriate latently infected cell targets. Larger $CD8^+$ CTL responses are not necessarily more protective ones. Therefore, extrapolating from CTL numbers and *in vitro* assays alone is not straightforward and does not necessarily translate into effective *in vivo* protection. A fundamental challenge in the control of γHV is to predict *in vivo* CTL efficacy. Proper selection of protective T cell populations and vaccine epitopes will be essential for optimal γHV infection control.

The $CD8^+$ T cell response to γHV has been extensively studied and several viral $CD8^+$ CTL targets have been identified. However, a comprehensive understanding of how epitope immune engagement functions *in vivo* and how it translates into effective infection control has been lacking. Work presented in this thesis provided a quantitative assessment of how MHC class I and $CD8^+$ T cell engagement, by a single latently expressed epitope, impacts on *in vivo* $CD8^+$ CTL control of virus-driven B cell proliferation and, thus, on host colonization.

MuHV-4 presents as a unique infection model to correlate biochemical interactions with *in vivo* γHV immune control. In this study, infection of mice with MuHV-4 allowed the identification of critical epitope binding characteristics for effective *in vivo* immune control by latent antigen-specific $CD8^+$ CTLs, highlighting the importance and the potential of predicting *in vivo* CTL efficacy from biochemical measures. This constitutes an important step towards the establishment of quantitative guidelines for γHV infection control.

Defining thresholds of immune engagement for effective *in vivo* control of γHV-driven B cell proliferation is fundamental for the design and development of successful immunotherapies and vaccination strategies.

CHAPTER 9

Materials and Methods

Materials and Methods

9.1. Materials

9.1.1. General Reagents

Analytical or molecular biology grade chemicals were obtained from Bio-Rad, Calbiochem, Fluka, Invitrogen, Merck, Roche and Sigma. Molecular biology reagents and enzymes were obtained from Fermentas, Invitrogen, Promega, New England Biolabs, Roche and Stratagene. Tissue culture reagents and supplements were obtained from Gibco BRL. Synthetic oligonucleotides and peptides were synthesized from Thermo Scientific. Antibodies for flow cytometry were obtained from BD Pharmingen, Biolegend and eBioscience. H-2K^{b} tetramers were a kind gift from Dr Hidde L. Ploegh (Whitehead Institute for Biomedical Research, Massachusetts Institute of Technology, Cambridge).

9.1.2. Mice

BALB/cByJ and C57BL/6J mice were purchased from Charles Rivers Laboratories International Inc.

B6.SJL-*Ptprc*^{a} *Pep3*^{b}/BoyJ (CD45.1 C57BL/6) is a congenic strain which carries the differential B cell antigen originally designated Ly5.1 and CD45.1. The *b* allele of *Ptprc* is normally present in the BALB and C57BL inbred strains.

C57BL/6-Tg (*TcraTcrb*)*1100Mjb*/J (OT-I) mice contain transgenic inserts for mouse Tcra-V2 and Tcrb-V5 genes. The transgenic TCR was designed to recognize ovalbumin residues 257-264 in the context of H2K^{b}.

B6.129S7-*Rag1*^{tm1Mom}/J (Rag1$^{-/-}$) mice are homozygous for the *Rag1*^{tm1Mom} mutation and produce no mature T cells or B cells (lack all mature lymphocytes i.e., are "non-leaky"). Rag1$^{-/-}$ mice have no CD3^{+} or TCRαβ^{+} cells.

B6.129S2-*Tcra*^{tm1Mom}/J (TCRα$^{-/-}$) mice are homozygous for the *Tcra*^{tm1Mom} targeted mutation and are deficient in the αβ TCR.

CD45.1 C57BL/6, OT-I, Rag1$^{-/-}$ and TCRα$^{-/-}$ mice were obtained from Jackson Laboratory.

CD45.1 Rag1$^{-/-}$ OT-I mice were obtained by breeding OT-I onto a CD45.1 Rag1$^{-/-}$ background. Mice were bred and housed under specific pathogen-free conditions at *Instituto de Medicina Molecular* animal facility, Lisbon, Portugal.

9.1.3. Cell lines

Baby hamster kidney (BHK-21) fibroblast cells were used for growing and titrating viral stocks, *in vitro* growth curves, *ex vivo* reactivation and plaque assays.

NIH-3T3-CRE cells were kindly provided by Dr Philip Stevenson (Division of Virology, Department of Pathology, University of Cambridge) and were used during the construction of MuHV-4 recombinant viruses, for removing the *lox*P-flanked BAC cassette. This cell line was established by transduction of NIH-3T3 cells with a retrovirus derived from Phoenix-ecotropic cells transfected with pMSCV-NEO (*cre* of bacteriophage P1 cloned into the *Eco*RI-*Xho*I sites of pMSCV-NEO) and selection with 1mg/ml G418 (Stevenson et al., 2002).

RMA-S cells (mutagenized Rauscher virus-induced T lymphoma cells of mouse origin) were kindly provided by Dr Hidde L. Ploegh (Whitehead Institute for Biomedical Research, Massachusetts Institute of Technology, Cambridge) and were used for H-2K^b stabilization assay and *ex vivo* stimulation of OT-I cells with OVA and APL peptides. Murine RMA-S cell line, was derived from the T lymphoma cell line RMA, and is transporter-associated with antigen processing (TAP) deficient (Karre et al., 1986). RMA-S cells have a defect in class I assembly and express markedly reduced levels of class I molecules at the cell surface (Karre et al., 1986; Ljunggren and Karre, 1985; Powis et al., 1991).

9.1.4. Viruses

Murid herpesvirus-4 (MuHV-4) used in this study belongs to the strain MHV-68 (murine herpesvirus 68) that was originally isolated by Prof. Dr Blaskovic (Blaskovic et al., 1980). Clone G2.4 was isolated from virus grown in BHK-21 cells by Dr Stacey Efstathiou (Efstathiou et al., 1990b).

Wild type virus (vWT) used in animal experiments was derived from a genomic bacterial artificial chromosome (BAC) and was a kind gift from Dr Heiko Adler and Dr Ulrich Koszinowski. This virus is essentially MHV-68 clone G2.4 but contains a single *lox*P site (Adler et al., 2001; Adler et al., 2000).

M2-OVA virus (vOVA) was constructed by Dr Sofia Marques in our laboratory by fusing the H2K^b-restricted OVA$_{257-264}$ (SIINFEKL) epitope, derived from chicken ovalbumin, to the C-terminus of M2. This virus contains a 33 nucleotide insertion immediately downstream of M2 last coding codon (nt 4031-4033) followed by a TAA-stop codon. The first six nucleotide insertion generated a new *Hind*III site and codes for a lysine (K) and a leucine (L). The following three nucleotides encode an arginine (K) and the next 24 nucleotides correspond

to the SIINFEKL epitope coding region. This virus was obtained by mutagenesis of the virus genome in *E.coli* using MuHV-4 BAC pHA3.

M2-Q4 virus (vQ4) was constructed by Dr Marta Alenquer in our laboratory using the same strategy employed by Dr Sofia Marques to construct vOVA. It expresses the $H2K^b$-restricted OVA APL Q4 (SIIQFEKL) epitope in fusion with the C-terminus of M2. It differs from vOVA by a single amino acid residue, asparagine (N) at position 4 of the OVA epitope was replaced by a glutamine (Q).

M2-V4 virus (vV4) was engineered by Dr Marta Alenquer in our laboratory by fusing the $H2K^b$-restricted OVA APL V4 (SIIVFEKL) epitope to the C-terminus of M2. It contains asparagine (N) at position 4 of the OVA epitope replaced by a valine (V).

M2-G4 virus (vG4) was engineered by Dr Sofia Marques and Dr Bruno Frederico in our laboratory. It expresses in fusion with the C-terminus of M2 the $H2K^b$-restricted OVA APL G4 (SIIGFEKL) epitope. It contains asparagine (N) at position 4 of the OVA epitope substituted by a glycine (G).

M2-R4 virus (vR4) was constructed by Dr Sofia Marques and Dr Bruno Frederico in our laboratory by fusing the $H2K^b$-restricted OVA APL R4 (SIIRFEKL) epitope to the C-terminus of M2. It contains the asparagine (N) residue at position 4 of the OVA epitope substituted by an arginine (R).

M2-E1 virus (vE1) was engineered by Dr Sofia Marques and Dr Bruno Frederico in our laboratory by fusing the $H2K^b$-restricted OVA APL E1 (EIINFEKL) epitope to the C-terminus of M2. It contains the serine (S) residue at position 1 of the OVA epitope replaced by a glutamic acid (E).

M2-A8 virus (vA8) was engineered in this study by mutagenesis of the virus genome in *E.coli* using the MuHV-4 bacterial artificial chromosome (BAC) pHA3 (Adler et al., 2000) as described in detail in section 9.2.5. It expresses in fusion with the C-terminus of M2 the $H2K^b$-restricted OVA A8 (SIINFEKA) epitope. Leucine (L) at position 8 of the OVA epitope, an anchor residue, was replaced by an alanine (A). This virus was engineered using the same strategy for construction of the previously described MuHV-4 epitope recombinants.

YFP-expressing MuHV-4 recombinant virus (vYFP) used in animal experiments was derived from a genomic bacterial artificial chromosome (BAC) and was a kind gift from Dr Samuel Speck. This virus expresses the enhanced yellow fluorescent protein (YFP), driven by the human cytomegalovirus (HCMV) immediate-early (IE) promoter and enhancer, from a neutral locus in the viral genome located between open reading frames 27 and 29b (Collins et al.,

2009). The expression cassette is flanked by a chromatin insulator from the human major histocompatibility complex II locus, an attempt to prolong YFP expression after the onset of latency. This virus allows direct detection of infected cells based on YFP expression and phenotypic analysis of the infected cell populations and was used in animal experiments with reconstituted TCRα$^{-/-}$ mice.

M2-OVA, -Q4, -V4, -G4 and -R4 expressing MuHV-4 YFP recombinant viruses were engineered in this study by mutagenesis of the virus genome in *E. coli* using the YFP MuHV-4 BAC (Collins et al., 2009), as described in detailed in section 9.2.5. These recombinants were used in animal experiments with reconstituted TCRα$^{-/-}$ mice to facilitate, based on YFP expression, tracking of infected cells, phenotypic analysis of infected cell populations and quantification of infection, by flow cytometry.

9.1.5. Bacterial strains

Plasmids were grown for the general purpose in *E. coli* strain DH5α (Invitrogen) with the following genotype F$^-$ Φ80*lac*ZΔM15 Δ(*lac*ZYA-*arg*F)U169 *rec*A1 *end*A1 *hsd*R17 (r_K^-, m_K^+) *pho*A *sup*E44 λ- *thi*-1 *gyr*A96 *rel*A1.

E. coli strain XL10-Gold ultracompetent (Stratagene), genotype Tet^r Δ(*mcrA*)*183* Δ(*mcrCB-hsdSMR-mrr*)*173 endA1 supE44 thi-1 recA1 gyrA96 relA1 lac* Hte [F´ *proAB lacI*^{q}*ZΔM15* Tn*10* (Tet^r) Amy Cam^r], was used to grow shuttle vector derived plasmids.

E. coli strain DH10B (Invitrogen), genotype F$^-$ *mcr*A Δ(*mrr-hsd*RMS-*mcr*BC) Φ80*lac*ZΔM15 Δ*lac*X74 *rec*A1 *end*A1 *ara*D139 Δ(*ara leu*)7697 *gal*U *gal*K λ- *rps*L (Str^r) *nup*G, containing the MuHV-4 BAC pHA3 (Adler et al., 2000) was provided by Dr Heiko Adler and Dr Ulrich Koszinowski and was used for mutagenesis of MuHV-4 BAC pHA3.
E. coli strain DH10B containing the YFP MuHV-4 BAC was used for mutagenesis of YFP MuHV-4 BAC.

9.1.6. Plasmids

pSP72-M2flank is a pSP72 (Promega) based plasmid in which the *Bgl*II/*Xho*I MuHV-4 genomic fragment (nt 3846 to 5367) was cloned by Dr Sofia Marques. This vector contains the *M2* coding and flanking regions. An engineered *Hind*III restriction site was introduced immediately before the *M2* stop codon.

pST76K-SR (shuttle vector) (Adler et al., 2000) was a kind gift from Dr Heiko Adler and Dr Ulrich Koszinowski.

*Hind*III-E shuttle plasmid, constructed by Dr Sofia Marques in our laboratory, is the 6.1 kb *Hind*III-E genomic fragment of MuHV-4 (nt 107 to 6261) cloned in the pST76K-SR plasmid.

pHA3 is the MuHV-4 genome cloned as a bacterial artificial chromosome (BAC) (Adler et al., 2000) and was kindly provided by Dr Heiko Adler and Dr Ulrich Koszinowski.

pEH1.4 is a pBluescript based plasmid containing the 1.4 kb *Hind*III-*Eco*RI subfragment of the *Hind*III-E MuHV-4 genomic fragment (nt 107 to 1518) cloned in an antigenomic orientation. It contains viral tRNA 1 to 4 and viral miRNA miR-M1-1 to 6, 10 and 11 transcripts. This plasmid was used to generate the digoxigenin (DIG)-labelled probe used to detect viral tRNA 1 to 4 and viral miRNA miR-M1-1 to 6, 10 and 11 transcripts by *in situ* hybridization. Plasmid was linearized with *Hind*III and DIG-labelled antisense probes were synthesised by *in vitro* transcription with T7 RNA polymerase via the T7 phage promoter. This plasmid was constructed by Dr Rory Bowden (Bowden et al., 1997).

9.2. Methods

9.2.1. Isolation and analysis of nucleic acids

9.2.1.1. High molecular weight cellular/viral DNA extractions

High molecular weight (HMW) DNA was extracted from BHK-21 cells infected with a high multiplicity of infection (MOI) (5 PFU/cell). To this end 6 cm cell culture dishes of cells with cytopathic effect (cpe) were harvested by cell scrapping and centrifuged for 5 min at 1,500 rpm. Cell pellet was resuspended in 750 µl of TE lysis buffer (10 mM Tris-HCl pH 8.0, 50 Mm ethylenediaminetetraacetic acid (EDTA), 0.5% SDS and 20 µg/ml Proteinase K) and incubated overnight at 37ºC.

DNA samples containing proteins and salts were purified by deproteinization using phenol/chloroform extraction and concentrated by ethanol precipitation. Typically, an equal volume of TE-buffered phenol:chroloform:isoamyl alcohol (25:24:1) was added to the DNA solution, mixed well by vigorous shaking or vortexing, incubated for 5 min at room temperature (RT) and centrifuged at 10, 000 rpm in a bench top centrifuge, for 5 min at RT. The upper aqueous phase containing DNA was transferred to a clean tube and re-extracted twice with an equal volume of chloroform.

DNA solutions were precipitated using 0.1 volumes of 3M KOAc or NaOAc (pH 5.5) and 2.5 volumes of 100% ethanol. Samples were gently mixed well, left for 10 min at RT and HMW DNA was extracted by spooling onto a glass Pasteur pipette. DNA was washed with cold 70% ethanol, left for 10-20 min at RT to air-dry and then resuspended in MiliQ water or TE.

9.2.1.2. Plasmid DNA isolation

Plasmid DNA was isolated from plasmid-containing *E. coli* strains (section 9.1.5) grown in Luria Bertani (LB) (tryptone 1%, yeast extract 0.5%, NaCl 1%) broth containing the appropriate antibiotic(s), using an alkaline lysis method modified accordingly to the scale of the preparation and plasmid size. Antibiotics were used at the following concentrations: 100 µg/ml ampicilin, 17 µg/ml chloramphenicol and 30 µg/ml kanamycin.

Small scale plasmid preparation

For small scale plasmid preparations (plasmid minipreps), 2-5 ml of LB broth cultures containing the appropriate antibiotic(s) were inoculated from single bacterial colonies and incubated with vigorous shaking 12-18h at 37 or 30ºC. Cultures were pelleted by centrifugation for 10 min at 3,500 rpm. Plasmid DNA was obtained using the Wizard Plus SV Minipreps DNA purification System (Promega), by column purification of DNA prepared by alkaline lysis, according to manufacturer's instructions. DNA was eluted in 50 µl of MiliQ water and stored at -20ºC.

Medium scale plasmid preparation

Cultures of plasmid-containing bacteria were prepared by inoculation of 5 ml LB broth cultures containing the appropriate antibiotic(s) from single colonies and incubation with shaking 12-18h at 37 or 30ºC. Bacteria were sub-cultured 1:500 into 100 ml LB containing the appropriate antibiotic(s) and incubated under the same conditions. Bacterial cultures were concentrated by centrifugation at 6,000 rpm for 15 min at 4ºC and DNA was obtained using the Qiagen Plasmid Midi Kit, following manufacturer's instructions. DNA was resuspended in 200 µl of MiliQ water and stored at -20ºC.

Large scale plasmid preparation

Cultures of plasmid-containing bacteria were prepared by inoculation of 5 ml LB broth cultures containing the appropriate antibiotic(s) from single colonies and incubation with shaking 12-18h at 37 or 30ºC. Bacteria were sub-cultured 1:500 into 200 ml LB containing the appropriate antibiotic(s) and incubated under the same conditions. Bacterial cultures were pelleted by centrifugation at 6,000 rpm for 15 min at 4ºC and DNA was purified using the LFU / Plasmid Purification MAXI Kit (JETSTAR), following manufacturer's instructions. DNA was resuspended in 500 µl of MiliQ water and stored at -20ºC.

Small scale BAC plasmid preparation

For small scale BAC plasmid preparations (BAC plasmid minipreps) 10 ml of LB broth containing 17 µg/ml chloramphenicol were inoculated from single bacterial colonies and incubated with vigorous shaking 12-18h at 37ºC. Bacteria were pelleted by centrifugation at 3,500 rpm for 10 min at 4ºC. Pellet was thoroughly resuspended in 200 µl of buffer P1 (50mM Tris-HCl pH 8.0, 10mM EDTA; from Quiagen) plus 100 µg/ml RNase A. 300 µl of buffer P2 (200mM NaOH, 1% SDS; from Qiagen) were promptly added and the suspension was mixed by gentle inversion and left at RT for 5 min. 300 µl of chilled buffer P3 (3.0 M KOAc pH 5.5; from Qiagen) were added, tubes were gently inverted to mix solution, incubated on ice for 15 min and centrifuged for 10 min at 13,000 rpm and 4ºC. Supernatants were transferred to 2 ml tubes, 1 ml phenol/chloroform (1:1) was added and mixed by inversion. Mixture was left 5 min at RT and then centrifuged 10 min at 13,000 rpm and 4ºC. Aqueous phase was recovered and precipitated with 0.7 volumes of isopropanol and left at RT for 5 min. BAC plasmid DNA was pelleted by centrifugation for 20 min at 13,000 rpm and 4ºC. Supernatant was discharged and the pellet was washed with 70% ethanol, centrifuged another 10 min, drained and air dried. DNA was resuspended in 50 µl of TE (10mM Tris, 1mM EDTA, pH 8.0) supplemented with RNase A (10µg/ml) and stored at 4ºC.

Large scale BAC plasmid preparation

Confluent cultures of BAC plasmid-containing bacteria were prepared by inoculation of 5 ml LB broth cultures supplemented with 17µg/ml chrolamphenicol from single colonies and incubating with shaking 12-18h at 37ºC. Bacteria were sub-cultured 1:500 into 500 ml LB chrolamphenicol and incubated 12-18h at 37ºC with shaking. Bacteria were pelleted by centrifugation at 5,000 rpm

for 15 min at 4ºC. BAC plasmid DNA was isolated using BAC 100 plasmid purification kit (Nucleobond), according to manufacturer's instructions. BAC DNA was resuspended in 100-200 µl TE (10mM Tris-HCl, 1mM EDTA, pH 8.0) supplemented with RNaseA (10 µg/ml) and stored at 4ºC.

9.2.1.3. Mouse tail, toe or ear DNA extractions

Mouse tail, toe or ear were digested by overnight incubation at 55ºC with 100 µl of DirectPCR Lysis Reagent (mouse tail) (Viagen Biotec Inc.) supplemented with 0.2-0.4 mg/ml of Proteinase K. In the next day Proteinase K was inactivated by heating at 85ºC for 1h. 1 µl of lysate was used directly in PCR reactions for mice genotyping (section 9.2.2).

9.2.1.4. Quantification of nucleic acids

DNA was quantified by UV spectrophotometry using a Nanodrop (ND-1000) spectrophotometer.

9.2.1.5. Restriction digestion

Restriction endonuclease digestion of plasmids or PCR products was used either to prepare linear or insert purified DNA, or to screen DNA for a desired digestion profile or for the presence of inserts cloned in expression vectors. Restriction enzyme assays were performed using the appropriate restriction endonucleases and correspondent reaction buffers, according to manufacturer's instructions. Volume of the reaction as well as amount of DNA and enzymes used depended on purpose of the assay.

Digestion of plasmids or PCR products for subsequent ligation and cloning was performed for 1-4h, with 5-10 µg of DNA and 1-10U of restriction endonuclease per µg of DNA, using the manufacturer's recommended conditions in a volume of 50 µl.
Diagnosis digestion was performed typically with 1 µg of DNA, 1-10 U of restriction endonuclease, using manufacturer´s recommended conditions, in a volume of 20 µl for 1-2h.
Multiple digestions of the same DNA were performed when possible with the same buffer; otherwise salt conditions were adjusted for subsequent digestion steps or DNA was re-purified in column. Restriction profile and completeness of the digestion were assessed by analytical agarose gel electrophoresis.

9.2.1.6. Analysis and isolation of DNA by gel electrophoresis

Linear DNAs were size fractioned and visualized on agarose gels stained with ethidium bromide, gel red (Biotium) or red safe (iNtRON Biotechnology), according to manufacturer's instructions. Gels were prepared using 0.7-2% agarose in 1x TAE (40mM Tris-acetate, 1mM EDTA, pH 8.0). DNA samples were mixed with the appropriate volume of DNA loading buffer (10mM EDTA, 5% glycerol, 0.025% bromophenol blue and 0.025% xylene cyanol) prior to loading on wells at the end of the gel. Samples were electrophoresed at 0.5-5.0 V/cm in 1x TAE buffer. DNA was

visualised by UV transillumination. Size of DNA bands was estimated by comparison with linear DNA standards of known molecular weight (1 Kb plus DNA ladder, Invitrogen) run along with samples.

Following analysis of DNA by agarose gel electrophoresis, DNA fragments of interest were purified by excision of the resolved bands from the gel and recovered on QIAquick gel extraction columns (Qiagen), according to manufacturer´s instructions. Typically, DNA was eluted in 50 µl of MiliQ water and a fraction of the purified samples (usually 1/10 of the total volume of the eluate) was re-run on an agarose gel, in order to check the DNA purification.

9.2.1.7. DNA sequencing

Integrity of the plasmids constructed in this study was confirmed by sequencing the PCR generated inserts. During recombinant virus construction all PCR-derived regions were sequenced to confirm the integrity of the introduced epitopes and of the MuHV-4 M2 flanking regions in the *Hind*III-E shuttle plasmid. The stability of the introduced epitopes was checked following BAC mutagenesis in *E.coli* and virus reconstitution in mammalian cells by viral DNA sequencing across the *M2 ORF* in the BAC vector and in HMW DNA extracted from virus infected BHK-21 cells, respectively. Recombinant viruses were also sequenced in the region subjected to mutagenesis to confirm the retention of the introduced epitopes following *in vivo* infection.

DNA was sequenced at STAB VIDA according to the Sanger method and using an automatic DNA sequencer (ABI 3730XL). DNA sequences were analysed and compared to sequences deposited in the NCBI (National Centre for Biotechnology Information) database using the BioEdit Sequence Alignment Editor software.

9.2.2. Polymerase Chain Reaction (PCR)

Polymerase chain reaction was used in this study for different purposes.
During construction of recombinant virus the A8 epitope was introduced by PCR in fusion with the M2 C-terminus using MuHV-4 genomic DNA as a template (section 9.2.5.1). A flanking primer and a mutagenic primer (Table 9.5) were used to obtain the M2 downstream region containing a *Hind*III restriction site followed by the epitope coding region and a stop codon.
PCR reactions were performed using the high fidelity *Pfu* DNA polymerase (Promega). PCR reaction mixes were prepared in a total volume of 50 µl (made up in sterile MiliQ water) and consisted of 300nM of each primer, 1x PCR buffer (Promega), 200 µM of each dNTP, 1U of *Pfu* DNA polymerase (Promega) and <100 ng of template DNA. DNA was amplified on a MyCycler thermal cycler (BioRad), under the following conditions: a initial melting step of 95ºC for 2 min followed by 25-30 cycles of amplification, composed of denaturation at 95ºC for 30 sec, annealing at 55ºC- 57ºC for 30 sec (depending on the optimal annealing temperature for each specific set of primers) and extension at 72ºC for 2 min. A final extension step was performed at 72ºC for 10

min. PCR products were analysed by gel electrophoresis (section 9.2.1.6) to assess if products had the expected size.

M2 ORF DNA region was PCR amplified from HMW DNA for subsequent verification of the introduced epitopes in recombinant viruses by DNA sequencing. Primers used are specific for *M2* gene and generate a fragment of 834 bp (Table 9.1).

Genome integrity of the recombinant viruses in the *Hind*III-E region subjected to homologous recombination was analysed by PCR; primers used and size of the amplified fragments are represented in Table 9.2, Figure 2.2, panels B and C and Figure 2.3, panels A and B.

PCR reactions were performed essentially as previously described but using 1U of *Taq* DNA polymerase (Promega) and the corresponding buffer (Promega).

PCR products were analysed by gel electrophoresis to assess if the products had the expected size. PCR products for subsequent sequencing reactions were purified with QIAquick PCR purification kit (Qiagen), according to manufacturer´s instructions.

Table 9.1. Primers used to amplify *M2* gene.

Oligonucleotide	Sequence	Genomic coordinates	Amplicon
Upper primer	5'-CTGGCTCTCCTAGGGTTGTAAAA-3'	3900-3922	834
Lower primer	5'-GTGTGGTCGAGACTGGAGGTTC-3'	4713-4734	

Table 9.2. Primers used for analysing genome integrity of the recombinant viruses in the *Hind*III-E region.

PCR	Oligonucleotide	Sequence	Genomic coordinates	Amplicon
1	Upper primer	5'-TCTCTGGTTCTGCAAAGCTT-3'	92-111	1596
	Lower primer	5'-CTTAGGAGGTTACCGCACCT-3'	1668-1687	
2	Upper primer	5'-TAAACATGGGCCATTAAAAG-3'	1970-1989	2765
	Lower primer	5'-GTGTGGTCGAGACTGGAGGTTC-3'	4713-4734	
3	Upper primer	5'-CTGGCTCTCCTAGGGTTGTAAAA-3'	3900-3922	2374
	Lower primer	5'-TCCAGCAAGCTTTATCATT-3'	6254-6273	
4	Upper primer	5'-TCTCTGGTTCTGCAAAGCTT-3'	92-111	4244
	Lower primer	5'-CGTTAAAGTCCCCATGGAAGCC-3'	4314-4335	

PCR was also used for genotyping OT-I and CD45.1 Rag1$^{-/-}$ OT-I mice. OT-I positive transgenic mice were identified using sets of primers specific for the VDJ region of the transgenic TCRα and TCRβ chains (Table 9.3). An additional set of primers was used in parallel as an internal positive control. Genotyping of Rag1 deficient strains was performed using the primers described in Table 9.4. PCR reactions and conditions were performed according to the recommendations of Jackson Laboratory. PCR products were analysed by gel electrophoresis.

Table 9.3. Primers used for OT-I genotyping.

Allele	Oligonucleotide	Sequence	Amplicon (bp)
Tg(Tcra)1100Mjb	Upper primer	5'-CAGCAGCAGGTGAGACAAAGT-3'	300
	Lower primer	5'-GGCTTTATAATTAGCTTGGTCC-3'	
Tg(Tcrb)1100Mjb	Upper primer	5'-AAGGTGGAGAGAGACAAAGGATTC-3'	300
	Lower primer	5'-TTGAGAGCTGTCTCC-3'	
Internal positive control	Upper primer	5'-CAAATGTTGCTTGTCTGGTG-3'	200
	Lower primer	5'-GTCAGTCGAGTGCACAGTTT-3'	

Table 9.4. Primers used for Rag1$^{-/-}$ genotyping.

Allele	Oligonucleotide	Sequence	Amplicon (bp)
Rag1^{tm1Mom}	WT forward primer	5'- GAGGTTCCGCTACGACTCTG-3'	WT: 474
	Mutant forward primer	5'- TGGATGTGGAATGTGTGCGAG-3'	Mutant: 530
	Common reverse primer	5'- CCGGACAAGTTTTTCATCGT-3'	Heterozygote: 474 + 530

9.2.3. Cloning procedures

9.2.3.1. Cloning of insert into the pSP72-M2flank vector

Insert was obtained by PCR (section 9.2.2), purified on QIAquick PCR purification column (Qiagen), according to manufacturer's instructions, and digested with *Bgl*II and *Hind*III restriction endonucleases (section 9.2.1.5). Digested insert was then isolated by gel electrophoresis and purified from agarose gel using the QIAquick gel Extraction Kit (Qiagen) (section 9.2.1.6). pSP72-M2flank plasmid contains the *Bgl*II/*Xho*I MuHV-4 genomic fragment (nt 3846 to 5367) in which a *Hind*III restriction site was introduced immediately before the *M2* stop codon. This plasmid was linearized with *Bgl*II (nt 3846) and *Hind*III restriction endonucleases, creating compatible cohesive ends with the insert. Digested vector was isolated by gel electrophoresis and purified from agarose gel using the QIAquick Gel Extraction Kit (Qiagen) (section 9.2.1.6). Prepared insert and vector were ligated as described in section 9.2.3.3 and ligations were transformed into *E. coli* DH5α competent cells (section 9.2.3.4). DNA was isolated from colonies by plasmid miniprep (section 9.2.1.2) and plasmid structure was screened by restriction analysis with the appropriate endonucleases (section 9.2.1.5).

9.2.3.2. Subcloning of insert into the HindIII-E shuttle vector

The previously described construct was subcloned into a *Hind*III-E MuHV-4 genomic fragment (nt 107 to 6261) cloned into the pST76K-SR plasmid by Dr S. Marques. Both plasmids were linearized with *Bln*I (*Hind*III-E nt 3908) and *Xho*I (*Hind*III-E nt 5362) restriction enzymes, creating compatible cohesive ends. Digested insert and vector were then isolated by gel electrophoresis and purified from agarose gel using the QIAquick Gel Extraction Kit (Qiagen) (section 9.2.1.6). Insert and vector were ligated as described in section 9.2.3.3 and ligations were transformed into XL10-Gold ultracompetent cells (Stratagene) (section 9.2.3.4). DNA was isolated from colonies

by plasmid miniprep (section 9.2.1.2) and plasmid structure was screened by restriction analysis with appropriate endonucleases (section 9.2.1.5).

9.2.3.3. DNA ligation

Digested inserts and vectors were ligated using T4 DNA ligase (Roche Applied Science). Approximately 100 ng of vector DNA were ligated with approximately a 1-3 fold excess of insert in 20 µl reactions containing 1x ligase buffer (Roche Applied Science) and 1U of T4 DNA ligase (Roche Applied Science) (made up in sterile MiliQ water). Cohesive-end ligations were performed overnight at 14ºC.

9.2.3.4. Bacterial transformation

Preparation of chemically competent cells

Competent *E. coli* strain DH5α was prepared by the modified H. Inoue method (Inoue et al., 1990). Approximately 5 µl of *E. coli* glycerol stock were inoculated into 10 ml of LB and incubated with vigorous shaking 12-18h at 37ºC. 10 ml of the resulting culture were inoculated into 400 ml of fresh LB and incubated at 37ºC, 225 rpm. When the bacterial culture reached an optical density $(OD)_{600nm}$ of 0.6 the cell culture was cooled on ice. Cells were pelleted by centrifugation at 4,000 rpm for 15 min at 4ºC. Cell pellet was gently resuspended in 100 ml of ice cold sterile solution A (0.03M KCH_3COO, 0.05M $MnCl_2$, 0.01M $CaCl_2$, 0.1M KCl and 15% glycerol in sterile MiliQ water). Cells were centrifuged at 4,000 rpm for 8 min at 4ºC and resulting pellet was resuspended in 20 ml of ice cold solution B (0.01M NaMOPS pH 7.0, 0.075M $CaCl_2$, 0.01M KCl and 15% glycerol in sterile MiliQ water). 100 µl and 300 µl aliquots were made. Each aliquot was quickly frozen by transferring the vials to dry ice immersed in ethanol. Competent cells were stored at -80ºC until further use.

Preparation of TSS competent cells

Competent *E. coli* strain DH10B containing MuHV-4 BAC or YFP MuHV-4 BAC plasmid, were prepared according to the method of (Chung et al., 1989). Briefly, ~5 µl of *E. coli* glycerol stock were inoculated into 5 ml of LB containing 17 µg/ml chloramphenicol and incubated with vigorous shaking 12-18h at 37ºC. 1 ml of the fresh overnight bacteria culture was diluted 1/100 into 100 ml of LB containing 17 µg/ml chloramphenicol and incubated with vigorous shaking at 37ºC. When cells reached an OD_{600nm} of 0.3-0.4 bacterial culture was centrifuged for 10 min at 2,500 rpm and 4ºC. Cell pellet was kindly resuspended in 1/20 (5 ml) of original volume of ice cold LB. Another 1/20 (5 ml) of original volume of 2xTSS (1x LB, 20% polyethylene glycol, 10% dimethyl sulfoxide, 50 mM $MgCl_2$) were added to the cells and 100 µl aliquots were made. Aliquots were quickly frozen by transferring the vials to dry ice immersed in ethanol. Competent cells were stored at -80ºC until further use.

Transformation of competent cells

Competent *E.coli* were transformed by the heat shock method. Competent cells were incubated on ice for 30 min with 100 ng of plasmid DNA or 10 µl of ligation mix. Cells were heat shocked for 45 sec at 42ºC and subsequently chilled on ice for 2 min. 800 µl of SOC medium (2% tryptone, 0.5% yeast extract, 10mM NaCl, 2.5mM $MgCl_2$, 10mM $MgSO_4$, 20mM glucose) were added to each vial and cells were incubated for 1 h at 37 or 30ºC, with vigorous shaking. Cells were then spread onto LB agar plates containing the appropriate antibiotic(s) and incubated at 37 or 30ºC, overnight or until colonies were visible. Ampicilin was used at 100 µg/ml ampicilin, chloramphenicol at 17 µg/ml and kanamycin at 30 µg/ml.

When using XL10-Gold ultracompetent cells (Stratagene) 4 µl of β-Mercaptoethanol mix provided with the kit were added to each aliquot of cells and incubated on ice for 10 min before adding the DNA.

9.2.4. Cell culture and transfections

9.2.4.1. Media and culture conditions

BHK-21 cells were cultured in Glasgow's modified Eagle's medium (GMEM) supplemented with 10% foetal calf serum, 2 mM L-glutamine, 100 U/ml of penicillin and streptomycin and 10% tryptose phosphate broth.

NIH-3T3-CRE cells were grown in Dulbecco's modified Eagle's medium (DMEM) supplemented with 10% foetal calf serum, 2 mM L-glutamine, 100 U/ml of penicillin and streptomycin.

RMA-S cells were grown in RPMI 1640 medium supplemented with 10% foetal calf serum, 2mM L-glutamine and 100 U/ml of penicillin and streptomycin.

All cell cultures were grown in a humidified tissue culture incubator at 37ºC under 5% CO_2.

9.2.4.2. Isolation and purification of OT-I cells

OT-I cells were obtained and purified from spleens of naïve OT-I mice. Briefly, spleens were collected into 5 ml of complete RPMI and kept on ice until mechanical disruption to obtain single splenocyte suspensions. Cell debris was removed by filtering through a 100 µm cell strainer and red blood cells were lysed by incubation with red blood cell lysis buffer (154mM ammonium chloride, 14mM sodium hydrogen carbonate, 1mM EDTA pH7.3) for 5 min on ice. Cell suspensions were washed, resuspended in ice-cold sterile MACS buffer (0.5% bovine serum albumine and 2mM EDTA in PBS pH 7.2) and filtered through a 40 µm cell strainer. OT-I cells were purified by depletion of indirect magnetically labeled non-$CD8\alpha^+$ T cells (negative selection) using mouse $CD8\alpha^+$ T cell isolation kit (MACS, Miltenyi Biotech), according to manufacturer's instructions. The purity of the enriched $CD8\alpha^+$ T cell population was evaluated by flow cytometry and was consistently >97%. Purified splenic OT-I cells were used for determining OVA and APLs stimulatory potency (section 9.2.11.1).

9.2.4.3. Isolation of CD45.1 Rag1$^{-/-}$ OT-I cells

CD45.1 Rag1$^{-/-}$ OT-I T cells were obtained from naïve CD45.1 Rag1$^{-/-}$ OT-I mice pooled lymph nodes (superficial and deep cervicals, axillary, brachial, mesenteric, renal, inguinal, lumbar and caudal). Briefly, pooled lymph nodes were collected into complete RPMI and kept on ice until mechanical disruption to obtain single lymphocyte suspensions. Cell debris was removed by filtering through a 100 µm cell strainer and residual red blood cells were lysed by incubation with red blood cell lysis buffer (154mM ammonium chloride, 14mM sodium hydrogen carbonate, 1mM EDTA pH7.3) for 5 min on ice. Lymphocyte suspension was washed, resuspended in ice-cold PBS and filtered through a 40 µm cell strainer. An aliquot of 10 µl of the obtained lymphocyte suspension was mixed with equal volume of trypan blue (Lonza), transferred to a haemacytometer and the total number of viable lymphocytes was determined by microscopy. CD45.1 Rag1$^{-/-}$ OT-I T cells were kept on ice until adoptive transfer to TCRα$^{-/-}$ recipient mice (section 9.2.6.2).

9.2.4.4. Isolation and purification of CD4^{+} T cells

CD4^{+} T cells were obtained and purified from pooled lymph nodes (superficial and deep cervicals, axillary, brachial, mesenteric, renal, inguinal, lumbar and caudal) of naïve C57BL/6 mice. Lymph nodes were prepared essentially as previously described (section 9.2.4.3). CD4^{+} T cells were purified by depletion of indirect magnetically labeled non-CD4^{+} T cells (negative selection) using mouse CD4^{+} T cell isolation kit (MACS, Miltenyi Biotech), according to manufacturer's instructions. Purity of the enriched CD4^{+} T cell population was evaluated by flow cytometry and was consistently >97%. Total number of viable CD4^{+} T cells was determined by trypan blue staining. CD4^{+} T cells were maintained in PBS, on ice, until adoptive transfer to TCRα$^{-/-}$ recipient mice (section 9.2.6.2).

9.2.4.5. Transfection of BHK-21 cells

BHK-21 cells were transiently transfected using FuGENE 6 or X-tremeGENE HP DNA transfection reagent from Roche Applied Science, according to manufacturer's instruction. Briefly, in the day before the transfection 10^6 BHK-21 cells were plated in 6 cm dishes and grown to semi-confluence.

When using FuGENE 6, 3 µl of FuGENE 6 DNA reagent were added to 300 µl of non-supplemented GMEM, gently mixed and incubated for 5 min at RT. 1 µg of BAC DNA was added to the solution, gently mixed and incubated at RT for 15-45 min.

When using X-tremeGENE HP, 1 µg of BAC DNA was added to 500 µl of non-supplemented GMEM and gently mixed. 2 µl of X-tremeGENE HP were subsequently added and the mix was incubated for 15 min at RT.

The obtained solution was drop wise added to semi-confluent cultures and cells were incubated in a tissue culture incubator at 37ºC with 5% CO_2, until approximately 50% cpe was visible (3-5 days).

9.2.5. Recombinant viruses construction

MuHV-4 recombinants and YFP-expressing MuHV-4 recombinants were derived from a BAC-cloned MuHV-4 pHA3 (Adler et al., 2001; Adler et al., 2000) and a BAC-cloned YFP MuHV-4 (Collins et al., 2009), respectively. Site-directed mutagenesis of MuHV-4-BAC genome was performed by homologous recombination in *E. coli*, using a two step replacement procedure (Adler et al., 2003). Viral progeny was reconstituted by transfection of the recombinant BAC plasmid into eukaryotic cells.

9.2.5.1. Shuttle vector cloning

The first step in the generation of recombinant viruses is the construction of a recombinant plasmid (shuttle plasmid) containing the desired epitope flanked by sequences homologous to the integration site (2 to 3 kb on each side).

OVA A8 epitope was introduced by PCR (section 9.2.2) in fusion with the M2 C-terminus using MuHV-4 genomic DNA as a template. Briefly, the *M2* downstream region (genomic coordinates 3805-4027) containing a *Hind*III restriction site followed by the epitope coding region and a stop codon was PCR amplified using the primers described in Table 9.5 (Figure 9.1). The obtained PCR product was inserted downstream of M2 in pSP72-M2flank plasmid, containing *Bgl*II/*Xho*I MuHV-4 genomic fragment (nt 3846-5367), using the genomic *Bgl*II (nt 3846) and the engineered *Hind*III (nt 4028) restriction sites, thereby attaching the epitope to the M2 C-terminus (section 9.2.3.1). Obtained construct was then subcloned into a *Hind*III-E MuHV-4 genomic fragment (Efstathiou et al., 1990b) cloned in the pST76K-SR shuttle plasmid (Adler et al., 2001), using genomic *Bln*I (nt 3908) and *Xho*I (nt 5362) restriction sites (section 9.2.3.2) (Figure 9.1). PCR-derived region was sequenced to confirm the integrity of the introduced epitope and of the MuHV-4 *M2* flanking region (section 9.2.1.7).

Table 9.5. Primers used to introduce the A8 epitope at the MuHV-4 M2 C-terminus.

Virus	Oligonucleotide	Sequence	Genomic coordinates[a]
vA8	Upper primer	AAAGAATTCCTTTACCAGCACTCACT	3805-3821
	Mutagenic primer	AAAAAGCTT**AGGAGTATAATCAACTTTGAAAAAGCCTAA** CAGTGAAGGTGCTAACGCAGAA	4006-4027

Engineered *Hind*III restriction site is underlined.
OVA A8 epitope coding region is in bold.
Stop codon is in bold and underlined.

9.2.5.2. BAC mutagenesis in E.coli

Recombinant shuttle plasmids were transformed into *E. coli* strain DH10B containing MuHV-4 BAC or YFP MuHV-4 BAC. Bacteria were plated on LB plates containing kanamycin (shuttle plasmid resistance marker) and chloramphenicol (BAC plasmid resistance marker) and incubated overnight at 30ºC, due to the temperature-sensitive replication mode of the shuttle vector. The shuttle plasmid encodes the recA protein which promotes complete integration of the shuttle plasmid into the viral BAC genome by homologous recombination (Adler et al., 2003). Bacteria containing the cointegrate were selected by incubation overnight at 43ºC on LB plates containing kanamycin and chloramphenicol. Clones were replated on LB plates containing chloramphenicol and grown for one day at 30ºC. Under these conditions cointegrates can spontaneously resolve by homologous recombination (bacteria are $recA^+$ at 30ºC) to either wild type or mutant BAC plasmid. Bacteria harbouring resolved cointegrates were selected by replating on LB plates containing chloramphenicol and 5% sucrose (counterselection against SacB encoded by the shuttle plasmid) and grown at 30ºC (selection for sucrose-resistance works best at 30ºC). Finally, colonies were plated in parallel on kanamycin and chloramphenicol containing LB plates and grown overnight at 37ºC. BAC plasmids from chloramphenicol-resistant kanamycin-sensitive clones were isolated by small or large scale BAC plasmid preparations (section 9.2.1.2) and characterized by *Hind*III restriction digestion of BAC DNA to identify the mutant clones (sections 9.2.1.5). The structure and integrity of the viral genome was verified by digestion of BAC DNA with *Bam*HI and *Eco*RI restriction enzymes and analysis of the resulting restriction patterns by agarose gel electrophoresis (section 9.2.1.6). YFP MuHV-4 BAC DNA was also digested with *Apa*I to confirm the present of the YFP cassette.

9.2.5.3. Virus reconstitution

Recombinant BAC DNA was transfected into BHK-21 cells using FuGENE 6 or X-tremeGENE HP DNA transfection reagent (section 9.2.4.5). When approximately 50% cpe was visible, cells and media were harvested and subjected to a freeze-thawing cycle to disrupt the cells. 1 ml aliquots were made and stored at -80ºC until further use. The obtained viral aliquots constituted the BAC^+ virus master stock.

9.2.5.4. Removal of BAC sequences

NIH-3T3-CRE cells were infected with the obtained BAC^+ master stock (section 9.2.7.1) to remove the *lox*P-flanked BAC cassette. The obtained $BAC^{+/-}$ master stock was then subjected to limiting dilution in NIH-3T3-CRE cells to obtain the BAC^- master stock. Briefly, 10^2 PFU of $BAC^{+/-}$ were mixed with 10^6 NIH-3T3-CRE cells and shaken at 37ºC for 1 h in 10 ml of complete DMEM. 100 µl of mixture were added to each well of a 96-well plate. Cells were incubated in a humidified tissue culture incubator at 37ºC under 5% CO_2 until cpe was visible. Wells containing GFP^- plaques (BAC^-) were selected. Cells from selected wells were resuspended in culture supernatant and transferred to a 1.5 ml tube. Half of the obtained suspension was stored at -80ºC while the

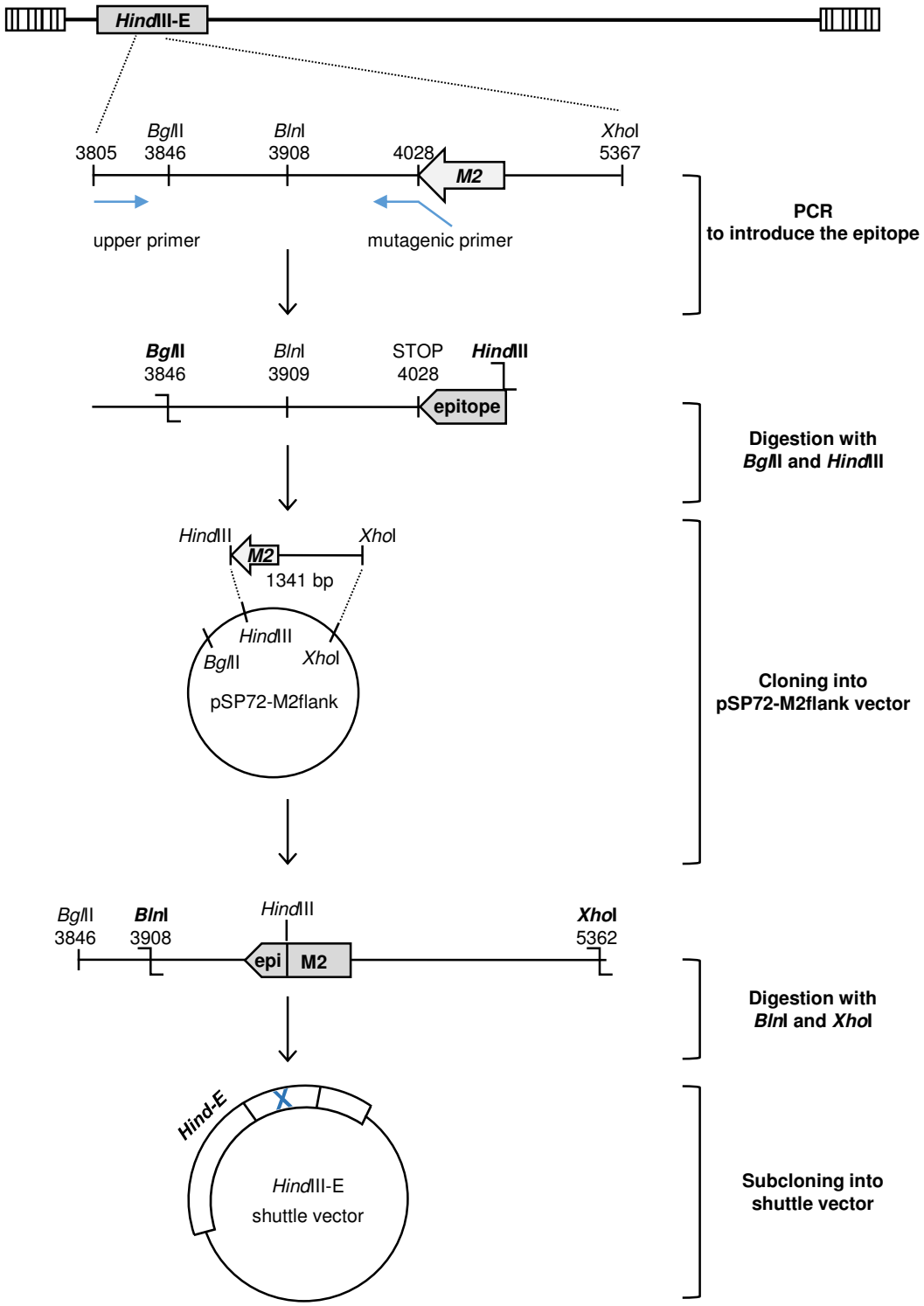

Figure 9.1. Schematic representation of the construction of a recombinant shuttle plasmid. The epitope was introduced by PCR at the M2 C-terminus. In the first step the M2 downstream region containing a *Hind*III restriction site followed by the epitope coding region and a stop codon were PCR amplified to attach the epitope to the M2 C-terminus. PCR product was inserted downstream of a *Hind*III/*Xho*I MuHV-4 genomic fragment in pSP72-M2flank, using a genomic *Bgl*II site and the engineered *Hind*III. The construct was then digested with *Bln*I and *Xho*I and inserted into the *Hind*III-E shuttle vector. Blue cross denotes the introduced epitope.

other half was added to 10^6 NIH-3T3-CRE cells in 1 ml of complete DMEM and incubated for 1 h at 37ºC with shaking. Cells were plated in a 6-well cell culture plate in 4 ml of complete DMEM and incubated at 37ºC until viral plaques appear. Viral plaques were analysed by fluorescence microscopy and, if GFP negative, cells and media were harvested by cell scrapping and centrifuged at 1,500 rpm for 10 min. Pellet was resuspended in 1 ml supernatant and freeze-thawed. 200 µl aliquots were made and constituted the recombinant virus master stock.

9.2.5.5. Analysis of the stability of the introduced epitopes following in vivo infection

Spleens were dissected from mice at 14 days post-infection and single splenocyte suspension were obtained (section 9.2.7.5). Approximately $5x10^6$ splenocytes were added to $5x10^5$ BHK-21 cells in 5 ml of complete GMEM and mixed by inversion. The suspension was plated out in 6 cm cell culture dishes and incubated at 37ºC with 5% CO_2 in a humidified incubator. When cpe was visible cells were harvested, HMW DNA was extracted from infected cells (section 9.2.1.1) and used as a template for a PCR to amplify the *M2* gene (section 9.2.2). PCR products were sequenced to analyse the retention of the introduced epitopes following *in vivo* infection (section 9.2.1.7).

9.2.6. Animal experiments

9.2.6.1. Ethics statement

This study was carried out in strict accordance with the recommendations of the Portuguese official Veterinary Directorate, which complies with the Portuguese Law (Portaria 1005/92). The Portuguese Experiments on Animal Act strictly comply with the European Guideline 86/609/EEC and follow the FELASA (Federation of European Laboratory Animal Science Associations) guidelines and recommendations concerning laboratory animal welfare. Animal experiments were approved by the Portuguese official veterinary department for welfare licensing under the protocol number AEC_2010_017_PS_Rdt_General and the IMM Animal Ethics Committee.

9.2.6.2. Adoptive transfers

CD45.1 $Rag1^{-/-}$ OT-I T cells and purified $CD4^+$ T cells were adoptively transferred to $TCR\alpha^{-/-}$ transgenic mice. CD45.1 $Rag1^{-/-}$ OT-I cells were obtained from pooled lymph nodes of naïve CD45.1 $Rag1^{-/-}$ OT-I mice (section 9.2.4.3). $CD4^+$ T cells were isolated and purified from pooled lymph nodes of naïve C57BL/6 mice (section 9.2.4.4). 10^6 CD45.1 $Rag1^{-/-}$ OT-I cells and $2x10^6$ $CD4^+$ T cells were adoptively transferred into age and sex matched $TCR\alpha^{-/-}$ recipients, via tail vein injection in 200 µl of PBS, one day prior to virus infection.

9.2.6.3. Mice infection

Female BALB/c and C57BL/6 mice (Charles Rivers Laboratories International Inc) were delivered to *Instituto de Medicina Molecular* animal facility at least three days before infections with virus were carried out. 6- to 8-week old female BALB/c and C57BL/6 mice were inoculated intranasally with 10^4 PFU of MuHV-4 or MuHV-4 recombinants. OT-I and TCR$\alpha^{-/-}$ mice were breed and housed at *Instituto de Medicina Molecular*. 8- to 12-week old, male or female, OT-I and reconstituted TCR$\alpha^{-/-}$ mice (section 9.2.6.2) were intranasally inoculated with 10^3 PFU of virus. All virus inoculations were performed in 20 µl of PBS under the effect of light isofluorane anaesthesia. At different time points after infection, mice were sacrificed by CO_2 inhalation or cervical dislocation, lungs or spleens were removed and processed for subsequent analysis.

9.2.6.4. CD8$^+$ T cell depletions

MuHV-4 infected OT-I mice were depleted of CD8$^+$ T cells by 5 intraperitoneal injections of 200 µg monoclonal antibody YTS 169.4, in 200 µl of PBS (Cobbold et al., 1984). Splenocytes from control or depleted mice were stained with anti-CD8α (53-6.7) (BD Pharmingen) (section 9.2.8.1) and analysed on a LRS Fortessa (BD Biosciences) (section 9.2.8.3).

9.2.7. Virus Assays

9.2.7.1. Virus infection of cells

Cells were seeded in tissue culture flasks or plates and grown to semi-confluence for low multiplicity of infection or to confluence for high multiplicity of infection. Cell monolayers were adsorbed with virus suspension in 10% of the final appropriate culture medium for 1h at 37ºC, then covered with the remaining 90% of medium and incubated for the appropriate time.

9.2.7.2. Virus working stocks

Virus working stocks were grown by low multiplicity infection of BHK-21 cells (0.001 PFU/cell) in 175cm^2 culture flasks. When approximately 50% cpe was visible (3-5 days), cells and supernatants were transferred to 50 ml tubes and centrifuged at 1,500 rpm for 10 min at 4ºC. Cell-associated virus was resuspended in 2 ml of fresh complete GMEM medium, subjected to freeze-thawing, and kept at -80ºC in 200 µl aliquots. Supernatant-associated virus was centrifuged at 15,000 rpm for 2 h at 4ºC and pellet was resuspended in 2 ml of fresh medium. 100 µl aliquots were made and stored at -80ºC. Virus titres were determined in duplicates by suspension assay.

9.2.7.3. In vitro multi-step growth curves

Low multiplicity growth curves were performed on confluent cell monolayers in 24-well plates. One day prior to infection 5x10^4 BHK-21 cells were plated per well in a 24 well plate. BHK-21 cells were infected at MOI of 0.01 PFU/cell, in 200 µl of complete GMEM, and virus was allowed to

adsorb for 1 h at 37ºC. Cells were washed in PBS and 1 ml of fresh complete GMEM was added. At each time point after infection, cells and supernatants were harvested, subjected to freeze-thawing and kept at -80ºC. Virus titres were determined by suspension assay for duplicate plates.

9.2.7.4. Plaque assay (suspension assay)

Virus stocks, *in vitro* multi-step growth curves and infectious virus in the lung and spleen of infected mice were titrated by plaque assay (or suspension assay).

Lungs and spleens were dissected into 15 ml tubes containing 5 ml of complete GMEM and frozen at -80ºC. Thawed lungs were homogenized in a glass homogenizer and frozen at -80ºC. Tissue homogenates, previously subjected to freeze-thawing to disrupt cells, were 10-fold serial diluted in 1ml of complete GMEM. $5x10^5$ BHK-21 cells were added to the serial 10-fold dilutions of virus suspensions in 1 ml of complete GMEM and adsorbed for 1 h at 37ºC with shaking. 3 ml of complete GMEM were added and then the suspension was plated out into 6 cm cell culture dishes. After 4 days incubation at 37ºC with 5% CO_2 in a humidified incubator, cell monolayers were fixed with 10% formaldehyde in phosphate-buffered saline (PBS) and stained with 0.1% toluidine blue. Viral plaques were counted using a magnifier lenses (Olympus SZ51 zoom stereo microscope) and virus titres were calculated from the number of viral plaques on duplicate dishes.

9.2.7.5. Infectious centre assay

Spleens were dissected from mice into 5 ml of complete GMEM and kept on ice during the procedure. Single cell suspensions were obtained by mechanical disruption and cell debris was removed by filtering through a 100 µl cell strainer. Cells were pelleted by centrifugation at 1,200 rpm for 5 min at 4ºC. Red blood cells were lysed by incubation with 1 ml of red blood cell lysis buffer (154mM ammonium chloride, 14mM sodium hydrogen carbonate, 1mM EDTA pH7.3) for 5 min on ice. 5 ml of complete GMEM were added, cells were centrifuged and resuspended in 5 ml of fresh medium. Cell suspensions were 10-fold serial diluted and $5x10^5$ BHK-21 cells were added. Final volume was made up to 5 ml with complete GMEM, suspension was mixed by inversion and plated out in 6 cm cell culture dishes. Assays were incubated for 5 days at 37ºC in a humidified incubator with 5% CO_2. Cell monolayers were fixed with 10% formaldehyde in PBS and stained with 0.1% toluidine blue. Viral plaques were counted using an Olympus SZ51 zoom stereo microscope and infectious centres were determined from duplicate dishes.

9.2.8. Flow cytometry

9.2.8.1. Staining of splenocytes

Spleens were dissected from mice into 5 ml 2% FCS in PBS and kept on ice until mechanical disruption to obtain single splenocyte suspensions. Cell debris was removed by filtering through a 100 µl cell strainer. Red blood cells were lysed by incubation with red blood cell lysis buffer for 5 min on ice. Cell suspensions were washed with 2% FCS in PBS and blocked by incubation with anti-CD16/32 (2.4G2) (BD Pharmingen) for 10 min at 4ºC. Splenocytes were stained by incubation for 30 min, at 4ºC, in the dark, with the appropriated antibodies diluted in PBS with 2% FCS (Table 9.6). Unbound antibodies were removed by washing twice with 2% FCS in PBS. For biotinylated antibodies, additional 20 min incubation with streptavidin was performed. MuHV-4 infected cells were identified based on YFP expression. Cells were resuspended in PBS with 2% FCS and flow analysed (section 9.2.8.3).

Table 9.6. List of antibodies used in flow cytometry analysis.

Antigen	Clone	Company
CD19	1D3	BD Pharmingen
CD95	Jo2	
CD8α	53-6.7	
IFNγ	XMG1.2	
CD45.1	A20	Biolegend
CD45.2	104	
CD44	IM7	
CD62L	MEL-14	
GL7	GL7	EBioscience
$H2K^b$	AF6-88.5.5.3	
TCRβ	H57-597	
GranzymeB	NGZB	
IgG2ak	eBR2a	

9.2.8.2. Purification of germinal centre B cell populations

Single cell suspensions of 4-5 pooled spleens stained with anti-CD19 (1D3) APC-H7 (BD Pharmingen), anti-CD95 (Jo2) PE (BD Pharmingen) and anti-GL7 T and B cell activation marker (GL7) eFluor660 (eBioscience) were enriched for the germinal centre B cell population $CD19^{+}CD95^{hi}GL7^{hi}$ using a BD FACSAria Flow Cytometer (BD Biosciences). Cells were recovered into 50% FCS in PBS and kept on ice until further use.

9.2.8.3. Flow cytometry analysis

Total splenocytes, lymph node cells or enriched cell populations were analysed on a LSR Fortessa (BD Biosciences), using FACSDiva software (BD Biosciences) for acquisition and FlowJo (Tree Star, Inc.) for analysis.

9.2.9. Limiting dilution analysis of infected splenocytes

Total single cell splenocyte suspensions or FACS-purified GC B cells (section 9.2.8.2) were 2-fold serial diluted in 2% FCS in PBS and 8 replicates were made per dilution. Cells were lysed by incubation in lysis buffer (10 mM Tris-HCl pH 8.3, 0.45% Tween-20, 0.45% NP-40, 3 mM $MgCl_2$, 50 mM KCl and 0.5mg/ml Proteinase K) at 37ºC overnight. In the next day Proteinase K was inactivated by incubation at 95ºC for 5 min. Samples were analysed by real time PCR (section 9.2.9.2) with primer/probe sets specific for *M9*. For each dilution, the number of negative PCR reactions, corresponding to a failure to obtain an amplification curve during the PCR cycles, was determined.

9.2.9.1. Statistical analysis of limiting dilution assay

Statistical analysis of limiting dilution assay to estimate the frequency of virus DNA+ cells was performed according to the method developed by Dr Sofia Marques (Marques et al., 2003).
The frequency of virus DNA+ cells (*f*) was calculated according to the single-hit Poison Model (SHPM) by maximum likelihood estimation (Bonnefoix et al., 2001). This model assumes that one limiting cell of one cell subset is necessary and sufficient for generating a positive response.
To evaluate the fit of the SHPM to our limiting dilution experiments, a method developed by Bonnefoix *et al*., (2001) was employed. This method consists in modelling the limiting dilution data according to the linear log-log regression model fitting the SHPM $\left(-log\left(log(\mu_i)\right) = \log(f) + \log(x_i)\right)$, where μ_i is the theoretical fraction of negative wells and x_i is the number of cells plated in each replicate well) and checking this model by an appropriate slope test (Bonnefoix et al., 2001).
Being *f* the frequency of virus DNA+ cells, the maximum likelihood of *f* is the value of *f* that maximizes the following function:

$$\log(L) = \sum_{i=1}^{k}\left[log\left(\frac{n_i!}{r_i!(n_i!-r_i!)}\right) + r_i\log(P_i) + (n_i - r_i)\log(1 - P_i^k)\right]$$

Where log(L) is the natural logarithm of the likelihood function L, P_i is given by $P_i = \exp(-f x_i)$ according to the SHPM. k is the number of groups of replicate PCR reactions, numbered i=1,2,3,…,k; n_i is the number of replicate reactions and r_i is the number of observed negative PCR reactions.
The standard error of *f* was calculated as the square root of the negative reciprocal of the second derivate of log(L):

$$SE(f) = \sqrt{\frac{-1}{d^2\log(L)/df^2}}$$

The 95% confidence interval (CI) of *f* was calculated as 95% CI(*f*) = $f \pm 1.96SE(f)$.

9.2.9.2. Real time PCR

Real time PCR was performed on a Rotor Gene 6000 (Corbett Life Science) according to manufacturer's instructions, using the fluorescent Taqman methodology. Primer/probe sets specific for MuHV-4 *M9* gene were used (Table 9.7). Reactions were performed in a final volume of 25 µl, containing 2.5 µl of cell lysate, 200 µM of each primer, 300 µM of probe, 1x Platinum Quantitative PCR SuperMix-UDG (Invitrogen), 5 mM of $MgCl_2$ and 1x Rox reference dye. Samples were subjected to a melting step of 95ºC for 10 min followed by 40 cycles of 15 s at 95ºC and 1 min at 60ºC. Real time PCR results were analysed on the Rotor Gene 6000 software.

Table 9.7. Primers and probe specific to *M9* gene used to detect MuHV-4 DNA.

Oligonucleotide	Sequence	Genomic coordinates[a]
Upper primer	5'-GCCACGGTGGCCCTCTA-3'	94176-94192
Lower primer	5'-CAGGCCTCCCTCCCTTTG-3'	94140-94157
Probe	5'-6-FAM-CTTCTGTTGATCTTCC-MGB-3'[b]	94159-94174

[a]According to GenBank accession no NC_001826.
[b]Oligonucleotide with fluorophore (6FAM) and quencher (MGB) covalently attached to the 5´- and 3´-ends, respectively.

9.2.10. *In situ* hybridization (ISH)

9.2.10.1. Generation of digoxigenin UTP-labelled riboprobes

Riboprobe used in this study was *in vitro* transcribed from pEH1.4 plasmid using the digoxigenin (DIG) RNA labeling kit T7/SP6 (Roche Applied Science), according to manufacturer´s instructions. Briefly, 1 µg of *Hind*III-linearized plasmid was transcribed in a 20 µl reaction containing 2 µl of 10x transcription buffer, 2 µl of 10x NTP labeling mixture, 1 µl of Protector RNase inhibitor and 2 µl of T7 RNA polymerase. After 2 h incubation at 37ºC template DNA was removed by addition of 2 µl of DNase and incubation for 15 min at 37ºC. Reaction was stopped by adding 2 ml of 0.2 M EDTA (pH8.0).

RNA was precipitated by addition of 2.5 µl of 4 M LiCl and 75 µl of ice-cold 100% ethanol, and incubation at -80ºC for at least 30 min. RNA was centrifuged at 13,000 rpm and 4ºC for 15 min, supernatant was discarded and pellet was washed with 50 µl of ice-cold 70% ethanol. Pellet was resuspended in 100 µl MiliQ water and incubated for 30 min at 37ºC. 20 µl aliquots were made and stored at -80ºC until required.

Concentration of labelled RNA was analysed by spot test assay, according to instructions provided in the DIG RNA labelling kit manual (Roche Applied Science).

9.2.10.2. Preparation of tissue for ISH

Spleens for ISH were dissected from groups of mice and fixed in 10% formalin, overnight at RT. Spleens were then embedded in paraffin in the Histology Service located in the Histology facilities of the Histology Institute of *Faculdade de Medicina de Lisboa*. Serial 5 µm sections were cut on a Minot Microtome Leica RM 2145 and mounted on Superfrost Plus slides (Menzel-Glaser).

9.2.10.3. In situ hybridization

In situ hybridization was performed as described by J. P. Simas *et al*. (1999). Sections were dewaxed in xylene for 20 min, rehydrated through graded ethanol solutions: 100% for 5 min, 90%, 70% and 50% for 2 min each and finally PBS for 5 min. Sections were then fixed in 0.1% v/v glutaraldehyde in PBS for 30 min at 4ºC, washed twice in PBS for 5 min and then digested with 100 µg/ml of Proteinase K in 20 mM Tris pH 7.5 and 2 mM $CaCl_2$ in dH_2O for 8-10 min at 37ºC. Sections were rinsed in PBS for 2 min at RT, re-fixed in 0.1% v/v glutaraldehyde for 15 min at 4ºC, rinsed in PBS again for 2 min at RT, then acetylated with fresh 0.25% v/v acetic anhydride in 0.1 M triethanolamine pH 8.0 while being stirred for 10 min at RT. Sections were washed in 2x saline sodium citrate (SSC) (300 mM NaCl and 30 mM Tri-sodium-citrate) for 5 min at 4ºC before being dehydrated through graded ethanol (50% to 100%) and left to air dry.

For 100 µl of probe mix, 2 µl of DIG-labelled riboprobe were mixed with 50 µl of deionised formamide, 5 µl of sonicated salmon sperm (10 mg/ml) and 5 µl of tRNA (10 mg/ml). Mix was denatured by heating for 5 min at 80ºC and then quenched on ice. 20 µl of 5x hybridization buffer, 1 µl of DTT (100 mM) and 100 U of Protector RNase inhibitor were added with MiliQ water to a final volume of 100 µl. 30 µl of probe mix were added to each section, covered with parafilm and incubated overnight at 55ºC on a humidified incubator.

After hybridization, probes were washed in 2x SSC and 10 mM Tris pH 7.5 for 15 min at RT with stirring and then in 0.1x SSC and 10 mM Tris pH 7.5 for additional 15 min. The stringency wash was performed in 30% deionised formamide, 0.1x SSC and 10 mM Tris pH 7.5, for 30 min, at 58ºC. Finally sections were rinsed in 0.1x SSC and 10 mM Tris pH 7.5 for 5 min at RT with stirring.

Hybridized probe was detected with alkaline phosphatase (AP)-conjugated anti-DIG antibody (Roche Applied Science). Sections were rinsed for 5 min, while stirring, in buffer 1 (100 mM Tris pH 7.5 and 150 mM NaCl in dH_2O), then blocked by incubation in blocking buffer (1% Boehringer Blocking Reagent, Roche, in buffer 1) for 30 min at RT. Sections were then dried around the edges and incubated with 100 µl anti-DIG-AP antibody (1:500 in blocking buffer) for 1 h at RT in a humidified chamber. Unbound antibody was removed by washing twice with buffer 1 for 15 min at RT.

Bound antibody was revealed by colorimetric detection with NBT. Sections were rinsed in buffer 3 (100 mM Tris pH 9.5, 100 mM NaCl and 50 mM $MgCl_2$ in dH_2O) for 10 min at RT. Colour development was performed in the dark by incubation of sections with NBT and X-Phos (Roche) in buffer 3 for at least 2 h. Reaction was stopped by rising with dH_2O. Sections were counter stained with 10% Mayer´s Haemalum, rinsed in tap H_2O and mounted with Aquatex (Merck).

9.2.11. T cell assays

9.2.11.1. OVA and APLs stimulatory potency

To measure the *ex vivo* stimulation of naïve OT-I cells by OVA and derived APL peptides, OT-I cells were isolated and purified from spleens of naïve OT-I mice (section 9.2.4.2). TAP deficient RMA-S cells were used as antigen presenting cells to ensure equivalent peptide/MHC class I numbers. 10^6/ml RMA-S cells were first incubated overnight at 26ºC with 5% CO_2 in a humidified incubator, to increase the level of empty surface $H2K^b$ molecules. In the next day, cells were counted and $2.5x10^5$ cells/ml were irradiated for 12 min 33 seg with 7500 rads in a Gammacell 3000 Elan Irradiator. 100 µl of RMA-S cells were plated per well of a round bottom 96 well-plate, then loaded with titrated doses of soluble OVA and APL peptides (Thermo Scientific) in 50 µl and incubated at 26ºC in complete RPMI supplemented with 1x non-essential amino acids, 1x sodium piruvate, 1x hepes and 1 x 2-mercaptoethanol. $5x10^4$ purified OT-I cells were then added to $2.5x10^4$ peptide-loaded RMA-S cells and incubated for 72 h at 37ºC with 5% CO_2 in a humidified tissue culture incubator. At the end of the incubation period culture supernatants were harvested and frozen at -20ºC until further analysis. IFNγ levels were measured in the culture supernatants by ELISA using the DuoSet ELISA development kit (R&D Systems), according to manufacturer's instructions. The data obtained were analysed and fit to sigmoidal dose-response curves and the EC_{50} values for half-maximum response concentrations were calculated using GraphPad Prism software.

9.2.11.2. Tetramer staining

Tetramer staining was performed with $H\text{-}2K^b$ tetramers, a kind gift from Dr Hidde L. Ploegh, produced by exchange of conditional ligand for SIINFEKL ($OVA_{257\text{-}264}$), SIIQFEKL (Q4), SIIVFEKL (V4), SIIGFEKL (G4), SIIRFEKL (R4), EIINFEKL (E1), SIINFEKA (A8) or RGYVYQGL (VSV $NP_{52\text{-}59}$) peptides (Thermo Scientific).

Class I MHC peptide exchange

1 µg of tetramer was diluted to 50 µl of RPMI without phenol red and supplemented with 10% FCS, 2mM L-glutamine and 100 U/ml of penicillin and streptomycin. The solution was deposited in a 96-well plate (round bottom) and 10 µg of peptide was added. The plate was placed (without the lid) in a flat bucket on ice, with aluminium foil underneath the plate, and UV cross linked two times, rotating the plate 90º in between, 7.5 min each time. Irradiation was performed in a Stratalinker 2400 UV cross-linker equipped with 365-nm UV lamps at an ≈ 10- to 20-cm distance from the UV source. After 1 h of incubation on ice and in the dark, the plate was centrifuged 3,000 x g for 20 min to remove any aggregates, and 50 µl of the supernatant was transferred into a new 96-well plate.

Tetramer staining

Splenocytes were distributed over a round bottom 96-well plate ($2x10^6$ in 50 µl per well) containing freshly prepared MHC tetramers and anti-CD8α (53-6.7) (BD Pharmingen) (50 µl per well) and were incubated for 45 min at 4ºC in the dark. Cells were washed twice with ice-cold PBS and fixed with 0.5% formaldehyde in PBS, overnight at 4ºC in the dark. In the next day cells were transferred to FACS tubes and flow analysed.

9.2.11.3. Ex vivo stimulation and intracellular cytokine staining

Freshly isolated splenocytes ($2x10^6$) obtained from infected mice were stimulated in 96-well round-bottom plates, for 5h at 37ºC and 5% CO_2, with 10 µg/ml peptide (OVA, APLs, A8 or VSV NP_{52-59}), 10 U/ml recombinant murine IL-2 (PeproTech) and 10 µg/ml Brefeldin A, in RPMI 1640 medium supplemented with 10% FCS, 2mM glutamine, 100 U/ml penicillin and streptomycin and 50 µM 2-mercaptoethanol (200 µl per well).

At the end of the incubation period cell surface staining followed by intracellular cytokine staining was performed. Briefly, cells were washed with 2% FCS in PBS (200 µl per well), blocked with anti-CD16/32 (2.4G2) (BD Pharmingen) for 15 minutes at 4ºC (40 µl per well) and cell surface stained by addition of 10 µl of anti-CD8α (53-6.7) (BD Pharmingen) or anti-CD8α and anti-CD45.1 (A20) (Biolegend) (for detection of OT-I cells) in PBS with 2% FCS. Cells were incubated for 30 min at 4ºC in the dark. After incubation, cells were fixed and permeabilized with Fix/Perm solution (Foxp3 staining buffer set, eBioscience) (100 µl per well) for 30 minutes at 4ºC, washed once with PERM buffer (Foxp3 staining buffer set, eBioscience) (100 µl per well) and blocked again by 15 min incubation with anti-CD16/32 diluted in PERM buffer (40 µl per well). Cells were then intracellular stained by addition of 10 µl of anti-IFNγ (XMG1.2) (BD Pharmingen), anti-Granzyme B (NGZB) or anti-IgG2ak Isotype control (eBioscience) in PERM buffer. Following 30 min incubation at 4ºC in the dark cells were washed twice with PERM buffer (100 µl per well) and resuspended in PBS with 2% FCS. Samples were collected and flow analysed on a LSR Fortessa (BD Biosciences).

9.2.11.4. In vivo cytotoxicity assay

Preparation of splenocytes

Total splenocytes from naïve congenic CD45.1 C57BL/6 mice were used as target and control cells. Spleens were pooled from CD45.1 C57BL/6 mice into 5 ml of complete RPMI and kept on ice until mechanical disruption to obtain single splenocyte suspensions. Cell debris was removed by filtering through a 100 µm cell strainer. Red blood cells were lysed by incubation with red blood cell lysis buffer for 5 min on ice. Cell suspensions were washed, resuspended in RPMI and filtered through a 100 µm cell strainer. An aliquot of 10 µl of the obtained cell suspension was transferred to an haemacytometer and the total number of splenocytes was determined by microscopy.

Peptide pulsing of splenocytes

$2x10^6$ splenocytes/ml were incubated with 1 µM of SIINFEKL (OVA), EIINFEKL (E1) or A8 (SIINFEKA) peptides (Thermo Scientific), for 1 h at 37ºC, in pre-warmed RPMI. Control splenocytes were left unpulsed. Cells were washed in RPMI without FCS and maintained at $2x10^6$/ml.

CFSE labeling

Target peptide-pulsed cells were labeled with a high (1µM) concentration of carboxyfluorescein succinimidyl ester (CFSE) (Molecular Probes). Control unpulsed cells were labeled with a low (0.1µM) concentration of CFSE. CFSE labeling was performed for 10 min at 37ºC in pre-warmed RPMI without FCS. At the end of the incubation period cells were immediately washed once with ice-cold complete RPMI, three times with ice-cold PBS and filtered through a 40 µm cell strainer. The total number of viable splenocytes was determined for each condition by trypan blue staining followed by microscopy analysis. $2x10^6$ targets and equal numbers of control cells (50:50 mixes of $CFSE^{hi}$ and $CFSE^{lo}$ cells) were prepared in 200 µl of ice-cold PBS. An aliquot of 10 µl from each mix was used for subsequent flow cytometry analysis of prepared mixes (section 9.2.8.1).

Adoptive transfer and analysis

Mixes were injected intravenously into the tail vein of vWT infected C57BL/6 controls to ensure equal transfer, and vOVA, vE1 or vA8 infected mice. In the next day splenocytes were harvested from recipient mice and the proportion of $CFSE^{hi}$ and $CFSE^{lo}$ cells among transferred $CD45.1^+$ splenocytes was analysed by flow cytometry (section 9.2.8.1). Dead cells were excluded by addition of propidium iodide (Sigma) to each sample immediately before acquisition.
Target cell killing was calculated as:

$$\% \text{ target cell killing} = 100 - \left(\frac{(\% CFSE^{lo} / \% CFSE^{hi}) \; in \; vWT \; infected \; controls}{(\% CFSE^{lo} / \% CFSE^{hi}) \; in \; vOVA, \; vE1 \; or \; vA8 \; infected \; mice}\right) \times 100$$

9.2.12. $H2K^b$ stabilization assay

Stabilization of $H2K^b$ was determined using TAP-deficient RMA-S cells. RMA-S cells at exponential phase ($1x10^6$ cells/ml) were collected, washed with RPMI 1640 and cultured for 16 h at 26 °C in RPMI 1640 to allow empty MHC class I molecules to accumulate on the cell surface. Cells (4–$5x10^5$ cells per well of a round bottom 96 well-plate) were then washed with RPMI 1640 and incubated with 4-fold serial dilutions of synthetic peptides (starting at 10^{-5} M) for 2h at 26ºC with 5% CO_2, and subsequently incubated for an additional 2h at 37ºC to destroy empty cell surface $H2K^b$ molecules. After incubation, cells were washed once and incubated on ice for 30 min with anti-$H2K^b$ (AF6-88.5.5.3) (eBioscience) followed by PerCP anti-mouse antibody as secondary reagent. Stained cells were fixed with 1% paraformaldehyde and analysed by flow cytometry. The stabilizing effect of the peptides was determined as mean fluorescence intensity

(MFI) using FlowJo software. The data obtained was then analysed, expressed as the percentage of maximum surface $H2K^b$ stabilization and fit to sigmoidal dose-response curves using GraphPad Prism software. The half-maximum effective concentration (EC_{50}) values required for surface $H2K^b$ stabilization were obtained from the constructed sigmoidal dose-response curves.

9.2.13. Statistical analysis

Data comparisons between groups were performed by unpaired two-tailed Student *t*-test or ordinary one-way ANOVA as appropriate. Mean values, s.e.m. and statistics were calculated with GraphPad Prism software.

CHAPTER 10

References

References

Abbott, R.J., L.L. Quinn, A.M. Leese, H.M. Scholes, A. Pachnio, and A.B. Rickinson. 2013. CD8+ T cell responses to lytic EBV infection: late antigen specificities as subdominant components of the total response. *Journal of immunology* 191:5398-5409.

Adhikary, D., U. Behrends, H. Boerschmann, A. Pfunder, S. Burdach, A. Moosmann, K. Witter, G.W. Bornkamm, and J. Mautner. 2007. Immunodominance of lytic cycle antigens in Epstein-Barr virus-specific CD4+ T cell preparations for therapy. *PloS one* 2:e583.

Adler, H., M. Messerle, and U.H. Koszinowski. 2001. Virus reconstituted from infectious bacterial artificial chromosome (BAC)-cloned murine gammaherpesvirus 68 acquires wild-type properties in vivo only after excision of BAC vector sequences. *Journal of virology* 75:5692-5696.

Adler, H., M. Messerle, and U.H. Koszinowski. 2003. Cloning of herpesviral genomes as bacterial artificial chromosomes. *Reviews in medical virology* 13:111-121.

Adler, H., M. Messerle, M. Wagner, and U.H. Koszinowski. 2000. Cloning and mutagenesis of the murine gammaherpesvirus 68 genome as an infectious bacterial artificial chromosome. *Journal of virology* 74:6964-6974.

Alam, S.M., G.M. Davies, C.M. Lin, T. Zal, W. Nasholds, S.C. Jameson, K.A. Hogquist, N.R. Gascoigne, and P.J. Travers. 1999. Qualitative and quantitative differences in T cell receptor binding of agonist and antagonist ligands. *Immunity* 10:227-237.

Alam, S.M., P.J. Travers, J.L. Wung, W. Nasholds, S. Redpath, S.C. Jameson, and N.R. Gascoigne. 1996. T-cell-receptor affinity and thymocyte positive selection. *Nature* 381:616-620.

Almeida, J.R., D.A. Price, L. Papagno, Z.A. Arkoub, D. Sauce, E. Bornstein, T.E. Asher, A. Samri, A. Schnuriger, I. Theodorou, D. Costagliola, C. Rouzioux, H. Agut, A.G. Marcelin, D. Douek, B. Autran, and V. Appay. 2007. Superior control of HIV-1 replication by CD8+ T cells is reflected by their avidity, polyfunctionality, and clonal turnover. *The Journal of experimental medicine* 204:2473-2485.

Altman, J.D., P.A. Moss, P.J. Goulder, D.H. Barouch, M.G. McHeyzer-Williams, J.I. Bell, A.J. McMichael, and M.M. Davis. 1996. Phenotypic analysis of antigen-specific T lymphocytes. *Science* 274:94-96.

Aman, P., B. Ehlin-Henriksson, and G. Klein. 1984. Epstein-Barr virus susceptibility of normal human B lymphocyte populations. *The Journal of experimental medicine* 159:208-220.

Ambroziak, J.A., D.J. Blackbourn, B.G. Herndier, R.G. Glogau, J.H. Gullett, A.R. McDonald, E.T. Lennette, and J.A. Levy. 1995. Herpes-like sequences in HIV-infected and uninfected Kaposi's sarcoma patients. *Science* 268:582-583.

Annels, N.E., M.F. Callan, L. Tan, and A.B. Rickinson. 2000. Changing patterns of dominant TCR usage with maturation of an EBV-specific cytotoxic T cell response. *Journal of immunology* 165:4831-4841.

Apcher, S., C. Daskalogianni, B. Manoury, and R. Fahraeus. 2010. Epstein Barr virus-encoded EBNA1 interference with MHC class I antigen presentation reveals a close correlation between mRNA translation initiation and antigen presentation. *PLoS pathogens* 6:e1001151.

Apcher, S., A. Komarova, C. Daskalogianni, Y. Yin, L. Malbert-Colas, and R. Fahraeus. 2009. mRNA translation regulation by the Gly-Ala repeat of Epstein-Barr virus nuclear antigen 1. *Journal of virology* 83:1289-1298.

Argaet, V.P., C.W. Schmidt, S.R. Burrows, S.L. Silins, M.G. Kurilla, D.L. Doolan, A. Suhrbier, D.J. Moss, E. Kieff, T.B. Sculley, and I.S. Misko. 1994. Dominant selection of an invariant T cell antigen receptor in response to persistent infection by Epstein-Barr virus. *The Journal of experimental medicine* 180:2335-2340.

Arico, E., K.A. Robertson, F. Belardelli, M. Ferrantini, and A.A. Nash. 2004. Vaccination with inactivated murine gammaherpesvirus 68 strongly limits viral replication and latency and protects type I IFN receptor knockout mice from a lethal infection. *Vaccine* 22:1433-1440.

Babcock, G.J., L.L. Decker, M. Volk, and D.A. Thorley-Lawson. 1998. EBV persistence in memory B cells in vivo. *Immunity* 9:395-404.

Babcock, G.J., D. Hochberg, and A.D. Thorley-Lawson. 2000. The expression pattern of Epstein-Barr virus latent genes in vivo is dependent upon the differentiation stage of the infected B cell. *Immunity* 13:497-506.

Balfour, H.H., Jr. 2007. Epstein-Barr virus vaccine for the prevention of infectious mononucleosis--and what else? *The Journal of infectious diseases* 196:1724-1726.

Balfour, H.H., Jr. 2014. Progress, prospects, and problems in Epstein-Barr virus vaccine development. *Current opinion in virology* 6C:1-5.

Ballestas, M.E., P.A. Chatis, and K.M. Kaye. 1999. Efficient persistence of extrachromosomal KSHV DNA mediated by latency-associated nuclear antigen. *Science* 284:641-644.

Ballon, G., K. Chen, R. Perez, W. Tam, and E. Cesarman. 2011. Kaposi sarcoma herpesvirus (KSHV) vFLIP oncoprotein induces B cell transdifferentiation and tumorigenesis in mice. *The Journal of clinical investigation* 121:1141-1153.

Barcy, S., S.C. De Rosa, J. Vieira, K. Diem, M. Ikoma, C. Casper, and L. Corey. 2008. Gamma delta+ T cells involvement in viral immune control of chronic human herpesvirus 8 infection. *Journal of immunology* 180:3417-3425.

Barker, J.N., E. Doubrovina, C. Sauter, J.J. Jaroscak, M.A. Perales, M. Doubrovin, S.E. Prockop, G. Koehne, and R.J. O'Reilly. 2010. Successful treatment of EBV-associated posttransplantation lymphoma after cord blood transplantation using third-party EBV-specific cytotoxic T lymphocytes. *Blood* 116:5045-5049.

Barozzi, P., C. Bonini, L. Potenza, M. Masetti, G. Cappelli, P. Gruarin, D. Whitby, G.E. Gerunda, A. Mondino, G. Riva, D. Vallerini, C. Quadrelli, R. Bosco, F. Ciceri, C. Bordignon, T.F. Schulz, G. Torelli, and M. Luppi. 2008. Changes in the immune responses against human herpesvirus-8 in the disease course of posttransplant Kaposi sarcoma. *Transplantation* 86:738-744.

Barozzi, P., M. Luppi, F. Facchetti, C. Mecucci, M. Alu, R. Sarid, V. Rasini, L. Ravazzini, E. Rossi, S. Festa, B. Crescenzi, D.G. Wolf, T.F. Schulz, and G. Torelli. 2003. Post-transplant Kaposi sarcoma originates from the seeding of donor-derived progenitors. *Nature medicine* 9:554-561.

Barton, E., P. Mandal, and S.H. Speck. 2011. Pathogenesis and host control of gammaherpesviruses: lessons from the mouse. *Annual review of immunology* 29:351-397.

Baylis, S.A., D.J. Purifoy, and E. Littler. 1989. The characterization of the EBV alkaline deoxyribonuclease cloned and expressed in E. coli. *Nucleic acids research* 17:7609-7622.

Beisser, P.S., D. Verzijl, Y.K. Gruijthuijsen, E. Beuken, M.J. Smit, R. Leurs, C.A. Bruggeman, and C. Vink. 2005. The Epstein-Barr virus BILF1 gene encodes a G protein-coupled receptor that inhibits phosphorylation of RNA-dependent protein kinase. *Journal of virology* 79:441-449.

Belz, G.T., H. Liu, S. Andreansky, P.C. Doherty, and P.G. Stevenson. 2003. Absence of a functional defect in CD8+ T cells during primary murine gammaherpesvirus-68 infection of I-A(b-/-) mice. *The Journal of general virology* 84:337-341.

Benavente, Y., G. Mbisa, N. Labo, D. Casabonne, N. Becker, M. Maynadie, L. Foretova, P.L. Cocco, A. Nieters, A. Staines, P. Bofetta, P. Brennan, D. Whitby, and S. de Sanjose. 2011. Antibodies against lytic and latent Kaposi's sarcoma-associated herpes virus antigens and lymphoma in the European EpiLymph case-control study. *British journal of cancer* 105:1768-1771.

Bennett, N.J., J.S. May, and P.G. Stevenson. 2005. Gamma-herpesvirus latency requires T cell evasion during episome maintenance. *PLoS biology* 3:e120.

Benninger-Doring, G., S. Pepperl, L. Deml, S. Modrow, H. Wolf, and W. Jilg. 1999. Frequency of CD8(+) T lymphocytes specific for lytic and latent antigens of Epstein-Barr virus in healthy virus carriers. *Virology* 264:289-297.

Bhatt, A.P., P.M. Bhende, S.H. Sin, D. Roy, D.P. Dittmer, and B. Damania. 2010. Dual inhibition of PI3K and mTOR inhibits autocrine and paracrine proliferative loops in PI3K/Akt/mTOR-addicted lymphomas. *Blood* 115:4455-4463.

Bhatt, A.P., S.R. Jacobs, A.J. Freemerman, L. Makowski, J.C. Rathmell, D.P. Dittmer, and B. Damania. 2012. Dysregulation of fatty acid synthesis and glycolysis in non-Hodgkin lymphoma. *Proceedings of the National Academy of Sciences of the United States of America* 109:11818-11823.

Bihl, F., N. Frahm, L. Di Giammarino, J. Sidney, M. John, K. Yusim, T. Woodberry, K. Sango, H.S. Hewitt, L. Henry, C.H. Linde, J.V. Chisholm, 3rd, T.M. Zaman, E. Pae, S. Mallal, B.D. Walker, A. Sette, B.T. Korber, D. Heckerman, and C. Brander. 2006. Impact of HLA-B alleles, epitope binding affinity, functional avidity, and viral coinfection on the immunodominance of virus-specific CTL responses. *Journal of immunology* 176:4094-4101.

Bihl, F., M. Narayan, J.V. Chisholm, 3rd, L.M. Henry, T.J. Suscovich, E.E. Brown, T.M. Welzel, D.E. Kaufmann, T.M. Zaman, S. Dollard, J.N. Martin, F. Wang, D.T. Scadden, K.M. Kaye, and C. Brander. 2007. Lytic and latent antigens of the human gammaherpesviruses Kaposi's sarcoma-

associated herpesvirus and Epstein-Barr virus induce T-cell responses with similar functional properties and memory phenotypes. *Journal of virology* 81:4904-4908.

Blackman, M.A., and E. Flano. 2002. Persistent gamma-herpesvirus infections: what can we learn from an experimental mouse model? *The Journal of experimental medicine* 195:F29-32.

Blackman, M.A., E. Flano, E. Usherwood, and D.L. Woodland. 2000. Murine gamma-herpesvirus-68: a mouse model for infectious mononucleosis? *Molecular medicine today* 6:488-490.

Blake, N., T. Haigh, G. Shaka'a, D. Croom-Carter, and A. Rickinson. 2000. The importance of exogenous antigen in priming the human CD8+ T cell response: lessons from the EBV nuclear antigen EBNA1. *Journal of immunology* 165:7078-7087.

Blasdell, K., C. McCracken, A. Morris, A.A. Nash, M. Begon, M. Bennett, and J.P. Stewart. 2003. The wood mouse is a natural host for Murid herpesvirus 4. *The Journal of general virology* 84:111-113.

Blasig, C., C. Zietz, B. Haar, F. Neipel, S. Esser, N.H. Brockmeyer, E. Tschachler, S. Colombini, B. Ensoli, and M. Sturzl. 1997. Monocytes in Kaposi's sarcoma lesions are productively infected by human herpesvirus 8. *Journal of virology* 71:7963-7968.

Blaskovic, D., M. Stancekova, J. Svobodova, and J. Mistrikova. 1980. Isolation of five strains of herpesviruses from two species of free living small rodents. *Acta virologica* 24:468.

Bogerd, H.P., H.W. Karnowski, X. Cai, J. Shin, M. Pohlers, and B.R. Cullen. 2010. A mammalian herpesvirus uses noncanonical expression and processing mechanisms to generate viral MicroRNAs. *Molecular cell* 37:135-142.

Bollard, C.M., S. Gottschalk, A.M. Leen, H. Weiss, K.C. Straathof, G. Carrum, M. Khalil, M.F. Wu, M.H. Huls, C.C. Chang, M.V. Gresik, A.P. Gee, M.K. Brenner, C.M. Rooney, and H.E. Heslop. 2007. Complete responses of relapsed lymphoma following genetic modification of tumor-antigen presenting cells and T-lymphocyte transfer. *Blood* 110:2838-2845.

Bollard, C.M., S. Gottschalk, V. Torrano, O. Diouf, S. Ku, Y. Hazrat, G. Carrum, C. Ramos, L. Fayad, E.J. Shpall, B. Pro, H. Liu, M.F. Wu, D. Lee, A.M. Sheehan, Y. Zu, A.P. Gee, M.K. Brenner, H.E. Heslop, and C.M. Rooney. 2014. Sustained complete responses in patients with lymphoma receiving autologous cytotoxic T lymphocytes targeting epstein-barr virus latent membrane proteins. *Journal of clinical oncology : official journal of the American Society of Clinical Oncology* 32:798-808.

Bollard, C.M., C.M. Rooney, and H.E. Heslop. 2012. T-cell therapy in the treatment of post-transplant lymphoproliferative disease. *Nature reviews. Clinical oncology* 9:510-519.

Boname, J.M., H.M. Coleman, J.S. May, and P.G. Stevenson. 2004a. Protection against wild-type murine gammaherpesvirus-68 latency by a latency-deficient mutant. *The Journal of general virology* 85:131-135.

Boname, J.M., B.D. de Lima, P.J. Lehner, and P.G. Stevenson. 2004b. Viral degradation of the MHC class I peptide loading complex. *Immunity* 20:305-317.

Boname, J.M., J.S. May, and P.G. Stevenson. 2005. The murine gamma-herpesvirus-68 MK3 protein causes TAP degradation independent of MHC class I heavy chain degradation. *European journal of immunology* 35:171-179.

Boname, J.M., and P.G. Stevenson. 2001. MHC class I ubiquitination by a viral PHD/LAP finger protein. *Immunity* 15:627-636.

Bonnefoix, T., P. Bonnefoix, M. Callanan, P. Verdiel, and J.J. Sotto. 2001. Graphical representation of a generalized linear model-based statistical test estimating the fit of the single-hit Poisson model to limiting dilution assays. *Journal of immunology* 167:5725-5730.

Borza, C.M., and L.M. Hutt-Fletcher. 2002. Alternate replication in B cells and epithelial cells switches tropism of Epstein-Barr virus. *Nature medicine* 8:594-599.

Boshoff, C. 2002. Kaposi's sarcoma biology. *IUBMB life* 53:259-261.

Boss, I.W., P.E. Nadeau, J.R. Abbott, Y. Yang, A. Mergia, and R. Renne. 2011. A Kaposi's sarcoma-associated herpesvirus-encoded ortholog of microRNA miR-155 induces human splenic B-cell expansion in NOD/LtSz-scid IL2Rgammanull mice. *Journal of virology* 85:9877-9886.

Boss, I.W., K.B. Plaisance, and R. Renne. 2009. Role of virus-encoded microRNAs in herpesvirus biology. *Trends in microbiology* 17:544-553.

Bowden, R.J., J.P. Simas, A.J. Davis, and S. Efstathiou. 1997. Murine gammaherpesvirus 68 encodes tRNA-like sequences which are expressed during latency. *The Journal of general virology* 78 (Pt 7):1675-1687.

Bower, M., J. Weir, N. Francis, T. Newsom-Davis, S. Powles, T. Crook, M. Boffito, B. Gazzard, and M. Nelson. 2009. The effect of HAART in 254 consecutive patients with AIDS-related Kaposi's sarcoma. *Aids* 23:1701-1706.

Braaten, D.C., J.S. McClellan, I. Messaoudi, S.A. Tibbetts, K.B. McClellan, J. Nikolich-Zugich, and H.W. Virgin. 2006. Effective control of chronic gamma-herpesvirus infection by unconventional MHC Class Ia-independent CD8 T cells. *PLoS pathogens* 2:e37.

Brander, C., P. O'Connor, T. Suscovich, N.G. Jones, Y. Lee, D. Kedes, D. Ganem, J. Martin, D. Osmond, S. Southwood, A. Sette, B.D. Walker, and D.T. Scadden. 2001. Definition of an optimal cytotoxic T lymphocyte epitope in the latently expressed Kaposi's sarcoma-associated herpesvirus kaposin protein. *The Journal of infectious diseases* 184:119-126.

Brewin, J., C. Mancao, K. Straathof, H. Karlsson, S. Samarasinghe, P.J. Amrolia, and M. Pule. 2009. Generation of EBV-specific cytotoxic T cells that are resistant to calcineurin inhibitors for the treatment of posttransplantation lymphoproliferative disease. *Blood* 114:4792-4803.

Bridgeman, A., P.G. Stevenson, J.P. Simas, and S. Efstathiou. 2001. A secreted chemokine binding protein encoded by murine gammaherpesvirus-68 is necessary for the establishment of a normal latent load. *The Journal of experimental medicine* 194:301-312.

Brooks, J.M., S.P. Lee, A.M. Leese, W.A. Thomas, M. Rowe, and A.B. Rickinson. 2009. Cyclical expression of EBV latent membrane protein 1 in EBV-transformed B cells underpins heterogeneity of epitope presentation and CD8+ T cell recognition. *Journal of immunology* 182:1919-1928.

Brooks, J.W., A.M. Hamilton-Easton, J.P. Christensen, R.D. Cardin, C.L. Hardy, and P.C. Doherty. 1999. Requirement for CD40 ligand, CD4(+) T cells, and B cells in an infectious mononucleosis-like syndrome. *Journal of virology* 73:9650-9654.

Buisson, M., T. Geoui, D. Flot, N. Tarbouriech, M.E. Ressing, E.J. Wiertz, and W.P. Burmeister. 2009. A bridge crosses the active-site canyon of the Epstein-Barr virus nuclease with DNase and RNase activities. *Journal of molecular biology* 391:717-728.

Burkhardt, A.L., J.B. Bolen, E. Kieff, and R. Longnecker. 1992. An Epstein-Barr virus transformation-associated membrane protein interacts with src family tyrosine kinases. *Journal of virology* 66:5161-5167.

Burrows, J.M., S.R. Burrows, L.M. Poulsen, T.B. Sculley, D.J. Moss, and R. Khanna. 1996. Unusually high frequency of Epstein-Barr virus genetic variants in Papua New Guinea that can escape cytotoxic T-cell recognition: implications for virus evolution. *Journal of virology* 70:2490-2496.

Cadwell, K., and L. Coscoy. 2005. Ubiquitination on nonlysine residues by a viral E3 ubiquitin ligase. *Science* 309:127-130.

Cadwell, K., and L. Coscoy. 2008. The specificities of Kaposi's sarcoma-associated herpesvirus-encoded E3 ubiquitin ligases are determined by the positions of lysine or cysteine residues within the intracytoplasmic domains of their targets. *Journal of virology* 82:4184-4189.

Caldwell, R.G., J.B. Wilson, S.J. Anderson, and R. Longnecker. 1998. Epstein-Barr virus LMP2A drives B cell development and survival in the absence of normal B cell receptor signals. *Immunity* 9:405-411.

Callan, M.F., N. Annels, N. Steven, L. Tan, J. Wilson, A.J. McMichael, and A.B. Rickinson. 1998a. T cell selection during the evolution of CD8+ T cell memory in vivo. *European journal of immunology* 28:4382-4390.

Callan, M.F., C. Fazou, H. Yang, T. Rostron, K. Poon, C. Hatton, and A.J. McMichael. 2000. CD8(+) T-cell selection, function, and death in the primary immune response in vivo. *The Journal of clinical investigation* 106:1251-1261.

Callan, M.F., N. Steven, P. Krausa, J.D. Wilson, P.A. Moss, G.M. Gillespie, J.I. Bell, A.B. Rickinson, and A.J. McMichael. 1996. Large clonal expansions of CD8+ T cells in acute infectious mononucleosis. *Nature medicine* 2:906-911.

Callan, M.F., L. Tan, N. Annels, G.S. Ogg, J.D. Wilson, C.A. O'Callaghan, N. Steven, A.J. McMichael, and A.B. Rickinson. 1998b. Direct visualization of antigen-specific CD8+ T cells during the primary immune response to Epstein-Barr virus In vivo. *The Journal of experimental medicine* 187:1395-1402.

Cardin, R.D., J.W. Brooks, S.R. Sarawar, and P.C. Doherty. 1996. Progressive loss of CD8+ T cell-mediated control of a gamma-herpesvirus in the absence of CD4+ T cells. *The Journal of experimental medicine* 184:863-871.

Casola, S., K.L. Otipoby, M. Alimzhanov, S. Humme, N. Uyttersprot, J.L. Kutok, M.C. Carroll, and K. Rajewsky. 2004. B cell receptor signal strength determines B cell fate. *Nature immunology* 5:317-327.

Catalina, M.D., J.L. Sullivan, K.R. Bak, and K. Luzuriaga. 2001. Differential evolution and stability of epitope-specific CD8(+) T cell responses in EBV infection. *Journal of immunology* 167:4450-4457.

Catalina, M.D., J.L. Sullivan, R.M. Brody, and K. Luzuriaga. 2002. Phenotypic and functional heterogeneity of EBV epitope-specific CD8+ T cells. *Journal of immunology* 168:4184-4191.

Cesarman, E. 2011. Gammaherpesvirus and lymphoproliferative disorders in immunocompromised patients. *Cancer letters* 305:163-174.

Cesarman, E. 2014. Gammaherpesviruses and lymphoproliferative disorders. *Annual review of pathology* 9:349-372.

Cesarman, E., Y. Chang, P.S. Moore, J.W. Said, and D.M. Knowles. 1995a. Kaposi's sarcoma-associated herpesvirus-like DNA sequences in AIDS-related body-cavity-based lymphomas. *The New England journal of medicine* 332:1186-1191.

Cesarman, E., P.S. Moore, P.H. Rao, G. Inghirami, D.M. Knowles, and Y. Chang. 1995b. In vitro establishment and characterization of two acquired immunodeficiency syndrome-related lymphoma cell lines (BC-1 and BC-2) containing Kaposi's sarcoma-associated herpesvirus-like (KSHV) DNA sequences. *Blood* 86:2708-2714.

Chadburn, A., E.M. Hyjek, W. Tam, Y. Liu, T. Rengifo, E. Cesarman, and D.M. Knowles. 2008. Immunophenotypic analysis of the Kaposi sarcoma herpesvirus (KSHV; HHV-8)-infected B cells in HIV+ multicentric Castleman disease (MCD). *Histopathology* 53:513-524.

Chang, H., D.P. Dittmer, Y.C. Shin, Y. Hong, and J.U. Jung. 2005. Role of Notch signal transduction in Kaposi's sarcoma-associated herpesvirus gene expression. *Journal of virology* 79:14371-14382.

Chang, Y., E. Cesarman, M.S. Pessin, F. Lee, J. Culpepper, D.M. Knowles, and P.S. Moore. 1994. Identification of herpesvirus-like DNA sequences in AIDS-associated Kaposi's sarcoma. *Science* 266:1865-1869.

Chapman, A.L., A.B. Rickinson, W.A. Thomas, R.F. Jarrett, J. Crocker, and S.P. Lee. 2001. Epstein-Barr virus-specific cytotoxic T lymphocyte responses in the blood and tumor site of Hodgkin's disease patients: implications for a T-cell-based therapy. *Cancer research* 61:6219-6226.

Chen, W., S. Khilko, J. Fecondo, D.H. Margulies, and J. McCluskey. 1994. Determinant selection of major histocompatibility complex class I-restricted antigenic peptides is explained by class I-peptide affinity and is strongly influenced by nondominant anchor residues. *The Journal of experimental medicine* 180:1471-1483.

Chen, Y., K. Yao, B. Wang, J. Qing, and G. Liu. 2008. Potent dendritic cell vaccine loaded with latent membrane protein 2A (LMP2A). *Cellular & molecular immunology* 5:365-372.

Chia, W.K., M. Teo, W.W. Wang, B. Lee, S.F. Ang, W.M. Tai, C.L. Chee, J. Ng, R. Kan, W.T. Lim, S.H. Tan, W.S. Ong, Y.B. Cheung, E.H. Tan, J.E. Connolly, S. Gottschalk, and H.C. Toh. 2014. Adoptive T-cell transfer and chemotherapy in the first-line treatment of metastatic and/or locally recurrent nasopharyngeal carcinoma. *Molecular therapy : the journal of the American Society of Gene Therapy* 22:132-139.

Christensen, J.P., R.D. Cardin, K.C. Branum, and P.C. Doherty. 1999. CD4(+) T cell-mediated control of a gamma-herpesvirus in B cell-deficient mice is mediated by IFN-gamma. *Proceedings of the National Academy of Sciences of the United States of America* 96:5135-5140.

Chung, C.T., S.L. Niemela, and R.H. Miller. 1989. One-step preparation of competent Escherichia coli: transformation and storage of bacterial cells in the same solution. *Proceedings of the National Academy of Sciences of the United States of America* 86:2172-2175.

Clarke, S.R., M. Barnden, C. Kurts, F.R. Carbone, J.F. Miller, and W.R. Heath. 2000. Characterization of the ovalbumin-specific TCR transgenic line OT-I: MHC elements for positive and negative selection. *Immunology and cell biology* 78:110-117.

Cobbold, S.P., A. Jayasuriya, A. Nash, T.D. Prospero, and H. Waldmann. 1984. Therapy with monoclonal antibodies by elimination of T-cell subsets in vivo. *Nature* 312:548-551.

Cocco, M., C. Bellan, R. Tussiwand, D. Corti, E. Traggiai, S. Lazzi, S. Mannucci, L. Bronz, N. Palummo, C. Ginanneschi, P. Tosi, A. Lanzavecchia, M.G. Manz, and L. Leoncini. 2008. CD34+ cord blood cell-transplanted Rag2-/- gamma(c)-/- mice as a model for Epstein-Barr virus infection. *The American journal of pathology* 173:1369-1378.

Cohen, J.I., A.S. Fauci, H. Varmus, and G.J. Nabel. 2011. Epstein-Barr virus: an important vaccine target for cancer prevention. *Science translational medicine* 3:107fs107.

Cohen, J.I., E.S. Mocarski, N. Raab-Traub, L. Corey, and G.J. Nabel. 2013. The need and challenges for development of an Epstein-Barr virus vaccine. *Vaccine* 31 Suppl 2:B194-196.

Collins, C.M., J.M. Boss, and S.H. Speck. 2009. Identification of infected B-cell populations by using a recombinant murine gammaherpesvirus 68 expressing a fluorescent protein. *Journal of virology* 83:6484-6493.

Collins, C.M., and S.H. Speck. 2014. Expansion of murine gammaherpesvirus latently infected B cells requires T follicular help. *PLoS pathogens* 10:e1004106.

Conrad, J.A., R.K. Ramalingam, R.M. Smith, L. Barnett, S.L. Lorey, J. Wei, B.C. Simons, S. Sadagopal, D. Meyer-Olson, and S.A. Kalams. 2011. Dominant clonotypes within HIV-specific T cell responses are programmed death-1high and CD127low and display reduced variant cross-reactivity. *Journal of immunology* 186:6871-6885.

Correia, B., S.A. Cerqueira, C. Beauchemin, M. Pires de Miranda, S. Li, R. Ponnusamy, L. Rodrigues, T.R. Schneider, M.A. Carrondo, K.M. Kaye, J.P. Simas, and C.E. McVey. 2013. Crystal structure of the gamma-2 herpesvirus LANA DNA binding domain identifies charged surface residues which impact viral latency. *PLoS pathogens* 9:e1003673.

Coscoy, L. 2007. Immune evasion by Kaposi's sarcoma-associated herpesvirus. *Nature reviews. Immunology* 7:391-401.

Coscoy, L., and D. Ganem. 2000. Kaposi's sarcoma-associated herpesvirus encodes two proteins that block cell surface display of MHC class I chains by enhancing their endocytosis. *Proceedings of the National Academy of Sciences of the United States of America* 97:8051-8056.

Coscoy, L., D.J. Sanchez, and D. Ganem. 2001. A novel class of herpesvirus-encoded membrane-bound E3 ubiquitin ligases regulates endocytosis of proteins involved in immune recognition. *The Journal of cell biology* 155:1265-1273.

Couedel, C., M. Bodinier, M.A. Peyrat, M. Bonneville, F. Davodeau, and F. Lang. 1999. Selection and long-term persistence of reactive CTL clones during an EBV chronic response are determined by avidity, CD8 variable contribution compensating for differences in TCR affinities. *Journal of immunology* 162:6351-6358.

Croft, N.P., C. Shannon-Lowe, A.I. Bell, D. Horst, E. Kremmer, M.E. Ressing, E.J. Wiertz, J.M. Middeldorp, M. Rowe, A.B. Rickinson, and A.D. Hislop. 2009. Stage-specific inhibition of MHC class I presentation by the Epstein-Barr virus BNLF2a protein during virus lytic cycle. *PLoS pathogens* 5:e1000490.

Cush, S.S., K.M. Anderson, D.H. Ravneberg, J.L. Weslow-Schmidt, and E. Flano. 2007. Memory generation and maintenance of CD8+ T cell function during viral persistence. *Journal of immunology* 179:141-153.

Cush, S.S., and E. Flano. 2009. Protective antigen-independent CD8 T cell memory is maintained during {gamma}-herpesvirus persistence. *Journal of immunology* 182:3995-4004.

Damania, B. 2004. Oncogenic gamma-herpesviruses: comparison of viral proteins involved in tumorigenesis. *Nature reviews. Microbiology* 2:656-668.

Damania, B., J.K. Choi, and J.U. Jung. 2000. Signaling activities of gammaherpesvirus membrane proteins. *Journal of virology* 74:1593-1601.

Daniels, M.A., E. Teixeiro, J. Gill, B. Hausmann, D. Roubaty, K. Holmberg, G. Werlen, G.A. Hollander, N.R. Gascoigne, and E. Palmer. 2006. Thymic selection threshold defined by compartmentalization of Ras/MAPK signalling. *Nature* 444:724-729.

De Angelis, B., G. Dotti, C. Quintarelli, L.E. Huye, L. Zhang, M. Zhang, F. Pane, H.E. Heslop, M.K. Brenner, C.M. Rooney, and B. Savoldo. 2009. Generation of Epstein-Barr virus-specific cytotoxic T lymphocytes resistant to the immunosuppressive drug tacrolimus (FK506). *Blood* 114:4784-4791.

de Campos-Lima, P.O., R. Gavioli, Q.J. Zhang, L.E. Wallace, R. Dolcetti, M. Rowe, A.B. Rickinson, and M.G. Masucci. 1993. HLA-A11 epitope loss isolates of Epstein-Barr virus from a highly A11+ population. *Science* 260:98-100.

de Campos-Lima, P.O., V. Levitsky, J. Brooks, S.P. Lee, L.F. Hu, A.B. Rickinson, and M.G. Masucci. 1994. T cell responses and virus evolution: loss of HLA A11-restricted CTL epitopes in Epstein-Barr virus isolates from highly A11-positive populations by selective mutation of anchor residues. *The Journal of experimental medicine* 179:1297-1305.

Delgado-Eckert, E., and M. Shapiro. 2011. A model of host response to a multi-stage pathogen. *Journal of mathematical biology* 63:201-227.

Delgado, T., P.A. Carroll, A.S. Punjabi, D. Margineantu, D.M. Hockenbery, and M. Lagunoff. 2010. Induction of the Warburg effect by Kaposi's sarcoma herpesvirus is required for the maintenance of latently infected endothelial cells. *Proceedings of the National Academy of Sciences of the United States of America* 107:10696-10701.

Delgado, T., E.L. Sanchez, R. Camarda, and M. Lagunoff. 2012. Global metabolic profiling of infection by an oncogenic virus: KSHV induces and requires lipogenesis for survival of latent infection. *PLoS pathogens* 8:e1002866.

Denton, A.E., R. Wesselingh, S. Gras, C. Guillonneau, M.R. Olson, J.D. Mintern, W. Zeng, D.C. Jackson, J. Rossjohn, P.D. Hodgkin, P.C. Doherty, and S.J. Turner. 2011. Affinity thresholds for naive CD8+ CTL activation by peptides and engineered influenza A viruses. *Journal of immunology* 187:5733-5744.

Dewan, M.Z., H. Terunuma, M. Toi, Y. Tanaka, H. Katano, X. Deng, H. Abe, T. Nakasone, N. Mori, T. Sata, and N. Yamamoto. 2006. Potential role of natural killer cells in controlling growth and infiltration of AIDS-associated primary effusion lymphoma cells. *Cancer science* 97:1381-1387.

Di Stasi, A., B. De Angelis, C.M. Rooney, L. Zhang, A. Mahendravada, A.E. Foster, H.E. Heslop, M.K. Brenner, G. Dotti, and B. Savoldo. 2009. T lymphocytes coexpressing CCR4 and a chimeric antigen receptor targeting CD30 have improved homing and antitumor activity in a Hodgkin tumor model. *Blood* 113:6392-6402.

Diebel, K.W., A.L. Smith, and L.F. van Dyk. 2010. Mature and functional viral miRNAs transcribed from novel RNA polymerase III promoters. *Rna* 16:170-185.

Dittmer, D., M. Lagunoff, R. Renne, K. Staskus, A. Haase, and D. Ganem. 1998. A cluster of latently expressed genes in Kaposi's sarcoma-associated herpesvirus. *Journal of virology* 72:8309-8315.

Dittmer, D.P. 2011. Restricted Kaposi's sarcoma (KS) herpesvirus transcription in KS lesions from patients on successful antiretroviral therapy. *mBio* 2:e00138-00111.

Dittmer, D.P., and B. Damania. 2013. Kaposi sarcoma associated herpesvirus pathogenesis (KSHV)--an update. *Current opinion in virology* 3:238-244.

Doherty, P.C., J.P. Christensen, G.T. Belz, P.G. Stevenson, and M.Y. Sangster. 2001. Dissecting the host response to a gamma-herpesvirus. *Philosophical transactions of the Royal Society of London. Series B, Biological sciences* 356:581-593.

Doubrovina, E., B. Oflaz-Sozmen, S.E. Prockop, N.A. Kernan, S. Abramson, J. Teruya-Feldstein, C. Hedvat, J.F. Chou, G. Heller, J.N. Barker, F. Boulad, H. Castro-Malaspina, D. George, A. Jakubowski, G. Koehne, E.B. Papadopoulos, A. Scaradavou, T.N. Small, R. Khalaf, J.W. Young, and R.J. O'Reilly. 2012. Adoptive immunotherapy with unselected or EBV-specific T cells for biopsy-proven EBV+ lymphomas after allogeneic hematopoietic cell transplantation. *Blood* 119:2644-2656.

Dunne, P.J., J.M. Faint, N.H. Gudgeon, J.M. Fletcher, F.J. Plunkett, M.V. Soares, A.D. Hislop, N.E. Annels, A.B. Rickinson, M. Salmon, and A.N. Akbar. 2002. Epstein-Barr virus-specific CD8(+) T cells that re-express CD45RA are apoptosis-resistant memory cells that retain replicative potential. *Blood* 100:933-940.

Dupin, N., C. Fisher, P. Kellam, S. Ariad, M. Tulliez, N. Franck, E. van Marck, D. Salmon, I. Gorin, J.P. Escande, R.A. Weiss, K. Alitalo, and C. Boshoff. 1999. Distribution of human herpesvirus-8 latently infected cells in Kaposi's sarcoma, multicentric Castleman's disease, and primary effusion lymphoma. *Proceedings of the National Academy of Sciences of the United States of America* 96:4546-4551.

Duraiswamy, J., M. Bharadwaj, J. Tellam, G. Connolly, L. Cooper, D. Moss, S. Thomson, P. Yotnda, and R. Khanna. 2004. Induction of therapeutic T-cell responses to subdominant tumor-associated viral oncogene after immunization with replication-incompetent polyepitope adenovirus vaccine. *Cancer research* 64:1483-1489.

Dutia, B.M., J.P. Stewart, R.A. Clayton, H. Dyson, and A.A. Nash. 1999. Kinetic and phenotypic changes in murine lymphocytes infected with murine gammaherpesvirus-68 in vitro. *The Journal of general virology* 80 (Pt 10):2729-2736.

Edelman, D.C. 2005. Human herpesvirus 8--a novel human pathogen. *Virology journal* 2:78.

Efstathiou, S., Y.M. Ho, S. Hall, C.J. Styles, S.D. Scott, and U.A. Gompels. 1990a. Murine herpesvirus 68 is genetically related to the gammaherpesviruses Epstein-Barr virus and herpesvirus saimiri. *The Journal of general virology* 71 (Pt 6):1365-1372.

Efstathiou, S., Y.M. Ho, and A.C. Minson. 1990b. Cloning and molecular characterization of the murine herpesvirus 68 genome. *The Journal of general virology* 71 (Pt 6):1355-1364.

Ehtisham, S., N.P. Sunil-Chandra, and A.A. Nash. 1993. Pathogenesis of murine gammaherpesvirus infection in mice deficient in CD4 and CD8 T cells. *Journal of virology* 67:5247-5252.

Elliott, S.L., A. Suhrbier, J.J. Miles, G. Lawrence, S.J. Pye, T.T. Le, A. Rosenstengel, T. Nguyen, A. Allworth, S.R. Burrows, J. Cox, D. Pye, D.J. Moss, and M. Bharadwaj. 2008. Phase I trial of a CD8+ T-cell peptide epitope-based vaccine for infectious mononucleosis. *Journal of virology* 82:1448-1457.

Epstein, M.A. 1976. Epstein-Barr virus--is it time to develop a vaccine program? *Journal of the National Cancer Institute* 56:697-700.

Epstein, M.A., B.G. Achong, and Y.M. Barr. 1964. Virus Particles in Cultured Lymphoblasts from Burkitt's Lymphoma. *Lancet* 1:702-703.

Evans, A.G., J.M. Moser, L.T. Krug, V. Pozharskaya, A.L. Mora, and S.H. Speck. 2008. A gammaherpesvirus-secreted activator of Vbeta4+ CD8+ T cells regulates chronic infection and immunopathology. *The Journal of experimental medicine* 205:669-684.

Feederle, R., H. Bannert, H. Lips, N. Muller-Lantzsch, and H.J. Delecluse. 2009. The Epstein-Barr virus alkaline exonuclease BGLF5 serves pleiotropic functions in virus replication. *Journal of virology* 83:4952-4962.

Feng, P., A. Moses, and K. Fruh. 2013. Evasion of adaptive and innate immune response mechanisms by gamma-herpesviruses. *Current opinion in virology* 3:285-295.

Flano, E., S.M. Husain, J.T. Sample, D.L. Woodland, and M.A. Blackman. 2000. Latent murine gamma-herpesvirus infection is established in activated B cells, dendritic cells, and macrophages. *Journal of immunology* 165:1074-1081.

Flano, E., Q. Jia, J. Moore, D.L. Woodland, R. Sun, and M.A. Blackman. 2005. Early establishment of gamma-herpesvirus latency: implications for immune control. *Journal of immunology* 174:4972-4978.

Flano, E., I.J. Kim, J. Moore, D.L. Woodland, and M.A. Blackman. 2003. Differential gamma-herpesvirus distribution in distinct anatomical locations and cell subsets during persistent infection in mice. *Journal of immunology* 170:3828-3834.

Flano, E., I.J. Kim, D.L. Woodland, and M.A. Blackman. 2002. Gamma-herpesvirus latency is preferentially maintained in splenic germinal center and memory B cells. *The Journal of experimental medicine* 196:1363-1372.

Foster, A.E., G. Dotti, A. Lu, M. Khalil, M.K. Brenner, H.E. Heslop, C.M. Rooney, and C.M. Bollard. 2008. Antitumor activity of EBV-specific T lymphocytes transduced with a dominant negative TGF-beta receptor. *Journal of immunotherapy* 31:500-505.

Fowler, P., and S. Efstathiou. 2004. Vaccine potential of a murine gammaherpesvirus-68 mutant deficient for ORF73. *The Journal of general virology* 85:609-613.

Fowler, P., S. Marques, J.P. Simas, and S. Efstathiou. 2003. ORF73 of murine herpesvirus-68 is critical for the establishment and maintenance of latency. *The Journal of general virology* 84:3405-3416.

Franceschi, S., L.D. Maso, M. Rickenbach, J. Polesel, B. Hirschel, M. Cavassini, A. Bordoni, L. Elzi, S. Ess, G. Jundt, N. Mueller, and G.M. Clifford. 2008. Kaposi sarcoma incidence in the Swiss HIV Cohort Study before and after highly active antiretroviral therapy. *British journal of cancer* 99:800-804.

Francois, S., S. Vidick, M. Sarlet, D. Desmecht, P. Drion, P.G. Stevenson, A. Vanderplasschen, and L. Gillet. 2013. Illumination of murine gammaherpesvirus-68 cycle reveals a sexual transmission route from females to males in laboratory mice. *PLoS pathogens* 9:e1003292.

Frederico, B., B. Chao, J.S. May, G.T. Belz, and P.G. Stevenson. 2014. A murid gamma-herpesviruses exploits normal splenic immune communication routes for systemic spread. *Cell host & microbe* 15:457-470.

Frederico, B., R. Milho, J.S. May, L. Gillet, and P.G. Stevenson. 2012. Myeloid infection links epithelial and B cell tropisms of Murid Herpesvirus-4. *PLoS pathogens* 8:e1002935.

Freeman, M.L., C.E. Burkum, K.G. Lanzer, M.K. Jensen, M. Ahmed, E.J. Yager, E. Flano, G.M. Winslow, D.L. Woodland, and M.A. Blackman. 2011. Cutting edge: activation of virus-specific CD4 T cells throughout gamma-herpesvirus latency. *Journal of immunology* 187:6180-6184.

Freeman, M.L., C.E. Burkum, D.L. Woodland, R. Sun, T.T. Wu, and M.A. Blackman. 2012. Importance of antibody in virus infection and vaccine-mediated protection by a latency-deficient recombinant murine gamma-herpesvirus-68. *Journal of immunology* 188:1049-1056.

Freeman, M.L., K.G. Lanzer, T. Cookenham, B. Peters, J. Sidney, T.T. Wu, R. Sun, D.L. Woodland, A. Sette, and M.A. Blackman. 2010. Two kinetic patterns of epitope-specific CD8 T-cell responses following murine gammaherpesvirus 68 infection. *Journal of virology* 84:2881-2892.

Fremont, D.H., E.A. Stura, M. Matsumura, P.A. Peterson, and I.A. Wilson. 1995. Crystal structure of an H-2Kb-ovalbumin peptide complex reveals the interplay of primary and secondary anchor positions in the major histocompatibility complex binding groove. *Proceedings of the National Academy of Sciences of the United States of America* 92:2479-2483.

Gallot, G., S. Vollant, S. Saiagh, B. Clemenceau, R. Vivien, E. Cerato, J.D. Bignon, C. Ferrand, A. Jaccard, S. Vigouroux, S. Choquet, J.H. Dalle, I. Frachon, B. Bruno, M. Mothy, F. Mechinaud, V. Leblond, N. Milpied, and H. Vie. 2014. T-cell Therapy Using a Bank of EBV-specific Cytotoxic T Cells: Lessons From a Phase I/II Feasibility and Safety Study. *Journal of immunotherapy* 37:170-179.

Ganem, D. 2010. KSHV and the pathogenesis of Kaposi sarcoma: listening to human biology and medicine. *The Journal of clinical investigation* 120:939-949.

Gaspar, M., J.S. May, S. Sukla, B. Frederico, M.B. Gill, C.M. Smith, G.T. Belz, and P.G. Stevenson. 2011. Murid herpesvirus-4 exploits dendritic cells to infect B cells. *PLoS pathogens* 7:e1002346.

Gerdemann, U., A.S. Christin, J.F. Vera, C.A. Ramos, Y. Fujita, H. Liu, D. Dilloo, H.E. Heslop, M.K. Brenner, C.M. Rooney, and A.M. Leen. 2009. Nucleofection of DCs to generate Multivirus-specific T cells for prevention or treatment of viral infections in the immunocompromised host. *Molecular therapy : the journal of the American Society of Gene Therapy* 17:1616-1625.

Gerdemann, U., U.L. Katari, A. Papadopoulou, J.M. Keirnan, J.A. Craddock, H. Liu, C.A. Martinez, A. Kennedy-Nasser, K.S. Leung, S.M. Gottschalk, R.A. Krance, M.K. Brenner, C.M. Rooney, H.E. Heslop, and A.M. Leen. 2013. Safety and clinical efficacy of rapidly-generated trivirus-directed T cells as treatment for adenovirus, EBV, and CMV infections after allogeneic hematopoietic stem cell transplant. *Molecular therapy : the journal of the American Society of Gene Therapy* 21:2113-2121.

Gerdemann, U., J.M. Keirnan, U.L. Katari, R. Yanagisawa, A.S. Christin, L.E. Huye, S.K. Perna, S. Ennamuri, S. Gottschalk, M.K. Brenner, H.E. Heslop, C.M. Rooney, and A.M. Leen. 2012. Rapidly generated multivirus-specific cytotoxic T lymphocytes for the prophylaxis and treatment of viral infections. *Molecular therapy : the journal of the American Society of Gene Therapy* 20:1622-1632.

Giannoni, F., A. Shea, C. Inglis, L.N. Lee, and S.R. Sarawar. 2008. CD40 engagement on dendritic cells, but not on B or T cells, is required for long-term control of murine gammaherpesvirus 68. *Journal of virology* 82:11016-11022.

Giffin, L., and B. Damania. 2014. KSHV: pathways to tumorigenesis and persistent infection. *Advances in virus research* 88:111-159.

Gires, O., U. Zimber-Strobl, R. Gonnella, M. Ueffing, G. Marschall, R. Zeidler, D. Pich, and W. Hammerschmidt. 1997. Latent membrane protein 1 of Epstein-Barr virus mimics a constitutively active receptor molecule. *The EMBO journal* 16:6131-6140.

Gottschalk, S., C.Y. Ng, M. Perez, C.A. Smith, C. Sample, M.K. Brenner, H.E. Heslop, and C.M. Rooney. 2001. An Epstein-Barr virus deletion mutant associated with fatal lymphoproliferative disease unresponsive to therapy with virus-specific CTLs. *Blood* 97:835-843.

Gottschalk, S., C.M. Rooney, and H.E. Heslop. 2005. Post-transplant lymphoproliferative disorders. *Annual review of medicine* 56:29-44.

Gottwein, E., X. Cai, and B.R. Cullen. 2006. Expression and function of microRNAs encoded by Kaposi's sarcoma-associated herpesvirus. *Cold Spring Harbor symposia on quantitative biology* 71:357-364.

Gottwein, E., D.L. Corcoran, N. Mukherjee, R.L. Skalsky, M. Hafner, J.D. Nusbaum, P. Shamulailatpam, C.L. Love, S.S. Dave, T. Tuschl, U. Ohler, and B.R. Cullen. 2011. Viral microRNA targetome of KSHV-infected primary effusion lymphoma cell lines. *Cell host & microbe* 10:515-526.

Gredmark-Russ, S., E.J. Cheung, M.K. Isaacson, H.L. Ploegh, and G.M. Grotenbreg. 2008. The CD8 T-cell response against murine gammaherpesvirus 68 is directed toward a broad repertoire of epitopes from both early and late antigens. *Journal of virology* 82:12205-12212.

Gregory, S.M., L. Wang, J.A. West, D.P. Dittmer, and B. Damania. 2012. Latent Kaposi's sarcoma-associated herpesvirus infection of monocytes downregulates expression of adaptive immune response costimulatory receptors and proinflammatory cytokines. *Journal of virology* 86:3916-3923.

Griffin, B.D., A.M. Gram, A. Mulder, D. Van Leeuwen, F.H. Claas, F. Wang, M.E. Ressing, and E. Wiertz. 2013. EBV BILF1 evolved to downregulate cell surface display of a wide range of HLA class I molecules through their cytoplasmic tail. *Journal of immunology* 190:1672-1684.

Gu, S.Y., T.M. Huang, L. Ruan, Y.H. Miao, H. Lu, C.M. Chu, M. Motz, and H. Wolf. 1995. First EBV vaccine trial in humans using recombinant vaccinia virus expressing the major membrane antigen. *Developments in biological standardization* 84:171-177.

Guihot, A., N. Dupin, A.G. Marcelin, I. Gorin, A.S. Bedin, P. Bossi, L. Galicier, E. Oksenhendler, B. Autran, and G. Carcelain. 2006. Low T cell responses to human herpesvirus 8 in patients with AIDS-related and classic Kaposi sarcoma. *The Journal of infectious diseases* 194:1078-1088.

Habison, A.C., C. Beauchemin, J.P. Simas, E.J. Usherwood, and K.M. Kaye. 2012. Murine gammaherpesvirus 68 LANA acts on terminal repeat DNA to mediate episome persistence. *Journal of virology* 86:11863-11876.

Hadinoto, V., M. Shapiro, T.C. Greenough, J.L. Sullivan, K. Luzuriaga, and D.A. Thorley-Lawson. 2008. On the dynamics of acute EBV infection and the pathogenesis of infectious mononucleosis. *Blood* 111:1420-1427.

Hadinoto, V., M. Shapiro, C.C. Sun, and D.A. Thorley-Lawson. 2009. The dynamics of EBV shedding implicate a central role for epithelial cells in amplifying viral output. *PLoS pathogens* 5:e1000496.

Hao, Q.F., Y.X. Yang, Y. Wang, L.M. Chen, G.Y. Sheng, and Z. Luan. 2014. Rapid generation of Epstein-Barr virus-specific T cells for cellular therapy. *Transplantation proceedings* 46:21-25.

Haque, T., K.A. McAulay, D. Kelly, and D.H. Crawford. 2010. Allogeneic T-cell therapy for Epstein-Barr virus-positive posttransplant lymphoproliferative disease: long-term follow-up. *Transplantation* 90:93-94.

Haque, T., G.M. Wilkie, M.M. Jones, C.D. Higgins, G. Urquhart, P. Wingate, D. Burns, K. McAulay, M. Turner, C. Bellamy, P.L. Amlot, D. Kelly, A. MacGilchrist, M.K. Gandhi, A.J. Swerdlow, and D.H. Crawford. 2007. Allogeneic cytotoxic T-cell therapy for EBV-positive posttransplantation lymphoproliferative disease: results of a phase 2 multicenter clinical trial. *Blood* 110:1123-1131.

Hardy, C.L., S.L. Silins, D.L. Woodland, and M.A. Blackman. 2000. Murine gamma-herpesvirus infection causes V(beta)4-specific CDR3-restricted clonal expansions within CD8(+) peripheral blood T lymphocytes. *International immunology* 12:1193-1204.

Hassman, L.M., T.J. Ellison, and D.H. Kedes. 2011. KSHV infects a subset of human tonsillar B cells, driving proliferation and plasmablast differentiation. *The Journal of clinical investigation* 121:752-768.

Hawkins, J.B., E. Delgado-Eckert, D.A. Thorley-Lawson, and M. Shapiro. 2013. The cycle of EBV infection explains persistence, the sizes of the infected cell populations and which come under CTL regulation. *PLoS pathogens* 9:e1003685.

Hayward, G.S. 1999. KSHV strains: the origins and global spread of the virus. *Seminars in cancer biology* 9:187-199.

He, B., N. Raab-Traub, P. Casali, and A. Cerutti. 2003. EBV-encoded latent membrane protein 1 cooperates with BAFF/BLyS and APRIL to induce T cell-independent Ig heavy chain class switching. *Journal of immunology* 171:5215-5224.

Henle, G., W. Henle, and V. Diehl. 1968. Relation of Burkitt's tumor-associated herpes-ytpe virus to infectious mononucleosis. *Proceedings of the National Academy of Sciences of the United States of America* 59:94-101.

Herskowitz, J.H., M.A. Jacoby, and S.H. Speck. 2005. The murine gammaherpesvirus 68 M2 gene is required for efficient reactivation from latently infected B cells. *Journal of virology* 79:2261-2273.

Herskowitz, J.H., A.M. Siegel, M.A. Jacoby, and S.H. Speck. 2008. Systematic mutagenesis of the murine gammaherpesvirus 68 M2 protein identifies domains important for chronic infection. *Journal of virology* 82:3295-3310.

Heslop, H.E., M.K. Brenner, and C.M. Rooney. 1994. Donor T cells to treat EBV-associated lymphoma. *The New England journal of medicine* 331:679-680.

Heslop, H.E., K.S. Slobod, M.A. Pule, G.A. Hale, A. Rousseau, C.A. Smith, C.M. Bollard, H. Liu, M.F. Wu, R.J. Rochester, P.J. Amrolia, J.L. Hurwitz, M.K. Brenner, and C.M. Rooney. 2010. Long-term outcome of EBV-specific T-cell infusions to prevent or treat EBV-related lymphoproliferative disease in transplant recipients. *Blood* 115:925-935.

Hewitt, E.W., L. Duncan, D. Mufti, J. Baker, P.G. Stevenson, and P.J. Lehner. 2002. Ubiquitylation of MHC class I by the K3 viral protein signals internalization and TSG101-dependent degradation. *The EMBO journal* 21:2418-2429.

Hislop, A.D., N.E. Annels, N.H. Gudgeon, A.M. Leese, and A.B. Rickinson. 2002. Epitope-specific evolution of human CD8(+) T cell responses from primary to persistent phases of Epstein-Barr virus infection. *The Journal of experimental medicine* 195:893-905.

Hislop, A.D., N.H. Gudgeon, M.F. Callan, C. Fazou, H. Hasegawa, M. Salmon, and A.B. Rickinson. 2001. EBV-specific CD8+ T cell memory: relationships between epitope specificity, cell phenotype, and immediate effector function. *Journal of immunology* 167:2019-2029.

Hislop, A.D., M. Kuo, A.B. Drake-Lee, A.N. Akbar, W. Bergler, N. Hammerschmitt, N. Khan, U. Palendira, A.M. Leese, J.M. Timms, A.I. Bell, C.D. Buckley, and A.B. Rickinson. 2005. Tonsillar homing of Epstein-Barr virus-specific CD8+ T cells and the virus-host balance. *The Journal of clinical investigation* 115:2546-2555.

Hislop, A.D., M.E. Ressing, D. van Leeuwen, V.A. Pudney, D. Horst, D. Koppers-Lalic, N.P. Croft, J.J. Neefjes, A.B. Rickinson, and E.J. Wiertz. 2007a. A CD8+ T cell immune evasion protein specific to Epstein-Barr virus and its close relatives in Old World primates. *The Journal of experimental medicine* 204:1863-1873.

Hislop, A.D., and S. Sabbah. 2008. CD8+ T cell immunity to Epstein-Barr virus and Kaposi's sarcoma-associated herpes virus. *Seminars in cancer biology* 18:416-422.

Hislop, A.D., G.S. Taylor, D. Sauce, and A.B. Rickinson. 2007b. Cellular responses to viral infection in humans: lessons from Epstein-Barr virus. *Annual review of immunology* 25:587-617.

Hladik, W., S.C. Dollard, J. Mermin, A.L. Fowlkes, R. Downing, M.M. Amin, F. Banage, E. Nzaro, P. Kataaha, T.J. Dondero, P.E. Pellett, and E.M. Lackritz. 2006. Transmission of human herpesvirus 8 by blood transfusion. *The New England journal of medicine* 355:1331-1338.

Hoegh-Petersen, M., A.R. Thomsen, J.P. Christensen, and P.J. Holst. 2009. Mucosal immunization with recombinant adenoviral vectors expressing murine gammaherpesvirus-68 genes M2 and M3 can reduce latent viral load. *Vaccine* 27:6723-6730.

Hogquist, K.A., S.C. Jameson, W.R. Heath, J.L. Howard, M.J. Bevan, and F.R. Carbone. 1994. T cell receptor antagonist peptides induce positive selection. *Cell* 76:17-27.

Hommel, M., and P.D. Hodgkin. 2007. TCR affinity promotes CD8+ T cell expansion by regulating survival. *Journal of immunology* 179:2250-2260.

Horst, D., W.P. Burmeister, I.G. Boer, D. van Leeuwen, M. Buisson, A.E. Gorbalenya, E.J. Wiertz, and M.E. Ressing. 2012. The "Bridge" in the Epstein-Barr virus alkaline exonuclease protein BGLF5 contributes to shutoff activity during productive infection. *Journal of virology* 86:9175-9187.

Horst, D., V. Favaloro, F. Vilardi, H.C. van Leeuwen, M.A. Garstka, A.D. Hislop, C. Rabu, E. Kremmer, A.B. Rickinson, S. High, B. Dobberstein, M.E. Ressing, and E.J. Wiertz. 2011. EBV protein BNLF2a exploits host tail-anchored protein integration machinery to inhibit TAP. *Journal of immunology* 186:3594-3605.

Horst, D., D. van Leeuwen, N.P. Croft, M.A. Garstka, A.D. Hislop, E. Kremmer, A.B. Rickinson, E.J. Wiertz, and M.E. Ressing. 2009. Specific targeting of the EBV lytic phase protein BNLF2a to the transporter associated with antigen processing results in impairment of HLA class I-restricted antigen presentation. *Journal of immunology* 182:2313-2324.

Hoshino, Y., T. Morishima, H. Kimura, K. Nishikawa, T. Tsurumi, and K. Kuzushima. 1999. Antigen-driven expansion and contraction of CD8+-activated T cells in primary EBV infection. *Journal of immunology* 163:5735-5740.

Hoyos, V., B. Savoldo, C. Quintarelli, A. Mahendravada, M. Zhang, J. Vera, H.E. Heslop, C.M. Rooney, M.K. Brenner, and G. Dotti. 2010. Engineering CD19-specific T lymphocytes with interleukin-15 and a suicide gene to enhance their anti-lymphoma/leukemia effects and safety. *Leukemia* 24:1160-1170.

Hu, Z., and E.J. Usherwood. 2014. Immune escape of gamma-herpesviruses from adaptive immunity. *Reviews in medical virology*

Hu, Z., W. Zhang, and E.J. Usherwood. 2013. Regulatory CD8+ T cells associated with erosion of immune surveillance in persistent virus infection suppress in vitro and have a reversible proliferative defect. *Journal of immunology* 191:312-322.

Hughes, D.J., A. Kipar, S.G. Milligan, C. Cunningham, M. Sanders, M.A. Quail, M.A. Rajandream, S. Efstathiou, R.J. Bowden, C. Chastel, M. Bennett, J.T. Sample, B. Barrell, A.J. Davison, and J.P. Stewart. 2010. Characterization of a novel wood mouse virus related to murid herpesvirus 4. *The Journal of general virology* 91:867-879.

Hui, E.P., G.S. Taylor, H. Jia, B.B. Ma, S.L. Chan, R. Ho, W.L. Wong, S. Wilson, B.F. Johnson, C. Edwards, D.D. Stocken, A.B. Rickinson, N.M. Steven, and A.T. Chan. 2013. Phase I trial of recombinant modified vaccinia ankara encoding Epstein-Barr viral tumor antigens in nasopharyngeal carcinoma patients. *Cancer research* 73:1676-1688.

Husain, S.M., E.J. Usherwood, H. Dyson, C. Coleclough, M.A. Coppola, D.L. Woodland, M.A. Blackman, J.P. Stewart, and J.T. Sample. 1999. Murine gammaherpesvirus M2 gene is latency-associated

and its protein a target for CD8(+) T lymphocytes. *Proceedings of the National Academy of Sciences of the United States of America* 96:7508-7513.

Huye, L.E., Y. Nakazawa, M.P. Patel, E. Yvon, J. Sun, B. Savoldo, M.H. Wilson, G. Dotti, and C.M. Rooney. 2011. Combining mTor inhibitors with rapamycin-resistant T cells: a two-pronged approach to tumor elimination. *Molecular therapy : the journal of the American Society of Gene Therapy* 19:2239-2248.

Icheva, V., S. Kayser, D. Wolff, S. Tuve, C. Kyzirakos, W. Bethge, J. Greil, M.H. Albert, W. Schwinger, M. Nathrath, M. Schumm, S. Stevanovic, R. Handgretinger, P. Lang, and T. Feuchtinger. 2013. Adoptive transfer of epstein-barr virus (EBV) nuclear antigen 1-specific t cells as treatment for EBV reactivation and lymphoproliferative disorders after allogeneic stem-cell transplantation. *Journal of clinical oncology : official journal of the American Society of Clinical Oncology* 31:39-48.

Iglesias, M.C., J.R. Almeida, S. Fastenackels, D.J. van Bockel, M. Hashimoto, V. Venturi, E. Gostick, A. Urrutia, L. Wooldridge, M. Clement, S. Gras, P.G. Wilmann, B. Autran, A. Moris, J. Rossjohn, M.P. Davenport, M. Takiguchi, C. Brander, D.C. Douek, A.D. Kelleher, D.A. Price, and V. Appay. 2011. Escape from highly effective public CD8+ T-cell clonotypes by HIV. *Blood* 118:2138-2149.

Incrocci, R., M. McCormack, and M. Swanson-Mungerson. 2013. Epstein-Barr virus LMP2A increases IL-10 production in mitogen-stimulated primary B-cells and B-cell lymphomas. *The Journal of general virology* 94:1127-1133.

Inoue, H., H. Nojima, and H. Okayama. 1990. High efficiency transformation of Escherichia coli with plasmids. *Gene* 96:23-28.

Ishido, S., C. Wang, B.S. Lee, G.B. Cohen, and J.U. Jung. 2000. Downregulation of major histocompatibility complex class I molecules by Kaposi's sarcoma-associated herpesvirus K3 and K5 proteins. *Journal of virology* 74:5300-5309.

Jacoby, M.A., H.W.t. Virgin, and S.H. Speck. 2002. Disruption of the M2 gene of murine gammaherpesvirus 68 alters splenic latency following intranasal, but not intraperitoneal, inoculation. *Journal of virology* 76:1790-1801.

Jameson, S.C., and M.J. Bevan. 1992. Dissection of major histocompatibility complex (MHC) and T cell receptor contact residues in a Kb-restricted ovalbumin peptide and an assessment of the predictive power of MHC-binding motifs. *European journal of immunology* 22:2663-2667.

Jameson, S.C., F.R. Carbone, and M.J. Bevan. 1993. Clone-specific T cell receptor antagonists of major histocompatibility complex class I-restricted cytotoxic T cells. *The Journal of experimental medicine* 177:1541-1550.

Jameson, S.C., K.A. Hogquist, and M.J. Bevan. 1994. Specificity and flexibility in thymic selection. *Nature* 369:750-752.

Jensen, K.K., S.C. Chen, R.W. Hipkin, M.T. Wiekowski, M.A. Schwarz, C.C. Chou, J.P. Simas, A. Alcami, and S.A. Lira. 2003. Disruption of CCL21-induced chemotaxis in vitro and in vivo by M3, a chemokine-binding protein encoded by murine gammaherpesvirus 68. *Journal of virology* 77:624-630.

Jia, Q., M.L. Freeman, E.J. Yager, I. McHardy, L. Tong, D. Martinez-Guzman, T. Rickabaugh, S. Hwang, M.A. Blackman, R. Sun, and T.T. Wu. 2010. Induction of protective immunity against murine gammaherpesvirus 68 infection in the absence of viral latency. *Journal of virology* 84:2453-2465.

Jochum, S., A. Moosmann, S. Lang, W. Hammerschmidt, and R. Zeidler. 2012. The EBV immunoevasins vIL-10 and BNLF2a protect newly infected B cells from immune recognition and elimination. *PLoS pathogens* 8:e1002704.

Johnston, C., J. Orem, F. Okuku, M. Kalinaki, M. Saracino, E. Katongole-Mbidde, M. Sande, A. Ronald, K. McAdam, M.L. Huang, L. Drolette, S. Selke, A. Wald, L. Corey, and C. Casper. 2009. Impact of HIV infection and Kaposi sarcoma on human herpesvirus-8 mucosal replication and dissemination in Uganda. *PloS one* 4:e4222.

Jones, K., J.P. Nourse, L. Morrison, D. Nguyen-Van, D.J. Moss, S.R. Burrows, and M.K. Gandhi. 2010. Expansion of EBNA1-specific effector T cells in posttransplantation lymphoproliferative disorders. *Blood* 116:2245-2252.

Joseph, A.M., G.J. Babcock, and D.A. Thorley-Lawson. 2000. EBV persistence involves strict selection of latently infected B cells. *Journal of immunology* 165:2975-2981.

Karre, K., H.G. Ljunggren, G. Piontek, and R. Kiessling. 1986. Selective rejection of H-2-deficient lymphoma variants suggests alternative immune defence strategy. *Nature* 319:675-678.

Karrer, U., S. Sierro, M. Wagner, A. Oxenius, H. Hengel, U.H. Koszinowski, R.E. Phillips, and P. Klenerman. 2003. Memory inflation: continuous accumulation of antiviral CD8+ T cells over time. *Journal of immunology* 170:2022-2029.

Kayhan, B., E.J. Yager, K. Lanzer, T. Cookenham, Q. Jia, T.T. Wu, D.L. Woodland, R. Sun, and M.A. Blackman. 2007. A replication-deficient murine gamma-herpesvirus blocked in late viral gene expression can establish latency and elicit protective cellular immunity. *Journal of immunology* 179:8392-8402.

Khan, N., A. Hislop, N. Gudgeon, M. Cobbold, R. Khanna, L. Nayak, A.B. Rickinson, and P.A. Moss. 2004. Herpesvirus-specific CD8 T cell immunity in old age: cytomegalovirus impairs the response to a coresident EBV infection. *Journal of immunology* 173:7481-7489.

Khan, N., N. Shariff, M. Cobbold, R. Bruton, J.A. Ainsworth, A.J. Sinclair, L. Nayak, and P.A. Moss. 2002. Cytomegalovirus seropositivity drives the CD8 T cell repertoire toward greater clonality in healthy elderly individuals. *Journal of immunology* 169:1984-1992.

Khanna, R., S. Bell, M. Sherritt, A. Galbraith, S.R. Burrows, L. Rafter, B. Clarke, R. Slaughter, M.C. Falk, J. Douglass, T. Williams, S.L. Elliott, and D.J. Moss. 1999. Activation and adoptive transfer of Epstein-Barr virus-specific cytotoxic T cells in solid organ transplant patients with posttransplant lymphoproliferative disease. *Proceedings of the National Academy of Sciences of the United States of America* 96:10391-10396.

Khanna, R., S.R. Burrows, M.G. Kurilla, C.A. Jacob, I.S. Misko, T.B. Sculley, E. Kieff, and D.J. Moss. 1992. Localization of Epstein-Barr virus cytotoxic T cell epitopes using recombinant vaccinia: implications for vaccine development. *The Journal of experimental medicine* 176:169-176.

Kim, I.J., E. Flano, D.L. Woodland, and M.A. Blackman. 2002. Antibody-mediated control of persistent gamma-herpesvirus infection. *Journal of immunology* 168:3958-3964.

Kim, I.J., E. Flano, D.L. Woodland, F.E. Lund, T.D. Randall, and M.A. Blackman. 2003. Maintenance of long term gamma-herpesvirus B cell latency is dependent on CD40-mediated development of memory B cells. *Journal of immunology* 171:886-892.

Kimball, L.E., C. Casper, D.M. Koelle, R. Morrow, L. Corey, and J. Vieira. 2004. Reduced levels of neutralizing antibodies to Kaposi sarcoma-associated herpesvirus in persons with a history of Kaposi sarcoma. *The Journal of infectious diseases* 189:2016-2022.

Krown, S.E., D. Roy, J.Y. Lee, B.J. Dezube, E.G. Reid, R. Venkataramanan, K. Han, E. Cesarman, and D.P. Dittmer. 2012. Rapamycin with antiretroviral therapy in AIDS-associated Kaposi sarcoma: an AIDS Malignancy Consortium study. *Journal of acquired immune deficiency syndromes* 59:447-454.

Kumar, G.R., and B.A. Glaunsinger. 2010. Nuclear import of cytoplasmic poly(A) binding protein restricts gene expression via hyperadenylation and nuclear retention of mRNA. *Molecular and cellular biology* 30:4996-5008.

Kurth, J., M.L. Hansmann, K. Rajewsky, and R. Kuppers. 2003. Epstein-Barr virus-infected B cells expanding in germinal centers of infectious mononucleosis patients do not participate in the germinal center reaction. *Proceedings of the National Academy of Sciences of the United States of America* 100:4730-4735.

Kurth, J., T. Spieker, J. Wustrow, G.J. Strickler, L.M. Hansmann, K. Rajewsky, and R. Kuppers. 2000. EBV-infected B cells in infectious mononucleosis: viral strategies for spreading in the B cell compartment and establishing latency. *Immunity* 13:485-495.

Kutok, J.L., and F. Wang. 2006. Spectrum of Epstein-Barr virus-associated diseases. *Annual review of pathology* 1:375-404.

Kwun, H.J., S.R. da Silva, I.M. Shah, N. Blake, P.S. Moore, and Y. Chang. 2007. Kaposi's sarcoma-associated herpesvirus latency-associated nuclear antigen 1 mimics Epstein-Barr virus EBNA1 immune evasion through central repeat domain effects on protein processing. *Journal of virology* 81:8225-8235.

Lagos, D., M.W. Trotter, R.J. Vart, H.W. Wang, N.C. Matthews, A. Hansen, O. Flore, F. Gotch, and C. Boshoff. 2007. Kaposi sarcoma herpesvirus-encoded vFLIP and vIRF1 regulate antigen presentation in lymphatic endothelial cells. *Blood* 109:1550-1558.

Lagunoff, M., and D. Ganem. 1997. The structure and coding organization of the genomic termini of Kaposi's sarcoma-associated herpesvirus. *Virology* 236:147-154.

Lagunoff, M., R. Majeti, A. Weiss, and D. Ganem. 1999. Deregulated signal transduction by the K1 gene product of Kaposi's sarcoma-associated herpesvirus. *Proceedings of the National Academy of Sciences of the United States of America* 96:5704-5709.

Laichalk, L.L., D. Hochberg, G.J. Babcock, R.B. Freeman, and D.A. Thorley-Lawson. 2002. The dispersal of mucosal memory B cells: evidence from persistent EBV infection. *Immunity* 16:745-754.

Laichalk, L.L., and D.A. Thorley-Lawson. 2005. Terminal differentiation into plasma cells initiates the replicative cycle of Epstein-Barr virus in vivo. *Journal of virology* 79:1296-1307.

Lambert, M., M. Gannage, A. Karras, M. Abel, C. Legendre, D. Kerob, F. Agbalika, P.M. Girard, C. Lebbe, and S. Caillat-Zucman. 2006. Differences in the frequency and function of HHV8-specific CD8 T cells between asymptomatic HHV8 infection and Kaposi sarcoma. *Blood* 108:3871-3880.

Lee, B.S., S.H. Lee, P. Feng, H. Chang, N.H. Cho, and J.U. Jung. 2005. Characterization of the Kaposi's sarcoma-associated herpesvirus K1 signalosome. *Journal of virology* 79:12173-12184.

Lee, D.Y., and B. Sugden. 2008. The latent membrane protein 1 oncogene modifies B-cell physiology by regulating autophagy. *Oncogene* 27:2833-2842.

Lee, H., J. Guo, M. Li, J.K. Choi, M. DeMaria, M. Rosenzweig, and J.U. Jung. 1998a. Identification of an immunoreceptor tyrosine-based activation motif of K1 transforming protein of Kaposi's sarcoma-associated herpesvirus. *Molecular and cellular biology* 18:5219-5228.

Lee, H., R. Veazey, K. Williams, M. Li, J. Guo, F. Neipel, B. Fleckenstein, A. Lackner, R.C. Desrosiers, and J.U. Jung. 1998b. Deregulation of cell growth by the K1 gene of Kaposi's sarcoma-associated herpesvirus. *Nature medicine* 4:435-440.

Lee, J.S., Q. Li, J.Y. Lee, S.H. Lee, J.H. Jeong, H.R. Lee, H. Chang, F.C. Zhou, S.J. Gao, C. Liang, and J.U. Jung. 2009a. FLIP-mediated autophagy regulation in cell death control. *Nature cell biology* 11:1355-1362.

Lee, K.S., C.D. Cool, and L.F. van Dyk. 2009b. Murine gammaherpesvirus 68 infection of gamma interferon-deficient mice on a BALB/c background results in acute lethal pneumonia that is dependent on specific viral genes. *Journal of virology* 83:11397-11401.

Lee, K.S., S.D. Groshong, C.D. Cool, B.K. Kleinschmidt-DeMasters, and L.F. van Dyk. 2009c. Murine gammaherpesvirus 68 infection of IFNgamma unresponsive mice: a small animal model for gammaherpesvirus-associated B-cell lymphoproliferative disease. *Cancer research* 69:5481-5489.

Lee, S.P., R.J. Tierney, W.A. Thomas, J.M. Brooks, and A.B. Rickinson. 1997. Conserved CTL epitopes within EBV latent membrane protein 2: a potential target for CTL-based tumor therapy. *Journal of immunology* 158:3325-3334.

Lee, Y.J., and B.A. Glaunsinger. 2009. Aberrant herpesvirus-induced polyadenylation correlates with cellular messenger RNA destruction. *PLoS biology* 7:e1000107.

Leen, A.M., C.M. Bollard, A.M. Mendizabal, E.J. Shpall, P. Szabolcs, J.H. Antin, N. Kapoor, S.Y. Pai, S.D. Rowley, P. Kebriaei, B.R. Dey, B.J. Grilley, A.P. Gee, M.K. Brenner, C.M. Rooney, and H.E. Heslop. 2013. Multicenter study of banked third-party virus-specific T cells to treat severe viral infections after hematopoietic stem cell transplantation. *Blood* 121:5113-5123.

Lei, X., Z. Bai, F. Ye, J. Xie, C.G. Kim, Y. Huang, and S.J. Gao. 2010. Regulation of NF-kappaB inhibitor IkappaBalpha and viral replication by a KSHV microRNA. *Nature cell biology* 12:193-199.

Leidal, A.M., D.P. Cyr, R.J. Hill, P.W. Lee, and C. McCormick. 2012. Subversion of autophagy by Kaposi's sarcoma-associated herpesvirus impairs oncogene-induced senescence. *Cell host & microbe* 11:167-180.

Leslie, A., D.A. Price, P. Mkhize, K. Bishop, A. Rathod, C. Day, H. Crawford, I. Honeyborne, T.E. Asher, G. Luzzi, A. Edwards, C.M. Rousseau, J.I. Mullins, G. Tudor-Williams, V. Novelli, C. Brander, D.C. Douek, P. Kiepiela, B.D. Walker, and P.J. Goulder. 2006. Differential selection pressure exerted on HIV by CTL targeting identical epitopes but restricted by distinct HLA alleles from the same HLA supertype. *Journal of immunology* 177:4699-4708.

Leung, C., O. Chijioke, C. Gujer, B. Chatterjee, O. Antsiferova, V. Landtwing, D. McHugh, A. Raykova, and C. Munz. 2013. Infectious diseases in humanized mice. *European journal of immunology* 43:2246-2254.

Levitskaya, J., M. Coram, V. Levitsky, S. Imreh, P.M. Steigerwald-Mullen, G. Klein, M.G. Kurilla, and M.G. Masucci. 1995. Inhibition of antigen processing by the internal repeat region of the Epstein-Barr virus nuclear antigen-1. *Nature* 375:685-688.

Levitsky, V., Q.J. Zhang, J. Levitskaya, M.G. Kurilla, and M.G. Masucci. 1997. Natural variants of the immunodominant HLA A11-restricted CTL epitope of the EBV nuclear antigen-4 are nonimmunogenic due to intracellular dissociation from MHC class I:peptide complexes. *Journal of immunology* 159:5383-5390.

Li, Q., R. Means, S. Lang, and J.U. Jung. 2007. Downregulation of gamma interferon receptor 1 by Kaposi's sarcoma-associated herpesvirus K3 and K5. *Journal of virology* 81:2117-2127.

Liang, C., J.S. Lee, and J.U. Jung. 2008. Immune evasion in Kaposi's sarcoma-associated herpes virus associated oncogenesis. *Seminars in cancer biology* 18:423-436.

Liang, X., C.M. Collins, J.B. Mendel, N.N. Iwakoshi, and S.H. Speck. 2009. Gammaherpesvirus-driven plasma cell differentiation regulates virus reactivation from latently infected B lymphocytes. *PLoS pathogens* 5:e1000677.

Liang, X., R.L. Crepeau, W. Zhang, S.H. Speck, and E.J. Usherwood. 2013. CD4 and CD8 T cells directly recognize murine gammaherpesvirus 68-immortalized cells and prevent tumor outgrowth. *Journal of virology* 87:6051-6054.

Liang, X., C.R. Paden, F.M. Morales, R.P. Powers, J. Jacob, and S.H. Speck. 2011. Murine gammaherpesvirus immortalization of fetal liver-derived B cells requires both the viral cyclin D homolog and latency-associated nuclear antigen. *PLoS pathogens* 7:e1002220.

Liang, X., M.T. Pickering, N.H. Cho, H. Chang, M.R. Volkert, T.F. Kowalik, and J.U. Jung. 2006. Deregulation of DNA damage signal transduction by herpesvirus latency-associated M2. *Journal of virology* 80:5862-5874.

Liang, X., Y.C. Shin, R.E. Means, and J.U. Jung. 2004. Inhibition of interferon-mediated antiviral activity by murine gammaherpesvirus 68 latency-associated M2 protein. *Journal of virology* 78:12416-12427.

Liu, L., E. Flano, E.J. Usherwood, S. Surman, M.A. Blackman, and D.L. Woodland. 1999a. Lytic cycle T cell epitopes are expressed in two distinct phases during MHV-68 infection. *Journal of immunology* 163:868-874.

Liu, L., E.J. Usherwood, M.A. Blackman, and D.L. Woodland. 1999b. T-cell vaccination alters the course of murine herpesvirus 68 infection and the establishment of viral latency in mice. *Journal of virology* 73:9849-9857.

Ljunggren, H.G., and K. Karre. 1985. Host resistance directed selectively against H-2-deficient lymphoma variants. Analysis of the mechanism. *The Journal of experimental medicine* 162:1745-1759.

Ljunggren, H.G., N.J. Stam, C. Ohlen, J.J. Neefjes, P. Hoglund, M.T. Heemels, J. Bastin, T.N. Schumacher, A. Townsend, K. Karre, and et al. 1990. Empty MHC class I molecules come out in the cold. *Nature* 346:476-480.

Long, H.M., G.S. Taylor, and A.B. Rickinson. 2011. Immune defence against EBV and EBV-associated disease. *Current opinion in immunology* 23:258-264.

Lopes, L.F., K.W. Ruiz Miyazawa, E.R. de Almeida, K.G. Serafim, K. de Almeida Gualtieri, I.C. Costa, I. Felipe, W.R. Pavanelli, and M.A. Watanabe. 2013. Epstein-Barr virus (EBV) microRNAs: involvement in cancer pathogenesis and immunopathology. *International reviews of immunology* 32:271-281.

Louis, C.U., K. Straathof, C.M. Bollard, S. Ennamuri, C. Gerken, T.T. Lopez, M.H. Huls, A. Sheehan, M.F. Wu, H. Liu, A. Gee, M.K. Brenner, C.M. Rooney, H.E. Heslop, and S. Gottschalk. 2010. Adoptive transfer of EBV-specific T cells results in sustained clinical responses in patients with locoregional nasopharyngeal carcinoma. *Journal of immunotherapy* 33:983-990.

Lutzky, V.P., M. Corban, L. Heslop, L.E. Morrison, P. Crooks, D.F. Hall, W.B. Coman, S.A. Thomson, and D.J. Moss. 2010. Novel approach to the formulation of an Epstein-Barr virus antigen-based nasopharyngeal carcinoma vaccine. *Journal of virology* 84:407-417.

Lutzky, V.P., P. Crooks, L. Morrison, N. Stevens, J.E. Davis, M. Corban, D. Hall, B. Panizza, W.B. Coman, S. Coman, and D.J. Moss. 2014. Cytotoxic T cell adoptive immunotherapy as a treatment for nasopharyngeal carcinoma. *Clinical and vaccine immunology : CVI* 21:256-259.

Lybarger, L., X. Wang, M.R. Harris, H.W.t. Virgin, and T.H. Hansen. 2003. Virus subversion of the MHC class I peptide-loading complex. *Immunity* 18:121-130.

Mackay, L.K., H.M. Long, J.M. Brooks, G.S. Taylor, C.S. Leung, A. Chen, F. Wang, and A.B. Rickinson. 2009. T cell detection of a B-cell tropic virus infection: newly-synthesised versus mature viral proteins as antigen sources for CD4 and CD8 epitope display. *PLoS pathogens* 5:e1000699.

Macrae, A.I., E.J. Usherwood, S.M. Husain, E. Flano, I.J. Kim, D.L. Woodland, A.A. Nash, M.A. Blackman, J.T. Sample, and J.P. Stewart. 2003. Murid herpesvirus 4 strain 68 M2 protein is a B-cell-associated antigen important for latency but not lymphocytosis. *Journal of virology* 77:9700-9709.

Madureira, P.A., P. Matos, I. Soeiro, L.K. Dixon, J.P. Simas, and E.W. Lam. 2005. Murine gammaherpesvirus 68 latency protein M2 binds to Vav signaling proteins and inhibits B-cell receptor-

induced cell cycle arrest and apoptosis in WEHI-231 B cells. *The Journal of biological chemistry* 280:37310-37318.

Maini, M.K., N. Gudgeon, L.R. Wedderburn, A.B. Rickinson, and P.C. Beverley. 2000. Clonal expansions in acute EBV infection are detectable in the CD8 and not the CD4 subset and persist with a variable CD45 phenotype. *Journal of immunology* 165:5729-5737.

Marques, S., M. Alenquer, P.G. Stevenson, and J.P. Simas. 2008. A single CD8+ T cell epitope sets the long-term latent load of a murid herpesvirus. *PLoS pathogens* 4:e1000177.

Marques, S., S. Efstathiou, K.G. Smith, M. Haury, and J.P. Simas. 2003. Selective gene expression of latent murine gammaherpesvirus 68 in B lymphocytes. *Journal of virology* 77:7308-7318.

Marquitz, A.R., A. Mathur, C.S. Nam, and N. Raab-Traub. 2011. The Epstein-Barr Virus BART microRNAs target the pro-apoptotic protein Bim. *Virology* 412:392-400.

Matsumura, M., Y. Saito, M.R. Jackson, E.S. Song, and P.A. Peterson. 1992. In vitro peptide binding to soluble empty class I major histocompatibility complex molecules isolated from transfected Drosophila melanogaster cells. *The Journal of biological chemistry* 267:23589-23595.

Maurer, D.M., B. Harrington, and J.M. Lane. 2003. Smallpox vaccine: contraindications, administration, and adverse reactions. *American family physician* 68:889-896.

May, J.S., H.M. Coleman, B. Smillie, S. Efstathiou, and P.G. Stevenson. 2004. Forced lytic replication impairs host colonization by a latency-deficient mutant of murine gammaherpesvirus-68. *The Journal of general virology* 85:137-146.

McAulay, K.A., T. Haque, G. Urquhart, C. Bellamy, D. Guiretti, and D.H. Crawford. 2009. Epitope specificity and clonality of EBV-specific CTLs used to treat posttransplant lymphoproliferative disease. *Journal of immunology* 182:3892-3901.

McGeoch, D.J. 2001. Molecular evolution of the gamma-Herpesvirinae. *Philosophical transactions of the Royal Society of London. Series B, Biological sciences* 356:421-435.

McNally, J.M., and R.M. Welsh. 2002. Bystander T cell activation and attrition. *Current topics in microbiology and immunology* 263:29-41.

Meij, P., J.W. van Esser, H.G. Niesters, D. van Baarle, F. Miedema, N. Blake, A.B. Rickinson, I. Leiner, E. Pamer, B. Lowenberg, J.J. Cornelissen, and J.W. Gratama. 2003. Impaired recovery of Epstein-Barr virus (EBV)--specific CD8+ T lymphocytes after partially T-depleted allogeneic stem cell transplantation may identify patients at very high risk for progressive EBV reactivation and lymphoproliferative disease. *Blood* 101:4290-4297.

Merlo, A., R. Turrini, S. Bobisse, R. Zamarchi, R. Alaggio, R. Dolcetti, J. Mautner, P. Zanovello, A. Amadori, and A. Rosato. 2010. Virus-specific cytotoxic CD4+ T cells for the treatment of EBV-related tumors. *Journal of immunology* 184:5895-5902.

Mesri, E.A., E. Cesarman, and C. Boshoff. 2010. Kaposi's sarcoma and its associated herpesvirus. *Nature reviews. Cancer* 10:707-719.

Mesri, E.A., M.A. Feitelson, and K. Munger. 2014. Human viral oncogenesis: a cancer hallmarks analysis. *Cell host & microbe* 15:266-282.

Midgley, R.S., A.I. Bell, D.J. McGeoch, and A.B. Rickinson. 2003a. Latent gene sequencing reveals familial relationships among Chinese Epstein-Barr virus strains and evidence for positive selection of A11 epitope changes. *Journal of virology* 77:11517-11530.

Midgley, R.S., A.I. Bell, Q.Y. Yao, D. Croom-Carter, A.D. Hislop, B.M. Whitney, A.T. Chan, P.J. Johnson, and A.B. Rickinson. 2003b. HLA-A11-restricted epitope polymorphism among Epstein-Barr virus strains in the highly HLA-A11-positive Chinese population: incidence and immunogenicity of variant epitope sequences. *Journal of virology* 77:11507-11516.

Miles, J.J., D. Elhassen, N.A. Borg, S.L. Silins, F.E. Tynan, J.M. Burrows, A.W. Purcell, L. Kjer-Nielsen, J. Rossjohn, S.R. Burrows, and J. McCluskey. 2005a. CTL recognition of a bulged viral peptide involves biased TCR selection. *Journal of immunology* 175:3826-3834.

Miles, J.J., S.L. Silins, A.G. Brooks, J.E. Davis, I. Misko, and S.R. Burrows. 2005b. T-cell grit: large clonal expansions of virus-specific CD8+ T cells can dominate in the peripheral circulation for at least 18 years. *Blood* 106:4412-4413.

Milho, R., B. Frederico, S. Efstathiou, and P.G. Stevenson. 2012. A heparan-dependent herpesvirus targets the olfactory neuroepithelium for host entry. *PLoS pathogens* 8:e1002986.

Moghaddam, A., M. Rosenzweig, D. Lee-Parritz, B. Annis, R.P. Johnson, and F. Wang. 1997. An animal model for acute and persistent Epstein-Barr virus infection. *Science* 276:2030-2033.

Molloy, M.J., W. Zhang, and E.J. Usherwood. 2011. Suppressive CD8+ T cells arise in the absence of CD4 help and compromise control of persistent virus. *Journal of immunology* 186:6218-6226.

Mombaerts, P., A.R. Clarke, M.A. Rudnicki, J. Iacomini, S. Itohara, J.J. Lafaille, L. Wang, Y. Ichikawa, R. Jaenisch, M.L. Hooper, and et al. 1992. Mutations in T-cell antigen receptor genes alpha and beta block thymocyte development at different stages. *Nature* 360:225-231.

Moore, K.W., P. Vieira, D.F. Fiorentino, M.L. Trounstine, T.A. Khan, and T.R. Mosmann. 1990. Homology of cytokine synthesis inhibitory factor (IL-10) to the Epstein-Barr virus gene BCRFI. *Science* 248:1230-1234.

Moore, P.S., C. Boshoff, R.A. Weiss, and Y. Chang. 1996. Molecular mimicry of human cytokine and cytokine response pathway genes by KSHV. *Science* 274:1739-1744.

Moorman, N.J., C.Y. Lin, and S.H. Speck. 2004. Identification of candidate gammaherpesvirus 68 genes required for virus replication by signature-tagged transposon mutagenesis. *Journal of virology* 78:10282-10290.

Moorman, N.J., D.O. Willer, and S.H. Speck. 2003. The gammaherpesvirus 68 latency-associated nuclear antigen homolog is critical for the establishment of splenic latency. *Journal of virology* 77:10295-10303.

Moosmann, A., I. Bigalke, J. Tischer, L. Schirrmann, J. Kasten, S. Tippmer, M. Leeping, D. Prevalsek, G. Jaeger, G. Ledderose, J. Mautner, W. Hammerschmidt, D.J. Schendel, and H.J. Kolb. 2010. Effective and long-term control of EBV PTLD after transfer of peptide-selected T cells. *Blood* 115:2960-2970.

Moser, J.M., M.L. Farrell, L.T. Krug, J.W. Upton, and S.H. Speck. 2006. A gammaherpesvirus 68 gene 50 null mutant establishes long-term latency in the lung but fails to vaccinate against a wild-type virus challenge. *Journal of virology* 80:1592-1598.

Moser, J.M., J.W. Upton, R.D. Allen, 3rd, C.B. Wilson, and S.H. Speck. 2005. Role of B-cell proliferation in the establishment of gammaherpesvirus latency. *Journal of virology* 79:9480-9491.

Moutschen, M., P. Leonard, E.M. Sokal, F. Smets, M. Haumont, P. Mazzu, A. Bollen, F. Denamur, P. Peeters, G. Dubin, and M. Denis. 2007. Phase I/II studies to evaluate safety and immunogenicity of a recombinant gp350 Epstein-Barr virus vaccine in healthy adults. *Vaccine* 25:4697-4705.

Murray, R.J., M.G. Kurilla, J.M. Brooks, W.A. Thomas, M. Rowe, E. Kieff, and A.B. Rickinson. 1992. Identification of target antigens for the human cytotoxic T cell response to Epstein-Barr virus (EBV): implications for the immune control of EBV-positive malignancies. *The Journal of experimental medicine* 176:157-168.

Nador, R.G., E. Cesarman, A. Chadburn, D.B. Dawson, M.Q. Ansari, J. Sald, and D.M. Knowles. 1996. Primary effusion lymphoma: a distinct clinicopathologic entity associated with the Kaposi's sarcoma-associated herpes virus. *Blood* 88:645-656.

Nagy, S., R. Gyulai, L. Kemeny, P. Szenohradszky, and A. Dobozy. 2000. Iatrogenic Kaposi's sarcoma: HHV8 positivity persists but the tumors regress almost completely without immunosuppressive therapy. *Transplantation* 69:2230-2231.

Nash, A.A., B.M. Dutia, J.P. Stewart, and A.J. Davison. 2001. Natural history of murine gamma-herpesvirus infection. *Philosophical transactions of the Royal Society of London. Series B, Biological sciences* 356:569-579.

Nemerow, G.R., C. Mold, V.K. Schwend, V. Tollefson, and N.R. Cooper. 1987. Identification of gp350 as the viral glycoprotein mediating attachment of Epstein-Barr virus (EBV) to the EBV/C3d receptor of B cells: sequence homology of gp350 and C3 complement fragment C3d. *Journal of virology* 61:1416-1420.

Nicholas, J. 2005. Human gammaherpesvirus cytokines and chemokine receptors. *Journal of interferon & cytokine research : the official journal of the International Society for Interferon and Cytokine Research* 25:373-383.

Nicholas, J., V. Ruvolo, J. Zong, D. Ciufo, H.G. Guo, M.S. Reitz, and G.S. Hayward. 1997a. A single 13-kilobase divergent locus in the Kaposi sarcoma-associated herpesvirus (human herpesvirus 8) genome contains nine open reading frames that are homologous to or related to cellular proteins. *Journal of virology* 71:1963-1974.

Nicholas, J., V.R. Ruvolo, W.H. Burns, G. Sandford, X. Wan, D. Ciufo, S.B. Hendrickson, H.G. Guo, G.S. Hayward, and M.S. Reitz. 1997b. Kaposi's sarcoma-associated human herpesvirus-8 encodes homologues of macrophage inflammatory protein-1 and interleukin-6. *Nature medicine* 3:287-292.

Nutt, S.L., and D.M. Tarlinton. 2011. Germinal center B and follicular helper T cells: siblings, cousins or just good friends? *Nature immunology* 12:472-477.

O'Connor, D.H., T.M. Allen, T.U. Vogel, P. Jing, I.P. DeSouza, E. Dodds, E.J. Dunphy, C. Melsaether, B. Mothe, H. Yamamoto, H. Horton, N. Wilson, A.L. Hughes, and D.I. Watkins. 2002. Acute phase cytotoxic T lymphocyte escape is a hallmark of simian immunodeficiency virus infection. *Nature medicine* 8:493-499.

O'Hara, A.J., P. Chugh, L. Wang, E.M. Netto, E. Luz, W.J. Harrington, B.J. Dezube, B. Damania, and D.P. Dittmer. 2009. Pre-micro RNA signatures delineate stages of endothelial cell transformation in Kaposi sarcoma. *PLoS pathogens* 5:e1000389.

O'Reilly, R.J., T.N. Small, E. Papadopoulos, K. Lucas, J. Lacerda, and L. Koulova. 1997. Biology and adoptive cell therapy of Epstein-Barr virus-associated lymphoproliferative disorders in recipients of marrow allografts. *Immunological reviews* 157:195-216.

Obar, J.J., D.C. Donovan, S.G. Crist, O. Silvia, J.P. Stewart, and E.J. Usherwood. 2004. T-cell responses to the M3 immune evasion protein of murid gammaherpesvirus 68 are partially protective and induced with lytic antigen kinetics. *Journal of virology* 78:10829-10832.

Osman, M., T. Kubo, J. Gill, F. Neipel, M. Becker, G. Smith, R. Weiss, B. Gazzard, C. Boshoff, and F. Gotch. 1999. Identification of human herpesvirus 8-specific cytotoxic T-cell responses. *Journal of virology* 73:6136-6140.

Ouyang, Q., W.M. Wagner, S. Walter, C.A. Muller, A. Wikby, G. Aubert, T. Klatt, S. Stevanovic, T. Dodi, and G. Pawelec. 2003. An age-related increase in the number of CD8+ T cells carrying receptors for an immunodominant Epstein-Barr virus (EBV) epitope is counteracted by a decreased frequency of their antigen-specific responsiveness. *Mechanisms of ageing and development* 124:477-485.

Paden, C.R., J.C. Forrest, S.A. Tibbetts, and S.H. Speck. 2012. Unbiased mutagenesis of MHV68 LANA reveals a DNA-binding domain required for LANA function in vitro and in vivo. *PLoS pathogens* 8:e1002906.

Papadopoulos, E.B., M. Ladanyi, D. Emanuel, S. Mackinnon, F. Boulad, M.H. Carabasi, H. Castro-Malaspina, B.H. Childs, A.P. Gillio, T.N. Small, and et al. 1994. Infusions of donor leukocytes to treat Epstein-Barr virus-associated lymphoproliferative disorders after allogeneic bone marrow transplantation. *The New England journal of medicine* 330:1185-1191.

Parry, C.M., J.P. Simas, V.P. Smith, C.A. Stewart, A.C. Minson, S. Efstathiou, and A. Alcami. 2000. A broad spectrum secreted chemokine binding protein encoded by a herpesvirus. *The Journal of experimental medicine* 191:573-578.

Pauk, J., M.L. Huang, S.J. Brodie, A. Wald, D.M. Koelle, T. Schacker, C. Celum, S. Selke, and L. Corey. 2000. Mucosal shedding of human herpesvirus 8 in men. *The New England journal of medicine* 343:1369-1377.

Paulsen, S.J., M.M. Rosenkilde, J. Eugen-Olsen, and T.N. Kledal. 2005. Epstein-Barr virus-encoded BILF1 is a constitutively active G protein-coupled receptor. *Journal of virology* 79:536-546.

Pfeffer, S., A. Sewer, M. Lagos-Quintana, R. Sheridan, C. Sander, F.A. Grasser, L.F. van Dyk, C.K. Ho, S. Shuman, M. Chien, J.J. Russo, J. Ju, G. Randall, B.D. Lindenbach, C.M. Rice, V. Simon, D.D. Ho, M. Zavolan, and T. Tuschl. 2005. Identification of microRNAs of the herpesvirus family. *Nature methods* 2:269-276.

Philpott, K.L., J.L. Viney, G. Kay, S. Rastan, E.M. Gardiner, S. Chae, A.C. Hayday, and M.J. Owen. 1992. Lymphoid development in mice congenitally lacking T cell receptor alpha beta-expressing cells. *Science* 256:1448-1452.

Pires de Miranda, M., M. Alenquer, S. Marques, L. Rodrigues, F. Lopes, X.R. Bustelo, and J.P. Simas. 2008. The Gammaherpesvirus m2 protein manipulates the Fyn/Vav pathway through a multidocking mechanism of assembly. *PloS one* 3:e1654.

Pires de Miranda, M., F.B. Lopes, C.E. McVey, X.R. Bustelo, and J.P. Simas. 2013. Role of Src homology domain binding in signaling complexes assembled by the murid gamma-herpesvirus M2 protein. *The Journal of biological chemistry* 288:3858-3870.

Polizzotto, M.N., T.S. Uldrick, D. Hu, and R. Yarchoan. 2012. Clinical Manifestations of Kaposi Sarcoma Herpesvirus Lytic Activation: Multicentric Castleman Disease (KSHV-MCD) and the KSHV Inflammatory Cytokine Syndrome. *Frontiers in microbiology* 3:73.

Pope, J.H., M.K. Horne, and W. Scott. 1968. Transformation of foetal human keukocytes in vitro by filtrates of a human leukaemic cell line containing herpes-like virus. *International journal of cancer. Journal international du cancer* 3:857-866.

Powis, S.J., A.R. Townsend, E.V. Deverson, J. Bastin, G.W. Butcher, and J.C. Howard. 1991. Restoration of antigen presentation to the mutant cell line RMA-S by an MHC-linked transporter. *Nature* 354:528-531.

Pudney, V.A., A.M. Leese, A.B. Rickinson, and A.D. Hislop. 2005. CD8+ immunodominance among Epstein-Barr virus lytic cycle antigens directly reflects the efficiency of antigen presentation in lytically infected cells. *The Journal of experimental medicine* 201:349-360.

Qiu, J., K. Cosmopoulos, M. Pegtel, E. Hopmans, P. Murray, J. Middeldorp, M. Shapiro, and D.A. Thorley-Lawson. 2011. A novel persistence associated EBV miRNA expression profile is disrupted in neoplasia. *PLoS pathogens* 7:e1002193.

Rangaswamy, U.S., and S.H. Speck. 2014. Murine gammaherpesvirus M2 protein induction of IRF4 via the NFAT pathway leads to IL-10 expression in B cells. *PLoS pathogens* 10:e1003858.

Rees, L., E.J. Tizard, A.J. Morgan, W.D. Cubitt, S. Finerty, T.A. Oyewole-Eletu, K. Owen, C. Royed, S.J. Stevens, R.C. Shroff, M.K. Tanday, A.D. Wilson, J.M. Middeldorp, P.L. Amlot, and N.M. Steven. 2009. A phase I trial of epstein-barr virus gp350 vaccine for children with chronic kidney disease awaiting transplantation. *Transplantation* 88:1025-1029.

Regamey, N., M. Tamm, M. Wernli, A. Witschi, G. Thiel, G. Cathomas, and P. Erb. 1998. Transmission of human herpesvirus 8 infection from renal-transplant donors to recipients. *The New England journal of medicine* 339:1358-1363.

Renne, R., W. Zhong, B. Herndier, M. McGrath, N. Abbey, D. Kedes, and D. Ganem. 1996. Lytic growth of Kaposi's sarcoma-associated herpesvirus (human herpesvirus 8) in culture. *Nature medicine* 2:342-346.

Ressing, M.E., D. Horst, B.D. Griffin, J. Tellam, J. Zuo, R. Khanna, M. Rowe, and E.J. Wiertz. 2008. Epstein-Barr virus evasion of CD8(+) and CD4(+) T cell immunity via concerted actions of multiple gene products. *Seminars in cancer biology* 18:397-408.

Ricciardelli, I., J. Brewin, G. Lugthart, S.J. Albon, M. Pule, and P.J. Amrolia. 2013. Rapid generation of EBV-specific cytotoxic T lymphocytes resistant to calcineurin inhibitors for adoptive immunotherapy. *American journal of transplantation : official journal of the American Society of Transplantation and the American Society of Transplant Surgeons* 13:3244-3252.

Rice, J., B. de Lima, F.K. Stevenson, and P.G. Stevenson. 2002. A gamma-herpesvirus immune evasion gene allows tumor cells in vivo to escape attack by cytotoxic T cells specific for a tumor epitope. *European journal of immunology* 32:3481-3487.

Rickabaugh, T.M., H.J. Brown, D. Martinez-Guzman, T.T. Wu, L. Tong, F. Yu, S. Cole, and R. Sun. 2004. Generation of a latency-deficient gammaherpesvirus that is protective against secondary infection. *Journal of virology* 78:9215-9223.

Rickinson, A.B., H.M. Long, U. Palendira, C. Munz, and A.D. Hislop. 2014. Cellular immune controls over Epstein-Barr virus infection: new lessons from the clinic and the laboratory. *Trends in immunology* 35:159-169.

Rickinson, A.B., and D.J. Moss. 1997. Human cytotoxic T lymphocyte responses to Epstein-Barr virus infection. *Annual review of immunology* 15:405-431.

Robey, R.C., D. Lagos, F. Gratrix, S. Henderson, N.C. Matthews, R.J. Vart, M. Bower, C. Boshoff, and F.M. Gotch. 2009. The CD8 and CD4 T-cell response against Kaposi's sarcoma-associated herpesvirus is skewed towards early and late lytic antigens. *PloS one* 4:e5890.

Robey, R.C., S. Mletzko, and F.M. Gotch. 2010. The T-Cell Immune Response against Kaposi's Sarcoma-Associated Herpesvirus. *Advances in virology* 2010:340356.

Rodrigues, L., J. Filipe, M.P. Seldon, L. Fonseca, J. Anrather, M.P. Soares, and J.P. Simas. 2009. Termination of NF-kappaB activity through a gammaherpesvirus protein that assembles an EC5S ubiquitin-ligase. *The EMBO journal* 28:1283-1295.

Rodrigues, L., M. Pires de Miranda, M.J. Caloca, X.R. Bustelo, and J.P. Simas. 2006. Activation of Vav by the gammaherpesvirus M2 protein contributes to the establishment of viral latency in B lymphocytes. *Journal of virology* 80:6123-6135.

Rodrigues, L., N. Popov, K.M. Kaye, and J.P. Simas. 2013. Stabilization of Myc through heterotypic poly-ubiquitination by mLANA is critical for gamma-herpesvirus lymphoproliferation. *PLoS pathogens* 9:e1003554.

Rooney, C.M., C.A. Smith, C.Y. Ng, S. Loftin, C. Li, R.A. Krance, M.K. Brenner, and H.E. Heslop. 1995. Use of gene-modified virus-specific T lymphocytes to control Epstein-Barr-virus-related lymphoproliferation. *Lancet* 345:9-13.

Rosette, C., G. Werlen, M.A. Daniels, P.O. Holman, S.M. Alam, P.J. Travers, N.R. Gascoigne, E. Palmer, and S.C. Jameson. 2001. The impact of duration versus extent of TCR occupancy on T cell activation: a revision of the kinetic proofreading model. *Immunity* 15:59-70.

Roughan, J.E., and D.A. Thorley-Lawson. 2009. The intersection of Epstein-Barr virus with the germinal center. *Journal of virology* 83:3968-3976.

Roughan, J.E., C. Torgbor, and D.A. Thorley-Lawson. 2010. Germinal center B cells latently infected with Epstein-Barr virus proliferate extensively but do not increase in number. *Journal of virology* 84:1158-1168.

Rowe, M., B. Glaunsinger, D. van Leeuwen, J. Zuo, D. Sweetman, D. Ganem, J. Middeldorp, E.J. Wiertz, and M.E. Ressing. 2007. Host shutoff during productive Epstein-Barr virus infection is mediated by BGLF5 and may contribute to immune evasion. *Proceedings of the National Academy of Sciences of the United States of America* 104:3366-3371.

Rowe, M., and J. Zuo. 2010. Immune responses to Epstein-Barr virus: molecular interactions in the virus evasion of CD8+ T cell immunity. *Microbes and infection / Institut Pasteur* 12:173-181.

Roy, D., S.H. Sin, A. Lucas, R. Venkataramanan, L. Wang, A. Eason, V. Chavakula, I.B. Hilton, K.M. Tamburro, B. Damania, and D.P. Dittmer. 2013. mTOR inhibitors block Kaposi sarcoma growth by inhibiting essential autocrine growth factors and tumor angiogenesis. *Cancer research* 73:2235-2246.

Samols, M.A., R.L. Skalsky, A.M. Maldonado, A. Riva, M.C. Lopez, H.V. Baker, and R. Renne. 2007. Identification of cellular genes targeted by KSHV-encoded microRNAs. *PLoS pathogens* 3:e65.

Sangster, M.Y., D.J. Topham, S. D'Costa, R.D. Cardin, T.N. Marion, L.K. Myers, and P.C. Doherty. 2000. Analysis of the virus-specific and nonspecific B cell response to a persistent B-lymphotropic gammaherpesvirus. *Journal of immunology* 164:1820-1828.

Sarid, R., O. Flore, R.A. Bohenzky, Y. Chang, and P.S. Moore. 1998. Transcription mapping of the Kaposi's sarcoma-associated herpesvirus (human herpesvirus 8) genome in a body cavity-based lymphoma cell line (BC-1). *Journal of virology* 72:1005-1012.

Sashihara, J., P.D. Burbelo, B. Savoldo, T.C. Pierson, and J.I. Cohen. 2009. Human antibody titers to Epstein-Barr Virus (EBV) gp350 correlate with neutralization of infectivity better than antibody titers to EBV gp42 using a rapid flow cytometry-based EBV neutralization assay. *Virology* 391:249-256.

Sashihara, J., Y. Hoshino, J.J. Bowman, T. Krogmann, P.D. Burbelo, V.M. Coffield, K. Kamrud, and J.I. Cohen. 2011. Soluble rhesus lymphocryptovirus gp350 protects against infection and reduces viral loads in animals that become infected with virus after challenge. *PLoS pathogens* 7:e1002308.

Saulquin, X., C. Ibisch, M.A. Peyrat, E. Scotet, M. Hourmant, H. Vie, M. Bonneville, and E. Houssaint. 2000. A global appraisal of immunodominant CD8 T cell responses to Epstein-Barr virus and cytomegalovirus by bulk screening. *European journal of immunology* 30:2531-2539.

Savoldo, B., J.A. Goss, M.M. Hammer, L. Zhang, T. Lopez, A.P. Gee, Y.F. Lin, R.E. Quiros-Tejeira, P. Reinke, S. Schubert, S. Gottschalk, M.J. Finegold, M.K. Brenner, C.M. Rooney, and H.E. Heslop. 2006. Treatment of solid organ transplant recipients with autologous Epstein Barr virus-specific cytotoxic T lymphocytes (CTLs). *Blood* 108:2942-2949.

Schumacher, T.N., M.T. Heemels, J.J. Neefjes, W.M. Kast, C.J. Melief, and H.L. Ploegh. 1990. Direct binding of peptide to empty MHC class I molecules on intact cells and in vitro. *Cell* 62:563-567.

Sehrawat, S., O. Kirak, P.A. Koenig, M.K. Isaacson, S. Marques, G. Bozkurt, J.P. Simas, R. Jaenisch, and H.L. Ploegh. 2012. CD8(+) T cells from mice transnuclear for a TCR that recognizes a single H-2K(b)-restricted MHV68 epitope derived from gB-ORF8 help control infection. *Cell reports* 1:461-471.

Seto, E., A. Moosmann, S. Gromminger, N. Walz, A. Grundhoff, and W. Hammerschmidt. 2010. Micro RNAs of Epstein-Barr virus promote cell cycle progression and prevent apoptosis of primary human B cells. *PLoS pathogens* 6:e1001063.

Shultz, L.D., Y. Saito, Y. Najima, S. Tanaka, T. Ochi, M. Tomizawa, T. Doi, A. Sone, N. Suzuki, H. Fujiwara, M. Yasukawa, and F. Ishikawa. 2010. Generation of functional human T-cell subsets with HLA-restricted immune responses in HLA class I expressing NOD/SCID/IL2r gamma(null) humanized mice. *Proceedings of the National Academy of Sciences of the United States of America* 107:13022-13027.

Siegel, A.M., J.H. Herskowitz, and S.H. Speck. 2008. The MHV68 M2 protein drives IL-10 dependent B cell proliferation and differentiation. *PLoS pathogens* 4:e1000039.

Silins, S.L., S.M. Cross, S.L. Elliott, S.J. Pye, J.M. Burrows, D.J. Moss, and I.S. Misko. 1997. Selection of a diverse TCR repertoire in response to an Epstein-Barr virus-encoded transactivator protein BZLF1 by CD8+ cytotoxic T lymphocytes during primary and persistent infection. *International immunology* 9:1745-1755.

Simas, J.P., and S. Efstathiou. 1998. Murine gammaherpesvirus 68: a model for the study of gammaherpesvirus pathogenesis. *Trends in microbiology* 6:276-282.

Simas, J.P., S. Marques, A. Bridgeman, S. Efstathiou, and H. Adler. 2004. The M2 gene product of murine gammaherpesvirus 68 is required for efficient colonization of splenic follicles but is not necessary for expansion of latently infected germinal centre B cells. *The Journal of general virology* 85:2789-2797.

Simas, J.P., D. Swann, R. Bowden, and S. Efstathiou. 1999. Analysis of murine gammaherpesvirus-68 transcription during lytic and latent infection. *The Journal of general virology* 80 (Pt 1):75-82.

Sin, S.H., and D.P. Dittmer. 2013. Viral latency locus augments B-cell response in vivo to induce chronic marginal zone enlargement, plasma cell hyperplasia, and lymphoma. *Blood* 121:2952-2963.

Sin, S.H., F.D. Fakhari, and D.P. Dittmer. 2010. The viral latency-associated nuclear antigen augments the B-cell response to antigen in vivo. *Journal of virology* 84:10653-10660.

Sin, S.H., D. Roy, L. Wang, M.R. Staudt, F.D. Fakhari, D.D. Patel, D. Henry, W.J. Harrington, Jr., B.A. Damania, and D.P. Dittmer. 2007. Rapamycin is efficacious against primary effusion lymphoma (PEL) cell lines in vivo by inhibiting autocrine signaling. *Blood* 109:2165-2173.

Smith, C., J. Tsang, L. Beagley, D. Chua, V. Lee, V. Li, D.J. Moss, W. Coman, K.H. Chan, J. Nicholls, D. Kwong, and R. Khanna. 2012. Effective treatment of metastatic forms of Epstein-Barr virus-associated nasopharyngeal carcinoma with a novel adenovirus-based adoptive immunotherapy. *Cancer research* 72:1116-1125.

Smith, C., N. Wakisaka, T. Crough, J. Peet, T. Yoshizaki, L. Beagley, and R. Khanna. 2009. Discerning regulation of cis- and trans-presentation of CD8+ T-cell epitopes by EBV-encoded oncogene LMP-1 through self-aggregation. *Blood* 113:6148-6152.

Smith, C.A., C.Y. Ng, H.E. Heslop, M.S. Holladay, S. Richardson, E.V. Turner, S.K. Loftin, C. Li, M.K. Brenner, and C.M. Rooney. 1995. Production of genetically modified Epstein-Barr virus-specific cytotoxic T cells for adoptive transfer to patients at high risk of EBV-associated lymphoproliferative disease. *Journal of hematotherapy* 4:73-79.

Smith, C.M., M.B. Gill, J.S. May, and P.G. Stevenson. 2007. Murine gammaherpesvirus-68 inhibits antigen presentation by dendritic cells. *PloS one* 2:e1048.

Smith, C.M., G.T. Rosa, J.S. May, N.J. Bennett, A.M. Mount, G.T. Belz, and P.G. Stevenson. 2006. CD4+ T cells specific for a model latency-associated antigen fail to control a gammaherpesvirus in vivo. *European journal of immunology* 36:3186-3197.

Soares, M.V., F.J. Plunkett, C.S. Verbeke, J.E. Cook, J.M. Faint, L.L. Belaramani, J.M. Fletcher, N. Hammerschmitt, M. Rustin, W. Bergler, P.C. Beverley, M. Salmon, and A.N. Akbar. 2004. Integration of apoptosis and telomere erosion in virus-specific CD8+ T cells from blood and tonsils during primary infection. *Blood* 103:162-167.

Sokal, E.M., K. Hoppenbrouwers, C. Vandermeulen, M. Moutschen, P. Leonard, A. Moreels, M. Haumont, A. Bollen, F. Smets, and M. Denis. 2007. Recombinant gp350 vaccine for infectious mononucleosis: a phase 2, randomized, double-blind, placebo-controlled trial to evaluate the safety, immunogenicity, and efficacy of an Epstein-Barr virus vaccine in healthy young adults. *The Journal of infectious diseases* 196:1749-1753.

Song, M.J., S. Hwang, W.H. Wong, T.T. Wu, S. Lee, H.I. Liao, and R. Sun. 2005. Identification of viral genes essential for replication of murine gamma-herpesvirus 68 using signature-tagged mutagenesis. *Proceedings of the National Academy of Sciences of the United States of America* 102:3805-3810.

Soulier, J., L. Grollet, E. Oksenhendler, P. Cacoub, D. Cazals-Hatem, P. Babinet, M.F. d'Agay, J.P. Clauvel, M. Raphael, L. Degos, and et al. 1995. Kaposi's sarcoma-associated herpesvirus-like DNA sequences in multicentric Castleman's disease. *Blood* 86:1276-1280.

Souza, T.A., B.D. Stollar, J.L. Sullivan, K. Luzuriaga, and D.A. Thorley-Lawson. 2005. Peripheral B cells latently infected with Epstein-Barr virus display molecular hallmarks of classical antigen-selected memory B cells. *Proceedings of the National Academy of Sciences of the United States of America* 102:18093-18098.

Souza, T.A., B.D. Stollar, J.L. Sullivan, K. Luzuriaga, and D.A. Thorley-Lawson. 2007. Influence of EBV on the peripheral blood memory B cell compartment. *Journal of immunology* 179:3153-3160.

Sparks-Thissen, R.L., D.C. Braaten, K. Hildner, T.L. Murphy, K.M. Murphy, and H.W.t. Virgin. 2005. CD4 T cell control of acute and latent murine gammaherpesvirus infection requires IFNgamma. *Virology* 338:201-208.

Stebbing, J., D. Bourboulia, M. Johnson, S. Henderson, I. Williams, N. Wilder, M. Tyrer, M. Youle, N. Imami, T. Kobu, W. Kuon, J. Sieper, F. Gotch, and C. Boshoff. 2003. Kaposi's sarcoma-associated

herpesvirus cytotoxic T lymphocytes recognize and target Darwinian positively selected autologous K1 epitopes. *Journal of virology* 77:4306-4314.

Steven, N.M., A.M. Leese, N.E. Annels, S.P. Lee, and A.B. Rickinson. 1996. Epitope focusing in the primary cytotoxic T cell response to Epstein-Barr virus and its relationship to T cell memory. *The Journal of experimental medicine* 184:1801-1813.

Stevenson, P.G., G.T. Belz, J.D. Altman, and P.C. Doherty. 1999a. Changing patterns of dominance in the CD8+ T cell response during acute and persistent murine gamma-herpesvirus infection. *European journal of immunology* 29:1059-1067.

Stevenson, P.G., G.T. Belz, M.R. Castrucci, J.D. Altman, and P.C. Doherty. 1999b. A gamma-herpesvirus sneaks through a CD8(+) T cell response primed to a lytic-phase epitope. *Proceedings of the National Academy of Sciences of the United States of America* 96:9281-9286.

Stevenson, P.G., R.D. Cardin, J.P. Christensen, and P.C. Doherty. 1999c. Immunological control of a murine gammaherpesvirus independent of CD8+ T cells. *The Journal of general virology* 80 (Pt 2):477-483.

Stevenson, P.G., and P.C. Doherty. 1998. Kinetic analysis of the specific host response to a murine gammaherpesvirus. *Journal of virology* 72:943-949.

Stevenson, P.G., and P.C. Doherty. 1999. Non-antigen-specific B-cell activation following murine gammaherpesvirus infection is CD4 independent in vitro but CD4 dependent in vivo. *Journal of virology* 73:1075-1079.

Stevenson, P.G., and S. Efstathiou. 2005. Immune mechanisms in murine gammaherpesvirus-68 infection. *Viral immunology* 18:445-456.

Stevenson, P.G., S. Efstathiou, P.C. Doherty, and P.J. Lehner. 2000. Inhibition of MHC class I-restricted antigen presentation by gamma 2-herpesviruses. *Proceedings of the National Academy of Sciences of the United States of America* 97:8455-8460.

Stevenson, P.G., J.S. May, X.G. Smith, S. Marques, H. Adler, U.H. Koszinowski, J.P. Simas, and S. Efstathiou. 2002. K3-mediated evasion of CD8(+) T cells aids amplification of a latent gamma-herpesvirus. *Nature immunology* 3:733-740.

Stevenson, P.G., J.P. Simas, and S. Efstathiou. 2009. Immune control of mammalian gamma-herpesviruses: lessons from murid herpesvirus-4. *The Journal of general virology* 90:2317-2330.

Stewart, J.P., N. Micali, E.J. Usherwood, L. Bonina, and A.A. Nash. 1999. Murine gamma-herpesvirus 68 glycoprotein 150 protects against virus-induced mononucleosis: a model system for gamma-herpesvirus vaccination. *Vaccine* 17:152-157.

Stewart, J.P., E.J. Usherwood, A. Ross, H. Dyson, and T. Nash. 1998. Lung epithelial cells are a major site of murine gammaherpesvirus persistence. *The Journal of experimental medicine* 187:1941-1951.

Strowig, T., C. Gurer, A. Ploss, Y.F. Liu, F. Arrey, J. Sashihara, G. Koo, C.M. Rice, J.W. Young, A. Chadburn, J.I. Cohen, and C. Munz. 2009. Priming of protective T cell responses against virus-induced tumors in mice with human immune system components. *The Journal of experimental medicine* 206:1423-1434.

Stuller, K.A., S.S. Cush, and E. Flano. 2010. Persistent gamma-herpesvirus infection induces a CD4 T cell response containing functionally distinct effector populations. *Journal of immunology* 184:3850-3856.

Stuller, K.A., and E. Flano. 2009. CD4 T cells mediate killing during persistent gammaherpesvirus 68 infection. *Journal of virology* 83:4700-4703.

Sunil-Chandra, N.P., J. Arno, J. Fazakerley, and A.A. Nash. 1994. Lymphoproliferative disease in mice infected with murine gammaherpesvirus 68. *The American journal of pathology* 145:818-826.

Sunil-Chandra, N.P., S. Efstathiou, J. Arno, and A.A. Nash. 1992a. Virological and pathological features of mice infected with murine gamma-herpesvirus 68. *The Journal of general virology* 73 (Pt 9):2347-2356.

Sunil-Chandra, N.P., S. Efstathiou, and A.A. Nash. 1992b. Murine gammaherpesvirus 68 establishes a latent infection in mouse B lymphocytes in vivo. *The Journal of general virology* 73 (Pt 12):3275-3279.

Sunil-Chandra, N.P., S. Efstathiou, and A.A. Nash. 1993. Interactions of murine gammaherpesvirus 68 with B and T cell lines. *Virology* 193:825-833.

Suthaus, J., C. Stuhlmann-Laeisz, V.S. Tompkins, T.R. Rosean, W. Klapper, G. Tosato, S. Janz, J. Scheller, and S. Rose-John. 2012. HHV-8-encoded viral IL-6 collaborates with mouse IL-6 in the development of multicentric Castleman disease in mice. *Blood* 119:5173-5181.

Sutkowski, N., B. Conrad, D.A. Thorley-Lawson, and B.T. Huber. 2001. Epstein-Barr virus transactivates the human endogenous retrovirus HERV-K18 that encodes a superantigen. *Immunity* 15:579-589.

Svobodova, J., D. Blaskovic, and J. Mistrikova. 1982. Growth characteristics of herpesviruses isolated from free living small rodents. *Acta virologica* 26:256-263.

Swaminathan, S. 2008. Noncoding RNAs produced by oncogenic human herpesviruses. *Journal of cellular physiology* 216:321-326.

Tamburro, K.M., D. Yang, J. Poisson, Y. Fedoriw, D. Roy, A. Lucas, S.H. Sin, N. Malouf, V. Moylan, B. Damania, S. Moll, C. van der Horst, and D.P. Dittmer. 2012. Vironome of Kaposi sarcoma associated herpesvirus-inflammatory cytokine syndrome in an AIDS patient reveals co-infection of human herpesvirus 8 and human herpesvirus 6A. *Virology* 433:220-225.

Tan, L.C., N. Gudgeon, N.E. Annels, P. Hansasuta, C.A. O'Callaghan, S. Rowland-Jones, A.J. McMichael, A.B. Rickinson, and M.F. Callan. 1999. A re-evaluation of the frequency of CD8+ T cells specific for EBV in healthy virus carriers. *Journal of immunology* 162:1827-1835.

Tanner, J., J. Weis, D. Fearon, Y. Whang, and E. Kieff. 1987. Epstein-Barr virus gp350/220 binding to the B lymphocyte C3d receptor mediates adsorption, capping, and endocytosis. *Cell* 50:203-213.

Tarakanova, V.L., F. Suarez, S.A. Tibbetts, M.A. Jacoby, K.E. Weck, J.L. Hess, S.H. Speck, and H.W.t. Virgin. 2005. Murine gammaherpesvirus 68 infection is associated with lymphoproliferative disease and lymphoma in BALB beta2 microglobulin-deficient mice. *Journal of virology* 79:14668-14679.

Taylor, G.S., and D.J. Blackbourn. 2011. Infectious agents in human cancers: lessons in immunity and immunomodulation from gammaherpesviruses EBV and KSHV. *Cancer letters* 305:263-278.

Taylor, G.S., H.M. Long, T.A. Haigh, M. Larsen, J. Brooks, and A.B. Rickinson. 2006. A role for intercellular antigen transfer in the recognition of EBV-transformed B cell lines by EBV nuclear antigen-specific CD4+ T cells. *Journal of immunology* 177:3746-3756.

Tellam, J., C. Smith, M. Rist, N. Webb, L. Cooper, T. Vuocolo, G. Connolly, D.C. Tscharke, M.P. Devoy, and R. Khanna. 2008. Regulation of protein translation through mRNA structure influences MHC class I loading and T cell recognition. *Proceedings of the National Academy of Sciences of the United States of America* 105:9319-9324.

Tellam, J.T., L. Lekieffre, J. Zhong, D.J. Lynn, and R. Khanna. 2012. Messenger RNA sequence rather than protein sequence determines the level of self-synthesis and antigen presentation of the EBV-encoded antigen, EBNA1. *PLoS pathogens* 8:e1003112.

Thorley-Lawson, D.A. 2001. Epstein-Barr virus: exploiting the immune system. *Nature reviews. Immunology* 1:75-82.

Thorley-Lawson, D.A. 2005. EBV the prototypical human tumor virus--just how bad is it? *The Journal of allergy and clinical immunology* 116:251-261; quiz 262.

Thorley-Lawson, D.A., K.A. Duca, and M. Shapiro. 2008. Epstein-Barr virus: a paradigm for persistent infection - for real and in virtual reality. *Trends in immunology* 29:195-201.

Thorley-Lawson, D.A., and K. Geilinger. 1980. Monoclonal antibodies against the major glycoprotein (gp350/220) of Epstein-Barr virus neutralize infectivity. *Proceedings of the National Academy of Sciences of the United States of America* 77:5307-5311.

Thorley-Lawson, D.A., and A. Gross. 2004. Persistence of the Epstein-Barr virus and the origins of associated lymphomas. *The New England journal of medicine* 350:1328-1337.

Thorley-Lawson, D.A., J.B. Hawkins, S.I. Tracy, and M. Shapiro. 2013. The pathogenesis of Epstein-Barr virus persistent infection. *Current opinion in virology* 3:227-232.

Thorley-Lawson, D.A., and K.P. Mann. 1985. Early events in Epstein-Barr virus infection provide a model for B cell activation. *The Journal of experimental medicine* 162:45-59.

Thorley-Lawson, D.A., and C.A. Poodry. 1982. Identification and isolation of the main component (gp350-gp220) of Epstein-Barr virus responsible for generating neutralizing antibodies in vivo. *Journal of virology* 43:730-736.

Tibbetts, S.A., J.S. McClellan, S. Gangappa, S.H. Speck, and H.W.t. Virgin. 2003. Effective vaccination against long-term gammaherpesvirus latency. *Journal of virology* 77:2522-2529.

Tibbetts, S.A., L.F. van Dyk, S.H. Speck, and H.W.t. Virgin. 2002. Immune control of the number and reactivation phenotype of cells latently infected with a gammaherpesvirus. *Journal of virology* 76:7125-7132.

Toebes, M., M. Coccoris, A. Bins, B. Rodenko, R. Gomez, N.J. Nieuwkoop, W. van de Kasteele, G.F. Rimmelzwaan, J.B. Haanen, H. Ovaa, and T.N. Schumacher. 2006. Design and use of conditional MHC class I ligands. *Nature medicine* 12:246-251.

Tomescu, C., W.K. Law, and D.H. Kedes. 2003. Surface downregulation of major histocompatibility complex class I, PE-CAM, and ICAM-1 following de novo infection of endothelial cells with Kaposi's sarcoma-associated herpesvirus. *Journal of virology* 77:9669-9684.

Townsend, A., C. Ohlen, J. Bastin, H.G. Ljunggren, L. Foster, and K. Karre. 1989. Association of class I major histocompatibility heavy and light chains induced by viral peptides. *Nature* 340:443-448.

Tracy, S.I., K. Kakalacheva, J.D. Lunemann, K. Luzuriaga, J. Middeldorp, and D.A. Thorley-Lawson. 2012. Persistence of Epstein-Barr virus in self-reactive memory B cells. *Journal of virology* 86:12330-12340.

Tripp, R.A., A.M. Hamilton-Easton, R.D. Cardin, P. Nguyen, F.G. Behm, D.L. Woodland, P.C. Doherty, and M.A. Blackman. 1997. Pathogenesis of an infectious mononucleosis-like disease induced by a murine gamma-herpesvirus: role for a viral superantigen? *The Journal of experimental medicine* 185:1641-1650.

Tsai, C.Y., Z. Hu, W. Zhang, and E.J. Usherwood. 2011. Strain-dependent requirement for IFN-gamma for respiratory control and immunotherapy in murine gammaherpesvirus infection. *Viral immunology* 24:273-280.

Uhlin, M., M. Okas, J. Gertow, M. Uzunel, T.B. Brismar, and J. Mattsson. 2010. A novel haplo-identical adoptive CTL therapy as a treatment for EBV-associated lymphoma after stem cell transplantation. *Cancer immunology, immunotherapy : CII* 59:473-477.

Uldrick, T.S., V. Wang, D. O'Mahony, K. Aleman, K.M. Wyvill, V. Marshall, S.M. Steinberg, S. Pittaluga, I. Maric, D. Whitby, G. Tosato, R.F. Little, and R. Yarchoan. 2010. An interleukin-6-related systemic inflammatory syndrome in patients co-infected with Kaposi sarcoma-associated herpesvirus and HIV but without Multicentric Castleman disease. *Clinical infectious diseases : an official publication of the Infectious Diseases Society of America* 51:350-358.

Uldrick, T.S., and D. Whitby. 2011. Update on KSHV epidemiology, Kaposi Sarcoma pathogenesis, and treatment of Kaposi Sarcoma. *Cancer letters* 305:150-162.

Usherwood, E.J., A.J. Ross, D.J. Allen, and A.A. Nash. 1996. Murine gammaherpesvirus-induced splenomegaly: a critical role for CD4 T cells. *The Journal of general virology* 77 (Pt 4):627-630.

Usherwood, E.J., D.J. Roy, K. Ward, S.L. Surman, B.M. Dutia, M.A. Blackman, J.P. Stewart, and D.L. Woodland. 2000. Control of gammaherpesvirus latency by latent antigen-specific CD8(+) T cells. *The Journal of experimental medicine* 192:943-952.

Usherwood, E.J., K.A. Ward, M.A. Blackman, J.P. Stewart, and D.L. Woodland. 2001. Latent antigen vaccination in a model gammaherpesvirus infection. *Journal of virology* 75:8283-8288.

van Berkel, V., J. Barrett, H.L. Tiffany, D.H. Fremont, P.M. Murphy, G. McFadden, S.H. Speck, and H.I. Virgin. 2000. Identification of a gammaherpesvirus selective chemokine binding protein that inhibits chemokine action. *Journal of virology* 74:6741-6747.

van Berkel, V., K. Preiter, H.W.t. Virgin, and S.H. Speck. 1999. Identification and initial characterization of the murine gammaherpesvirus 68 gene M3, encoding an abundantly secreted protein. *Journal of virology* 73:4524-4529.

Vera, J.F., V. Hoyos, B. Savoldo, C. Quintarelli, G.M. Giordano Attianese, A.M. Leen, H. Liu, A.E. Foster, H.E. Heslop, C.M. Rooney, M.K. Brenner, and G. Dotti. 2009. Genetic manipulation of tumor-specific cytotoxic T lymphocytes to restore responsiveness to IL-7. *Molecular therapy : the journal of the American Society of Gene Therapy* 17:880-888.

Vereide, D.T., E. Seto, Y.F. Chiu, M. Hayes, T. Tagawa, A. Grundhoff, W. Hammerschmidt, and B. Sugden. 2014. Epstein-Barr virus maintains lymphomas via its miRNAs. *Oncogene* 33:1258-1264.

Victora, G.D., D. Dominguez-Sola, A.B. Holmes, S. Deroubaix, R. Dalla-Favera, and M.C. Nussenzweig. 2012. Identification of human germinal center light and dark zone cells and their relationship to human B-cell lymphomas. *Blood* 120:2240-2248.

Vigano, S., D.T. Utzschneider, M. Perreau, G. Pantaleo, D. Zehn, and A. Harari. 2012. Functional avidity: a measure to predict the efficacy of effector T cells? *Clinical & developmental immunology* 2012:153863.

Vinuesa, C.G., S.G. Tangye, B. Moser, and C.R. Mackay. 2005. Follicular B helper T cells in antibody responses and autoimmunity. *Nature reviews. Immunology* 5:853-865.

Virgin, H.W.t., P. Latreille, P. Wamsley, K. Hallsworth, K.E. Weck, A.J. Dal Canto, and S.H. Speck. 1997. Complete sequence and genomic analysis of murine gammaherpesvirus 68. *Journal of virology* 71:5894-5904.

Virgin, H.W.t., R.M. Presti, X.Y. Li, C. Liu, and S.H. Speck. 1999. Three distinct regions of the murine gammaherpesvirus 68 genome are transcriptionally active in latently infected mice. *Journal of virology* 73:2321-2332.

von Essen, M.R., M. Kongsbak, and C. Geisler. 2012. Mechanisms behind functional avidity maturation in T cells. *Clinical & developmental immunology* 2012:163453.

Vrazo, A.C., M. Chauchard, N. Raab-Traub, and R. Longnecker. 2012. Epstein-Barr virus LMP2A reduces hyperactivation induced by LMP1 to restore normal B cell phenotype in transgenic mice. *PLoS pathogens* 8:e1002662.

Wang, X., X. Liu, Y. Jia, Y. Chao, X. Xing, Y. Wang, and B. Luo. 2010. Widespread sequence variation in the Epstein-Barr virus latent membrane protein 2A gene among northern Chinese isolates. *The Journal of general virology* 91:2564-2573.

Wen, K.W., and B. Damania. 2010. Kaposi sarcoma-associated herpesvirus (KSHV): molecular biology and oncogenesis. *Cancer letters* 289:140-150.

Willer, D.O., and S.H. Speck. 2003. Long-term latent murine Gammaherpesvirus 68 infection is preferentially found within the surface immunoglobulin D-negative subset of splenic B cells in vivo. *Journal of virology* 77:8310-8321.

Woodberry, T., T.J. Suscovich, L.M. Henry, J.K. Davis, N. Frahm, B.D. Walker, D.T. Scadden, F. Wang, and C. Brander. 2005a. Differential targeting and shifts in the immunodominance of Epstein-Barr virus--specific CD8 and CD4 T cell responses during acute and persistent infection. *The Journal of infectious diseases* 192:1513-1524.

Woodberry, T., T.J. Suscovich, L.M. Henry, J.N. Martin, S. Dollard, P.G. O'Connor, J.K. Davis, D. Osmond, T.H. Lee, D.H. Kedes, A. Khatri, J. Lee, B.D. Walker, D.T. Scadden, and C. Brander. 2005b. Impact of Kaposi sarcoma-associated herpesvirus (KSHV) burden and HIV coinfection on the detection of T cell responses to KSHV ORF73 and ORF65 proteins. *The Journal of infectious diseases* 192:622-629.

Woodland, D.L., E. Flano, E.J. Usherwood, L. Liu, I.J. Kim, S.M. Husain, J.T. Sample, and M.A. Blackman. 2001a. Antigen expression during murine gamma-herpesvirus infection. *Immunobiology* 204:649-658.

Woodland, D.L., E.J. Usherwood, L. Liu, E. Flano, I.J. Kim, and M.A. Blackman. 2001b. Vaccination against murine gamma-herpesvirus infection. *Viral immunology* 14:217-226.

Wu, T.T., M.A. Blackman, and R. Sun. 2010. Prospects of a novel vaccination strategy for human gamma-herpesviruses. *Immunologic research* 48:122-146.

Wu, T.T., J. Qian, J. Ang, and R. Sun. 2012. Vaccine prospect of Kaposi sarcoma-associated herpesvirus. *Current opinion in virology* 2:482-488.

Wycisk, A.I., J. Lin, S. Loch, K. Hobohm, J. Funke, R. Wieneke, J. Koch, W.R. Skach, P.U. Mayerhofer, and R. Tampe. 2011. Epstein-Barr viral BNLF2a protein hijacks the tail-anchored protein insertion machinery to block antigen processing by the transport complex TAP. *The Journal of biological chemistry* 286:41402-41412.

Xiao, Z., M.F. Mescher, and S.C. Jameson. 2007. Detuning CD8 T cells: down-regulation of CD8 expression, tetramer binding, and response during CTL activation. *The Journal of experimental medicine* 204:2667-2677.

Yang, J., V.M. Lemas, I.W. Flinn, C. Krone, and R.F. Ambinder. 2000. Application of the ELISPOT assay to the characterization of CD8(+) responses to Epstein-Barr virus antigens. *Blood* 95:241-248.

Zaldumbide, A., M. Ossevoort, E.J. Wiertz, and R.C. Hoeben. 2007. In cis inhibition of antigen processing by the latency-associated nuclear antigen I of Kaposi sarcoma herpes virus. *Molecular immunology* 44:1352-1360.

Zehn, D., S.Y. Lee, and M.J. Bevan. 2009. Complete but curtailed T-cell response to very low-affinity antigen. *Nature* 458:211-214.

Zeidler, R., G. Eissner, P. Meissner, S. Uebel, R. Tampe, S. Lazis, and W. Hammerschmidt. 1997. Downregulation of TAP1 in B lymphocytes by cellular and Epstein-Barr virus-encoded interleukin-10. *Blood* 90:2390-2397.

Zhu, J.Y., M. Strehle, A. Frohn, E. Kremmer, K.P. Hofig, G. Meister, and H. Adler. 2010. Identification and analysis of expression of novel microRNAs of murine gammaherpesvirus 68. *Journal of virology* 84:10266-10275.

Zhu, Y., I. Haecker, Y. Yang, S.J. Gao, and R. Renne. 2013. gamma-Herpesvirus-encoded miRNAs and their roles in viral biology and pathogenesis. *Current opinion in virology* 3:266-275.

Zong, J.C., D.M. Ciufo, D.J. Alcendor, X. Wan, J. Nicholas, P.J. Browning, P.L. Rady, S.K. Tyring, J.M. Orenstein, C.S. Rabkin, I.J. Su, K.F. Powell, M. Croxson, K.E. Foreman, B.J. Nickoloff, S. Alkan, and G.S. Hayward. 1999. High-level variability in the ORF-K1 membrane protein gene at the left end of the Kaposi's sarcoma-associated herpesvirus genome defines four major virus subtypes and multiple variants or clades in different human populations. *Journal of virology* 73:4156-4170.

Zuo, J., A. Currin, B.D. Griffin, C. Shannon-Lowe, W.A. Thomas, M.E. Ressing, E.J. Wiertz, and M. Rowe. 2009. The Epstein-Barr virus G-protein-coupled receptor contributes to immune evasion by targeting MHC class I molecules for degradation. *PLoS pathogens* 5:e1000255.

Zuo, J., L.L. Quinn, J. Tamblyn, W.A. Thomas, R. Feederle, H.J. Delecluse, A.D. Hislop, and M. Rowe. 2011. The Epstein-Barr virus-encoded BILF1 protein modulates immune recognition of endogenously processed antigen by targeting major histocompatibility complex class I molecules trafficking on both the exocytic and endocytic pathways. *Journal of virology* 85:1604-1614.

Zuo, J., W. Thomas, D. van Leeuwen, J.M. Middeldorp, E.J. Wiertz, M.E. Ressing, and M. Rowe. 2008. The DNase of gammaherpesviruses impairs recognition by virus-specific CD8+ T cells through an additional host shutoff function. *Journal of virology* 82:2385-2393.

SUPPLEMENTARY INFORMATION

A

MuHV-4 Recombinants	Epitope Sequence
vORF8	M2 – KNYIFEEKL
vA4	M2 – KNYAFEEKL
vA6	M2 – KNYIFAEKL
vD6	M2 – KNYIFDEKL
vA9	M2 – KNYIFEEKA

B

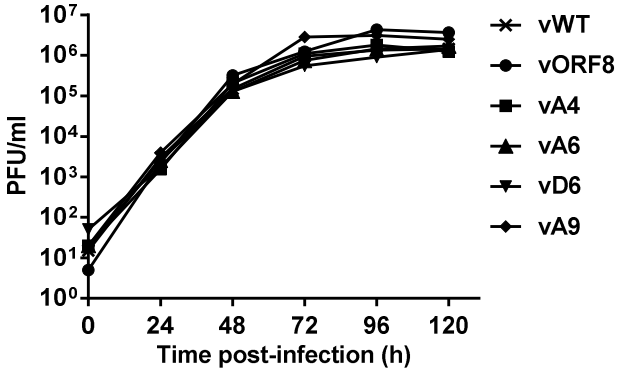

C

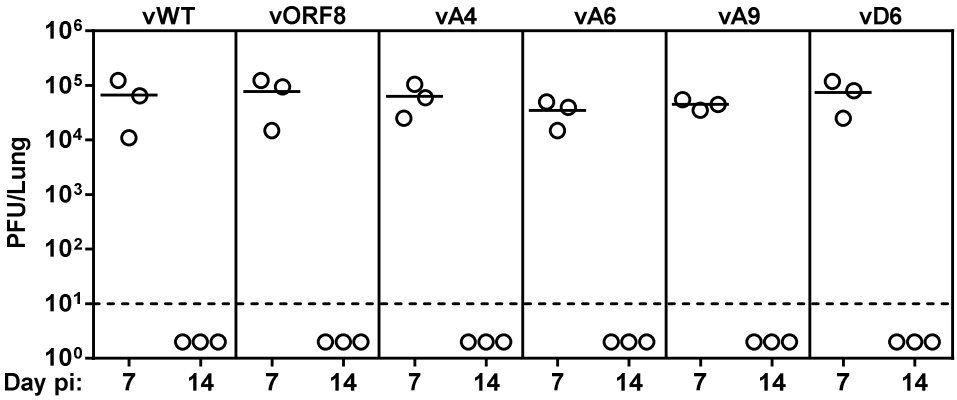

D

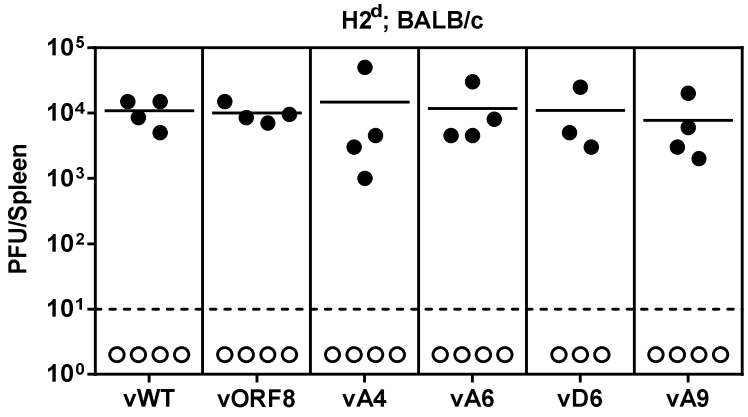

E

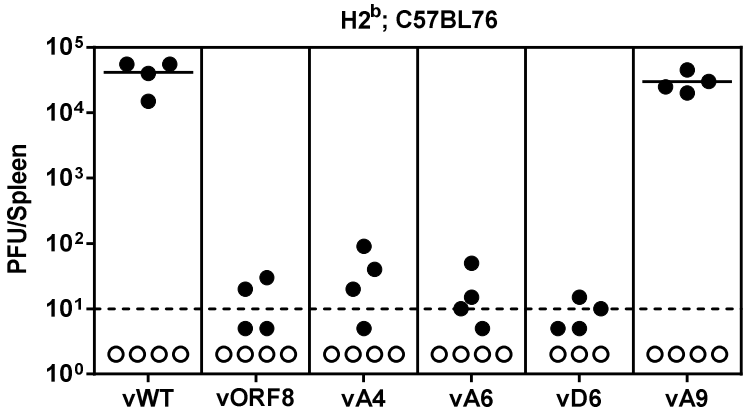

Supplementary Figure 1. Expression of the endogenous MuHV-4 ORF8 epitope or APL derivates during latency impairs virus-driven lymphoproliferation. (A) MuHV-4 recombinant viruses were generated to express from the M2 C-terminus the $H2K^b$-restricted epitope comprising amino acid residues 604-612 of MuHV-4 ORF8 glycoprotein B ($ORF8_{604-612}/K^b$) or APL derivates. Amino acid sequences introduced in each recombinant virus are presented. Blue residues denote amino acid alterations introduced into native ORF8 epitope. Amino acid substitutions in vA4, vA6 and vD6 comprise residues important for binding to the TCR, while vA9 contains a replacement in an anchor residue, as determined by ability to induce IFNγ production by activated ORF8 transnuclear $CD8^+$ T cells and $H2K^b$ stabilization on RMA-S, respectively (Sehrawat et al., 2012). MuHV-4 recombinant viruses were engineered by Diana Fontinha under the supervision of Dr Sofia marques in our laboratory. (B) Multi-step growth curves of recombinant viruses in BHK-21 cells infected at low multiplicity (0.01 PFU per cell). At the indicated times post-infection, samples were harvested, freeze-thawed and virus titres were determined by plaque assay on monolayers of BHK-21 cells. *In vitro* lytic replication kinetics of the recombinant viruses were not significantly different from vWT ($p>0.05$, by ordinary one-way ANOVA followed by Dunnett's multiple comparisons test). (C) Virus replication in lungs of intranasally infected (10^4 PFU) C57BL/6 ($H2^b$) mice was quantified by plaque assay at the indicated days p.i.. No MuHV-4 recombinant showed a deficit relative to vWT ($p>0.05$, using ordinary one-way ANOVA followed by Dunnett's multiple comparisons test). (D) Latent infection in spleens of intranasally infected (10^4 PFU) BALB/c ($H2^d$) mice was determined by *ex vivo* reactivation assay (closed symbols) at 14 days p.i.. Pre-formed infectious viruses were analysed by plaque assay (open symbols). Latent loads of MuHV-4 recombinants expressing the ORF8 epitope or APLs were not significantly different to vWT ($p>0.05$, by ordinary one-way ANOVA followed by Dunnett's multiple comparisons test). (E) Latent load in spleens of C57BL/6 ($H2^b$) mice at day 14 p.i. was quantified by *ex vivo* reactivation assay (closed symbols) and pre-form infectious virus was measured by plaque assay (open symbols). vORF8, vA4, vA6 and vD6 latent loads were significantly below those of vWT ($p=0.0047$, for each comparison using two-tailed unpaired t-test). vA9 latent loads were not significantly different from vWT ($p=0.3407$). In panels C, D and E each point represents the titre of an individual mouse, horizontal bars show arithmetic means and the dashed horizontal line indicates the limit of detection of the assay.

APPENDIX 1

OPEN ACCESS Freely available online

PLOS | PATHOGENS

Defining Immune Engagement Thresholds for *In Vivo* Control of Virus-Driven Lymphoproliferation

Cristina Godinho-Silva[1☯], Sofia Marques[1☯], Diana Fontinha[1], Henrique Veiga-Fernandes[1], Philip G. Stevenson[2], J. Pedro Simas[1*]

1 Instituto de Medicina Molecular, Faculdade de Medicina, Universidade de Lisboa, Lisboa, Portugal, **2** Sir Albert Sakzewski Virus Research Center and Queensland and Children's Medical Research Institute, University of Queensland, Brisbane, Queensland, Australia

Abstract

Persistent infections are subject to constant surveillance by $CD8^+$ cytotoxic T cells (CTL). Their control should therefore depend on MHC class I-restricted epitope presentation. Many epitopes are described for γ-herpesviruses and form a basis for prospective immunotherapies and vaccines. However the quantitative requirements of *in vivo* immune control for epitope presentation and recognition remain poorly defined. We used Murid Herpesvirus-4 (MuHV-4) to determine for a latently expressed viral epitope how MHC class-I binding and CTL functional avidity impact on host colonization. Tracking MuHV-4 recombinants that differed only in epitope presentation, we found little latitude for sub-optimal MHC class I binding before immune control failed. By contrast, control remained effective across a wide range of T cell functional avidities. Thus, we could define critical engagement thresholds for the *in vivo* immune control of virus-driven B cell proliferation.

Citation: Godinho-Silva C, Marques S, Fontinha D, Veiga-Fernandes H, Stevenson PG, et al. (2014) Defining Immune Engagement Thresholds for *In Vivo* Control of Virus-Driven Lymphoproliferation. PLOS Pathog 10(6): e1004220. doi:10.1371/journal.ppat.1004220

Editor: Edward Usherwood, Dartmouth Medical School, United States of America

Received March 26, 2014; **Accepted** May 13, 2014; **Published** June 26, 2014

Data Availability: The authors confirm that all data underlying the findings are fully available without restriction. All data included in manuscript and supporting file.

Funding: JPS was funded by Fundação para a Ciência e Tecnologia (PTDC/SAU-MII/099314/2008); HMSP-ICT/0021/2010) Portugal. CGS, SM, and DF were supported by scholarships from Fundação para a Ciência e Tecnologia, Portugal. PGS is an ARC Future Fellow. The funders had no role in study design, data collection and analysis, decision to publish, or preparation of the manuscript.

Competing Interests: The authors have declared that no competing interests exist.

* Email: psimas@fm.ul.pt

☯ These authors contributed equally to this study.

Introduction

The gamma-herpesviruses (γHVs) infect >90% of humans and cause diseases including nasopharyngeal carcinoma, African Burkitt's lymphoma and Kaposi's Sarcoma. Their colonization of circulating memory B cells is crucial to persistence and hence to disease ontogeny. Viral latency gene expression in B cells provides an immune target [1] that has been exploited to prevent lymphoproliferative disease in acutely immunodeficient patients by T cell transfer [2]. However, extending this approach to established cancers and developing related vaccines have proved difficult. A significant problem is that the narrow species tropisms of human γHVs severely restrict *in vivo* analysis, and hence an understanding of how empirical therapies such as adoptive T cell transfer work.

Immune recognition can be assayed *in vitro*; but while Epstein-Barr virus (EBV) latency gene products drive autonomous B cell proliferation *in vitro*, most *in vivo* infected cells are resting memory B cells that have passed though lymphoid germinal centers (GCs) [3]. This makes difficult *in vitro* analysis of *in vivo* immune control. One way to make progress is to study related viruses that are experimentally more accessible. Probably the best characterized is Murid Herpesvirus-4 (MuHV-4, archetypal strain MHV-68) [4–6]. MuHV-4 is more closely related to the Kaposi's Sarcoma-associated Herpesvirus (KSHV) than to EBV [7]. However it shares many features of host colonization with EBV, for example it exploits lymphoid GCs to establish persistence in circulating memory B cells [8–10]. Therefore it can be used to reveal fundamental mechanisms of γHV/host interaction.

MuHV-4 studies have shown that γHV-driven lymphoproliferation occurs in complex lesions incorporating T cell evasion and infected cells with distinct patterns of viral gene expression [10]. In addition to cis-acting T cell evasion during episome maintenance [11,12], EBV inhibits the transporter associated with antigen processing (TAP) via BNLF2a [13–15] and MHC class I export to the cell surface via BILF1 [16,17]; KSHV degrades MHC class I and other immune receptors via K3 and K5 [18]; and MuHV-4 degrades MHC class I and TAP via MK3 [19–21]. Disrupting MK3 impairs virus-driven lymphoproliferation [22].

The γHVs also evade immune recognition during latency by expressing few CTL targets. However a gene that modulates signaling through the B cell receptor - M2 in MuHV-4 [23–26], LMP-2A in EBV [27] and K1 in KSHV [28] - is expressed more widely than growth program genes [3], and shows protein sequence diversity [29–33] consistent with immune selection. More directly, the presence of an $H2K^d$ binding epitope in M2 [34,35] significantly reduces long-term MuHV-4 latent loads in BALB/c mice [29]. Therefore despite viral evasion, CTL help to regulate long-term infection [36,37], and CTL recognition of M2/K1/LMP-2A, which in EBV may extend also to EBNA3A/B/C

Author Summary

Chronic viral infections cause huge morbidity and mortality worldwide. γ-herpesviruses provide an example relevant to all human demographics, causing, *inter alia*, Hodgkin's disease, Burkitt's lymphoma, Kaposi's Sarcoma, and nasopharyngeal carcinoma. The proliferation of latently infected B cells and their control by $CD8^+$ T cells are central to pathogenesis. Although many viral T cell targets have been identified *in vitro*, the functional impact of their engagement *in vivo* remains ill-defined. With the well-established Murid Herpesvirus-4 infection model, we used a range of recombinant viruses to define functional thresholds for the engagement of a latently expressed viral epitope. These data advance significantly our understanding of how the immune system must function to control γ-herpesvirus infection, with implications for vaccination and anti-cancer immunotherapy.

[38,39], provides a potential point of attack. LMP-2A is also a candidate vaccine target for nasopharyngeal carcinoma [40]. Thus, how M2/K1/LMP-2A recognition works *in vivo* is important to understand.

CTL effector capacity broadly correlates with functional avidity, as determined by the capacity of T cell receptor (TcR) engagement to trigger CTL proliferation, cytokine production and target cell lysis at limiting antigen dose [41]. Therefore with limited γHV protein expression during latency, peptide affinity for MHC class I and TcR functional avidity are likely to be crucial for immune control. The diversity of LMP-2A, K1 and M2 prompted us to analyze *in vivo* the consequences of varying MHC class I binding and TcR functional avidity for a single epitope derived from M2. These parameters affected dramatically the control of virus-driven lymphoproliferation, even in the context of immune evasion. The capacity of MuHV-4 to correlate biochemical interactions with *in vivo* immune function allowed us to establish quantitative guidelines for infection control.

Results

Characterization of altered peptide ligands (APLs) by MHC class I binding and TcR functional avidity

To understand the CTL recognition requirements for γHV infection control, we expressed from MuHV-4 a well-characterized, $H2K^b$-restricted epitope comprising amino acid residues 257–264 of ovalbumin (OVA), or APL derivatives (Figure 1A). OVA binds to $H2K^b$ with high affinity ($K_D = 4.1$ nM) [42]. We compared OVA and APL binding by $H2K^b$ stabilization on TAP-deficient RMA/S cells (Figure 1B) [43]. The OVA concentration giving 50% maximal stabilization (EC_{50}) was 40 nM, in close agreement with published data [44]. APLs Q4, V4, G4 and R4 were similar to OVA (EC_{50} within 2-fold), consistent with residue 4 being solvent-exposed in the $H2K^b$-peptide complex [45]. E1 required 6-fold more peptide for equivalent $H2K^b$ stabilization, consistent with this residue being only partly exposed; A8, which has a mutated anchor residue, required 10-fold more peptide again; and the control peptide A5A8, with 2 mutated anchor residues, gave no significant stabilization. The $H2K^b$/OVA/β_2M complex has an estimated half-life of 8 h [44]. Its stability is determined primarily by the peptide off-rate, so the E1 complex is likely to have a half-life of approximately 1.3 h.

We assessed the functional avidity of the $H2K^b$-OVA-specific TcR of OT-I [46] for each APL by *ex vivo* stimulation of $CD8^+$ T cells from OT-I mice with graded peptide doses (Figure 1C). There was a clear hierarchy in dose-response, with OVA>Q4 (14-fold)>V4 (a further 279-fold)>G4 (53-fold further still), consistent with published data [47]. The R4 antagonist peptide [48,49] gave no stimulation. As predicted E1 and A8, which have lower MHC class I binding, generated the lowest dose-responses.

Generation of MuHV-4 recombinants expressing OVA or APLs linked to M2

We next introduced each epitope at the MuHV-4 M2 C-terminus to ensure expression in latency without compromising M2 function [29]. CTL recognition of an endogenous M2 epitope reduces long-term MuHV-4 latent loads in $H2^d$ mice [29]. The lack of an endogenous $H2^b$-restricted M2 epitope therefore allowed us to introduce new targets in a context where this is known to be important. Each recombinant virus was also made with a yellow fluorescent protein (YFP) reporter construct [50] to aid infection tracking (Figure S1). Correct epitope insertion and assembly of the surrounding genome were demonstrated by PCR of plaque-purified viral DNA (Figure 1D). Each recombinant virus showed equivalent *in vitro* growth (Figure 1E), equivalent lytic replication in the lungs of intranasally (i.n.) infected C57BL/6 mice (Figure 1F) - with peak titers at 4–7 days post-inoculation and clearance by day 11 - and normal latency establishment in $H2^d$ BALB/c mice - with equivalent splenic infectious center assay titers 14 days after i.n. inoculation (Figure 1G). Therefore none showed a replication defect independent of $H2^b$-restricted latent epitope expression.

MHC class I binding by a latency-associated epitope impairs host colonization

We then tested latency establishment in $H2^b$ mice. Infectious center assays (Figure 2A) showed attenuation of any virus with an $H2K^b$ binding epitope attached to M2 (vOVA, vQ4, vV4, vG4, vR4): splenic infection was established at day 11, but then cleared rather than amplified by days 14–21. In contrast, the virus expressing a poorly binding epitope (vA8) was indistinguishable from the epitope-negative wild-type (vWT). Interestingly vE1, which expresses an epitope with 6-fold lower EC_{50} for $H2K^b$ stabilization (Figure 1B), showed an intermediate phenotype with normal titers at day 11 followed by a gradual reduction.

Not every latently infected cell necessarily reactivates its virus *ex vivo*. We therefore used PCR of viral DNA at limiting dilution (Figure 2B; Table 1) as a second measure of infected cell frequency. We looked at the peak of latent infection (14 days post-inoculation) and at the steady state (50 days). These results supported the infectious centre assays: vOVA, vQ4, vV4, vG4 and vR4 were all markedly attenuated (>100-fold reduction); vA8 was equivalent to vWT; and vE1 showed an intermediate phenotype, with strongly decreased acute titers but long-term titers close to vA8 and vWT. MuHV-4-specific CTL responses peak at 14–21 days post-infection [51]. Thus a weakly binding latent epitope (E1) allowed some control when CTL responses were at their peak, but not in the long-term when CTL responses decrease in size.

MuHV-4 colonizes multiple cell types in acutely infected spleens. Many are B cells, which change in phenotype as they pass through germinal centers; others are myeloid cells. The main proliferating population is GC B cells, and these also connect most directly to the long-term latency reservoir of resting memory B cells [9,10]. Therefore to understand better the relationship between acute and long-term viral loads, we measured viral genome prevalence in flow cytometrically sorted GC B cells (Figure 2C; Table 2). They showed marked reductions for vOVA, vQ4, vV4, vG4 and vR4, equivalent frequencies for vA8 and

A

MuHV-4 recombinants	Epitope Sequence
vOVA	M2 - SIINFEKL
vQ4	M2 - SIIQFEKL
vV4	M2 - SIIVFEKL
vG4	M2 - SIIGFEKL
vR4	M2 - SIIRFEKL
vE1	M2 - EIINFEKL
vA8	M2 - SIINFEKA

B

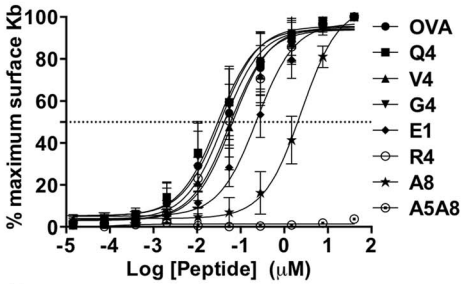

C

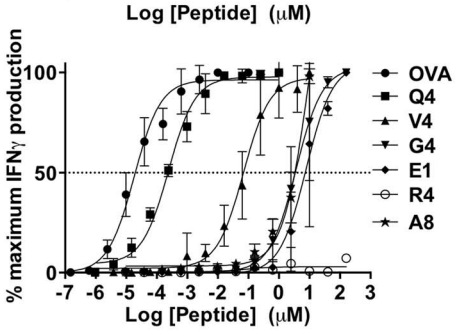

Peptide	EC_{50} (μM)	EC_{50} APL/OVA
OVA	0.040	1.0
Q4	0.030	0.8
G4	0.034	0.9
R4	0.056	1.4
V4	0.063	1.6
E1	0.235	5.9
A8	2.466	61.7
A5A8	-----	-----

OT-I sensitivity

Peptide	EC_{50} (μM)	EC_{50} APL/OVA
OVA	1.82E-05	1.00E+00
Q4	2.43E-04	1.35E+01
V4	6.85E-02	3.76E+03
G4	3.61E+00	1.98E+05
E1	7.78E+00	4.27E+05
R4	-------	-------
A8	1.03E+01	5.64E+06

D

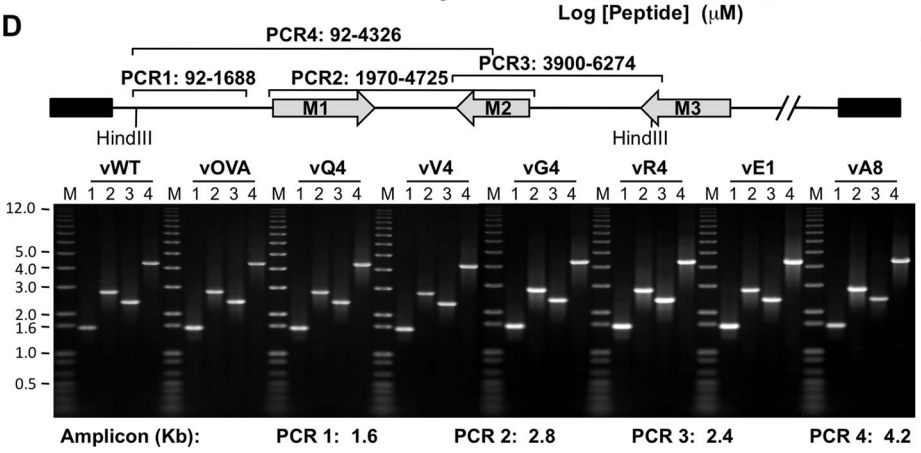

E

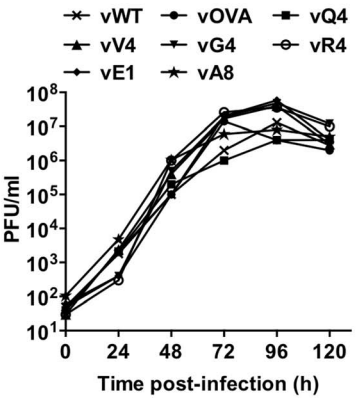

F

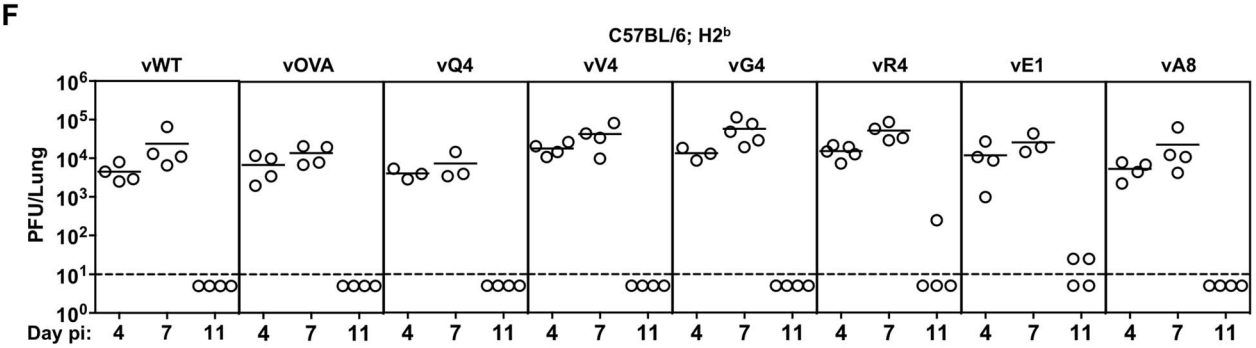

G

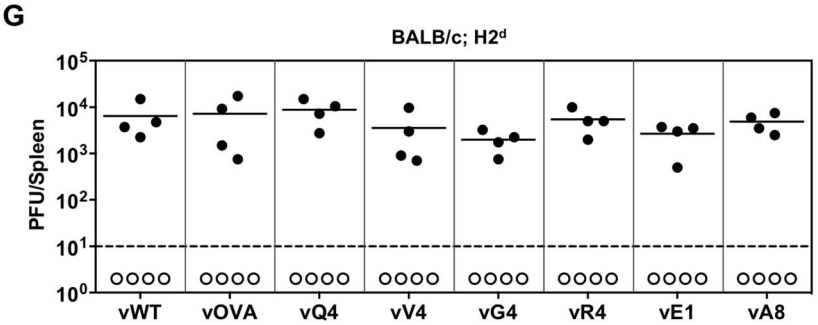

Figure 1. Characterization of APLs by MHC class I binding and TcR functional avidity, and generation of MuHV-4 recombinants expressing OVA or APLs linked to M2. (A) Amino acid sequences used to generate MuHV-4 recombinants. Blue residues denote amino acid alterations introduced into native OVA. (B) Capacity of OVA and APL peptides to stabilize $H2K^b$ on TAP deficient RMA/S cells. Half-maximum effective concentration (EC_{50}) values were calculated from dose-response curves. The experiment was repeated 3 times. (C) Functional avidities of OT-I CTL for OVA and APL peptides were determined by IFNγ production. EC_{50} and APL/OVA EC_{50} ratios are shown. This experiment was repeated in duplicates 4 times (D) PCR analysis of recombinant viral DNA to confirm genome integrity in the *Hin*DIII-E region, with schematic representation of the MuHV-4 genome, amplicon genomic co-ordinates and predicted PCR product sizes. (E) Multi-step growth curves of viruses in BHK-21 (0.01 PFU/cell). Virus titres were determined by plaque assay. *In vitro* lytic replication kinetics of the recombinant viruses were not significant different from vWT ($p>0.05$, by ordinary one-way ANOVA followed by Dunnett's multiple comparisons test). (F) Virus replication in lungs of i.n. infected C57BL/6 ($H2^b$) mice was quantified by plaque assay. No MuHV-4 recombinant showed a deficit relative to vWT ($p>0.05$, using ordinary one-way ANOVA followed by Tukey's multiple comparisons test). (G) Latent infection in spleens of BALB/c ($H2^d$) mice was determined by explant co-culture assay (closed symbols) at 14 days post-infection. Pre-formed infectious virus were measured by plaque assay (open symbols). Latent loads of MuHV-4 recombinants expressing OVA or APLs were not significantly different to vWT ($p>0.05$, by ordinary one-way ANOVA followed by Dunnett's multiple comparisons test). In panels F and G each point shows the titre of 1 mouse, horizontal lines show arithmetic means and dashed horizontal lines indicate the detection limit of the assay.
doi:10.1371/journal.ppat.1004220.g001

vWT, and intermediate frequencies for vE1. These data were further supported by *in situ* hybridization for latently expressed viral tRNA/miRNA homologs [29] (Figure 2D), which showed abundant GC infection by vWT and vA8, severely impaired infection by vOVA, vQ4, vV4, vG4 and vR4, and intermediate infection by vE1. Therefore susceptibility to CTL attack during acute lymphoproliferation varied with cell type, and the relative sparing of $vE1^+$ GC B cells appeared to allow high long-term viral loads.

CTL responses to epitopes expressed in latent infection

We measured epitope-specific CTL responses with $H2K^b$-peptide tetramers (Figure 2E) and by staining for intracellular IFN-γ after *ex vivo* stimulation (Figure 2F). Responses to vA8 were uniformly low despite high viral loads, presumably because this epitope was not produced in sufficient amounts to compensate for its poor $H2K^b$ binding. Responses to vOVA, vQ4, vV4, vG4 and vR4 were detectable, although small compared to those reported for lytic antigens [51]. Surprisingly, the largest CTL response was elicited by the intermediate phenotype virus, vE1. This could not be explained by lytic infection, since this was high in lungs for all viruses (Figure 1F).

We confirmed the functionality of vE1-specific CTL by *in vivo* killing of CFSE-labelled, peptide-exposed targets (Figure 2G,H): vE1-induced CTL showed target cell elimination comparable to vOVA, whereas mice infected with vWT or vA8 showed none. Therefore the relatively weak $H2K^b$ binding of E1 was sufficient to stimulate large, functional CTL responses, but not for those CTL to curtail efficiently virus-driven lymphoproliferation. This result suggested that at least for vE1, most CTL stimulation comes from a population distinct from that engaged in lymphoproliferation.

CTL functional avidity also determines infection control by latency epitope recognition

The capacity of C57BL/6 mice to control MuHV-4-driven lymphoproliferation through the recognition of latently expressed OVA, Q4, V4, G4 or R4 indicated that the key requirement in a polyclonal TcR setting is the availability of an epitope capable of strong MHC class I binding: T cells from the naive repertoire could recognize either OVA or an APL. However responses to EBV can involve oligoclonal or even monoclonal CTL expansions [52–54]. Therefore to understand better the quantitative requirements of TcR functional avidity for *in vivo* γHV control, we focussed on the well-characterized OT-I TcR (Figure 3).

We first infected OT-I mice with MuHV-4 expressing OVA or APLs with comparable $H2K^b$ binding (Q4, V4, G4, R4), and measured host colonization by infectious center assay of spleens 9 and 11 days later (Figure 3A). vE1 and vA8 were not utilized since they bind MHC class I less efficiently precluding analysis of T cell functional avidity because target concentrations are different. There was a clear correlation between CTL functional avidity (Figure 1C) and *in vivo* virus control. The antagonist epitope (R4) allowed no control - titers were equivalent to those of the epitope-negative vWT; the others showed a hierarchy of control (OVA> Q4>V4>G4) that matched exactly their hierarchy of functional avidity (and not their minor differences in $H2K^b$ binding). Low titers of pre-formed infectious virus were found in some mice, but generally in proportion to their latent titers, consistent with reactivation of a fixed fraction of the latent viral load; we saw no evidence that M2-associated epitope presentation created a significant new lytic CTL target.

To confirm that the immune control was by CTL, we treated mice with a depleting, CD8-specific mAb from the time of infection (Figure 3B–D). Each virus then reached equivalent titers to the wild-type. While the depletions were highly effective (Figure 3C), they had little effect on the day 11 spleen titers of vWT (Figure 3D). This result was consistent with previous publications [36,55] and with the lack of known $H2^b$-restricted MuHV-4 latency epitopes. Thus, introducing latent epitope recognition caused new, CD8-dependent virus attenuation in proportion to the functional avidity of that epitope for the dominant TcR.

CTL functional avidity in the context of normalized T cell repertoire

OT-I mice provided a useful starting point for *in vivo* analysis of single TcR function. However their limited $CD4^+$ T cell repertoire impairs GC formation and so the ability of MuHV-4 to drive B cell proliferation. Hence, to define the impact of TcR functional avidity in an environment more conducive to lymphoproliferation, we adoptively transferred lymphocytes from Rag-$1^{-/-}$OT-I mice and purified $CD4^+$ T cells from C57BL/6 mice into $TcR\alpha^{-/-}$ recipients (Figure 4A). Thus the reconstituted mice had polyclonal $CD4^+$ T cells and a $TcR\alpha\beta^+CD8^+$ T cell compartment of modest size that was restricted to OT-I cells. (Most $CD8^+$ T cells of $TcR\alpha^{-/-}$ mice are $TcR\gamma\delta^+TcR\alpha\beta^-$.) Infecting these with vWT led to a robust proliferation of infected GC B cells (Figure S2 and S3). Infecting them with vOVA elicited a strong OT-I response (Figure 4B) and suppression of splenic colonization (Figure 4C); by contrast vR4, which expressed an antagonist epitope, elicited no OT-I response and reached high titers (Figure 4C). Therefore these mice provided a new and informative window onto how TcR engagement by a latency epitope affects virus-driven lymphoproliferation.

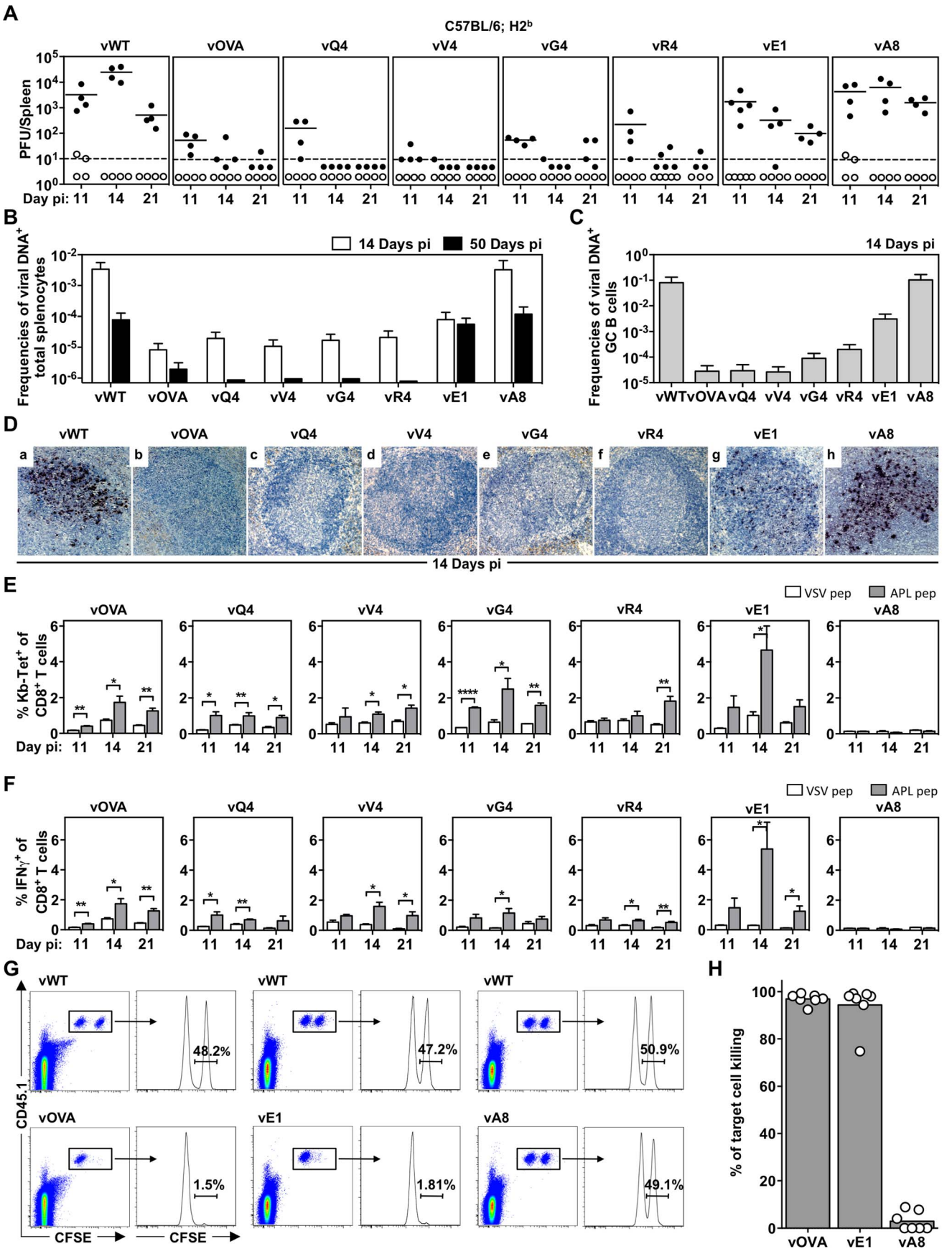
A
C57BL/6; H2b
vWT
vOVA
vQ4
vV4
vG4
vR4
vE1
vA8
PFU/Spleen
Day pi: 11 14 21
B
14 Days pi
50 Days pi
Frequencies of viral DNA+ total splenocytes
C
14 Days pi
Frequencies of viral DNA+ GC B cells
D
a
b
c
d
e
f
g
h
14 Days pi
E
VSV pep
APL pep
% Kb-Tet+ of CD8+ T cells
F
% IFNγ+ of CD8+ T cells
G
CD45.1
CFSE
48.2%
47.2%
50.9%
1.5%
1.81%
49.1%
H
% of target cell killing

Figure 2. MHC class I binding by a latency-associated epitope impairs host colonization. C57BL/6 mice were infected i.n. with 10^4 PFU of the indicated viruses. (A) The latent load in spleens was determined by explant co-culture assay (closed symbols) and pre-formed infectious virus was quantified by plaque assay (open symbols). Each point shows the titre of 1 mouse, horizontal lines arithmetic means and dashed horizontal line limit of detection of assay. At day 14, vOVA, vQ4, vV4, vG4, vR4 and vE1 latent loads were significantly below vWT ($p<0.05$, by two-tailed unpaired t-test). vA8 latency loads were not significantly different from vWT ($p = 0.07$). (B–C) Reciprocal frequencies of viral DNA^+ cells in (B) total splenocytes or (C) GC B cells. Bars represent the frequency of viral DNA^+ cells with 95% confidence intervals. (D) Representative spleen sections showing dark stained latently infected cells by *in situ* hybridization. (E) % tetramer positive $CD8^+$ T cells at each time point from spleens (arithmetic mean +/− SEM of 3 independent assays). * $p<0.05$, ** $p<0.01$, **** $p<0.0001$; using a two-tailed unpaired t-test. (F) Functional capacity of splenic CTL determined by intracellular interferon-gamma staining after *ex vivo* stimulation. Data show % $CD8^+$ T cells responding to each peptide (arithmetic mean +/− SEM of 3 independent assays). * $p<0.05$, ** $p<0.01$; using a two-tailed unpaired t-test. (G–H) *In vivo* CTL activity at 11 days post-infection. (G) At day 10 post-infection 50:50 mixes consisting of 2×10^6 unpulsed $CD45.1^+$ $CFSE^{lo}$ splenocytes and 2×10^6 OVA-, E1- or A8-pulsed $CD45.1^+$ $CFSE^{hi}$ splenocytes were transferred intravenously into vOVA, vE1 or vA8 infected C57BL/6 mice. The same mix of cells was transferred into vWT infected mice C57BL/6 as internal control. In the next day, the proportion of $CFSE^{hi}$ and $CFSE^{lo}$ cells among $CD45.1^+$ cells recovered from the spleen was analysed by FACS. Representative FACS plots showing % of unpulsed $CD45.1^+$ $CFSE^{lo}$ and OVA-, E1, or A8-pulsed $CD45.1^+$ $CFSE^{hi}$ splenocytes. (H) % target cell killing. Three to four mice were analyzed per group, and experiments repeated three times.
doi:10.1371/journal.ppat.1004220.g002

Sub-optimal CTL functional avidity still allows control of virus-driven lymphoproliferation

We then infected reconstituted mice with MuHV-4 expressing OVA or APLs (Figure 5). At day 16 post-infection OT-I T cell expansion was greatest for vOVA, reduced for vQ4, reduced further for vV4, and close to background for vG4 and vR4 (Figure 5A). Thus it correlated well with the epitope functional avidity measured in Figure 1C (OVA>Q4>V4>G4>R4). Specifically, the 14-fold avidity reduction of Q4 only modestly reduced CTL cell expansion, and the 4000-fold reduction of V4 caused further reduction but still did not ablate it entirely. The CTL response declined to background only when the avidity was reduced 200,000-fold (G4). Therefore the immune response showed a surprisingly large tolerance for sub-optimal TcR engagement.

Similar results were obtained for OT-I T cell activation (loss of CD62L, Figure 5B). We analyzed CTL function further by intracellular staining for IFN-γ (Figure 5C) and Granzyme B (Figure 5D) after *ex vivo* stimulation with the corresponding peptide epitope. The responses to vG4 and vR4 were hard to assess due to low CTL numbers; but those to vQ4 and vV4 showed comparable functionality to vOVA. (Note that the peptide concentration used was only just sufficient for maximal stimulation by V4 in Figure 1C) Therefore there was no sign of vQ4 and vV4 eliciting CTL responses that were functionally impaired (or functionally enhanced); they simply elicited responses that were smaller.

Virus titers (Figure 5E) were reduced markedly by OVA expression, only marginally less by Q4, and not significantly by G4 or R4. V4 expression gave an intermediate phenotype, with titers significantly below those of the vWT control and significantly above those of vOVA. The frequencies of viral DNA^+ cells in spleens (Figure 5F and Table S1) showed a similar hierarchy (vWT = vG4 = vR4>vV4>vQ4>vOVA). The viral DNA^+ frequencies of flow cytometrically sorted GC B cells (Figure 5G and Table 3) showed less discrimination. Nonetheless the trends were similar, and these results were further corroborated by analysis of YFP expression in GC B cells (Figure S4). Therefore high functional avidity (vOVA) gave marked CTL expansion and low virus titers; a 14-fold avidity reduction (vQ4) have remarkably similar results; a 200,000-fold avidity reduction abolished virus control (vG4); and a 4000-fold reduction gave an intermediate phenotype (vV4). OT-I TcR engagement by M2-derived OVA was therefore considerably above the threshold required for *in vivo* viral control, and low functional avidity compromised viral control via reduced CTL expansion, rather than by differentially affecting CTL effector function.

Table 1. Reciprocal frequency of MuHV-4 infection in total splenocytes[a] of C57BL/6 mice.

Virus	Day p.i.	Reciprocal frequency[b] of viral DNA^+ cells (95% CI)	
vWT	14	296	(179–856)
	50	12,770	(7,900–33,288)
vOVA	14	121,005	(75,230–309,065)
	50	517,114	(316,845–1,405,472)
vQ4	14	51,426	(32,333–125,586)
	50	id	≥1,149,446[c]
vV4	14	92,857	(57,599–239,405)
	50	id	≥1,053,659[c]
vG4	14	59,253	(37,537–140,588)
	50	id	≥1,053,659[c]
vR4	14	47,755	(29,622–123,123)
	50	id	≥1,264,391[c]
vE1	14	12,576	(7,445–40,375)
	50	17,810	(11,400–40,677)
vA8	14	307	(212–962)
	50	8462	(4970–28,436)

[a]Data were obtained from pools of 4 to 5 spleens.
[b]Frequencies were calculated by limiting-dilution analysis with 95% confidence intervals (CI).
[c]Estimated based upon less than 3 different dilution sets.
id; indeterminable.
doi:10.1371/journal.ppat.1004220.t001

Discussion

Gamma-herpesvirus epitope recognition by CTL has been studied extensively [1,54], but ours is the first quantitative assessment of how epitope/MHC class I/TcR complex formation affects host colonization. Where no latency epitope expression existed, introducing one led to a profound, CTL-dependent suppression of virus-driven lymphoproliferation. This was consistent with the impact of endogenous epitope presentation in $H2^d$ mice [29]. The latter affected only long-term viral loads; OVA expression in $H2^b$ mice also conferred susceptibility to CTL during acute lymphoproliferation, when trans-acting immune evasion operates [1]. This greater effect of epitope presentation possibly reflected differences in host susceptibility to immune evasion: the MuHV-4 K3 degrades $H2K^b$ relatively poorly [19] and degrades TAP better in $H2^d$ than $H2^b$ cells [20].

The precise cellular targets for $CD8^+$ T cell recognition of M2-linked epitopes remain unknown. One possibility is proliferating germinal centre B cells, as B cells are a major site of M2 expression

Table 2. Reciprocal frequency of MuHV-4 infection in GC B cells[a] of C57BL/6 mice at 14 days post-infection.

Virus	Reciprocal frequency[b] of viral DNA$^+$ cells (95% CI)		% Cells[c]	% Purity[d]
vWT	12	(8–34)	4.63	96.1
vOVA	35,463	(21,819–94,657)	4.06	96.3
vQ4	33,847	(19,882–113,738)	3.63	97.6
vV4	44,687	(23,952–92,597)	4.03	97.4
vG4	11,092	(7,184–24,318)	5.76	96.0
vR4	5,016	(3,268–10,785)	5.66	97.5
vE1	323	(211–687)	4.13	96.5
vA8	10	(6–25)	4.18	96.6

[a]Data were obtained from pools of 5 spleens.
[b]Frequencies were calculated by limiting-dilution analysis with 95% confidence intervals (CI).
[c]The percentage of GC B cells from total spleen was estimated by FACS analysis.
[d]The purity of sorted cells was determined by FACS analysis.
doi:10.1371/journal.ppat.1004220.t002

[10,34]. Infected B cells could also be recognized before the onset of proliferation; and as myeloid cells transfer infection to B cells [56], CD8$^+$ T cells could also suppress lymphoproliferation indirectly, by targeting infected myeloid cells [1].

A key point for physiologically relevant epitope presentation is that it conforms to normal latent gene expression. Exogenous promoters such as HCMV IE1 show activity independent of endogenous viral gene expression [57] and this can lead to attenuation [58]. Previous analysis of endogenous M2 epitope [29] established its importance for determining the different long-term latent loads of H2^d and H2^b mice. Here, to identify presentation thresholds, we made use of the well-characterized SIINFEKL epitope, attaching it to a neutral region of M2 (its C-terminus). This allowed the generation of a very well-defined model epitope with the kinetics and copy number of a known endogenous epitope. Epitope presentation varies with MHC class I genotype. C57BL/6 mice have only 2 MHC class I molecules and appear not to recognize an endogenous M2 epitope. In this context, M2-SIINFEKL illustrated the impact of strong epitope presentation, and wild-type M2 (or M2-vA8) that of poor epitope presentation. The SIINFEKL variants covered the range between, and so allowed us to identify functional recognition thresholds.

Small differences ($<$1.6-fold) in H2K^b epitope binding had no obvious impact on *in vivo* CTL efficacy, but a 60-fold reduction abolished protection and a 6-fold reduction showed a partial phenotype. Thus, M2-linked epitope presentation left little room for sub-optimal MHC class I binding. By contrast when H2K^b binding was maintained, reducing TcR functional avidity 14-fold had little effect, reducing it 200,000-fold abolished control, and reducing it 4,000-fold gave an intermediate phenotype. Therefore this aspect of recognition was more flexible even for monoclonal, Rag-1$^{-/-}$ CTL, and a polyclonal population could attack any epitope so long as its MHC class I binding was strong.

In complex viral infections, larger CTL responses are not necessarily more effective responses. These parameters can correlate: MuHV-4 lacking its K3 evasion gene elicits more CTL and achieves lower titers [22]; and our reconstituted mice showed a correlation between more CTL and less virus. But as with latent epitope presentation downstream of ORF73 [11], OVA-specific CTL responses that completely suppressed lymphoproliferation were small compared to lytic epitope responses [51]; and mice infected with vE1 made large epitope-specific responses yet showed poor virus control. We hypothesize that CTL can be stimulated by the key, self-renewing population of infected B cells, when infection is suppressed, but also by infected cells less important to host colonization, when large responses may achieve little. Crucially, viral evasion may make the self-renewing population harder to target. Thus, vE1 showed a strong acute reduction in total viral DNA$^+$ cell frequencies, but relative sparing of GC B cells and consequently high long-term virus loads. A position 1 mutation also impairs the control by Rag-1$^{-/-}$OT-I mice of MuHV-4 expressing OVA from an HCMV IE1 promoter [59]. However such mice lack B cells or CD4$^+$ T cells, and without CD4$^+$ T cells MuHV-4 causes a lethal, chronic lytic infection even with a strong, polyclonal CTL response [60,61]. Our reconstituted mice maintained both virus-driven lymphoproliferation and infection control without outgrowth of CTL escape mutants. Thus we could relate directly quantitative changes in epitope recognition to the control of lymphoproliferation.

An important task with EBV is to predict *in vivo* CTL efficacy. Extrapolating from CTL numbers and *in vitro* assays alone is clearly problematic. For example, large responses to lytic epitopes in infectious mononucleosis [54] could be interpreted as important, or simply as poor latency epitope recognition when better recognition might preclude large lytic responses and avoid symptoms. The precise relatedness of EBV memory B cell colonization via GCs to MuHV-4 memory B cell colonization via GCs is unknown. But all γHVs have evolved to colonize lymphocytes with maximal efficiency, within limits set ultimately by the immune system, so similar quantitative thresholds would not be surprising. Our data therefore have important general implications for γHV-specific CTL function, and for predicting *in vivo* CTL efficacy from biochemical measures.

Materials and Methods

Ethics statement

The study accorded with the Portuguese official Veterinary Directorate (Portaria 1005/92), European Guideline 86/609/EEC, and Federation of European Laboratory Animal Science Associations guidelines on laboratory animal welfare. It was approved by the Portuguese official veterinary department for welfare licensing (protocol AEC_2010_017_PS_Rdt_General) and by the IMM Animal Ethics Committee.

Mice

CD45.1 C57BL/6, OT-I, Rag-1$^{-/-}$ and TcRα$^{-/-}$ mice were obtained from Jackson Laboratories. CD45.1 Rag-1$^{-/-}$ OT-I

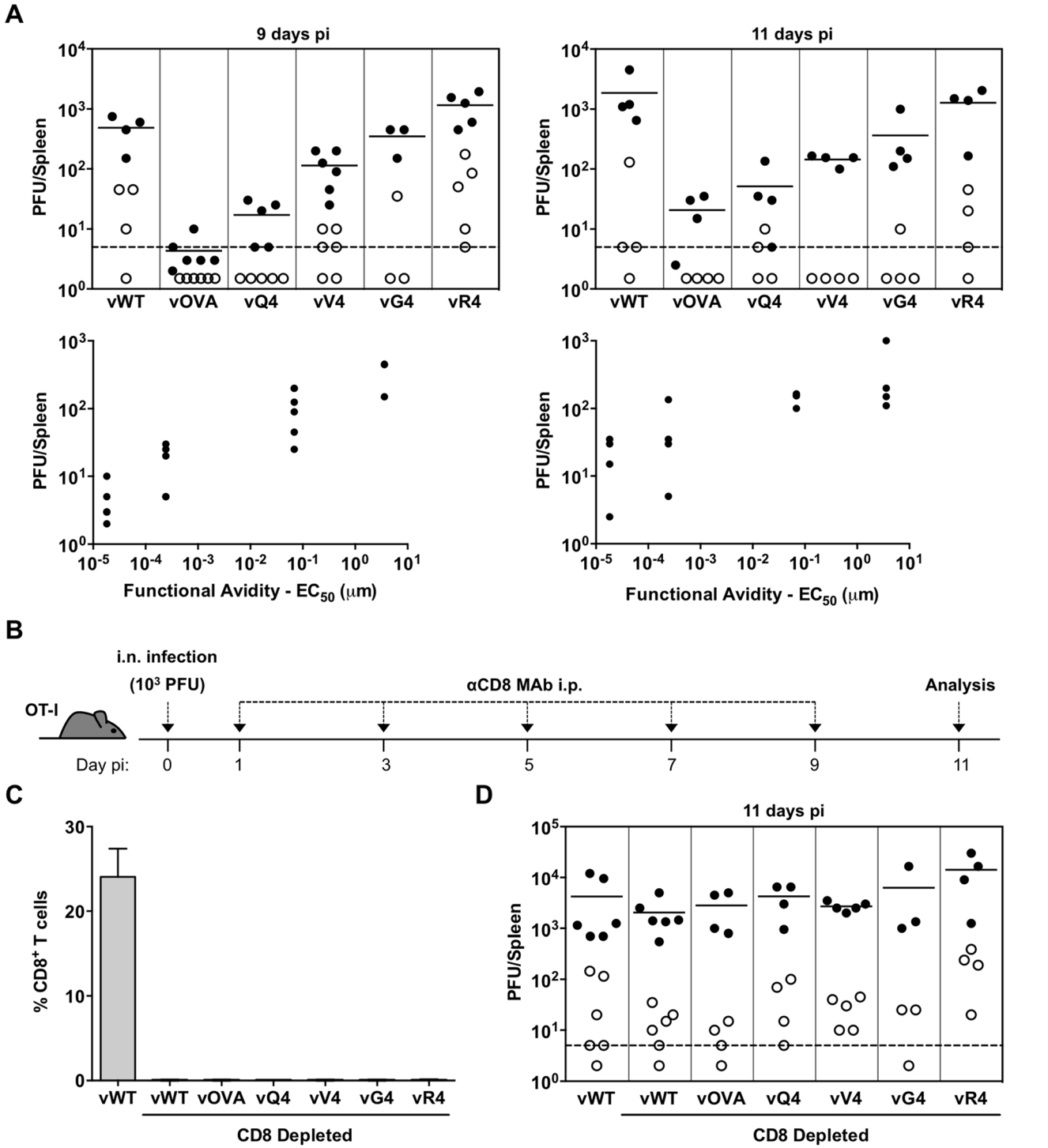

Figure 3. CTL functional avidity also determines infection control by latently expressed epitope recognition. (A) OT-I mice were infected i.n. (10^3 PFU). Splenocytes were titrated for latent virus by explant co-culture (closed circles) and for pre-formed infectious virus by plaque assay (open circles). At 9 days vOVA, vQ4 and vV4 showed significantly less latent infection compared to vWT (vOVA $p = 0.0014$, vQ4 $p = 0.004$, vV4 $p = 0.009$; by Student's 2-tailed unpaired t-test). vG4 and vR4 latent infections were not significantly different to vWT (vG4 $p = 0.46$, vR4 $p = 0.09$). Graphs show the correlation between TcR functional avidity (determined in Figure 1C) and splenic latent load (day 9: $p = 0.04$, $r_s = 0.91$; day 11 $p = 0.05$, $r_s = 0.90$; according to Pearson's correlation). (B) CD8 T^+ cells were depleted from i.n. infected OT-I mice by intraperitoneal injection of anti-CD8 monoclonal antibody (MAb). (B) Schematic diagram of the experimental setting. (C) Data show the percentage of $CD8^+$ T cells of total splenocytes (arithmetic mean +/− SEM) in control (non-depleted) and depleted mice. (D) Spleens were titrated for latent (closed circles) and lytic (open circles) infection. Latent loads of the epitope recombinants were not significantly different to vWT latent loads in CD8-depleted mice ($p > 0.05$; ordinary one-way ANOVA followed by Dunnett's multiple comparisons test). Data were reproduced in two independent experiments. Each point shows the titre of 1 mouse, horizontal lines arithmetic means and dashed lines the limit of detection of the assay.
doi:10.1371/journal.ppat.1004220.g003

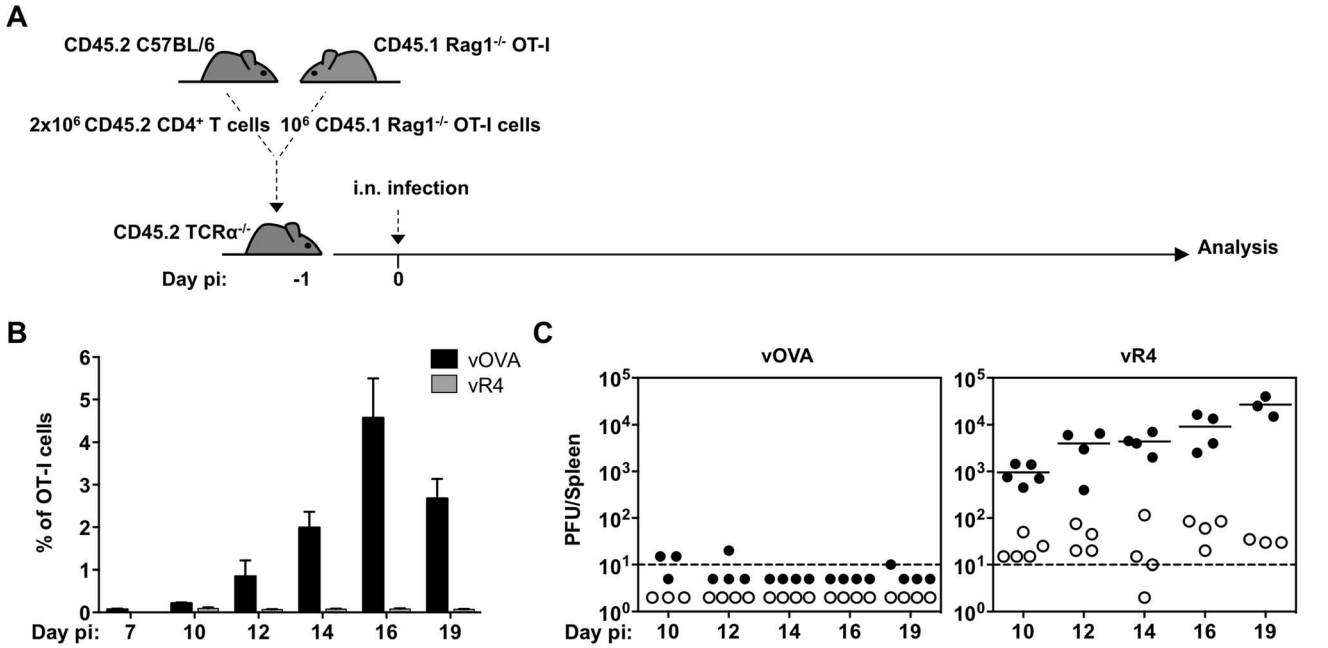

Figure 4. vOVA infection of TCR$\alpha^{-/-}$ mice reconstituted with CD4$^+$/OT-I T cells elicits a strong OT-I response and suppression of splenic colonization. CD4$^+$ T cells from C57BL/6 lymph nodes and OT-I T cells from CD45.1 Rag-1$^{-/-}$ OT-I lymph nodes were intravenously transferred to TcR$\alpha^{-/-}$ mice one day prior to infection with vOVA or vR4 (10^3 PFU). (A) Schematic diagram of the experimental setting. (B) Kinetics of *in vivo* OT-I CTL expansion in spleens of mice infected with vOVA (black bars) or vR4 (grey bars) determined by FACS staining of CD45.1$^+$CD8α^+ cells (arithmetic mean +/− SEM). (C) Latent infection in spleens was quantified by explant co-culture assay (closed circles) and pre-formed infectious virus by plaque assay (open circles). Each circle shows the titre of 1 mouse. Horizontal bars show arithmetic means. The dashed line shows the limit of detection of the assay.
doi:10.1371/journal.ppat.1004220.g004

mice were obtained by breeding OT-I onto a CD45.1 Rag-1$^{-/-}$ background. C57BL/6 and BALB/c mice were purchased from Charles River Laboratories. All mice were housed under specific pathogen-free conditions at the Instituto de Medicina Molecular and used when 6–12 weeks old. For adoptive transfers to TcR$\alpha^{-/-}$ mice, CD4$^+$ T cells were purified by negative selection from pooled lymph nodes of naïve C57BL/6 mice using the CD4$^+$ T cell isolation kit (Miltenyi Biotech). OT-I T cells were obtained from pooled lymph nodes of naïve CD45.1 Rag-1$^{-/-}$ OT-I mice. 2×10^6 CD4$^+$ T cells and 10^6 CD45.1 Rag-1$^{-/-}$ OT-I T cells were adoptively transferred to TcR$\alpha^{-/-}$ recipients via tail vein injection one day prior to infection.

Generation of recombinant viruses

MuHV-4 recombinants were generated from BAC-cloned viral genomes [29]. OVA and APL epitopes were introduced by PCR at the M2 C-terminus. Briefly, the M2 downstream region (genomic co-ordinates 3846-4029) containing a *Hind*III restriction site followed by the epitope coding region and a stop codon were PCR amplified (Table S2) to attach each epitope to the M2 C-terminus. The PCR products were inserted downstream of a *Hin*DIII/*Xho*I MuHV-4 genomic fragment (nt 4029–5362) in pSP72 (Promega), using a genomic *Bgl*II site (nt 3846) and the engineered *Hin*DIII (nt 4029) restriction site. The constructs were then subcloned into a *Hin*DIII-E MuHV-4 genomic fragment in the pST76K-SR shuttle plasmid, using genomic *Bln*I (nt 3908) and *Xho*I (nt 5362) restriction sites. All PCR-derived regions were sequenced to confirm the integrity of the introduced epitopes and the M2 flanking region. Each recombinant *Hin*DIII-E shuttle plasmid was transformed into *E.coli* carrying the wild type MuHV-4 BAC (pHA3) or a YFP$^+$ BAC [50] obtained from Dr Samuel Speck (Emory Vaccine Center, Atlanta). Following multi-step selection, recombinant BAC clones were identified by restriction digestion with *Hin*DIII. The integrity of each BAC was confirmed by digestion with *Bam*HI and *Eco*RI. All viruses were reconstituted by transfecting BAC DNA into BHK-21 cells using FuGENE 6 or X-tremeGENE HP (Roche Applied Science). The *lox*P-flanked BAC cassette was then removed by viral passage through NIH-3T3-CRE cells and limiting dilution cloning. The integrity of each reconstituted virus was checked by PCR of viral DNA across the *Hin*DIII-E region and DNA sequencing across M2.

Cell culture and viruses

Murine RMA/S cells were cultured in RPMI 1640 with 10% fetal calf serum, 2 mM glutamine and 100 U/ml penicillin and 100 μg/ml streptomycin. NIH-3T3 (ATCC)-CRE cells [22] were grown in Dulbecco's modified Eagle's medium (DMEM) with 10% fetal calf serum, 2 mM glutamine, 100 U/ml penicillin and 100 μg/ml streptomycin. Baby hamster kidney fibroblast cells (BHK-21, ATCC) were cultured in Glasgow's modified Eagle's medium (GMEM) supplemented as above plus 10% tryptose phosphate broth. To prepare viral stocks, low multiplicity infections (0.001 PFU per cell) of NIH-3T3-CRE or BHK-21 cells were harvested after 4 days and titrated by plaque assay [29].

H2K^b stabilization assay and OVA/APLs stimulatory potency

H2K^b stabilization was determined with TAP-deficient RMA/S cells. These were incubated overnight at 26°C to promote the export of empty H2K^b complexes, then loaded with graded concentrations of OVA or APL peptides (Thermo Scientific) for 2 h at 26°C and subsequently transferred to 37°C for 2 h to

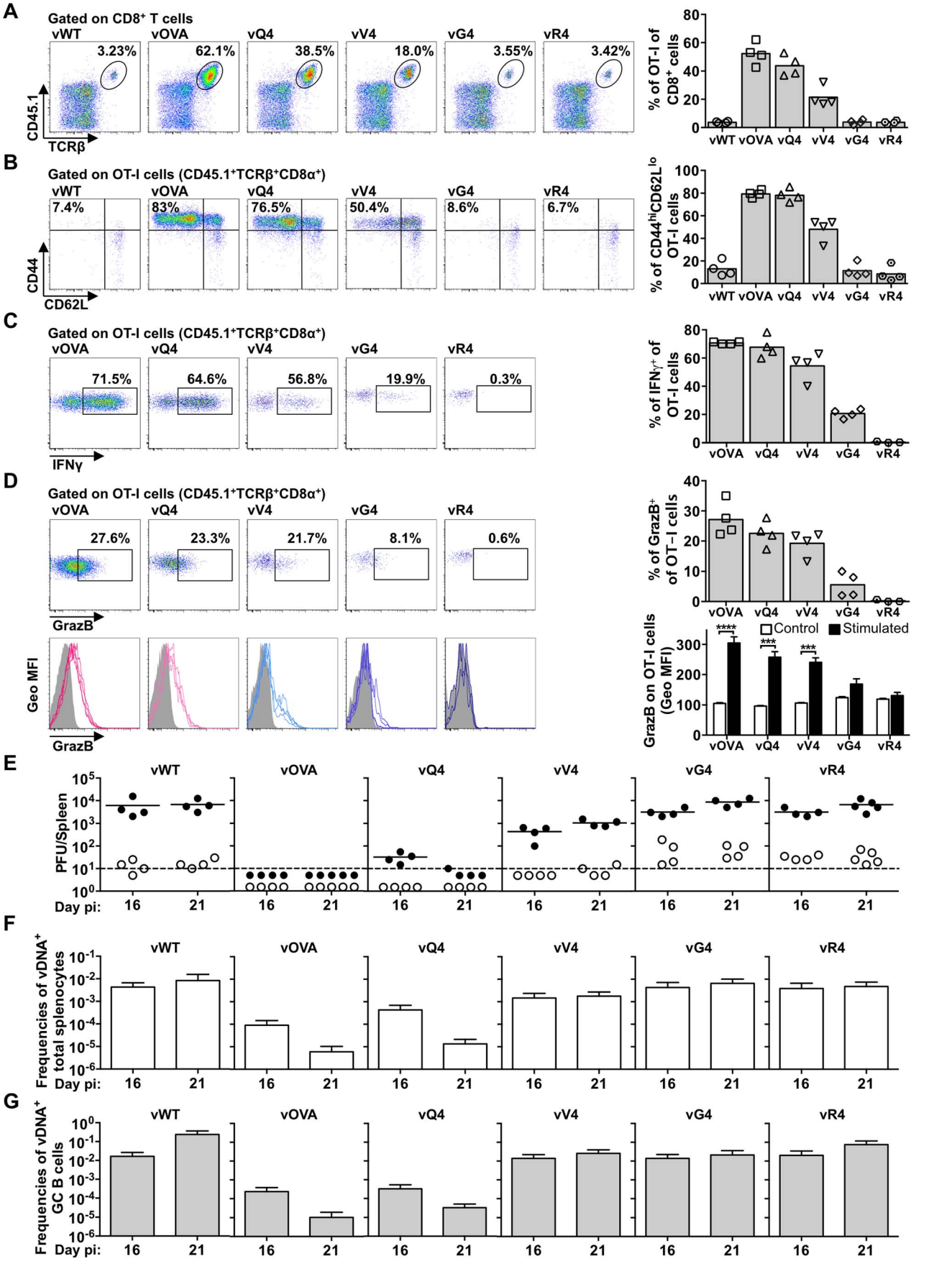
A
Gated on CD8+ T cells
vWT
vOVA
vQ4
vV4
vG4
vR4
3.23%
62.1%
38.5%
18.0%
3.55%
3.42%
CD45.1
TCRβ
% of OT-I of CD8+ cells
B
Gated on OT-I cells (CD45.1+TCRβ+CD8α+)
7.4%
83%
76.5%
50.4%
8.6%
6.7%
CD44
CD62L
% of CD44hiCD62Llo OT-I cells
C
Gated on OT-I cells (CD45.1+TCRβ+CD8α+)
71.5%
64.6%
56.8%
19.9%
0.3%
IFNγ
% of IFNγ+ of OT-I cells
D
Gated on OT-I cells (CD45.1+TCRβ+CD8α+)
27.6%
23.3%
21.7%
8.1%
0.6%
GrazB
Geo MFI
% of GrazB+ of OT-I cells
Control
Stimulated
GrazB on OT-I cells (Geo MFI)
E
PFU/Spleen
Day pi:
F
Frequencies of vDNA+ total splenocytes
G
Frequencies of vDNA+ GC B cells

Figure 5. Suboptimal CTL functional avidity still allows control of virus-driven lymphoproliferation. Reconstituted TcR$\alpha^{-/-}$ mice (described in Figure 4A). were i.n. infected. (A–D) At 16 days the frequency, phenotype and effector function of transferred OT-I T cells was analyzed by flow cytometry. (A) Representative FACS plots from individual animals show the frequency of OT-I (CD45.1$^+$TcRβ^+CD8α^+) cells within total CD8$^+$ T cells. vOVA, vQ4 and vV4 induced significant expansion of OT-I cells in comparison with vWT ($p<0.0001$, $p<0.0001$, $p = 0.002$, respectively; by ordinary one-way ANOVA followed by Tukey's multiple comparisons test). vWT, vG4 and vR4 did not significantly increase OT-I cell numbers ($p>0.9$). (B) The activation phenotype of OT-I cells was determined by staining he CD45.1$^+$TcRβ^+CD8α^+ population for CD44 and CD62L. vOVA, vQ4 and vV4 induced significantly more OT-I cell activation than vWT ($p<0.0001$); vG4 and vR4 were not significantly different from vWT ($p>0.9$). (C–D) The effector function of OT-I cells was determined as % CD45.1$^+$TcRβ^+CD8α^+ cells producing (C) IFN-γ and (D) granzyme B by intracellular cytokine staining following *ex vivo* stimulation with OVA or the corresponding APL peptide. Histograms show geometric mean fluorescence intensities of granzyme B staining relative to an antibody isotype control (shaded area). Representative FACS plots from individual animals (left panels) and compiled percentages (right panels) are shown. Each point shows 1 mouse; 4 mice were analyzed per group; the bars shows means. *** $p<0.001$, **** $p<0.0001$; using Student's 2-tailed unpaired t-test. (E) At 16 and 21 days, spleens were titrated for latent virus (closed circles) and infectious virus (open circles). Each circle shows the titre of 1 mouse and the horizontal bars show means. The dashed line shows the limit of detection of the assay. At 16 and 21 days vOVA, vQ4 and vV4 showed significantly lower latent loads than vWT (d16: vOVA $p = 0.02$, vQ4 $p = 0.02$, vV4 $p = 0.03$; d21: vOVA $p = 0.004$, vQ4 $p = 0.006$, vV4 $p = 0.02$; by ordinary one-way ANOVA and Dunnett's multiple comparisons test). Latent loads of vG4 and vR4 were not significantly different from vWT (d16: vG4 $p = 0.4$, vR4 $p = 0.4$; d21: vG4 $p = 0.8$, vR4 $p = 1.0$). (F–G) Reciprocal frequencies of viral DNA$^+$ cells in (F) total splenocytes and (G) purified GC B cells. Bars show frequencies of viral DNA-positive cells with 95% confidence intervals.
doi:10.1371/journal.ppat.1004220.g005

destabilize empty MHC molecules [43]. The cells were then washed twice, stained with anti-H2K^b (AF6-88.5.5.3, eBioscience), and analysed on a LSR Fortessa (BD Biosciences). Mean fluorescence intensities were determined with FlowJo (Tree Star). To measure the *ex vivo* stimulation of naïve OT-I T cells by OVA and APLs, CD8$^+$ T cells from the spleens of naïve OT-I mice were purified by negative selection (CD8$^+$ T cell isolation kit, Miltenyi Biotech); for equivalent peptide/MHC class I numbers, irradiated (7500 rads) RMA/S cells were loaded with different peptides at 26°C, then incubated at 37°C; and 5×10^4 OT-I T cells were cultured with 2.5×10^4 RMA/S cells for 72 h at 37°C. IFNγ levels in culture supernatants were measured by ELISA (DuoSet ELISA development kit, R&D Systems). The data were fitted to sigmoidal dose-response curves and EC_{50} values calculated using GraphPad Prism.

In vivo infections and virus assays

Groups of 6- to 8-week old BALB/c and C57BL/6 mice were inoculated i.n. with 10^4 PFU of MuHV-4. 8- to 12-week old OT-I and TCR$\alpha^{-/-}$ mice were inoculated i.n. with 10^3 PFU of MuHV-4. All virus inoculations were in 20 µl of PBS under isofluorane anaesthesia. At different days post-infection lungs or spleens were removed and processed for subsequent analysis. Titres of infectious virus were determined by plaque assay of freeze-thawed lung or spleen homogenates using BHK-21 cells. Latent virus loads were quantified by explant co-culture of splenocytes with BHK-21 cells. Plates were incubated for 4 (plaque assay) or 5 (explant co-culture assay) days, then fixed with 4% formaldehyde and stained with 0.1% toluidine blue. Viral plaques were counted with a plate microscope. The frequency of MuHV-4 genome-positive cells was determined by limiting dilution combined with real time PCR [10]. Splenocytes were pooled from 4–5 mice. GC B cells (CD19$^+$CD95^{hi}GL7^{hi}) were purified from pools of 4 or 5 spleens using a BD FACSAria Flow Cytometer (BD Biosciences). Cells were serially two-fold diluted and eight replicates of each dilution were analysed by real time PCR (Rotor Gene 6000, Corbett Life Science). The primer/probe sets were specific for the MuHV-4 M9 gene (5′ primer: GCCACGGTGGCCCTCTA; 3′ primer: CAGGCCTCCCTCCCTTTG; probe: 6-FAM-CTTCTGTTGATCTTCC-MGB). Samples

Table 3. Reciprocal frequency of MuHV-4 infection in GC B cells[a] of reconstituted TCR$\alpha^{-/-}$ mice.

Virus	Day p.i.	Reciprocal frequency[b] of viral DNA$^+$ cells (95% CI)		% Cells[c]	% Purity[d]
vWT	16	61	(38–158)	3.13	97.3
	21	4	(3–9)	6.36	97.4
vOVA	16	41,748	(25,873–108,104)	1.95	97.0
	21	id	>96,432[e]	4.88	98.4
vQ4	16	3,042	(1,874–8,064)	3.50	97.0
	21	29,920	(19,237–67,294)	4.87	97.0
vV4	16	72	(45–176)	3.00	98.2
	21	39	(25–84)	8.83	99.0
vG4	16	72	(45–176)	3.08	97.0
	21	32	(18–108)	6.68	98.0
vR4	16	50	(29–167)	2.46	97.4
	21	16	(9–53)	7.99	97.0

[a]Data were obtained from pools of 4 to 5 spleens.
[b]Frequencies were calculated by limiting-dilution analysis with 95% confidence intervals (CI).
[c]The percentage of GC B cells from total spleen was estimated by FACS analysis.
[d]The purity of sorted cells was determined by FACS analysis.
[e]Estimated based upon less than 3 different dilution sets.
id; indeterminable.
doi:10.1371/journal.ppat.1004220.t003

were subjected to a melting step of 95°C for 10 min followed by 40 cycles of 15 s at 95°C and 1 min at 60°C. Real-time PCR data was analysed on the Rotor Gene 6000 software. The purity of sorted populations was always >96%. *In situ* hybridization with a digoxigenin-labelled riboprobe encompassing MuHV-4 vtRNAs 1–4 and microRNAs 1–6 was performed on formalin-fixed, paraffin-embedded spleen sections [29], using probes generated by T7 transcription of pEH1.4.

In vivo cytotoxicity assay

Splenocytes from naïve CD45.1 C57BL/6 mice were used as targets and controls. Targets were pulsed with 1 μM OVA, E1 or A8 peptides for 1 h at 37°C, then labeled with 1 μM carboxyfluorescein succinimidyl ester (CFSE) (Molecular Probes). Controls were left unpulsed and labeled with 0.1 μM CFSE. Cells were washed three times then injected intravenously as a 50:50 mix of $CFSE^{hi}$ and $CFSE^{lo}$ cells (4×10^6) into mice infected with vWT, vOVA, vE1 or vA8. The same mixes were injected intravenously into vWT infected C57BL/6 controls to ensure equal transfer. On the next day splenocytes were harvested and the proportion of $CFSE^{hi}$ and $CFSE^{lo}$ cells among CD45.1 splenocytes was analysed by FACS. Target cell killing was calculated as (% $CFSE^{lo}$/% $CFSE^{hi}$), with % = 100−(ratio in vWT infected/ratio in vOVA, vE1 or vA8 infected)×100.

$CD8^+$ T cell depletions

MuHV-4 infected OT-I mice were depleted of $CD8^+$ T cells by 5 intraperitoneal injections of 200 μg monoclonal antibody YTS 169.4. Splenocytes from control or depleted mice were stained with anti-CD8α (53-6.7) (BD Pharmingen) and analysed on a LSR Fortessa (BD Biosciences).

Ex vivo stimulation and intracellular cytokine staining

Splenocytes (2×10^6) from infected mice were stimulated for 5 h at 37°C with 10 μg/ml peptide (OVA, APLs or VSV $NP_{52\text{-}59}$) in RPMI 1640/10% fetal calf serum/2 mM glutamine/100 U/ml penicillin/100 μg/ml streptomycin/50 μM 2-mercaptoethanol/10 U/ml recombinant murine IL-2 (PeproTech)/10 μg/ml Brefeldin A. Cells were then washed, blocked with anti-CD16/32 (2.4G2) (BD Pharmingen), surface stained with anti-CD8α ± anti-CD45.1 (for OT-I T cells), fixed and permeabilized with Foxp3 staining buffer (eBioscience) and stained with anti-IFNγ (XMG1.2) (BD Pharmingen), anti-Granzyme B (NGZB) or anti-IgG2ak Isotype control (eBioscience). Samples were analysed on a LSR Fortessa (BD Biosciences).

Flow cytometry

Splenocytes were treated with red blood cell lysis buffer, blocked with anti-CD16/32 (2.4G2, BD Pharmingen, 10 min), and stained at 4°C in PBS/2% FCS 30 minutes: anti-CD95 (Jo2), anti-CD19 (1D3), anti-CD8α (53-6.7), anti-IFNγ (XMG1.2) (BD Pharmingen); anti-CD45.1 (A20), anti-CD45.2 (104), anti-CD44 (IM7), anti-CD62L (MEL-14) (Biolegend); anti-GL7 (GL7), anti-$H2K^b$ (AF6-88.5.5.3), anti-TCRβ (H57-597), anti-GranzymeB (NGZB), anti-IgG2ak Iso control (eBR2a) (eBioscience). For biotinylated antibodies, an additional 20 minutes incubation with streptavidin was performed. MuHV-4 infected cells were identified by YFP expression. $H2K^b$ tetramers conjugated to PE were a kind gift from Dr Hidde L. Ploegh (Whitehead Institute for Biomedical Research, Massachusetts Institute of Technology, Cambridge). Conditional ligand was exchanged for SIINFEKL (OVA), SIIQFEKL (Q4), SIIVFEKL (V4), SIIGFEKL (G4), SIIRFEKL (R4), EIINFEKL (E1) or RGYVYQGL (VSV $NP_{52\text{-}59}$) peptides (Thermo Scientific). Streptavidin-APC or -PerCP (BD Pharmingen) was used to reveal biotinylated antibodies. Samples were acquired on a LSR Fortessa using DIVA (BD Biosciences) and analysed with FlowJo (Tree Star, Inc.).

Statistical analysis

Data comparisons between groups were performed by an unpaired two-tailed t-test or ordinary one-way ANOVA as appropriate. Mean +/− SEM and statistics were calculated with GraphPad Prism Software. For limiting dilution analysis 95% confidence intervals were determined as described [10].

PCR primers

Primers used for attaching each epitope to MuHV-4 M2 C-terminus are detailed in supplemental Table S2.

Supporting Information

Figure S1 Characterization of MuHV-4 YFP recombinants expressing OVA or APLs linked to M2. (A) PCR analysis of recombinant viral DNA to confirm genome integrity in the HinDIII-E region. High molecular weight DNA was purified from lytically infected BHK-21 cells. A schematic representation of the MuHV-4 genome, amplicon genomic coordinates and expected size for each PCR product are shown. (B) Latent infection in spleens of intranasally infected (10^4 PFU) BALB/c ($H2^d$) mice was quantified by explant co-culture assay (closed symbols) at day 14 post-infection. Pre-formed infectious virus was measured by plaque assay (open symbols). Latent loads of MuHV-4 YFP recombinants expressing OVA or APLs were not significantly different from MuHV-4 YFP (vWT) ($p>0.05$, by ordinary one-way ANOVA followed by Dunnett's multiple comparisons test). Each point shows the titre of 1 mouse, horizontal lines indicate arithmetic means and the dashed horizontal line the limit of detection of the assay. Data were reproduced in two independent experiments. (C) Phenotype of infected cells (YFP expressing cells) was analysed by FACS, by overlapping GC ($CD19^+CD95^{hi}GL7^{hi}$) B cells and YFP^+ B cells FACS plots. Representative FACS plots from individual animals are shown. Five animals were analysed per group and data were reproduced in two independent experiments.
(TIF)

Figure S2 Reconstitution of $TCR\alpha^{-/-}$ mice with $CD4^+$ T cells leads to robust GC reactions upon MuHV-4 infection. 2×10^6 $CD4^+$ T cells purified from pooled lymph nodes of naïve C57BL/6 mice were intravenously transferred into age and sex matched $TCR\alpha^{-/-}$ mice one day prior to infection with 10^3 PFU of MuHV-4 YFP (vWT). At 14 days post-infection mice were sacrificed, spleens were dissected and single splenocyte suspensions were stained for GC B cells and analysed by FACS. (A) Schematic diagram of the experimental setting. (B) Representative FACS plots show the frequency of GC ($CD19^+CD95^{hi}GL7^{hi}$) B cells in spleens of the following experimental controls: non-transferred naïve $TCR\alpha^{-/-}$ mice, CD4-transferred naïve $TCR\alpha^{-/-}$ mice, non-transferred $TCR\alpha^{-/-}$ mice infected with vWT, CD4-transferred $TCR\alpha^{-/-}$ mice infected with vWT, and CD4 and OT-I T cells co-transferred $TCR\alpha^{-/-}$ mice infected with vWT. Four mice were analysed per group and data were reproduced in two independent experiments.
(TIF)

Figure S3 $TCR\alpha^{-/-}$ mice reconstituted with $CD4^+$ and OT-I T cells show robust proliferation of MuHV-4 infected GC B cells. $CD4^+$ T cells from C57BL/6 lymph

nodes and OT-I T cells from CD45.1 Rag-1$^{-/-}$ OT-I mice lymph nodes were intravenously transferred to TCR$\alpha^{-/-}$ mice 1 day prior to infection with MuHV-4 YFP (10^3 PFU). (A) Schematic diagram of the experimental setting. (B) Frequencies of GC (CD19$^+$CD95^{hi}GL7^{hi}) B cells. (C) Frequency of YFP$^+$ cells in GC B cells. (D) Phenotype of infected cells analyzed by overlapping GC B cells and YFP$^+$ B cells FACS plots. Representative FACS plots from individual animals are shown (top panels) and compiled percentages are presented in the graphics below. Each point represents an individual mouse; grey bars indicate the average percentage.
(TIF)

Figure S4 YFP expression in GC B cells of reconstituted TCR$\alpha^{-/-}$ mice infected with MuHV-4 recombinants expressing OVA or APLs. TCR$\alpha^{-/-}$ mice were adoptively transferred with polyclonal CD4$^+$ T cells and CD45.1 Rag1$^{-/-}$ OT-I cells one day prior to infection (10^3 PFU) with MuHV-4 YFP (vWT) or MuHV-4 YFP expressing the indicated epitopes. At 16 (A and B) and 21 (C and D) days post-infection spleens were removed and analysed by FACS. (A and C) Frequencies of GC (CD19$^+$CD95^{hi}GL7^{hi}) B cells. (B and D) Frequency of YFP$^+$ cells in GC B cells. FACS plots show data obtained from pools of 4 or 5 spleens per group of animals.
(TIF)

Table S1 Reciprocal frequency of MuHV-4 infection in total splenocytes[a] of reconstituted TCR$\alpha^{-/-}$ mice.
(DOC)

Table S2 Primers used for attaching each epitope to MuHV-4 M2 C-terminus.
(DOC)

Acknowledgments

The authors thank Bruno Frederico for initial help making some recombinant viruses.

Author Contributions

Conceived and designed the experiments: CGS SM HVF PGS JPS. Performed the experiments: CGS SM DF. Analyzed the data: CGS SM DF HVF PGS JPS. Contributed reagents/materials/analysis tools: CGS SM. Contributed to the writing of the manuscript: CGS PGS JPS.

References

1. Stevenson PG, Simas JP, Efstathiou S (2009) Immune control of mammalian gamma-herpesviruses: lessons from murid herpesvirus-4. J Gen Virol 90: 2317–2330.
2. Bollard CM, Rooney CM, Heslop HE (2012) T-cell therapy in the treatment of post-transplant lymphoproliferative disease. Nat Rev Clin Oncol 9: 510–519.
3. Thorley-Lawson DA (2001) Epstein-Barr virus: exploiting the immune system. Nat Rev Immunol 1: 75–82.
4. Simas JP, Efstathiou S (1998) Murine gammaherpesvirus 68: a model for the study of gammaherpesvirus pathogenesis. Trends Microbiol 6: 276–282.
5. Speck SH, Ganem D (2010) Viral latency and its regulation: lessons from the gamma-herpesviruses. Cell Host Microbe 8: 100–115.
6. Nash AA, Dutia BM, Stewart JP, Davison AJ (2001) Natural history of murine gamma-herpesvirus infection. Philos Trans R Soc Lond B Biol Sci 356: 569–579.
7. Virgin HWt, Latreille P, Wamsley P, Hallsworth K, Weck KE, et al. (1997) Complete sequence and genomic analysis of murine gammaherpesvirus 68. J Virol 71: 5894–5904.
8. Simas JP, Marques S, Bridgeman A, Efstathiou S, Adler H (2004) The M2 gene product of murine gammaherpesvirus 68 is required for efficient colonization of splenic follicles but is not necessary for expansion of latently infected germinal centre B cells. J Gen Virol 85: 2789–2797.
9. Flano E, Kim IJ, Woodland DL, Blackman MA (2002) Gamma-herpesvirus latency is preferentially maintained in splenic germinal center and memory B cells. J Exp Med 196: 1363–1372.
10. Marques S, Efstathiou S, Smith KG, Haury M, Simas JP (2003) Selective gene expression of latent murine gammaherpesvirus 68 in B lymphocytes. J Virol 77: 7308–7318.
11. Bennett NJ, May JS, Stevenson PG (2005) Gamma-herpesvirus latency requires T cell evasion during episome maintenance. PLoS Biol 3: e120.
12. Levitskaya J, Coram M, Levitsky V, Imreh S, Steigerwald-Mullen PM, et al. (1995) Inhibition of antigen processing by the internal repeat region of the Epstein-Barr virus nuclear antigen-1. Nature 375: 685–688.
13. Hislop AD, Ressing ME, van Leeuwen D, Pudney VA, Horst D, et al. (2007) A CD8+ T cell immune evasion protein specific to Epstein-Barr virus and its close relatives in Old World primates. J Exp Med 204: 1863–1873.
14. Horst D, van Leeuwen D, Croft NP, Garstka MA, Hislop AD, et al. (2009) Specific targeting of the EBV lytic phase protein BNLF2a to the transporter associated with antigen processing results in impairment of HLA class I-restricted antigen presentation. J Immunol 182: 2313–2324.
15. Croft NP, Shannon-Lowe C, Bell AI, Horst D, Kremmer E, et al. (2009) Stage-specific inhibition of MHC class I presentation by the Epstein-Barr virus BNLF2a protein during virus lytic cycle. PLoS Pathog 5: e1000490.
16. Zuo J, Currin A, Griffin BD, Shannon-Lowe C, Thomas WA, et al. (2009) The Epstein-Barr virus G-protein-coupled receptor contributes to immune evasion by targeting MHC class I molecules for degradation. PLoS Pathog 5: e1000255.
17. Zuo J, Quinn LL, Tamblyn J, Thomas WA, Feederle R, et al. (2011) The Epstein-Barr virus-encoded BILF1 protein modulates immune recognition of endogenously processed antigen by targeting major histocompatibility complex class I molecules trafficking on both the exocytic and endocytic pathways. J Virol 85: 1604–1614.
18. Fruh K, Bartee E, Gouveia K, Mansouri M (2002) Immune evasion by a novel family of viral PHD/LAP-finger proteins of gamma-2 herpesviruses and poxviruses. Virus Res 88: 55–69.
19. Boname JM, Stevenson PG (2001) MHC class I ubiquitination by a viral PHD/LAP finger protein. Immunity 15: 627–636.
20. Boname JM, de Lima BD, Lehner PJ, Stevenson PG (2004) Viral degradation of the MHC class I peptide loading complex. Immunity 20: 305–317.
21. Boname JM, May JS, Stevenson PG (2005) The murine gamma-herpesvirus-68 MK3 protein causes TAP degradation independent of MHC class I heavy chain degradation. Eur J Immunol 35: 171–179.
22. Stevenson PG, May JS, Smith XG, Marques S, Adler H, et al. (2002) K3-mediated evasion of CD8(+) T cells aids amplification of a latent gamma-herpesvirus. Nat Immunol 3: 733–740.
23. Rodrigues L, Pires de Miranda M, Caloca MJ, Bustelo XR, Simas JP (2006) Activation of Vav by the gammaherpesvirus M2 protein contributes to the establishment of viral latency in B lymphocytes. J Virol 80: 6123–6135.
24. Pires de Miranda M, Lopes FB, McVey CE, Bustelo XR, Simas JP (2013) Role of Src homology domain binding in signaling complexes assembled by the murid gamma-herpesvirus M2 protein. J Biol Chem 288: 3858–3870.
25. Siegel AM, Herskowitz JH, Speck SH (2008) The MHV68 M2 protein drives IL-10 dependent B cell proliferation and differentiation. PLoS Pathog 4: e1000039.
26. Rangaswamy US, Speck SH (2014) Murine gammaherpesvirus M2 protein induction of IRF4 via the NFAT pathway leads to IL-10 expression in B cells. PLoS Pathog 10: e1003858.
27. Burkhardt AL, Bolen JB, Kieff E, Longnecker R (1992) An Epstein-Barr virus transformation-associated membrane protein interacts with src family tyrosine kinases. J Virol 66: 5161–5167.
28. Lee H, Guo J, Li M, Choi JK, DeMaria M, et al. (1998) Identification of an immunoreceptor tyrosine-based activation motif of K1 transforming protein of Kaposi's sarcoma-associated herpesvirus. Mol Cell Biol 18: 5219–5228.
29. Marques S, Alenquer M, Stevenson PG, Simas JP (2008) A single CD8+ T cell epitope sets the long-term latent load of a murid herpesvirus. PLoS Pathog 4: e1000177.
30. Wang X, Liu X, Jia Y, Chao Y, Xing X, et al. (2010) Widespread sequence variation in the Epstein-Barr virus latent membrane protein 2A gene among northern Chinese isolates. J Gen Virol 91: 2564–2573.
31. Stebbing J, Bourboulia D, Johnson M, Henderson S, Williams I, et al. (2003) Kaposi's sarcoma-associated herpesvirus cytotoxic T lymphocytes recognize and target Darwinian positively selected autologous K1 epitopes. J Virol 77: 4306–4314.
32. Guihot A, Dupin N, Marcelin AG, Gorin I, Bedin AS, et al. (2006) Low T cell responses to human herpesvirus 8 in patients with AIDS-related and classic Kaposi sarcoma. J Infect Dis 194: 1078–1088.
33. Brander C, O'Connor P, Suscovich T, Jones NG, Lee Y, et al. (2001) Definition of an optimal cytotoxic T lymphocyte epitope in the latently expressed Kaposi's sarcoma-associated herpesvirus kaposin protein. J Infect Dis 184: 119–126.
34. Husain SM, Usherwood EJ, Dyson H, Coleclough C, Coppola MA, et al. (1999) Murine gammaherpesvirus M2 gene is latency-associated and its protein a target for CD8(+) T lymphocytes. Proc Natl Acad Sci U S A 96: 7508–7513.
35. Usherwood EJ, Roy DJ, Ward K, Surman SL, Dutia BM, et al. (2000) Control of gammaherpesvirus latency by latent antigen-specific CD8(+) T cells. J Exp Med 192: 943–952.

36. Stevenson PG, Cardin RD, Christensen JP, Doherty PC (1999) Immunological control of a murine gammaherpesvirus independent of CD8+ T cells. J Gen Virol 80 (Pt 2): 477–483.
37. Tibbetts SA, van Dyk LF, Speck SH, Virgin HWt (2002) Immune control of the number and reactivation phenotype of cells latently infected with a gammaherpesvirus. J Virol 76: 7125–7132.
38. Midgley RS, Bell AI, McGeoch DJ, Rickinson AB (2003) Latent gene sequencing reveals familial relationships among Chinese Epstein-Barr virus strains and evidence for positive selection of A11 epitope changes. J Virol 77: 11517–11530.
39. Midgley RS, Bell AI, Yao QY, Croom-Carter D, Hislop AD, et al. (2003) HLA-A11-restricted epitope polymorphism among Epstein-Barr virus strains in the highly HLA-A11-positive Chinese population: incidence and immunogenicity of variant epitope sequences. J Virol 77: 11507–11516.
40. Chen Y, Yao K, Wang B, Qing J, Liu G (2008) Potent dendritic cell vaccine loaded with latent membrane protein 2A (LMP2A). Cell Mol Immunol 5: 365–372.
41. Vigano S, Utzschneider DT, Perreau M, Pantaleo G, Zehn D, et al. (2012) Functional avidity: a measure to predict the efficacy of effector T cells? Clin Dev Immunol 2012: 153863.
42. Matsumura M, Saito Y, Jackson MR, Song ES, Peterson PA (1992) In vitro peptide binding to soluble empty class I major histocompatibility complex molecules isolated from transfected Drosophila melanogaster cells. J Biol Chem 267: 23589–23595.
43. Schumacher TN, Heemels MT, Neefjes JJ, Kast WM, Melief CJ, et al. (1990) Direct binding of peptide to empty MHC class I molecules on intact cells and in vitro. Cell 62: 563–567.
44. Chen W, Khilko S, Fecondo J, Margulies DH, McCluskey J (1994) Determinant selection of major histocompatibility complex class I-restricted antigenic peptides is explained by class I-peptide affinity and is strongly influenced by nondominant anchor residues. J Exp Med 180: 1471–1483.
45. Fremont DH, Stura EA, Matsumura M, Peterson PA, Wilson IA (1995) Crystal structure of an H-2Kb-ovalbumin peptide complex reveals the interplay of primary and secondary anchor positions in the major histocompatibility complex binding groove. Proc Natl Acad Sci U S A 92: 2479–2483.
46. Alam SM, Travers PJ, Wung JL, Nasholds W, Redpath S, et al. (1996) T-cell-receptor affinity and thymocyte positive selection. Nature 381: 616–620.
47. Zehn D, Lee SY, Bevan MJ (2009) Complete but curtailed T-cell response to very low-affinity antigen. Nature 458: 211–214.
48. Jameson SC, Carbone FR, Bevan MJ (1993) Clone-specific T cell receptor antagonists of major histocompatibility complex class I-restricted cytotoxic T cells. J Exp Med 177: 1541–1550.
49. Hogquist KA, Jameson SC, Heath WR, Howard JL, Bevan MJ, et al. (1994) T cell receptor antagonist peptides induce positive selection. Cell 76: 17–27.
50. Collins CM, Boss JM, Speck SH (2009) Identification of infected B-cell populations by using a recombinant murine gammaherpesvirus 68 expressing a fluorescent protein. J Virol 83: 6484–6493.
51. Stevenson PG, Belz GT, Altman JD, Doherty PC (1999) Changing patterns of dominance in the CD8+ T cell response during acute and persistent murine gamma-herpesvirus infection. Eur J Immunol 29: 1059–1067.
52. Price DA, Brenchley JM, Ruff LE, Betts MR, Hill BJ, et al. (2005) Avidity for antigen shapes clonal dominance in CD8+ T cell populations specific for persistent DNA viruses. J Exp Med 202: 1349–1361.
53. Callan MF, Steven N, Krausa P, Wilson JD, Moss PA, et al. (1996) Large clonal expansions of CD8+ T cells in acute infectious mononucleosis. Nat Med 2: 906–911.
54. Hislop AD, Taylor GS, Sauce D, Rickinson AB (2007) Cellular responses to viral infection in humans: lessons from Epstein-Barr virus. Annu Rev Immunol 25: 587–617.
55. Ehtisham S, Sunil-Chandra NP, Nash AA (1993) Pathogenesis of murine gammaherpesvirus infection in mice deficient in CD4 and CD8 T cells. J Virol 67: 5247–5252.
56. Frederico B, Chao B, May JS, Belz GT, Stevenson PG (2014) A murid gammaherpesviruses exploits normal splenic immune communication routes for systemic spread. Cell Host Microbe 15: 457–470.
57. Smith CM, Gill MB, May JS, Stevenson PG (2007) Murine gammaherpesvirus-68 inhibits antigen presentation by dendritic cells. PLoS ONE 2: e1048.
58. El-Gogo S, Flach B, Staib C, Sutter G, Adler H (2008) In vivo attenuation of recombinant murine gammaherpesvirus 68 (MHV-68) is due to the expression and immunogenicity but not to the insertion of foreign sequences. Virology 380: 322–327.
59. Loh J, Popkin DL, Droit L, Braaten DC, Zhao G, et al. (2012) Specific mutation of a gammaherpesvirus-expressed antigen in response to CD8 T cell selection in vivo. J Virol 86: 2887–2893.
60. Cardin RD, Brooks JW, Sarawar SR, Doherty PC (1996) Progressive loss of CD8+ T cell-mediated control of a gamma-herpesvirus in the absence of CD4+ T cells. J Exp Med 184: 863–871.
61. Belz GT, Stevenson PG, Castrucci MR, Altman JD, Doherty PC (2000) Postexposure vaccination massively increases the prevalence of gamma-herpesvirus-specific CD8+ T cells but confers minimal survival advantage on CD4-deficient mice. Proc Natl Acad Sci U S A 97: 2725–2730.

APPENDIX 2

LETTER

doi:10.1038/nature13158

Maternal retinoids control type 3 innate lymphoid cells and set the offspring immunity

Serge A. van de Pavert[1]†*, Manuela Ferreira[2]*, Rita G. Domingues[2], Hélder Ribeiro[2], Rosalie Molenaar[1], Lara Moreira-Santos[2], Francisca F. Almeida[2], Sales Ibiza[2], Inês Barbosa[2], Gera Goverse[1], Carlos Labão-Almeida[2], Cristina Godinho-Silva[2], Tanja Konijn[1], Dennis Schooneman[1], Tom O'Toole[1], Mark R. Mizee[1], Yasmin Habani[1], Esther Haak[3], Fabio R. Santori[4], Dan R. Littman[4], Stefan Schulte-Merker[5], Elaine Dzierzak[3], J. Pedro Simas[2], Reina E. Mebius[1]* & Henrique Veiga-Fernandes[2]*

The impact of nutritional status during fetal life on the overall health of adults has been recognized[1]; however, dietary effects on the developing immune system are largely unknown. Development of secondary lymphoid organs occurs during embryogenesis and is considered to be developmentally programmed[2,3]. Secondary lymphoid organ formation depends on a subset of type 3 innate lymphoid cells (ILC3) named lymphoid tissue inducer (LTi) cells[2–5]. Here we show that mouse fetal ILC3s are controlled by cell-autonomous retinoic acid (RA) signalling *in utero*, which pre-sets the immune fitness in adulthood. We found that embryonic lymphoid organs contain ILC progenitors that differentiate locally into mature LTi cells. Local LTi cell differentiation was controlled by maternal retinoid intake and fetal RA signalling acting in a haematopoietic cell-autonomous manner. RA controlled LTi cell maturation upstream of the transcription factor RORγt. Accordingly, enforced expression of *Rorgt* restored maturation of LTi cells with impaired RA signalling, whereas RA receptors directly regulated the *Rorgt* locus. Finally, we established that maternal levels of dietary retinoids control the size of secondary lymphoid organs and the efficiency of immune responses in the adult offspring. Our results reveal a molecular link between maternal nutrients and the formation of immune structures required for resistance to infection in the offspring.

Haematopoietic cells that initially colonize secondary lymphoid organ (SLO) sites include $CD3^-$c-Kit^+IL-$7R\alpha^-\alpha4\beta7^+CD11c^+CD4^-$ lymphoid tissue initiator (LTin) cells and the prototypical member of type 3 ILCs, LTi cells[2–7]. Although most LTi cells express CD4, this is a late event in LTi differentiation and not all $ROR\gamma t^+$ LTi cells express this marker[5,6,8,9]. Thus, we proposed that $CD3^-$IL-$7R\alpha^+\alpha4\beta7^+ID2^+$c-$Kit^+CD11c^-CD4^-$ ILCs (hereafter called ILC_{4neg} cells) receive local cues giving rise to $ID2^+ROR\gamma t^+CD4^+$ LTi cells (LTi_4) within developing SLOs. Notably, enteric ILC_{4neg} cells include mainly $ID2^+ROR\gamma t^+CD4^-$ LTi cells (LTi_0) but also a small fraction of $ID2^+ROR\gamma t^-CD4^-$ precursors with LTi cell potential (hereafter called pre-ILC cells)[9]. In contrast, nearly 100% of lymph node ILC_{4neg} cells are LTi_0 cells (Extended Data Fig. 1a, b). Analysis of embryonic day 12.5 (E12.5) guts revealed that ILC_{4neg} cells are the only appreciable IL-$7R\alpha^+$ colonizing cells (Fig. 1a, b). Accordingly, non-cycling mature $Sca1^-$ LTi_4 cells increased throughout development, seemingly at the expense of $Sca1^+$ ILC_{4neg} cells (Fig. 1a–c and Extended Data Fig. 1c). Further evidence that ILC_{4neg} cells differentiate locally was provided by organ cultures and transplantation of E12.5 intestines. Despite absence of fetal liver output in these settings, LTi_4 cells increased with time at the expense of local ILC_{4neg} cells (Fig. 1d, e). Furthermore, in E14.5 $Rorgt^{-/-}$ embryos, ILC_{4neg} cells were attracted to the intestine and lymph nodes, supporting initial anlagen colonization by these cells (Extended Data Fig. 1d, e). Notably, RA stimulation of E13.5 lymph node cells showed increased frequency of LTi_4 cells and reduction of ILC_{4neg} cells, indicating that differentiation of LTi_4 cells is regulated by RA (Fig. 1f). To confirm the effect of RA in LTi differentiation *in vivo*, pregnant mice received a RA-enriched diet starting at E10.5. Supplementation of RA increased the proportion of LTi_4 cells in the embryo, to the detriment of ILC_{4neg} cells (Fig. 1f). In agreement with this finding, provision of the RA signalling inhibitor BMS493 to pregnant female mice resulted in a decrease of fetal LTi_4 cells despite normal frequency of fetal liver progenitors and enteric haematopoietic cells (Fig. 1f and Extended Data Fig. 1f). Consequently, despite normal embryo size, BMS493 administration led to a reduction in lymph node dimensions and Peyer's patch developmental failure (Fig. 1g–i and Extended Data Fig. 1g). Collectively, our data indicate that maternal retinoids control LTi cell differentiation within developing SLOs.

RA is a vitamin A metabolite that controls early vertebrate development, some immune processes in adulthood, and has been shown to mediate CXCL13 expression in fetal mesenchymal cells[10–16]. RA binds to heterodimers formed by the RA receptors (RARs) and retinoid X receptors (RXRs), which bind DNA RA response elements (RAREs)[11]. To address putative RA cell-autonomous responses, we assessed RAR and RXR expression in E15.5 ILC_{4neg}, LTi_4 and LTin cells. RARs and RXRs were predominantly expressed by ILC_{4neg} and LTi_4 cells, whereas LTin cells expressed these molecules at lower levels (Fig. 2a). RA stimulation revealed that only ILC_{4neg} and LTi_4 cells respond robustly, as shown by *Rarb* upregulation (Fig. 2b)[16]. Together, these data indicate that impaired SLO development in BMS493-treated mice might be the consequence of RA signal ablation in LTi cells. To test this hypothesis we used a lineage-targeted model to block RA signalling. We used a mouse line in which a truncated form of the RARα gene was knocked into the *ROSA26* locus preceded by a triple polyadenylation signal flanked by two *loxP* sites (*ROSA26*-RARα403). This line was bred to *Vav*-iCre mice that in contrast to other tested Cre lines ensured Cre activity in fetal LTin, ILC_{4neg} and LTi_4 cells (Extended Data Fig. 2a–d)[17,18]. Despite normal frequencies of fetal liver precursors, and SLO LTin, ILC_{4neg} and LTi_0 cells, *Vav*-iCre/*ROSA26*-RARα403 embryos (Rar mice) revealed a dose-dependent reduction of LTi_4 cells (Fig. 2c, d and Extended Data Fig. 3a–f). To assess whether the differentiation potential of ILC_{4neg} cells is controlled by RA thresholds, we cultured purified ILC_{4neg} cells from Rar heterozygous (Rar^{Het}), homozygous (Rar^{Hom}) and wild-type littermate control mice. Whereas wild-type ILC_{4neg} cells upregulated pro-inflammatory cytokines and chemokines and gave rise to LTi_4 cells *in vitro*, these were impaired proportionally to the degree of RA signalling abrogation in ILC_{4neg} cells (Fig. 2e, f and Extended Data Fig. 3g). Finally, despite normal frequency of colonizing ILC_{4neg} cells (Fig. 2d),

[1]Department of Molecular Cell Biology and Immunology, VU University Medical Center, van der Boechorststraat 7, 1081BT Amsterdam, The Netherlands. [2]Instituto de Medicina Molecular, Faculdade de Medicina de Lisboa, Av. Prof. Egas Moniz, Edifício Egas Moniz, 1649-028 Lisboa, Portugal. [3]Erasmus Stem Cell Institute, Department of Cell Biology, Erasmus Medical Center, 3000 CA Rotterdam, The Netherlands. [4]Howard Hughes Medical Institute, Molecular Pathogenesis Program, Skirball Institute of Biomolecular Medicine, New York University School of Medicine, New York, New York 10016, USA. [5]Hubrecht Institute–KNAW (Royal Netherlands Academy of Arts and Sciences) and University Medical Center Utrecht, 3584 CT Utrecht, Netherlands. †Present address: Hubrecht Institute–KNAW (Royal Netherlands Academy of Arts and Sciences) and University Medical Center Utrecht, 3584 CT Utrecht, Netherlands.
*These authors contributed equally to this work.

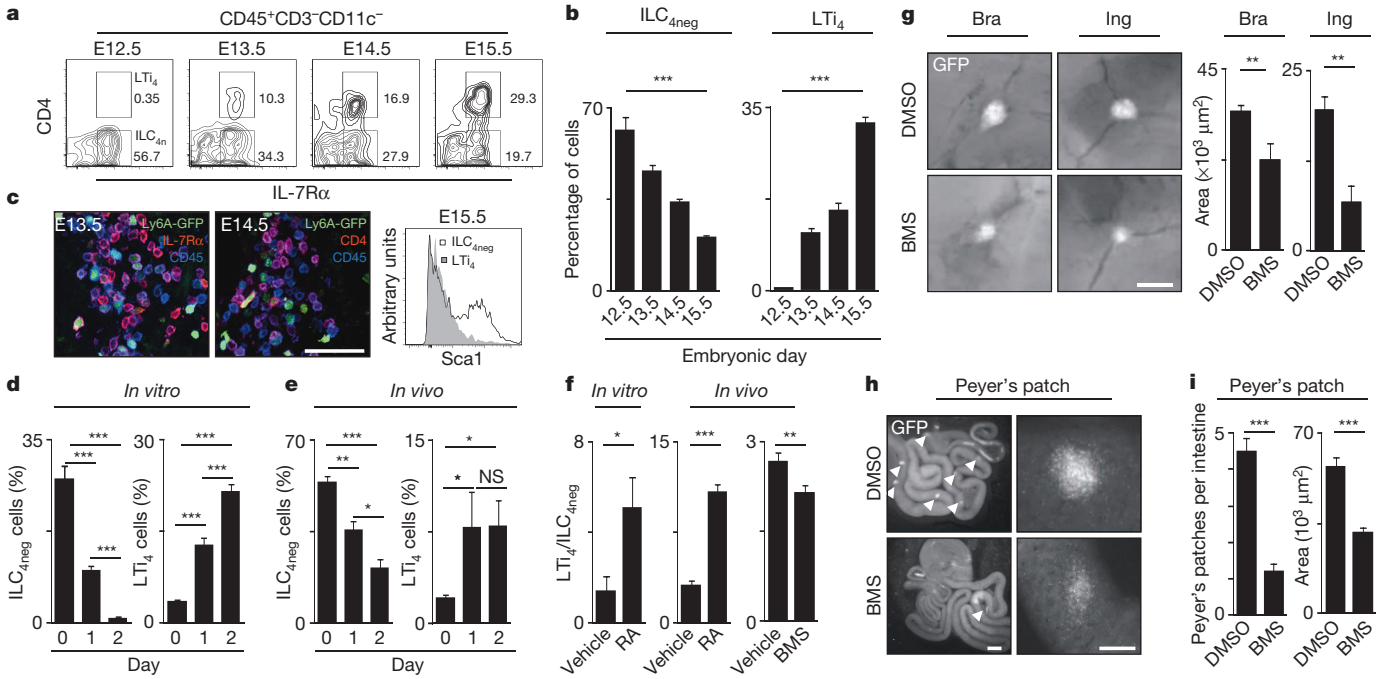

Figure 1 | Maternal RA controls LTi differentiation. **a**, Enteric fetal ILC_{4neg} and LTi_4 cells. **b**, Percentage of enteric fetal ILC_{4neg} and LTi_4 cells. E12.5, $n = 8$; E13.5, $n = 3$; E14.5, $n = 6$; E15.5, $n = 3$. **c**, Left: *Sca1-GFP* lymph nodes. Right: E15.5 gut cells. **d**, **e**, Cultured or transplanted E12.5 guts. **d**, Day 0, $n = 4$; day 1, $n = 6$; day 2, $n = 6$. **e**, Day 0, $n = 7$; day 1, $n = 3$; day 2, $n = 5$. **f**, Left: E13.5 lymph node cells; $n = 7$. Centre: RA was provided to females. E13.5 lymph node cells; $n = 8$. Right: females received BMS493; $n = 8$. LTi_4/ILC_{4neg} cell ratio is shown. **g**–**i**, *hCD2-GFP* females received BMS493. E17.5 SLOs. **g**, Brachial (Bra) and inguinal (Ing) lymph nodes; $n = 6$. **h**, Arrowheads indicate Peyer's patch. **i**, Peyer's patch number per intestine: DMSO, $n = 8$; BMS, $n = 22$. Area: DMSO, $n = 30$; BMS, $n = 25$. Scale bars: 50 μm (**c**), 200 μm (**g**, **h** right), 1 mm (**h**, left). Error bars show s.e. $*P < 0.05$; $**P < 0.01$; $***P < 0.001$. NS, not significant.

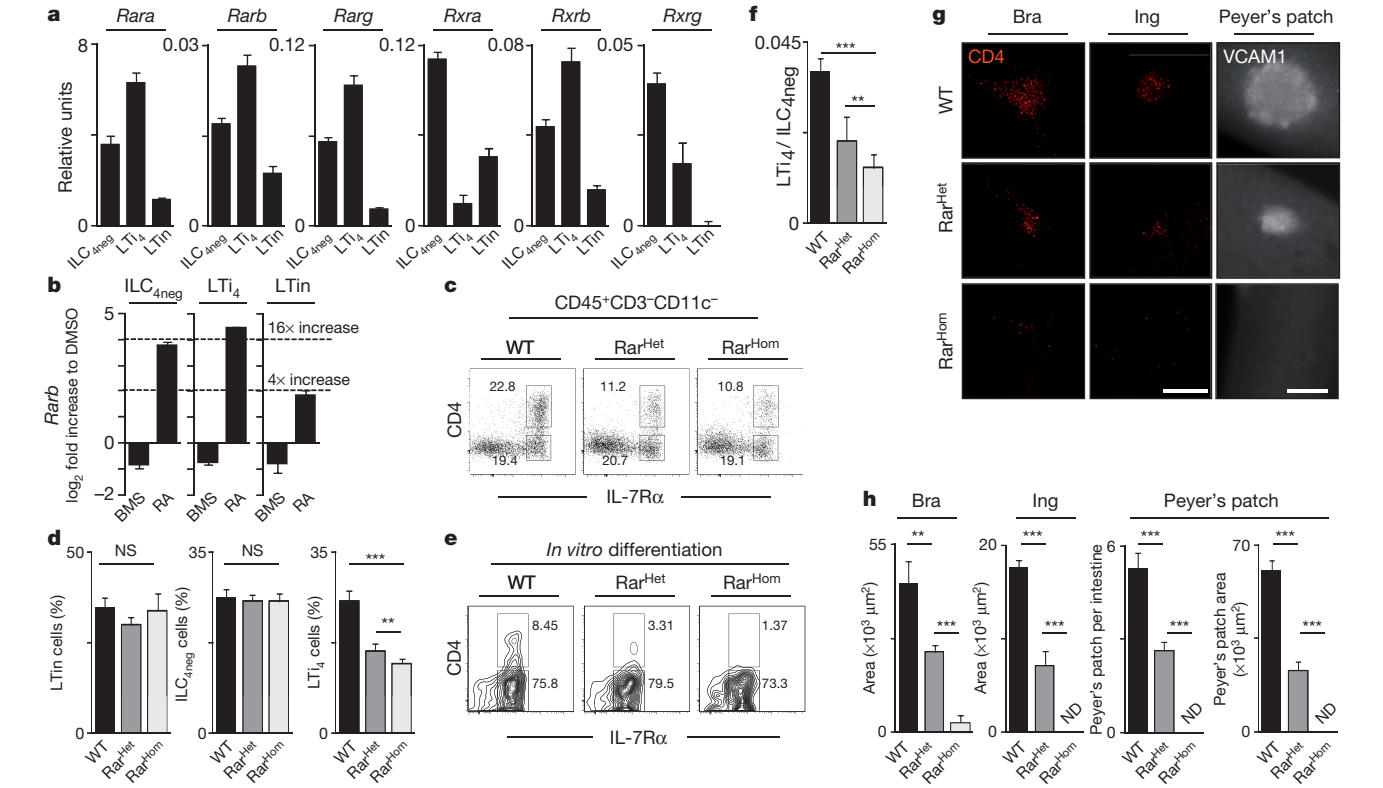

Figure 2 | Cell-autonomous RA controls LTi cells and SLO development. **a**, RT–PCR of enteric cells. Data represent three independent experiments. **b**, DMSO, BMS493 or RA stimulation. Data represent three independent experiments. **c**, E15.5 enteric ILC subsets. **d**, LTin, $n = 4$; ILC_{4neg}, $n = 5$; LTi_4, $n = 5$. **e**, E15.5 ILC_{4neg} cells cultured for 6 days. **f**, ILC_{4neg} cell cultures at day 6; $n = 5$. **g**, Immunostaining of E15.5 embryos and intestines. Developing brachial (Bra) and inguinal (Ing) lymph nodes and Peyer's patch are shown. CD4, red; VCAM1, grey. Scale bars: 200 μm. **h**, SLO size; $n = 6$. Error bars show s.e. $*P < 0.05$; $**P < 0.01$; $***P < 0.001$. NS, not significant. ND, not detected.

haematopoietic cell-autonomous impairment of RA responses resulted in severely diminished fetal lymph node size and reduced number of minute Peyer's patches (Fig. 2g, h and Extended Data Fig. 3h). Our data indicate that LTi cell differentiation is controlled by cell-autonomous RA signalling in developing SLOs.

Previous reports have identified key LTi cell regulators[2]. Mice mutant for the transcription factors ID2 and RORγt lack LTi cells and do not develop SLOs[19,20]. *Runx1*, *Tox* and *Notch1* were also implicated in LTi cell maturation[9,21–23]. We found that whereas most LTi-related genes were normally expressed in Rar^{Hom} and Rar^{Het} ILC_{4neg} and LTi_4 cells, *Runx1* was increased and *Rorgt* was reduced (Fig. 3a and Extended Data Fig. 4a–d). Expression of pro-inflammatory genes was also reduced in Rar^{Hom} and Rar^{Het} ILC_{4neg} and LTi_4 cells (Fig. 3a and Extended Data Fig. 4b–d). The marked reduction of *Rorgt* expression suggested that RA could provide ILC_{4neg} cells with signals leading to *Rorgt* regulation. Accordingly, RA stimulation of ILC_{4neg} cells resulted in *Rorgt* upregulation whereas most other transcription factors were unperturbed, notably *Runx1* (Fig. 3b). In agreement, BMS493 inhibited RA-induced *Rorgt* expression, and efficient block of RORγt by digoxin prevented RA-induced differentiation of ILC_{4neg} cells into LTi_4 cells, while cell viability was unaffected (Fig. 3c and Extended Data Fig. 5a–c). To test further whether RA-induced LTi maturation requires RORγt, we determined if differentiation of RAR dominant-negative ILC_{4neg} cells is restored by enforced *Rorgt* expression. Retroviral transduction of *Rorgt* revealed that RAR dominant-negative ILC_{4neg} cells restored high levels of pro-inflammatory genes and reacquired their potential to differentiate towards LTi_4 cells (Fig. 3d–f). Further evidence that RA can directly regulate *Rorgt* expression was provided by computational analysis of potential RARE sites and chromatin immunoprecipitation (ChIP) with pan-RAR and RXR antibodies. RA stimulation resulted in increased binding of RAR and RXR upstream and within the *Rorgt* locus (Fig. 3g, h and Extended Data Table 1). To analyse the role of these sites we introduced the RARE C (−5,478 *Rorg* transcription start site (TSS)), E (−1,800 *Rorg* TSS) and G (−1,619 *Rorgt* TSS) half-sites in a luciferase reporter vector. Mutations in these sites resulted in significant reduction of the regulatory function of these elements as measured by luciferase activity (Fig. 3i). Thus, cell-autonomous RA signalling provides LTi cells with critical differentiation signals via direct regulation of *Rorgt*.

Our data indicate that mature LTi cell numbers regulate the size of SLO primordia and may determine lymphoid organ size in adulthood[24]. Rar^{Het} adult mice had reduced SLOs and lymphocyte numbers when compared to their wild-type littermate controls (Fig. 4a, b and Extended Data Fig. 6a, b). In agreement, mice that received a vitamin-A-deficient (VAD) diet throughout life had reduced lymphoid organ size when compared to vitamin-A-control mice (VAC) (Fig. 4c). However, because Rar^{Het} and VAD lymphocytes are continuously exposed to altered levels of RA signals, it is possible that SLO size might be a consequence of altered lymphocyte pools[12–15]. To clarify this issue, we provided pregnant mice with a vitamin-A-high (VAH), VAD or VAC diet and switched all diets to the same VAC diet after birth. At 10 weeks of age mice that were exposed to a VAH diet exclusively *in utero* had larger SLOs, whereas mice exposed to a VAD diet had small SLOs when compared to VAC control mice (Fig. 4d). Notably, provision of variable vitamin A diet levels exclusively after birth no longer controlled SLO size (Extended Data Fig. 6c, d). Additional evidence that RA determines SLO size in early life was provided by transplantation of CD45.1 wild-type bone marrow into lethally irradiated Rar^{Het} (WT→Rar^{Het}) or wild-type (WT→WT) CD45.2 littermate control hosts at 2 weeks of age (Fig. 4e). Thus, we generated mice that pre- and perinatally received low input of RA signals in haematopoietic cells, but that on transplantation harbour a normal wild-type haematopoietic system. WT→Rar^{Het} mice, which received low RA cues *in utero*, exhibited small SLOs when compared to their WT→WT counterparts at 8 weeks after transplantation (Fig. 4f, g and Extended Data Fig. 6e, f). This phenotype also revealed reduced lymphocyte numbers, albeit normal SLO organization and similar haematopoietic cell reconstitution (Fig. 4h and Extended Data Figs 6f and 7a–d). In agreement, dendritic cells from WT→Rar^{Het} or WT→WT chimaeras had similar capacity to activate lymphocytes (Extended Data Fig. 7e, f).

Our data indicate that available RA *in utero* regulates the size of lymphocyte pools in the offspring, with possible consequences on their adaptive immune responses. To test this hypothesis, WT→Rar^{Het} or WT→WT chimaeras were infected intranasally with murid herpesvirus-4, resulting in acute lung infection. Analysis of draining intrathoracic lymph nodes revealed reduced expansion but normal frequency of $CD8^+$ T cells specific for the viral epitopes ORF61 and ORF75c in WT→Rar^{Het} mice (Fig. 4i and Extended Data Fig. 8a–c). Consequently, whereas

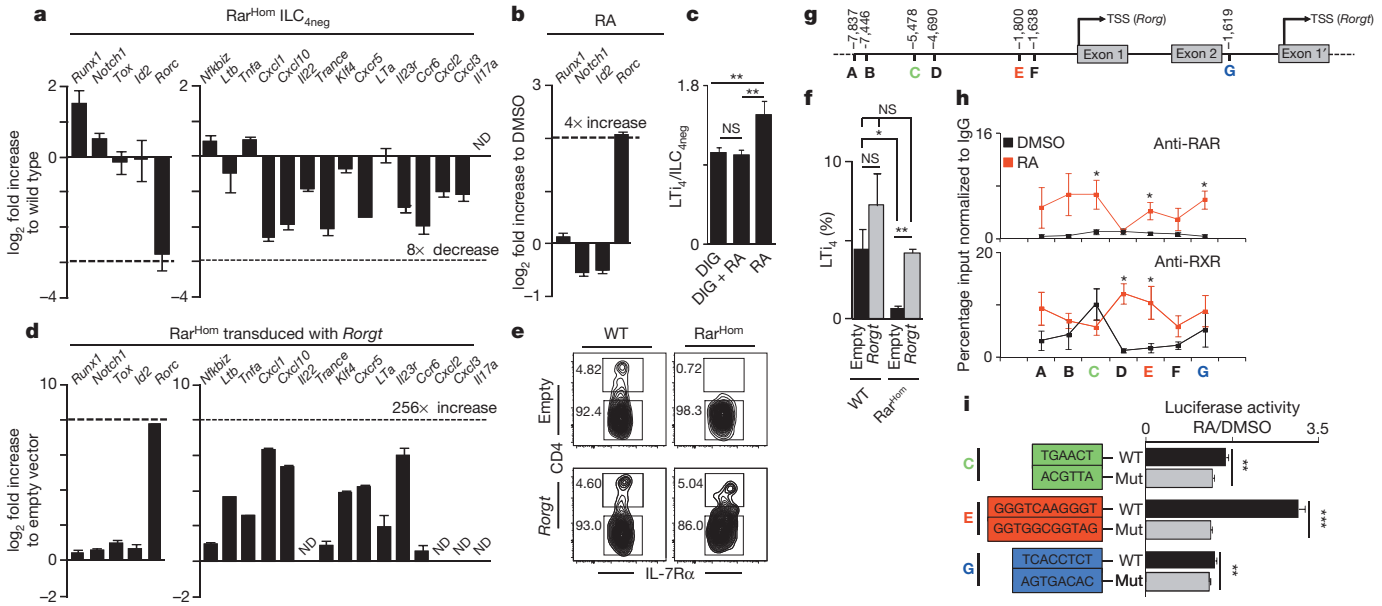

Figure 3 | RA controls LTi cells via RORγt. **a**, E15.5 ILC_{4neg} cells. Data represent three experiments. **b**, E15.5 ILC_{4neg} cells stimulated with RA. Data represent three experiments. **c**, E13.5 lymph node cells stimulated with RA and digoxin (DIG); $n = 16$. **d**–**f**, ILC_{4neg} cells transduced with pMig. *Rorgt*-IRES-GFP virus (day 6). **d**, Data represent three experiments. **e**, Cytometry analysis. **f**, Emergent LTi_4 cells. Wild type (WT), $n = 5$; Rar^{Hom}, $n = 3$. **g**, RARE sites. **h**, E15.5 ILC_{4neg} cells stimulated with RA. ChIP analysis of five biological replicates. **i**, Luciferase activity of RARE wild-type and mutated sites. C, $n = 6$; E, $n = 9$; G, $n = 6$. Error bars show s.e. $^*P < 0.05$; $^{**}P < 0.01$; $^{***}P < 0.001$. NS, not significant. ND, not detected.

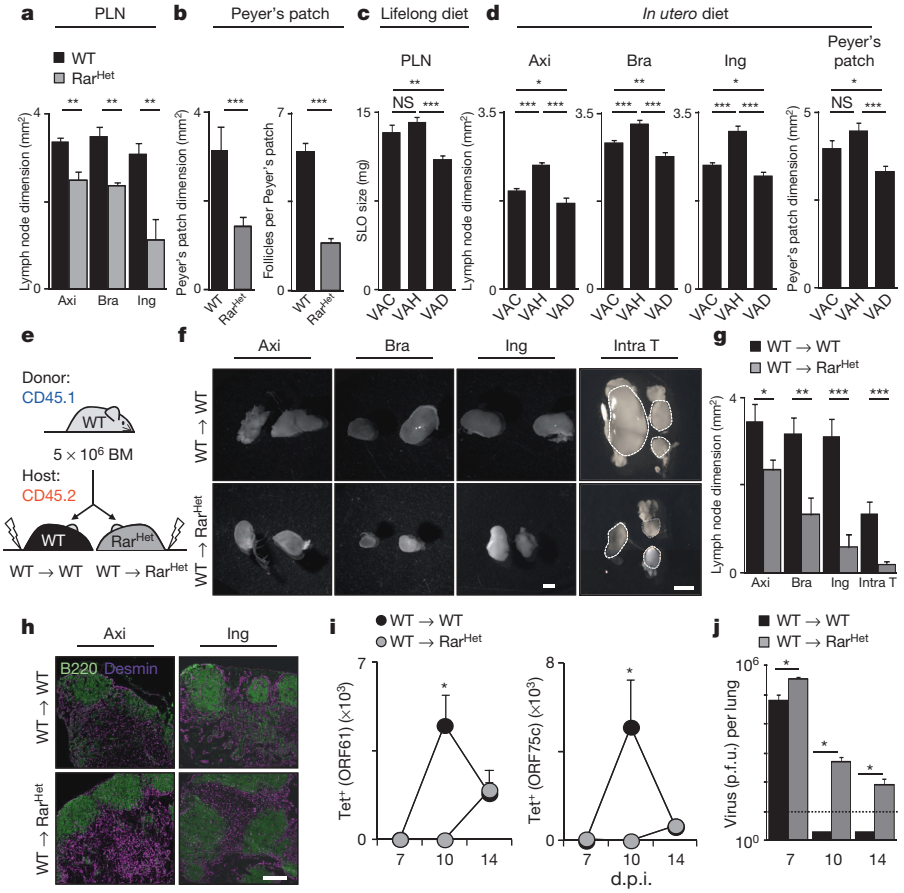

Figure 4 | Retinoid levels *in utero* determine the offspring resistance to infection. **a**, Adult axillary (Axi), brachial (Bra) and inguinal (Ing) peripheral lymph nodes (PLN). $n = 6$. **b**, Peyer's patch area and follicle number per Peyer's patch. Wild type (WT), $n = 26$; Rar^{Het}, $n = 23$. **c**, Females received diets that were maintained in the offspring. VAC, $n = 10$; VAH, $n = 8$; VAD, $n = 18$. **d**, Females received variable diets. Their offspring received VAC diet. Lymph node: VAC, $n = 18$; VAH, $n = 24$; VAD, $n = 25$. Peyer's patch: VAC, $n = 20$; VAH, $n = 40$; VAD, $n = 63$. **e**, Transplantation scheme. **f**, Chimaeric lymph nodes. Scale bar: 1 mm. **g**, Dimensions of chimaeric lymph nodes. $n = 6$. **h**, Chimaeric lymph node structure. Scale bar: 200 μm. **i**, Chimaeras infected with murid herpesvirus-4. Tetramer positive CD8 T cells in intrathoracic lymph nodes. **j**, Virus titres (plaque-forming units (p.f.u.) per lung). 7 days post infection (d.p.i.): WT→WT, $n = 3$; WT→Rar^{Het}, $n = 3$. 10 d.p.i.: WT→WT, $n = 4$; WT→Rar^{Het}, $n = 3$. 14 d.p.i.: WT→WT, $n = 8$; WT→Rar^{Het}, $n = 5$. Dashed line indicates the detection limit. Error bars show s.e. $^{*}P < 0.05$; $^{**}P < 0.01$; $^{***}P < 0.001$. NS, not significant.

WT→WT chimaeras efficiently cleared lytic virus by day 10, high viral titres were still detected in WT→Rar^{Het} chimaeras 14 days after infection (Fig. 4j)[25]. Thus, a deficit of RA signals within haematopoietic cells in early life results in small SLOs and poor capacity to control infection.

Defining the requirements that control SLO development is essential to understand how immunity may be regulated. We now show that RA controls LTi cells, regulating LTi pro-inflammatory genes and the frequency of LTi_4 cells (Extended Data Fig. 9). RA operates in a cell-autonomous fashion, via RORγt, although additional factors regulate *Rorgt* in ILC3s.

SLO development has been considered to be developmentally programmed; we now show that formation of these structures can be also controlled by dietary signals. Thus, in addition to the established impact of dietary plant-derived chemicals in postnatal immune cells, our work reveals dietary retinoids as key regulators of pre-natal ILCs with a lifelong impact on adult lymphoid organ size[26–28]. It was previously shown that complete absence of lymphoid organs leads to long-life virus persistence[29]. Our data reveal that the efficiency of adaptive immune responses to infection and possibly to other immune insults may be pre-tuned in early life through dietary signals from maternal origin.

We report here that cell-autonomous RA signalling is a key axis for *Rorgt* expression and LTi cell differentiation within developing SLOs. Similarly, RA may also be important after birth in infection and chronic inflammatory diseases[30]. Lineage-targeted strategies will be central to elucidate the contribution of dietary retinoids in these outcomes.

METHODS SUMMARY

Mice were maintained at Instituto de Medicina Molecular (IMM) or VU University Medical Centre according to national and international guidelines. Bone marrow cells were isolated from 8-week-old C57BL/6 CD45.1 mice and injected intravenously into 2-week-old lethally irradiated CD45.2 *ROSA26*-RARα403^{Het} (WT→Rar^{Het}) or wild-type littermate controls (WT→WT). C57BL/6 female mice received either vitamin-A-deficient (VAD), with no vitamin A (vitamin free casein), vitamin-A-high (VAH, 25,000 IU kg^{-1}) or vitamin-A-control (VAC, 4,000 IU kg^{-1}) diets. Retinoic acid was provided to pregnant mice from E10.5 until they were euthanized. Quantitative real-time PCR with reverse transcription (RT–PCR) was performed as previously described[6,7,10]. Computational analysis was performed with TESS. DNA–protein complexes were immunoprecipitated using antibodies against mouse pan-RAR, pan-RXR or control IgG.

Online Content Any additional Methods, Extended Data display items and Source Data are available in the online version of the paper; references unique to these sections appear only in the online paper.

Received 6 June 2013; accepted 18 February 2014.
Published online 19 March 2014.

1. Gluckman, P. D. & Hanson, M. A. Living with the past: evolution, development, and patterns of disease. *Science* **305,** 1733–1736 (2004).
2. van de Pavert, S. A. & Mebius, R. E. New insights into the development of lymphoid tissues. *Nature Rev. Immunol.* **10,** 664–674 (2010).
3. Randall, T. D., Carragher, D. M. & Rangel-Moreno, J. Development of secondary lymphoid organs. *Annu. Rev. Immunol.* **26,** 627–650 (2008).
4. Mebius, R. E., Rennert, P. & Weissman, I. L. Developing lymph nodes collect $CD4^{+}CD3^{-}LT\beta^{+}$ cells that can differentiate to APC, NK cells, and follicular cells but not T or B cells. *Immunity* **7,** 493–504 (1997).

5. Eberl, G. *et al.* An essential function for the nuclear receptor RORγt in the generation of fetal lymphoid tissue inducer cells. *Nature Immunol.* **5,** 64–73 (2004).
6. Veiga-Fernandes, H. *et al.* Tyrosine kinase receptor RET is a key regulator of Peyer's Patch organogenesis. *Nature* **446,** 547–551 (2007).
7. Patel, A. *et al.* Differential RET signaling pathways drive development of the enteric lymphoid and nervous systems. *Sci. Signal.* **5,** ra55 (2012).
8. Cupedo, T. *et al.* Presumptive lymph node organizers are differentially represented in developing mesenteric and peripheral nodes. *J. Immunol.* **173,** 2968–2975 (2004).
9. Cherrier, M., Sawa, S. & Eberl, G. Notch, Id2, and RORγt sequentially orchestrate the fetal development of lymphoid tissue inducer cells. *J. Exp. Med.* **209,** 729–740 (2012).
10. van de Pavert, S. A. *et al.* Chemokine CXCL13 is essential for lymph node initiation and is induced by retinoic acid and neuronal stimulation. *Nature Immunol.* **10,** 1193–1199 (2009).
11. Niederreither, K. & Dolle, P. Retinoic acid in development: towards an integrated view. *Nature Rev. Genet.* **9,** 541–553 (2008).
12. Iwata, M. Retinoic acid production by intestinal dendritic cells and its role in T-cell trafficking. *Semin. Immunol.* **21,** 8–13 (2009).
13. Hall, J. A. *et al.* Essential role for retinoic acid in the promotion of $CD4^+$ T cell effector responses via retinoic acid receptor alpha. *Immunity* **34,** 435–447 (2011).
14. Mora, J. R. & von Andrian, U. H. Role of retinoic acid in the imprinting of gut-homing IgA-secreting cells. *Semin. Immunol.* **21,** 28–35 (2009).
15. Mucida, D. *et al.* Retinoic acid can directly promote TGF-β-mediated $Foxp3^+$ Treg cell conversion of naive T cells. *Immunity* **30,** 471–472; Reply 472–473 (2009).
16. Hall, J. A., Grainger, J. R., Spencer, S. P. & Belkaid, Y. The role of retinoic acid in tolerance and immunity. *Immunity* **35,** 13–22 (2011).
17. de Boer, J. *et al.* Transgenic mice with hematopoietic and lymphoid specific expression of Cre. *Eur. J. Immunol.* **33,** 314–325 (2003).
18. Rosselot, C. *et al.* Non-cell-autonomous retinoid signaling is crucial for renal development. *Development* **137,** 283–292 (2010).
19. Sun, Z. *et al.* Requirement for RORγ in thymocyte survival and lymphoid organ development. *Science* **288,** 2369–2373 (2000).
20. Yokota, Y. *et al.* Development of peripheral lymphoid organs and natural killer cells depends on the helix-loop-helix inhibitor Id2. *Nature* **397,** 702–706 (1999).
21. Aliahmad, P., de la Torre, B. & Kaye, J. Shared dependence on the DNA-binding factor TOX for the development of lymphoid tissue-inducer cell and NK cell lineages. *Nature Immunol.* **11,** 945–952 (2010).
22. Possot, C. *et al.* Notch signaling is necessary for adult, but not fetal, development of $ROR\gamma t^+$ innate lymphoid cells. *Nature Immunol.* **12,** 949–958 (2011).
23. Tachibana, M. *et al.* Runx1/Cbfβ2 complexes are required for lymphoid tissue inducer cell differentiation at two developmental stages. *J. Immunol.* **186,** 1450–1457 (2011).
24. Meier, D. *et al.* Ectopic lymphoid-organ development occurs through interleukin 7-mediated enhanced survival of lymphoid-tissue-inducer cells. *Immunity* **26,** 643–654 (2007).
25. Gredmark-Russ, S., Cheung, E. J., Isaacson, M. K., Ploegh, H. L. & Grotenbreg, G. M. The CD8 T-cell response against murine gammaherpesvirus 68 is directed toward a broad repertoire of epitopes from both early and late antigens. *J. Virol.* **82,** 12205–12212 (2008).
26. Kiss, E. A. *et al.* Natural aryl hydrocarbon receptor ligands control organogenesis of intestinal lymphoid follicles. *Science* **334,** 1561–1565 (2011).
27. Lee, J. S. *et al.* AHR drives the development of gut ILC22 cells and postnatal lymphoid tissues via pathways dependent on and independent of Notch. *Nature Immunol.* **13,** 144–151 (2011).
28. Qiu, J. *et al.* The aryl hydrocarbon receptor regulates gut immunity through modulation of innate lymphoid cells. *Immunity* **36,** 92–104 (2011).
29. Karrer, U. *et al.* On the key role of secondary lymphoid organs in antiviral immune responses studied in alymphoplastic (*aly/aly*) and spleenless (*Hox11*$^{-/-}$) mutant mice. *J. Exp. Med.* **185,** 2157–2170 (1997).
30. Spencer, S. P. *et al.* Adaptation of innate lymphoid cells to a micronutrient deficiency promotes type 2 barrier immunity. *Science* **343,** 432–437 (2014).

Acknowledgements We thank the imaging, animal and flow cytometry facilities at IMM and UPC for technical assistance; C. Mendelsohn for providing *ROSA26*-RARα403 mice; N. Schmolka, J. G. van Rietschoten, R. E. van Kesteren, T. H. B. Geijtenbeek, S. Gringhuis, E. Keuning, J. Peterson-Maduro, M. G. Roukens, D. D'Astolfo, M. Vermunt, A. Rijerkerk, J. Koning, J. van der Meulen and B. Oliver for technical help; and G. Vilhais-Neto, M. C. Coles and G. Eberl for discussion. M.F., L.M.-S. and R.G.D. were supported by FCT, Portugal; H.V.-F. by EMBO (1648) and ERC (207057); D.R.L. by NIH (RO1AI080885) and HHMI; M.R.M. by Dutch MS research foundation (MS 12-797); S.A.vd.P. by NGI Breakthrough Horizon (40-41009-98-9077); and R.E.M. by a VICI (918.56.612) and ALW-TOP grant (09.048).

Author Contributions M.F. wrote the manuscript, designed, performed and analysed the experiments in Figs 1a, b, d, e, g–i, 2a–h, 3a, b, d–i and 4a, b, d–j and Extended Data Figs 1a, b, d–f, 2a–d, 3a–h, 4a–d, 5a–c, 6, 7a–f, 8a–d, 9a, b and 10a–c. S.A.vd.P. wrote the manuscript, designed, performed and analysed the experiments in Figs 1c, f, 3c, g–i and 4c and Extended Data Figs 1b, c, e, 5b, c and 6. R.G.D., H.R., R.M., L.M.-S., F.F.A., S.I., I.B., G.G., C.L.-A., T.K., D.S., T.O'T., M.R.M., Y.H. and S.S-M. contributed to several experiments. C.G.-S. and J.P.S. provided murid herpesvirus-4. D.R.L. and F.R.S provided *Rorgt*$^{-/-}$ embryos. E.H. and E.D. provided Ly-6A (*Sca1*)-*GFP* mice. R.E.M. and H.V.-F. supervised the work, planned the experiments and wrote the manuscript.

Author Information Reprints and permissions information is available at www.nature.com/reprints. The authors declare no competing financial interests. Readers are welcome to comment on the online version of the paper. Correspondence and requests for materials should be addressed to H.V.-F. (jhfernandes@medicina.ulisboa.pt).